NANOMATERIALS BASED ELECTROCHEMICAL AND OPTICAL SENSORS FOR FOOD ADDITIVES AND BIOMARKERS

Thesis submitted to

Cochin University of Science and Technology

in partial fulfilment of the requirements

for the award of the degree of

Doctor of Philosophy

in

Chemistry

by

Unni Sivasankaran

(Reg. No. 4794)

Department of Applied Chemistry

Cochin University of Science and Technology

Kochi – 22

June 2018

Nanomaterials Based Electrochemical and Optical Sensors for Food Additives and Biomarkers

Ph. D. Thesis under the Faculty of Sciences

By

Unni Sivasankaran
Research Fellow
Department of Applied Chemistry
Cochin University of Science and Technology
Kochi, India - 682022
Email: unni.siva.info@gmail.com

Supervising Guide

Dr. K. Girish Kumar
Professor & Head
Department of Applied Chemistry
Cochin University of Science and Technology
Kochi, India - 682022
Email: giri@cusat.ac.in

Department of Applied Chemistry
Cochin University of Science and Technology
Kochi, India 682022

June 2018

DEPARTMENT OF APPLIED CHEMISTRY
COCHIN UNIVERSITY OF SCIENCE AND TECHNOLOGY
KOCHI - 682022, INDIA

Dr. K. Girish Kumar
Professor and Head

Tel: 0484 - 2575804
E-mail: chem.@cusat.ac.in

Date: 06 June 2018

Certificate

Certified that the work entitled **"Nanomaterials Based Electrochemical and Optical Sensors for Food Additives and Biomarkers"**, submitted by Mr. Unni Sivasankaran, in partial fulfilment of the requirements for the degree of Doctor of Philosophy in Chemistry to Cochin University of Science and Technology, is an authentic and bonafide record of the original research work carried out by him under my supervision at the Department of Applied Chemistry. Further, the results embodied in this thesis, in full or in part, have not been submitted previously for the award of any other degree. All the relevant corrections and modifications suggested by the audience during the pre-synopsis seminar and recommended by the Doctoral committee have been incorporated in the thesis.

K. Girish Kumar
(Supervising Guide)

Declaration

I hereby declare that the work presented in this thesis entitled **"Nanomaterials Based Electrochemical and Optical Sensors for Food Additives and Biomarkers"** is based on the original work carried out by me under the guidance of Dr. K. Girish Kumar, Professor & Head, Department of Applied Chemistry, Cochin University of Science and Technology and has not been included in any other thesis submitted previously for the award of any degree.

Kochi-22 **Unni Sivasankaran**
06/06/2018

UNIVERSITY LIBRARY

COCHIN UNIVERSITY OF SCIENCE AND TECHNOLOGY

Cochin-682 022, Kerala, India

Phone: 0484-2575715, 2575092 e-mail: ul@cusat.ac.in

UNIVERSITY LIBRARIAN

UL/109/ 2018-19 31-5-2018

CERTIFICATE

Certified that the contents in the thesis entitled "**Nanomaterials based Electrochemical and Optical Sensors for food Additives and Biomarkers**" submitted by **Unni Sivasankaran (Reg.No.4794), Research Scholar, Department of Applied Chemistry, Cochin University of Science and Technology, Kochi-22** was subjected to plagiarism detection using the software 'URKUND' and found that significant level of plagiarism is **8%.**

DR.BEENA.C

Dedicated to

My Parents…

Acknowledgement

In life, there are many people whose support, encouragement and inspiration are needed to reach and accomplish major milestones, especially, if it involves realizing and fulfilling one's cherished dreams. For me, this thesis is such an important destiny that I am truly and forever indebted to lot of people for their wishes and blessings, with which I have been able to complete this journey.

First of all, I would like to express my immense gratitude to my research supervisor Prof. K. Girish Kumar for his guidance throughout my research work. Without his patient guidance, relentless persuasion and inspiration, I would not have been able to complete this journey. I am deeply indebted to Girish Sir for giving me the opportunity to work in the Sensor group. His support has been selfless in my endeavor for scientific knowledge and personal growth. His words have always inspired me and have instilled in me a higher level of thinking and understanding. He has been very affectionate and was always ready to help me, even in the midst of his busy schedule. I have been extremely lucky and blessed to have Prof. K. Girish Kumar as my research guide.

I am thanking Dr. P. V. Mohanan, with whom I initially joined as a research scholar due to the unavailability of vacancy in the Analytical Lab and subsequently becoming my doctoral committee member. He has been very generous to me with his suggestions and advices as and when it was required. I am deeply indebted to him for his kindness and understanding throughout my association with the department.

I take this opportunity to express my deep gratitude to Dr. K. Sreekumar and Dr. S. Prathapan, faculty members of Department of Applied Chemistry, CUSAT for their resolute guidance, critical appreciation and continuous help during the course of this study for which I shall remember both of them with great respect for all the time to come.

I express my gratefulness to all the faculty members of Department of Applied Chemistry, CUSAT for their inspiration and timely help. I also acknowledge the help of various non-teaching staff members for extending to me a lot of support.

Dr. Anitha I., Principal, KKTM Govt. College (Kodungallur), deserves a special mention here for her support and help.

My heartfelt gratitude to my friends Meegle, Vijesh, Sowmya chechi, Anjali chechi, Rakesh chettan and Nandagopal for helping me a lot in characterizing my samples. I am highly indebted to the divisional staffs of STIC (CUSAT), International School of Photonics (CUSAT), IISER (Trivandrum), IIST (Trivandrum), M. G. University (Kottayam) and Amrita Center for Nanosciences & Molecular Medicine for Analysis (Edappally) for their generous cooperation in characterizing my samples.

I am forever indebted to all my former teachers as they laid the foundation for this achievement. I also have to especially acknowledge my teachers in BSc. and MSc. classes for really nourishing my interest in the subject of Chemistry.

I would like to express my sincere thanks to my senior colleagues Theresa chechi, Divya chechi, Anuja chechi, Soumya chechi, Jesny chechi, Zafna chechi and Ammu for their valuable suggestions, fruitful criticisms and co-operation at various junctures of my work. With utmost pleasure, I express my thanks to my juniors and also my best friends during my research - Shalini, Ambily chechi, Sanu, Manna and Devika for their critical advice, invigorating discussions, constructive comments, kind co-operation and cheerful company in my day to day interactions. I would also like to take the opportunity to thank Monica chechi and Jintha chechi for being very helpful.

A special word of appreciation goes to Soumya chechi and Ammu for their willingness to help me even in the midst of their busy schedule. Monica chechi, Jintha chechi, Jesny chechi, Shalini and Ambily chechi took efforts to correct

grammatical mistakes and improve the language of my thesis. The friendship forged with Jerin, Tomson and Kiran chettan helped me push and tide through the gruesome period of this thesis documentation.

I remember with gratitude my friends- Jomon chettan, Mahesh chettan, Sreejith chettan, Rakesh chettan, Kiran chettan, Rashid, Shandev, Tomson, Jith, Midhun, Sowmya chechi, Anjali chechi, Sona chechi, Jisha chechi, Sneha chechi, Jessica chechi, Letcy, Nithya, Daly, Nishad, Lincy, Rani, Ambily chechi, Reshma chechi, Cisy chechi, Sherly Miss, Aswathy, Parvathi chechi and Vineetha chechi for their support and friendship that made the experience of working at CUSAT very enjoyable and memorable.

I am also thankful to Somashekhar, Sandeep, Sanoop and late Vishnu for giving me cherished memories. The good times I had while working with Sheela miss, Meera chechi, Sreejith chettan, Shruthy chechi, Noufia, Sreelakshmi, Arun, Kavya, Aparna, Shilpa, Jilsy, Akhila, Meera, Nihal, Radhika, Bhagyalakshmi and Lakshmi will always remain with me and I sincerely thank them.

I am grateful to the Cochin University of Science and Technology-Kochi for the fellowship, Directorate of Extramural Research and Property Rights (DRDO)-New Delhi, University Grants Commission (UGC)-New Delhi, Kerala State Council for Science, Technology and Environment and the Department of Science and Technology (DST)-New Delhi for the funding assistance in the form of projects.

I am deeply grateful to my family for their continuing encouragement and affection. I find no words to express the constant love and care of my parents who have always given me the best of everything. Their patience and sacrifice will remain my inspiration throughout my life.

Above all, I thank God; the almighty for this most amazing moment.

Though, many others have not been mentioned, none of them is forgotten.

Unni Sivasankaran

Preface

Improvement of quality of life is one of the most important objectives of the global research efforts. Naturally, the quality of life is closely related to a better control of diseases, food quality and safety. More and more measurements of analytes are performed in various locations, including hospital point-of-care settings, by caregivers in non-hospital settings and by patients at home.

The detection and determination of a particular quantity, whether chemical or physical, requires a sensing platform which can specifically or selectively monitor that quantity. A sensor is a device that detects and responds to some type of input from the physical environment. Sensing technology has captured the attention of scientists across the world due its vast number of applications in various fields such as clinical, quality control, environment monitoring etc.

A chemical sensor is a device that transforms chemical information into an analytically useful signal. This chemical information may relate to a wide range of chemical processes ranging from the composition or presence of a particular element or ion, concentration, chemical activity, partial pressure etc. The sensing process involves two major steps: recognition and transduction. Based on the principle of transduction, chemical sensors are classified in to four main classes such as heat sensitive, mass sensitive, electrochemical and optical sensors. Among which, electrochemical and optical sensors have become a growing field of scientific interest owing to their fast response, cost effectiveness and high selectivity and sensitivity. Development of nanomaterials based electrochemical and optical sensors for the quantification of food additives and biomarkers was carried out during the course of present study.

The thesis entitled "Nanomaterials based electrochemical and optical sensors for food additives and biomarkers" is divided in to twelve chapters. Brief descriptions of the chapters are given below.

Chapter 1 outlines a general introduction of principles behind the electrochemical and optical sensing, especially voltammetry, fluorimetry and colorimetry. Importance of three electrode system, various types of electrodes, modification etc. are discussed under the section called voltammetric sensor. Interaction of light with matter and important phenomenon behind the emission and absorption spectroscopy, probable mechanisms that can be occurred upon interaction of fluorescent or colorimetric probe with analyte is also discussed in detail. An adequate literature review of various voltammetric, fluorescent and colorimetric sensors are also included in this chapter.

Chapter 2 is devoted to the description of various chemicals and instruments used, preparation of various buffers and artificial physiological samples and cleaning procedures for electrodes. Procedures used for reference methods are also discussed.

Chapter 3 discusses the development of a voltammetric sensor for the phenolic antioxidant octyl gallate (OG). Gold nanoparticles and self-assembled monolayer of dodecane thiol modified glassy carbon electrode was used as working electrode. Optimization of various experimental parameters for the determination of OG was carried out. Determination of OG in commercial food samples was also done.

Chapter 4 describes the voltammetric determination of the important metabolite uric acid using polybromophenol blue – gold nanoparticle composite modified glassy carbon electrode. Based on the higher peak current and lower peak potential of modified electrode in comparison to the bare, optimization studies were carried out and the developed method was applied for analysis of urine and blood serum samples.

Chapter 5 deals with the development of a voltammetric sensor for propyl gallate (PG) by nickel nanoparticles modified glassy carbon electrode. Various experimental parameters for the electro-oxidation of PG was studied

and optimized. The developed sensor has been tried to determine PG in commercial food samples such as oils and fat.

Chapter 6 reports the application of L-cysteine stabilized cadmium sulphide quantum dots (L-cys-CdS) as fluorescent sensor for the food colorant brilliant blue FCF (BB). Determination was achieved using the quenching efficiency of BB on the fluorescence intensity of L-cys-CdS. Experimental parameters have been studied and optimized. Determination of BB from sports drink and candies are also studied for the applicability of the developed sensor.

Chapter 7 explains the development of a fluorescent sensor for quinoline yellow (QY) using L-cysteine stabilized copper nanoclusters (L-cys-CuNCs) as fluorophores. Fluorescence intensity of L-cys-CuNCs was dramatically quenched in presence of the food colorant QY. Based on this, a turn-off fluorescent sensor for QY is developed and is successfully applied for determination in commercial food samples.

Chapter 8 describes the synthesis of ethylene diamine passivated carbon dots (EDA-CDs) from tissue paper and its application as a fluorescent sensor for glutathione (GSH). Characterization of the synthesized EDA-CDs was done using several analytical techniques. In presence of GSH, fluorescence intensity of probe quenched dramatically and based on this response, a turn-off sensor was developed. Determination of GSH in artificial saliva samples were also carried out to verify the applicability of the developed sensor.

Chapter 9 focusses the development of a colorimetric sensor for dopamine (DA) using citrate stabilized gold nanoparticles (AuNPs). Aggregated AuNPs by NaOH was used for sensing purpose. On addition of DA to aggregated AuNPs, dispersion of AuNPs occurred with a significant change of absorption spectra. Color of the aggregated AuNPs solution changed from blue to yellowish green in presence of DA. Based on these responses,

colorimetric determination of DA has been carried out. Artificial urine samples and pharmaceutical formulations were used for application studies.

Chapter 10 details the application of L-cysteine stabilized copper nanoparticles (L-cys-CuNPs) as a colorimetric probe for creatinine (CR) sensing. Absorption of L-cys-CuNPs significantly decreased with a change in color from red to yellow after the addition of CR. Based on the above response, sensing of CR was achieved and developed sensor was applied for CR determination in synthetic urine and blood serum samples.

Chapter 11 presents the development of a dual channel sensing strategy for adrenaline (ADR) using $CuCl_2$ solution. Presence of ADR reduces the Cu (II) to Cu and there by oxidation of ADR takes place. Oxidized ADR produces cage like particles and the already produced CuNPs are trapped inside the cage. These changes occurred by a change in the color of the $CuCl_2$ solution from pale blue to yellowish brown. Production of CuNPs induced a new peak in absorption spectrum and a strong blue fluorescence of oxidized ADR via metal enhanced effect. By noting these changes fluorimetric and colorimetric sensing of ADR was achieved and the method was also applied for the analysis of artificial urine and pharmaceutical formulation.

Chapter 12 represents the summery and important conclusions of the work.

List of references cited in the chapters is compiled at the end of the thesis as a separate section.

Contents

Chapter 1

Chapter 2

Chapter 8

SYNTHESIS OF CARBON DOTS AND APPLICATION AS A FLUORESCENT SENSOR FOR GLUTATHIONE 171-193

List of Tables

List of Figures

List of Schemes

Chapter 1

INTRODUCTION

Contents

"Without health life is not life; it is a state of languor and suffering – an image of death" – Buddha

Modern science has tremendously added comfort and convenience to mankind. However, life style habits associated with modern world viz. fascination to junk food along with lack of exercise and exposure to environment pollutants can adversely affect quality of human life. In this scenario, consumer awareness about harmful effects and effective detection strategies is increasing. Chemical sensors a worthwhile achievement of modern science, the marvel of analysis, can play a vital role here. Based on the applicability, it is widely used in variety of fields such as clinical analysis, quality control, environment monitoring and defence.

Chemical sensors are devices that transform chemical information into analytically useful signals. The chemical information may be composition or presence of particular element or ion, its concentration or chemical activity, partial pressure etc. Based on the principle of transduction, chemical sensors are classified in to four main classes viz. heat sensitive, mass sensitive, electrochemical and optical sensors.

- Heat sensitive sensors are based on the measurement of heat effects such as heat liberated or absorbed during a chemical reaction and is usually called as calorimetric sensors.

- Mass sensitive sensors are based on the measurement of changes in mass triggered by accumulation of analyte at specially modified surface.

- In electrochemical sensors, a change in the electrical properties such as current, potential, resistance, capacitance etc. are measured and is related to the concentration or composition of the given sample. Here sensing element is the electrodes and chemical reaction of electro active compound occurring at the electrode surface is studied.

- Optical sensors deals with changes in optical properties such as light absorption, emission etc. by the interaction of analyte. Usually an optical indicator is used and changes in optical properties of the indicator is studied and related to concentration of analyte.

1.1 Electrochemical sensors

Electrochemical sensors are good choices for routine analysis due to its outstanding properties such as biocompatibility, cost effectiveness, simplicity etc. Here, oxidation or reduction of analytes is usually studied. Electrochemical reaction takes place at electrode surface is studied using same electrode, thereby it acts as sensing element.

1.1.1 Interfacial electrochemistry

To study possible reactions happening in electrochemical systems, scientists usually think about formation of an interface between electrode and electrolyte solution. Figure 1.1 illustrates diagrammatic representation of interface. Normally, electrode surface carries a charge with opposite sign and equal magnitude to that of charge from the solution side of the interface. The consequential charge distribution of these two fine sections of equal and opposite charge, similar to a capacitor is called as electrical double layer. Here, very high capacitance is produced between these two small effective plates. Reactions concerning transference of charge across the interface and thereby flow of current are generally called as electrochemical reactions.

For the determination of an analyte, we consider a system consisting of an electrode interacting with an electrolyte containing non-reacting cations and anions. Also, there is no or negligible decomposition of solvent in applied potential range. Based on thermodynamic concept, above discussed interface can be expressed as ideally polarizable. Potential range, at which the electrochemical processes are studied, is called as the potential window. Usually at this potential window electrochemical reaction under study should be devoid of interference by solvent.

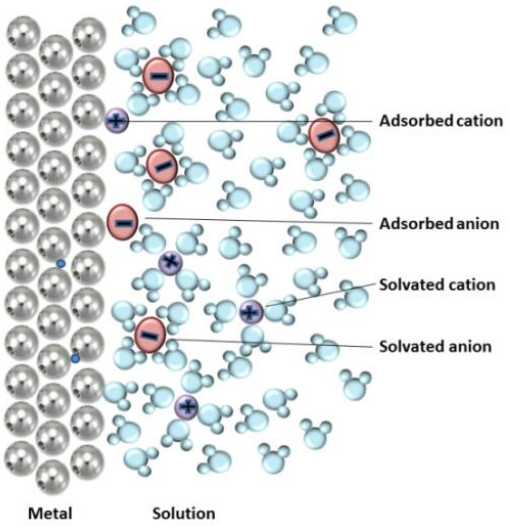

Figure 1.1: Structure and processes at the metal-solution interface.

Movement of current through electrode-electrolyte interface will be followed by either faradaic or non-faradaic process. Faradaic process is governed by Faraday's laws; where, oxidation or reduction occurs by transfer of electrons across interface. Changes occurring at electrode-solution interface are by either adsorption or desorption, resulting in a change in effective area of electrode. Reactions progressed by such developments are called non-faradaic processes. Current produced by faradaic and non-faradaic processes are known as faradaic current and non-faradaic currents, respectively. Generally faradaic processes are preferred in electrochemical reactions and it is influenced by mass transport of electroactive species.

1.1.1.1 Types of mass transport

Electrode reaction is preceded by mass transport of electroactive species from bulk solution to electrode surface. Three common forms of mass transport processes are migration, convection and diffusion.

1.1.1.1.1 Migration

It is the movement of charged species towards the opposite charge due to electrostatic attraction. Influence of migration can be minimized by addition of higher concentration of supporting electrolyte into solution.

1.1.1.1.2 Convection

This type of mass transport is due to movement of species by density gradient or by mechanical means. The former case is known as natural convection and latter case occurs by stirring or rotating the solution, so it is known as forced convection. By keeping the solution unstirred, effect of convection can be reduced.

1.1.1.1.3 Diffusion

Movement of species due to a difference in concentration gradient is known as diffusion. Usually diffusion of species occurs from a region of higher concentration to a region of lower concentration. Adolf Fick proposed two laws to explain diffusion process.

Using Fick's first law, rate of transfer of electroactive species (J_o) to a unit area of electrode surface can be related to concentration gradient ($\frac{\partial Co}{\partial x}$) and diffusion coefficient (D) as,

$$\boldsymbol{J_o = -D\frac{\partial C_o}{\partial x}}$$

According to Fick's second law, rate of diffusion of a species to the electrode surface from a distance of x can be expressed as,

$$\frac{\partial C_o}{\partial t} = D \frac{\partial^2 C_o}{\partial x^2}$$

Mass transport in electrochemical cell is multifaceted due to three modes of transport. In the case of voltammetry, mass transport is only due to diffusion process. This can be achieved by eliminating migration and convection via addition of excess concentration of inert supporting electrolyte to the reaction cell and conducting experiment in an unstirred condition.

1.1.2 Voltammetric sensors

In Voltammetric sensors, current produced is registered as a function of applied potential. Numerous voltammetric systems are manufactured commercially for quantification of certain species of scientific or industrial interest. These sensors can be applied for analysis of different analytes in various matrices.[1]

1.1.2.1 Instrumentation – cell set up

Electrochemists are interested in the investigation of reactions occurring at interface between electrode and electrolyte, where a minimum of two electrodes are necessary for the passage of current through the system. In voltammetry, three electrodes are used, the main electrode - working electrode, counter/auxiliary electrode and reference electrode. All three electrodes are immersed in an excess of supporting electrolyte which provides electrical conductivity between electrodes.

1.1.2.2 Working electrode

The electrode at which electrochemical reaction takes place is called working electrode. Selection of working electrode is important because it can influence the reaction characteristics. Working electrode must possesses properties such as inertness over broad potential window, high overvoltage for oxygen and hydrogen evolution, low residual current and low ohmic resistance. Along with the above discussed properties, good stability is an important characteristic needed for long term use.

Usually used working electrodes in voltammetric studies include electrodes of gold, platinum, carbon paste and glassy carbon. Among these, glassy carbon based electrodes (GCE) find great attention among electrochemists due to their exceptional mechanical and electrical properties *viz*., high resistance to solvents, wide potential window and reproducible outcomes.[2] In GCE, disk of glassy carbon, an isotropic and conducting material with low porosity prepared from polymeric resin is often used.[3] For the present studies in the development of electrochemical sensors, GCE is selected as the working electrode due to the above special properties.

1.1.2.3 Reference electrode

Reference electrode is a half-cell whose reduction potential is known and is used to measure and control the potential of working electrode. It is also known as unpolarized electrode. A good reference electrode must be stable with respect to temperature and time.

Standard hydrogen electrode can be used as reference electrode, but difficulty in construction and maintenance reduces its widespread use. Due to easiness in construction and maintenance, KCl saturated Ag/AgCl or

calomel electrodes are usually used for voltammetric studies. In the present study, KCl saturated Ag/AgCl was employed as reference electrode.

1.1.2.4 Auxiliary electrode

To retain constant potential for reference electrodes, no current should pass through it. So, auxiliary/counter electrode is used to allow passage of electrons through cell without any disturbance to reference electrode. Auxiliary electrode functions as sink or source for electrons.[4] Surface area of counter electrode must be equal or larger than that of working electrodes to support the current generated at working electrode. Because of its inert character, wires of platinum, gold or carbon are often used as auxiliary electrodes. In present studies, platinum wire is used as counter electrode.

1.1.3 Different techniques used for electrochemical analysis

To explore various phenomena such as reaction mechanism, kinetics, thermodynamics etc. different electrochemical techniques can be used. Among different electrochemical techniques available, cyclic voltammetry (CV), linear sweep voltammetry (LSV), square wave voltammetry (SWV), differential pulse voltammetry (DPV), chronoamperometry (CA) and electrochemical impedance spectroscopy (EIS) have been used for present study.

1.1.3.1 Cyclic voltammetry

CV is one of the widely used electrochemical techniques for attaining qualitative information of electrochemical processes. CV is always conducted at the beginning of every electrochemical study and it can be considered as an initial point of electrochemical analysis.[2]

CV is a potentiodynamic technique where potential of the electrode is changed linearly with time. In this technique, a triangular potential sweep is applied to working electrode using a potentiostat, whereby initial potential is varied to final potential and returns to the initial at a constant rate of potential sweep (Figure 1.2 a). Ensuing graph achieved by plotting current against applied potential is called cyclic voltammogram. Depending on the properties of electroactive species, one or more peaks corresponding to reduction and/or oxidation will observe on voltammogram. Observed current in voltammogram is proportional to concentration of the studied electroactive species. Imperative variables in a cyclic voltammogram are anodic peak potential (E_{pa}), cathodic peak potential (E_{pc}), anodic peak current (i_{pa}) and cathodic peak current (i_{pc}). In order to enhance the sensitivity and speed of quantitative analysis, pulse techniques are usually employed.[5]

1.1.3.2 Linear sweep voltammetry

Linear sweep voltammetry is almost similar to CV and only difference is in the mode of potential sweep. Here, potential is only swept from initial to final at a constant rate and no reversal of scan as in the case of CV (Figure 1.2 b). An increase in Faradaic current is observed with scan rates, which resulting in an increase in signal to noise ratio.[6] Compared to CV, this technique is often used for studies of irreversible reactions.

1.1.3.3 Square wave voltammetry

Square wave voltammetry (SWV) is the most widely used pulse technique for electrochemical analysis. This is because of its unique properties such as higher sensitivity compared to CV and LSV and fast

response in comparison to other pulsed techniques. Potential in SWV comprises of consistent square wave superimposed on a staircase (Figure 1.2 c). Observed currents at the end of frontward and backward pulses are recorded as a function of potential. Net current, obtained as difference between frontward and backward currents is estimated.[7]

1.1.3.4 Differential pulse voltammetry

In differential pulse voltammetry (DPV), potential is increased in a staircase fashion and difference between currents is measured just before and after each pulse (Figure 1.2 d). Difference in currents is plotted versus potential to get a wave form. DPV minimise the effect of charging current and there by only faradaic current is measured. Compared to the above discussed voltammetric techniques, DPV is more sensitive; but it is time consuming.

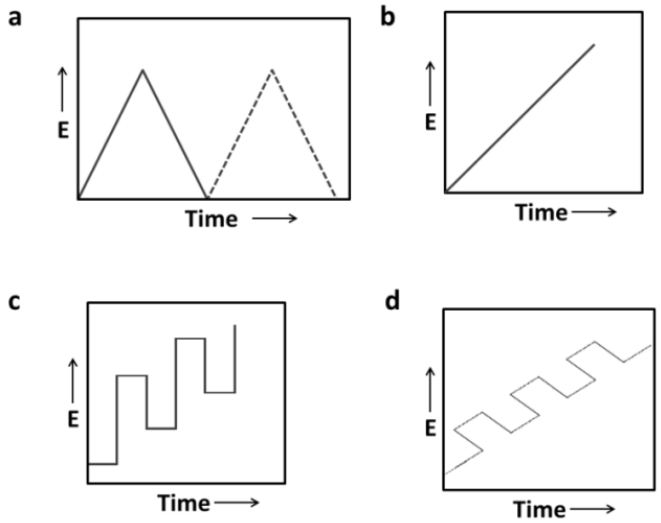

Figure 1.2: Modes of application of potential in (a) cyclic voltammetry, (b) linear sweep voltammetry, (c) square wave voltammetry and (d) differential pulse voltammetry.

1.1.3.5 Chronoamperometry

Chronoamperometry (CA) is one of the widely used electroanalytical techniques employed for examining mechanism or kinetics of electrode processes. Also, it is suitable for the determination of diffusion coefficient. As in the case of voltammetry, same electrode-cell system is used here. In CA, potential is applied in a square-wave fashion, from a point where no electrochemical reaction occurs to final point, at which concentration of species on surface of electrode approaches to zero and resultant current is recorded as a function of time. Here, deviations in current arise according to growth or depletion of diffusion layer at electrode surface.[8] CA studies can be performed either by single potential step or by double potential step. In single potential step method, resulting current from forward step is recorded. In double potential step, observed current is recorded when the potential is increased from low to high and returned to a final value (E_f) at a time period (τ).

Resultant current *vs* time is related in Cottrell equation as,[9]

$$\boldsymbol{I = nFAD^{1/2}C\pi^{-1/2}t^{-1/2}}$$

where, n is the number of electrons involved in reaction, F is Faraday's constant, A is surface area of electrode, D is diffusion coefficient and C is concentration of electroactive species respectively.

1.1.3.6 Electrochemical impedance spectroscopy

Electrochemical impedance spectroscopy (EIS) is a sensitive and powerful technique used for investigation of mechanism and charge transfer properties of electrochemical reactions taking place at the interface of

electrode and electrolyte. By changing frequency (f) of applied potential, complex impedance (Z) (sum of real (Z') and imaginary (-Z") components) is studied.[10]

EIS data is often represented by Bode and Nyquist plots. Bode plots are presented using impedance (real or imaginary) and phase angle as function of frequency. But in Nyquist plot, real impedance representing resistance of cell is plotted against imaginary impedance obtained from double-layer capacitance.[11] Among these two representations, Nyquist plot is quite simple and most commonly used. Nyquist plot usually contains two portions, a semicircular portion at higher frequency region represents electron transfer limited process and linear portion at lower frequency depicts diffusion limited process (Figure 1.3). From the diameter of semicircle, charge transfer resistance (R_{ct}) at electrode surface can be obtained. Usually semicircle with larger diameter is observed for sluggish electron transfer.[12]

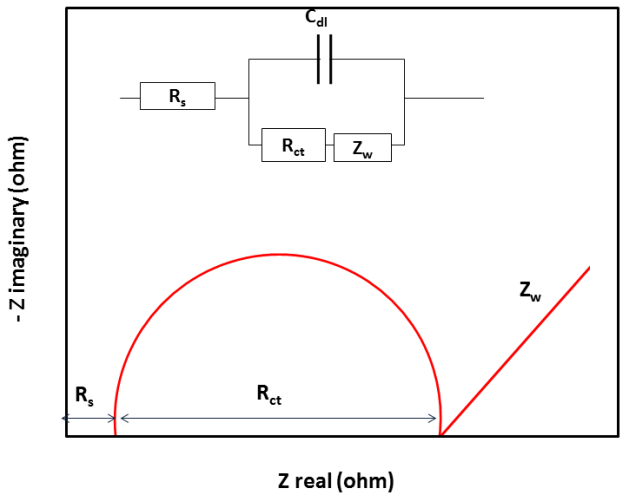

Figure 1.3: Nyquist plot of the Randel's circuit as shown in inset.

1.1.4 Kinetics of electrode reaction

1.1.4.1 Reversible systems

When electron transfer kinetics is faster than mass transport of an electroactive species towards electrode surface, such electrochemical system is said to be reversible. According to Nernst equation, concentration of electroactive species in reversible systems is given by,

$$\boldsymbol{E_e = E_e^o + \frac{RT}{nF} ln \frac{C_o}{C_R}}$$

where E_e, E_e^o, n, C_o and C_R are the equilibrium potential, standard potential, number of electrons involved, surface concentrations of oxidized and reduced species respectively. R, T and F have their usual meaning.

Using Randles - Sevcik equation, peak current (i_p) of a reversible system (at 25°C) can be equated to concentration (C) as,

$$\boldsymbol{i_p = \left(2.69 \times 10^5\right) n^{3/2} A D^{1/2} C v^{1/2}}$$

where A, D and ν refers to surface area of electrode (cm^2), diffusion coefficient ($cm^2\ s^{-1}$) and scan rate (Vs^{-1}), respectively. According to the above equation, peak current increases with square root of scan rate. For a perfectly reversible redox couple, ratio of anodic and cathodic current $(i_{p,c}/i_{p,a})$ is unity.

1.1.4.2 Irreversible systems

When electron transfer kinetics is slower than mass transport of an electroactive species towards electrode surface, such electrochemical system

is said to be irreversible. In this case, there is no equilibrium between concentration of oxidized and reduced species. Here, peak currents and peak potential are dependent of scan rate. In irreversible process, peak potential increases with scan rate. Peak potential of an irreversible process can be expressed as,

$$E_p = E^0 - \frac{RT}{\alpha F}[0.780 + ln(\frac{D_0^{1/2}}{k_0}) + ln(\frac{\alpha F v}{RT})^{1/2}]$$

where 'α' is transfer coefficient

According to Randles – Sevcik equation, peak current for totally irreversible process can be related to scan rate by,

$$i_p = (2.99 \times 10^5)\alpha^{1/2} A C_o D^{1/2} v^{1/2}$$

For irreversible reaction, value of α is nearly equal to 0.50.

1.1.5 Need and advantages of chemically modified electrodes

Electrochemical analyses using bare working electrodes will face several difficulties such as surface fouling, poor sensitivity, higher over potential and slow electron transfer kinetics, which confines its practical efficacy.[13] To solve these problems, electrochemists introduced concept of chemically modified electrodes (CME). Modification of electrode surface using intentionally immobilized foreign molecules has opened up innovative prospects in sensing technology. In 1975, Murray and co-workers introduced the idea of immobilization of foreign species on surface of electrodes.[14]

According to IUPAC, CME is *an electrode made of a conducting or semiconducting material that is coated with a selected monomolecular, multi molecular, ionic or polymeric film of a chemical modifier and that by means of faradaic (charge-transfer) reactions or interfacial potential differences (no net charge transfer) exhibits chemical, electrochemical, and/or optical properties of the film.*[15]

Modification of electrode surface offers more control over its surface characteristics. Compared to bare electrodes, CMEs significantly enhance sensitivity and selectivity of the system. In addition to these advantages, it speeds up rate of electron transfer of analyte and also decreases its over potential. Based on these advantages, CME have been widely used in various fields such as sensing, electrochromic display devices, electro-catalysis and fuel cells. Several methodologies adopted for fabrication of CMEs includes adsorption, electro deposition and electro polymerization of various functionalities on electrode surface.

By utilising the exceptional characteristics, present investigation have been focussed to develop electrochemical sensors based on nanomaterials modified glassy carbon electrodes.

1.1.5.1 Nanomaterials as efficient electrode modifiers

Materials or matrices having at least one dimension ranging between 1 nm and 100 nm are known as nanomaterials or nano-matrices. With difference in size, nanomaterials exhibit distinctive physical and chemical features leading to innovative sensor characteristics. Compared to bulk materials, nanoparticles (NPs) are chemically more active owing to their high surface energy. During reduction in size of structure, surface to volume

ratio increases substantially with variations in surface phenomena than that of the bulk. Upon modification with NPs, overpotential of electrochemical reaction can be decreased together with enhancement in peak current. In some cases, irreversible reactions of analytes on bare electrode become reversible after modification with NPs.[16]

Even if NPs show different roles in diverse electrochemical sensing systems; basic purposes of modification with NPs can be categorized as enhancement of electron transfer or as platforms for immobilization of other species as reactants.

1.1.5.1.1 Enhancement of electron transfer

Conductive properties of NPs can be used for increasing the electron transfer between analyte and electrodes, performing as "mediators" or "electrical wires". Recently, non-metal NPs, like oxide NPs or semiconductor NPs were also used to enhance electron transfer between electrodes and enzymes. Enhanced electron transfer rate in presence of NPs was not only due to conductivity, but also due to specific arrangement of NPs.[17] An ordered arrangement of NPs can be achieved using nanotechnology, thereby enhancing electron transfer properties of sensors.

1.1.5.1.2 Immobilization of foreign species on electrode surface

Owing to large surface area and high surface free energy, NPs shows greater tendency to adsorb foreign species like biomolecules and play an important role in biosensor production. Due to equivalent dimensions, biomolecules retain the natural structure/conformation and functionality while conjugated to NPs.

Functionalization of NPs using foreign species can be achieved through three main mechanisms:

(i) Electrostatic adsorption

(ii) Chemisorption of thiol derivatives

(iii) Specific affinity interactions

Electrostatic adsorption: Charged biomolecules or chemical species can be adsorbed on surface of NPs having opposite charge with that of the compound to be adsorbed.[18,19] This approach permits the preparation of well-designed films on NPs with enzyme molecules having high density.

Chemisorption of thiol derivatives: Chemisorption of thiols on noble NPs originates by binding of -SH groups to the surface of Au molecule. Among the NPs used for immobilization of thiols, AuNPs are most commonly used because of the inert character of gold (it does not form stable oxide films) and it has a strong specific interaction with sulfur.[20,21] It is understood that chemisorption of thiol on gold surface lose hydrogen from –SH group as H_2 molecule,[22] resulting in a strong covalent Au-S bond formation.[20,22]

Specific affinity interactions: To study the presence or quantity of a species like antigens in a sample, specific interactions between antigen and corresponding antibody can be utilized. For this purpose, NPs functionalized with antibodies provides spots for binding of antigens and corresponding signal changes are studied.[23]

1.1.5.1.3 Nanoparticles acting as a reactant

As discussed earlier, during reduction in size of particles, some species exhibit special chemical properties which are not shown by the bulk material. For example, compared to bulk MnO_2, its nano form can easily react with H_2O_2.[16] These properties can be efficiently utilized for studying the sensing characteristics.

By taking advantage of NPs, new sensor devices can be constructed for various analytes. Increased sensitivity of the system results in lower limits of detection, so very low volume of samples is needed. Properties of NPs can be controlled by their preparation conditions.[2] Both physical and chemical methods are usually used for preparation of NPs for various applications. For electrochemical sensing, electrodeposition is a suitable method because it can form reproducible - uniform films at each time of analysis. Electro-polymerization on NPs modified electrode can be done to enhance properties of both films, because usually it forms a composite structure.

1.1.6 A brief literature review of electrochemical sensors based on nanomaterials

As in the case of a variety of fields, sensor research has also attracted by the fascinating properties of nanomaterials. A number of electrochemical sensors based on nanomaterials are reported in literature. A few of them are described below.

A Simultaneous voltammetric determination of catechol, resorcinol and hydroquinone was reported by Yang et al. using poly-

BPB/MWNT/GCE.[24] CV was used to study the electrochemical behavior of analytes. Linear range and limit of detection were reported to be 1.0×10^{-4} to 1.0×10^{-6} M and 3.0×10^{-7} M respectively. Excellent reproducibility and stability was obtained for modified electrode. Water sample from a photo studio was used for application study.

Using modified GCE, two electrochemical sensors were developed by Jos et al. for the determination of tinidazole (TIN).[25] GCE was modified with L-Cys and L-Cys/AuNPs and surface morphology studies was done using SEM. Linear range was obtained from 1.0×10^{-5} to 7.0×10^{-7} M. Developed sensors exhibited advantages such as nano molar detection limit and good stability. Incorporation of AuNPs showed more catalytic activity towards the reduction of TIN, thereby a decrease in overpotential from –0.581 to -0.487 V was observed. Application studies were carried out in pharmaceutical formulations and in spiked urine samples.

Simultaneous determination of dopamine (DA), uric acid (UA) and ascorbic acid (AA) was reported by Zhang et al. using poly(glycine)/carbon nanohorns composite modified GCE (CNHs/PGLY/GCE).[26] Modified electrode was characterized using various electrochemical techniques such as CV, DPV and EIS. Modified electrode exhibited good linear range and detection limit for all three analytes. Linear range obtained for UA are 3.5×10^{-4} - 2.0×10^{-6} M, for AA 4.5×10^{-4} - 3.0×10^{-6} M and for DA 2.8×10^{-4} - 1.0×10^{-6} M. Detection limit of UA, AA and DA were calculated to be 1.8×10^{-7}, 3.4×10^{-7} and 3.0×10^{-8} M, respectively. Successful application of developed sensor in analysis of human urine samples was reported for all three analytes.

Vikraman et al. reported a differential pulse voltammetric method for quantification of synthetic phenolic antioxidant, propyl gallate (PG).[27] Here, multiwalled carbon nanotube (MWCNT)-modified gold electrode (GE) was fabricated and used for the determination of PG. 0.1 M acetate buffer of pH 7 was chosen as the supporting electrolyte for the study. Compared to bare electrode, modified electrode exhibited an excellent catalytic activity and stability towards oxidation of PG. Various analytical parameters such as interference caused by coexisting species, pH of the supporting electrolyte and effect of scan rate were studied. The developed method allowed a determination of PG as low as 6.3×10^{-7} M. Analysis of PG concentration in commercial vegetable oil samples were also carried out.

By taking the advantages of polymer nanocomposite of gold nanoparticle (AuNP) and poly(p-aminobenzenesulfonic acid) (poly(*p*-ABSA)), determination of PG was carried out by Cyriac et al..[28] Compared to bare glassy carbon electrode (GCE), AuNP/poly(*p*-ABSA)/GCE showed a decrease in oxidation potential and a large increase in peak current. Various analytical parameters such as number of cycles of electro deposition, thickness of polymer film, effect of pH and scan rate were studied and optimized. Calibration curve was obtained in the concentration range of 1.0×10^{-4} to 9.0×10^{-6} M and limit of detection was 1.9×10^{-7} M. Application studies were carried out in edible vegetable oils and recoveries between 98.9 and 101.3% were obtained.

A cost-effective sensing strategy for the quantification of glucose was reported by Guo et al. using the electrocatalytic activity of nickel nanoparticles (NiNPs).[29] Using SEM analysis, morphology of NiNPs

modified GCE was studied and a porous structure was proposed. Here a non-enzymatic oxidation of glucose was reported using the modified electrode by amperometry. A linear concentration range of 1.1×10^{-3} - 5×10^{-6} M was obtained with a detection limit of 1.0×10^{-6} M. Interference study was carried out and it reveals ascorbic acid, dopamine and uric acid, do not interfere the quantification. Determination of glucose in serum samples was also carried out using the developed method.

Dai and coworkers explored the electro catalytic activity of polytetraphenylporphyrin, polypyrrole, and graphene oxide composite for the determination of uric acid (UA).[30] Nanocomposite of PPy/GO was synthesized by in-situ chemical oxidation and polymerization and was characterized using scanning electron microscopy, Raman spectroscopy and FTIR. Composite modified electrode was used for differential pulse voltammetric analysis and found that oxidation peak current varies with concentration of UA in the range from 2.0×10^{-4} to 5.0×10^{-6} M and lower detection limit was found to be 1.1×10^{-6} M. Authors also found out that, modified electrode showed excellent selectivity for UA even in the presence of ascorbic acid and dopamine.

Mukdasai et al. developed a simple and sensitive electrochemical sensor for ascorbic acid (AA) and uric acid (UA).[31] Here carbon paste electrode (CPE) was modified with porous graphitized carbon monolith (CM) and palladium nanoparticles (PdNPs). Among the bare and modified CPE, PdNPs/CM/CPE showed better response (a decrease in potential and enhancement in peak current) for the oxidation. Detection limits for the determination of AA and UA using the developed sensor was found to be

5.3×10^{-7} M and 6.6×10^{-7} M respectively. Further, developed sensor was applied for the determination of AA and UA in human serum sample.

Individual and simultaneous determination of dopamine and uric acid using CdTe quantum dots-modified carbon paste electrode was reported by Beitollahi et al.[32] In SWV, the determination was found to be sensitive for dopamine and uric acid. Linear ranges for dopamine and uric acid was 7.5×10^{-8} to 6.0×10^{-4} M and 7.5×10^{-6} to 1.4×10^{-3} M respectively. Using these responses, quantification of dopamine and uric acid in real samples was also achieved.

1.2 Optical sensors

Optical sensors measure the changes in optical properties such as colour, wavelength or intensity (absorbed or emitted) of light. Based on the read out, optical sensors are mainly divided in to three broad categories such as Phosphorimetry, Fluorimetry and Colorimetry.

1.2.1 Interaction of light with matter

Interaction of light with matter is an interesting field in scientific research since it provides information regarding characteristic features of different materials, which can be used for design of optical devices for various applications. Upon irradiation, electromagnetic field of light interacts with the localized electromagnetic field of atoms in matter.[33] This may result in a change in characteristics of emitted light from matter. This characteristic interaction is generally governed by field strength and wavelength of the light and also by nature of matter itself. Some of the

phenomena resulting from such type of interactions include reflection, transmission, absorption and emission.

1.2.1.1 Reflection

Reflection is a phenomenon of light resulting when light travelled between two mediums having a difference in refractive index. In fact, a definite portion of light is reflected from interface, and rest is refracted through the medium. Generally two types of reflections are observed, ie., specular and diffuse reflection. In specular reflection, the reflecting surface is very smooth and this allows 100% reflection of incident light. Diffuse reflection occurs when unidirectional light is deflected into many directions and this forms the principal mechanism for physical observation.

1.2.1.2 Transmission

Transmission is the process of passage of electromagnetic radiation through a medium and it is of two types viz., direct (regular) transmission and diffuse transmission. When no diffusion of light occurs, transmission of a unidirectional light beam results in a unidirectional beam according to the laws of geometrical optics. Reflection, transmission and scattering leave the frequency of the radiation unchanged. Exception is seen in Doppler Effect, where a change in frequency occurs when the reflecting material or surface is in motion.

1.2.1.3 Absorption

Transference of radiant energy from radiation to matter by interaction is called absorption. The term absorbance denotes capacity of a

medium to absorb light energy and is defined as ratio between absorbed and incident radiant powers.

Lambert's law proposes that absorbance of a material is directly proportional to thickness or path length of the material. Later, Beer proposed another law, which states that; absorbance is directly proportional to concentration of sample. During further derivations, these two laws were combined, which states that absorbance is correlated to path length and concentration of material.

Mathematically, absorbance (A) is related to optical depth (l) and concentration (c) as

$$A = \varepsilon c l$$, where ε is the molar absorptivity.

Beer–Lambert law is commonly applied to analysis of chemicals and used in recognizing attenuation for photons, neutrons or rarefied gases.

Absorption and reflection of light are strongly influenced by the surface properties of material such as particle size, roughness, charge and corrosive wear.[33] Thus any change in particle size can induce a change in the interaction between particle and light[34] which ultimately results in the variation in absorption or reflection of light. This phenomenon is widely used in developing nanomaterial based optical sensors.

1.2.1.4 Phenomena of luminescence

If radiative absorption takes place, there is possibility of formation of higher energy levels and since the higher energy state is less stable, it returns to ground state by losing its energy via radiative or non-radiative

transition. Emission of light which occurs from electronically excited states of substances is known as Luminescence, which is divided into two broad categories—fluorescence and phosphorescence, based on the nature of excited state.[35]

1.2.1.4.1 Jablonski diagram

Jablonski diagram illustrates the electronic states in a molecule and possible transitions between them. In this diagram, electronic states are arranged vertically in accordance with energy levels and grouped horizontally in accordance with spin multiplicity. The vibrational ground states of each electronic state are indicated with thick lines and higher vibrational states with thinner lines.[36] Arrows are used to show the transitions between the states. Non-radiative transitions are depicted by wavy arrows and radiative transitions by straight arrows.

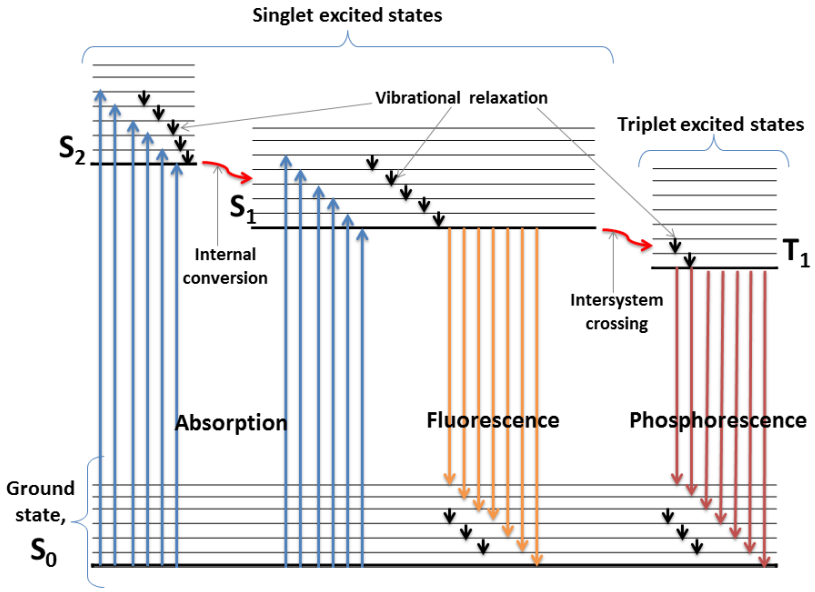

Figure 1.4: Jablonski diagram showing various transitions from various electronic states.

Upon irradiation, the electrons from ground state (S_0) get excited to higher energy state (S_n). During its relaxation to ground state, the absorbed energy will be released to the environment by internal conversion or intersystem crossing.

Internal conversion is the non-radiative transition from higher excited state (S_n) to lower vibrational states of same spin multiplicity ($S_{n-1, n-2 \ldots}$). This process takes place in a time period of 10^{-12} s or less and is identical to vibrational relaxation, where energy is transferred through collisions. Emission of photons during transition from S_1 to S_0 state is termed fluorescence and is a spin allowed process. Internal conversion always occurs prior to fluorescence.[36]

Transition from excited singlet state (S_1) to first excited triplet state (T_1) is possible in certain cases and is termed as intersystem crossing. Compared to internal conversion, intersystem crossing is a slow process, it usually occurs at 10^{-8} s after absorption of light. This intersystem crossing result in a phenomenon called phosphorescence. Phosphorescence occurs when there is transition of the electron from T_1 to S_0 state, accompanied by emission of photons. Compared to fluorescence, phosphorescence is a spin forbidden process and hence it is less intense.

1.2.2 Optical properties of nanomaterials

As discussed earlier, optical properties are size dependent. Properties shown by various nanomaterials upon interaction of light are explained below.

1.2.2.1 Surface plasmon resonance

Plasmonic properties of nanoparticles have gained wide interest during the past decade, owing to their suitability for practical applications in sensing and prototypes for nano-photonic devices. Localized surface plasmon resonance (LSPR), occurs by collective electronic oscillations of nanoparticles upon interaction with electromagnetic radiation, leading to selective photon absorption and radiation, as well as an enhanced electromagnetic field around nanoparticles (Figure 1.5). This selective absorption of radiation gives rise to bright colors, leading to their use in colorimetric sensors. Enhancement of electromagnetic field of nanomaterials upon interaction with light is widely used for surface-enhanced Raman spectroscopy (SERS). LSPR of nanomaterials depends on material's nature, shape, size and environment. Small changes in the surface properties of nanomaterial will results in variations in LSPR absorption which could be easily identified.[37] Thus, LSPR of nanomaterials is used in a large number of sensing methods.

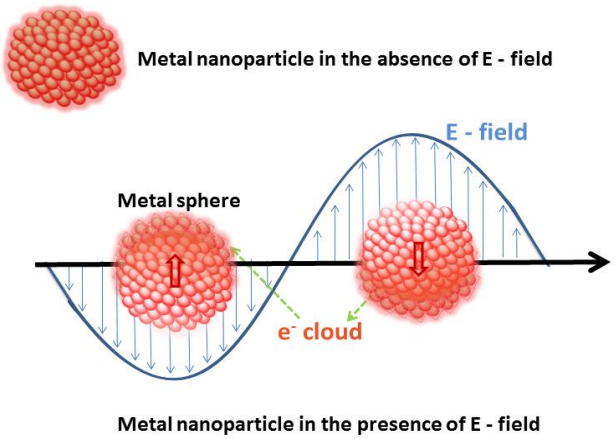

Figure 1.5: Surface plasmon resonance of nanoparticle upon interaction of electromagnetic radiation.

1.2.2.2 Quantum confinement

Phenomenon of change in electronic and optical properties of material samples by decrease in size (typically 10 nanometers or less) is known as quantum confinement. As the size of nanostructure decreases, their bandgap increases. As a result of these geometrical constraints, electrons and holes being squeezed into a dimension which approaches a critical quantum measurement, called exciton Bohr radius. Figure 1.6 shows the photographs of fluorescence produced by cadmium telluride quantum dots (CdTe QDs) having various particle sizes synthesized by hydrothermal method.

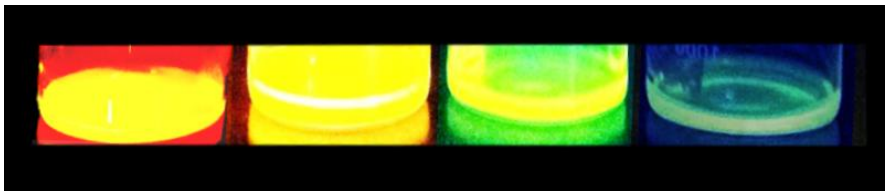

Figure 1.6: Photographs of fluorescence exhibited by CdTe QDs having various particle sizes kept under UV light.

Effect of quantum confinement in distribution of energy levels of CdTe QDs is illustrated in Figure 1.7. Evaluation of Figure 1.7 clearly shows that, upon reduction in size of QD's, an increase in band gap of energy level results.

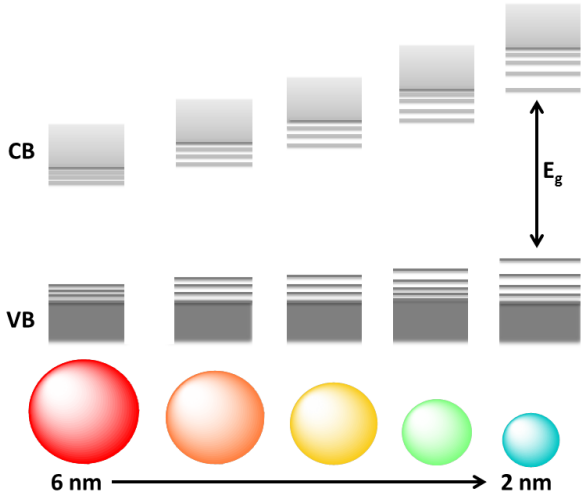

Figure 1.7: Schematic illustration of the quantum confinement effects.

1.2.2.3 Photo stability

Major parameters to be considered while analyzing nanomaterials include morphology (size and shape) of particles and their stability in solution (colloid). Control over size and shape is of paramount importance since they determine the properties of the nanoparticles. Further, stability of the nanomaterials can be achieved by proper addition of a stabilizing or capping agent. For example, citrate-capped nanoparticles are negatively charged, which can attract positively charged particles/ions from solution, resulting in electrical double layer formation, which in turn creates repulsive forces between particles preventing agglomeration.[38] Sometimes, colloidal stability is lost by intense radiation, usually known as photo bleaching. Due to this, nanoparticle's ability to produce color/luminescence is reduced. During illumination, brakeage of stabilizing group is facilitated, resulting in alteration in stability/emission property.

1.2.3 Fluorescence sensors

In fluorescence sensing, variation in emission properties of a fluorophore (fluorescent molecule) is studied as a function of analyte concentration. Since emission is more sensitive property than absorption, fluorescence sensing is used for analysis of a wide variety of target species.

1.2.3.1 Characteristics of fluorescence emission

Loss of vibrational energy occurs during relaxation of excited electrons in to their ground state. This loss of energy results in a shift (longer wavelength) in emission spectrum compared to excitation spectrum, which is known as Stokes shift. A wide separation of excitation and emission spectra was observed in the case of greater stokes shift.

1.2.3.2 Lifetime and quantum yield

Fluorescence lifetime is a characteristic feature of fluorophore, depicting the time spends by a fluorophore at the excited state before returning to ground state by emitting a photon.[39] Lifetimes of fluorophores can range from hundreds of nanoseconds to picoseconds. Fluorescence lifetime analysis has been extensively used during characterization of fluorescence species and proteins.

Fluorescence quantum yield is an important characteristic feature of a fluorophore, which is a measure of its efficiency to emit the absorbed photons. Quantum yield is the ratio of number of quanta (photon) emitted to that of absorbed.

$$\varphi = \frac{\textbf{Number of quanta emitted}}{\textbf{Number of quanta absorbed}}$$

Value of quantum yield ranges typically between zero to one. Generally, it is determined by comparing absorbance and fluorescence intensity of sample with that of a reference material, whose **φ** value is known. The following equation is used for this purpose,

$$\boldsymbol{\varphi_S} = \boldsymbol{\varphi_R} \times \frac{\mu_S}{\mu_R} \times \left(\frac{\boldsymbol{\eta_S}}{\boldsymbol{\eta_R}}\right)^2$$

Here φ_S is quantum yield of sample (fluorescent probe) and φ_R is quantum yield of reference material. μ_S and μ_R represents slopes of plot of integral fluorescence intensity vs absorbance of sample and reference respectively. The η_S and η_R denotes refractive indices of solutions of sample and reference.

1.2.3.3 Turn off and turn on fluorescence sensors

Fluorescence sensors are classifieds into two, based on changes in intensity of fluorophores. They are turn-off and turn-on sensors. In turn-off fluorescence sensor, intensity of emission is reduced after interaction with analyte. But in turn-on fluorescent sensor, intensity of emission increases or fluorescence is produced on interaction with analyte. In nutshell, turn-off sensors work in accordance with principle of fluorescence quenching (decrease in intensity) and turn-on sensor works with principle of enhancement (increase in intensity).

1.2.3.3.1 Mechanism of fluorescence quenching

Mechanisms of fluorescence quenching have been a subject of much scientific debate. Static and dynamic quenching are the two basic types of

quenching processes usually studied. Both types require an interaction between fluorophore and quencher (analyte).

Static quenching: This type of quenching arises due to ground state interactions between fluorophore and analyte. Here, a non-fluorescent complex may be formed between fluorophore and quencher.[35] Since formation of this complex is a ground state process, it does not depend on population of excited state. Hence no change in fluorescence lifetime of fluorophore can be observed after interaction with analyte.[35]

Dynamic quenching: It is also known as collisional quenching. In this case, excited state interaction between fluorophore and analyte takes place.[35] Excited fluorophore returns to ground state without emission of a photon upon collision with analyte. Since interaction of fluorophore and quencher occurs at excited state, significant changes in fluorescence lifetime can be observed.[35]

Inner filter effect (IFE): This effect can be considered as another type of quenching arises during fluorescence studies. Sometimes it occurs along with static and/or dynamic quenching. In such cases, inner filter corrections are needed for observing the effect of the former alone. Radiative energy transfer arises when absorption spectrum of absorber (here analyte) overlaps with excitation and/or emission spectrum of fluorophore in IFE, converting the absorption into corresponding fluorescence signal.[40] If only IFE is operative, sensing can be done using this mechanism. Recently several analytical methods based on IFE have been reported.

Analysis of absorption spectrum of fluorescent probes before and after addition of analyte, provides information regarding the type of quenching process. Because, only static quenching shows some perturbation in absorption spectrum due to complex formation, it can be easily identified from others. Lifetime analysis also reveals dynamic quenching. A significant property of both types of quenching process is that they show characteristic changes with variations in temperature. If temperature is increased during analysis, dynamic quenching will also increases, but static quenching will be decreased. This occurs due to increase in diffusion or due to increased solubility/decreased stability of formed complex in dynamic and static quenching respectively. IFE has no effect on changes in temperature and it does not change the fluorescence lifetime of a fluorophore.

1.2.3.3.2 Reasons for fluorescence enhancement

Although most of the fluorescence sensors function on the mechanism of fluorescence quenching, a few sensors based on mechanism of fluorescence enhancement are also reported. In most of these cases, substitution of surface groups or replacement of special reagent via analyte binding is observed.

Binding induced: A major category of fluorescence enhancement is based on binding of analytes with either surface or surface groups of fluorophores and basis of such analysis is "probe environment". Here conformational changes are induced in the probe environment through binding of analytes. Generally two types of approaches are used in this category, one is direct binding of analyte via covalent bonding to surface or

surface groups of fluorophores and another one is based on turn-off-on approach. In the former case, analytes are selectively/specifically bind to the surface through 'Lewis' - basic groups, thereby reducing the surface traps (surface passivation) and they increase availability of electrons for excitation, leading to fluorescence enhancement.[41] In the latter case, a quencher is added to fluorescence system, which quenches the fluorescence intensity. Further, the analyte of interest is added, which separates the quencher from fluorophore by binding with quencher, leading to fluorescence enhancement. Thus, in turn-off-on case, reappearance of fluorescence takes place resulting in selective binding of analyte with quencher and not with fluorophore.

Metal induced: metal enhanced fluorescence (MEF) or plasmon enhanced fluorescence is a characteristic feature shown by metal nanoparticles (NPs) having surface plasmon absorption. This approach is explained on the basis of Mie theory. Principle behind MEF is ascribed to combination effect of increase in excitation rate of fluorophores and increase in quantum yield of metal nanoparticle-fluorophores system. MEF is dependent on parameters such as distance between nanoparticle and fluorophores, spectral overlap of LSPR band of metal nanoparticle with emission/excitation wavelength of fluorophore, structure and morphology of NPs and properties of fluorophores (quantum yield, lifetime). Among these parameters, distance between plasmonic NPs and fluorophores is more important. Studies have shown that as maximum efficiency of MEF is obtained only at a critical distance range of 5 to10 nm.[42] Silver NPs based fluorescence enhancement is well studied.[43] Further, sensors based on CuNPs are also reported in recent years.[44]

1.2.3.4 Fluorescence probes

A wide variety of compounds are used as fluorescent materials for sensor development. However, most fluorescent probes based on organic dyes have narrow excitation spectra, poor photo-stability and broad emission bands with red tailing, thus limiting its wide applications.[45] Therefore, nanomaterials based probes are widely utilized, since it overcome above limitations. Nanomaterials based fluorophores includes dye-doped NPs, NPs made of organic polymers, silica-based NPs, quantum dots and metal nanoclusters. Quantum dots and metal nanoclusters based fluorophores were used during present studies.

1.2.3.4.1 Quantum dots

Generally quantum dots (QDs) are nanocrystals having semiconductor properties. It works via quantum confinement effect and excitons are confined in all three special dimensions. Particle diameter of QDs ranges from 2 to 10 nm. Like gold nanoparticles, QDs are also found in antique materials, indicating its use in early 20^{th} century. Louis E. Brus discovered the 'special particles' as colloidal suspension in 1982 and the term 'quantum dot' was proposed by Mark A. Reed. Due to its exceptional size related properties, QDs have found wide applications in diverse scientific fields. Commonly used QDs are cadmium based materials such as cadmium selenide, cadmium telluride and cadmium sulphide. Synthesis and application studies of carbon based quantum dots is a growing field of scientific research.

1.2.3.4.1.1 Cadmium sulphide quantum dots

Among the semiconductor family of group II–VI (as per Mendaleeve's periodic table), cadmium sulphide (CdS) QDs are widely used because of their special characteristics such as size dependent optical properties, availability of discrete energy levels, tunable bandgap, well-developed and simple preparation procedures and good stability.[46] On account of CdS, the band gap can be tuned in vicinity of 4.5 eV to 2.5 eV as size is changed from molecular to the nanocrystal form and correspondingly its radiative life time ranges from tens of picosecond (10^{-12} s) to a few nanoseconds (10^{-9} s).[47] In this manner, energy of exciton is estimated to endure a blue shift if size of particle falls below 6 nm.[48]

1.2.3.4.1.2 Carbon dots

Carbon quantum dots or carbon dots (CDs) are a special class of carbon nanomaterials, with sizes lower than 10 nm. They are generally pseudo-spherical in shape consisting of sp^2 or sp^3 carbon, oxygen/nitrogen based groups, post-modified chemical groups and they possess amorphous to nano-crystalline states.[49]

In 2004, CDs were discovered accidentally during synthesis of single walled carbon nanotubes by arc-discharge method.[50] Ever since, unique properties and simplicity in synthesis have led to innovative synthesis methods of CDs, employing different types of precursors.

CDs possess special properties such as high (aqueous) solubility, chemical inertness and high resistance to photo bleaching, in comparison with traditional semiconductor quantum dots and organic dyes. In addition to these advantages, good biocompatibility and low toxicity of CDs make

them suitable for bio-imaging, bio-sensing and drug delivery.[51] For fluorescence applications, size and surface groups of CDs must be carefully modified.

Surface passivation is usually needed for CDs having higher quantum yield and stability. In addition to stability, presence of hydroxyl, carboxyl or amine groups in passivating agents can impart higher solubility in water. Even though, mechanisms behind fluorescence emission of CDs attract much debate among researchers; suggested mechanisms are based on quantum effect or transitions involving conjugated π-domains or surface defects.

1.2.3.4.2 Nanoclusters

Metal nanoclusters, comprising of a few to about 100 atoms (size typically less than 2 nm)[52] exhibit unique electronic, optical and chemical properties compared to their larger counterparts.[53] Nanoclusters often behave like molecules, without plasmonic behavior and are known as bridging link between atoms and nanoparticles.[54] Commonly used nanoclusters are based on expensive noble metals viz. gold and silver. Although, copper nanoclusters (CuNCs) are comparatively cheap, their use in the field of sensing is not much explored.[55]

1.2.3.4.2.1 Copper nanoclusters

Because of high conductivity, cost effectiveness and molecular properties similar to gold and silver, copper is widely used for diverse industrial applications. However, studies relating nanostructures of copper have received less scientific attention due to their susceptibility to oxidation.

Copper nanoclusters (CuNCs) are nanoparticles containing few to hundreds of Cu atoms surrounded by capping agents. Usually CuNCs posess size below 2 nm. Due to their extreme small size; molecule-like properties are shown by CuNCs compared to bulk metals or even nanoparticles (Figure 1.8). This includes HOMO–LUMO transitions, magnetism and photoluminescence (PL). Among these, phenomenon of PL makes CuNCs more attractive than conventional fluorophores or other metal nanoclusters. Also, CuNCs possess other advantages including cost effectiveness, non-toxicity, large Stoke shifts and high photo stability.[56]

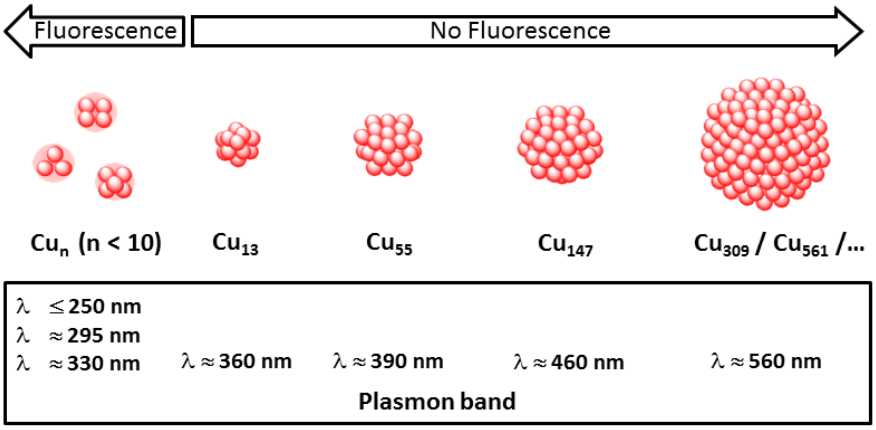

Figure 1.8: Chronological illustration of particles of copper with size and their optical properties.

Unlike large sized Cu nanoparticles, CuNCs exhibit a discrete electronic structure, so the characteristic absorption peak corresponding to surface plasmonic resonance of CuNPs in the range of 500 – 600 nm is not observed. Instead, peaks attributed to inter-band electronic transitions are often observed in the UV wavelength range.[57,58]

1.2.3.5 A brief literature review on fluorescent sensors based on nanomaterials

Several fluorescent sensing strategies are reported for the quantification of wide variety of compounds. Among them, nanomaterials based sensing systems stands out due to excellent limit of detection and wide linear range. Some of the reported methods are detailed as follows.

Wang and coworkers developed a fluorescence sensing strategy for melamine using thioglycolic acid capped CdS QDs.[59] This is a type of turn on sensor and fluorescence enhancement was achieved by the passivation of amine groups. Developed sensor showed a linear range between 5.0×10^{-5} M to 2.0×10^{-9} M with a detection limit of 1.0×10^{-9} M. Application of developed method for quantification of melamine in raw milk was done and satisfactory results were obtained.

Sensing of adenosine-5'-triphosphate (ATP) based on fluorescence enhancement of cysteamine capped CdS QDs was reported by Tedsana et al.[60] Developed sensor showed excellent selectivity towards ATP over other phosphate metabolites and anions. Linear working range was observed from 8.0×10^{-5} M – 2.0×10^{-5} M of ATP. The reported method allows the detection of ATP as low as 1.7×10^{-5} M. Further, quantification of ATP was carried out from urine samples and satisfactory results were obtained.

Liu et al. reported a fluorescent sensor for sulfadiazine based on quenching of fluorescence intensity of CdS QDs protected by thioglycolic acid.[61] Here QDs were synthesized by microwave assisted method. Electrostatic interaction of sulfadiazine and QDs allows the determination of

sulfadiazine in the linear range of 2.3×10^{-3} to 1.2×10^{-5} M with a detection limit of 8.0×10^{-6} M. Application of developed sensor was done in injection samples of sulfadiazine and results obtained were satisfactory.

A green synthesis method for CDs production and its application as a sensor for tartrazine has been reported by Xu et al.[62] Reported synthesis was based on hydrothermal route using aloe as carbon source. Synthesized CDs were characterized using various analytical techniques such as TEM, AFM, UV-vis absorption spectroscopy, fluorescence spectroscopy and FTIR. Synthetic food colorant-tartrazine produced a strong fluorescence quenching of the synthesized CDs. Using this response, a fluorescent sensor was fabricated having a linear range of 3.2×10^{-5} to 2.5×10^{-7} M. This sensor was successfully applied for the quantification of tartrazine in commercially available food samples.

Yuan et al. proposed a method for the synthesis of CDs from N-(2-Hydroxyethyl) ethylenediamine triacetic acid by heating HEDTA in air.[63] Developed probe was also used for the fluorescence sensing of sunset yellow in soft drink samples. Linear range for the determination was found to be 8.0×10^{-7} to 3.0×10^{-7}M with a limit of detection of 7.9×10^{-8} M. Also application on soft drinks samples reveals the usefulness of the developed sensor for food analysis.

A ratiometric fluorescent sensor for Al (III) ions using CDs was reported by Zou et al.[64] Using the coordinating capacity of Quercetin and its complex with Al (III) to surface of CDs sensing was achieved. Mechanism behind the sensing was proposed to be fluorescence resonance energy

transfer from CDs to complex of Al (III). The developed method allowed detection as low as 5.6×10^{-7} M of Al (III).

Das and coworkers developed an efficient protocol for the synthesis of luminescent CuNCs using glutathione GSH as a stabilizing as well as reducing agent.[65] Characterization was done using MALDI-TOF mass spectrometry and TEM analysis. Using the synthesized CuNCs, metal ion sensing was carried out and studies revealed that, the probe selectively responds to Fe (III) ions at nanomolar concentration. Further, developed CuNCs was also used for bioimaging purpose.

A label-free determination strategy for nitrofurantoin (NFT) using CuNCs stabilized with adenosine was reported by Wang et al.[66] NFT induced quenching of photoluminescence intensity of CuNCs and using this response, sensing strategy was developed. Mechanism behind the sensing was attributed to the inner filter effect. The proposed sensor showed a linear range of 4.0×10^{-6} to 5.0×10^{-8} M. Limit of detection of the method was found to be 3.0×10^{-9} M. Developed sensor was effectively applied for determination of NFT in lake water.

Ghosh et al. reported a new synthetic route for fluorescent CuNCs via reduction of Cu (II) by hydrazine in presence of lysozyme.[67] Number of copper atoms in the cluster was studied using mass spectrometric analyses and it revealed that, 2 to 9 numbers are present in CuNCs. Also, formation of cluster was established using TEM and it showed the formation of particles having average diameter of 2.3 nm. Imaging of cancer cells was achieved successfully using the developed CuNCs.

1.2.4 Colorimetric sensors

Colorimetric sensing is often carried out using indicators that changes its colour upon interaction with analyte. Though this change is visibly observed, a spectrophotometer is usually used for accurate quantification.[68] Frequently used indicator in colorimetry includes organic / inorganic compounds, inorganic complexes and nanomaterials.

1.2.4.1 Principle of spectrophotometry

Basic principle governing spectrophotometry is Beer – Lambert law. This method can be carried out quickly and conveniently when target species under study is colored or when it has absorption in UV range.

From spectrophotometric analysis, qualitative as well as quantitative information can be obtained about an analyte by analyzing its absorption spectra. Study of absorption spectra by a compound at different wavelengths provides information regarding its structure. Quantification is achieved directly by relating the absorbance to concentration, as expressed by Beer–Lambert law. Almost all of the organic compounds having biological significance show absorption in UV or visible range of spectrum. Thus, a number of biologically relevant compounds can be determined semi-quantitatively with the use of UV-visible spectrophotometer.

1.2.4.2 Reason for color change

In colorimetry, concentration of analyte is indirectly measured by observing variations in optical properties of indicator. If indicators are nanomaterials (in solution phase), alterations in colloidal stability is often studied. Inter-particle distance is one of the major factors affecting surface

plasmon properties of a metal nanoparticle. Under the influence of analytes, nanoparticles approach each other, leading to interactions between their electric fields. Due to this, inter-particle plasmon coupling results with a shift in LSPR and color change is observed.[69,70]

The above discussed alterations may be due to the analyte induced surface effects such as detachment of stabilizing / capping agent, binding of analyte to surface or to stabilizing groups. Sometimes analytes functions as linkers between particles, resulting in aggregation of nanoparticles. Rarely, analytes remove the capping agents from surface of nanoparticles through bond formation and this will lead to reduction in their stability resulting in aggregation. There are several examples known for these types of color changes via aggregation. Also, few examples are available for analyte induced breakdown of aggregated nanoparticles. Here, analytes are acting as stabilizing agents, thereby increasing colloidal stability of aggregated probe particles. Above all cases, together with spectral changes, a color change of probe solution is observed, enabling visual detection. Thus, research on nanoparticles with different stabilizing / capping agents offers great potential for specific applications.

1.2.4.3 Colorimetric probes

Owing to their exceptional optical properties, coinage metal (copper, silver and gold) nanoparticles have been extensively used for colorimetric sensor development of various analytes. By changing the composition of nanoparticles and/or capping agents, selectivity of probe can be altered. Au, Cu and Ag are the metals which show bright and sharp surface plasmon

absorbance.[71] In the present investigations, main focus have been given to development of colorimetric sensors using gold and copper nanoparticles.

1.2.4.3.1 Gold nanoparticles

For development of colorimetric assays, use of gold nanoparticles (AuNPs) have been studied broadly amid other coinage metal nanoparticles. In most cases, colloidal solution of AuNPs were synthesized by reduction of Au(III) ions to Au(0) using sodium citrate as reducing agent. In this case citrate ions were also acting as capping agents. Further, functionalization of Citrate-capped AuNPs was also carry out. Stability of gold-sulphur linkage enables functionalization/capping with thiol compounds. A few sensors are developed recently based on the above linkages.

AuNPs (diameter of 10–50 nm) solution exhibits ruby red colour in well-dispersed state, whereas aggregation of smaller AuNPs or larger AuNPs (diameter > 50 nm) show purple or blue colour. So, change in colour of solution together with shift in band in the visible region of electromagnetic spectrum can be related to inter particle plasmon coupling.[72] Red shift in absorption maximum of AuNPs, caused by aggregation has effectively been exploited in various assays as a recognition mechanism.

Although most of the AuNPs based sensors are aggregation based, few sensors with anti-aggregation phenomenon is also reported. Here, aggregation of citrate capped AuNPs is achieved by addition of suitable reagents. Upon addition of the analyte of interest, anti-aggregation results via binding of analyte on surface of nanoparticles. Main advantage of above approach is the minimal interference caused by coexisting species. Due to

higher species concentrations, citrate stabilized AuNPs usually shows some extent of aggregation.

1.2.4.3.2 Copper nanoparticles

Compared to noble metal nanoparticles viz., gold and silver, copper nanoparticles (CuNPs) are considered to be cost-effective and more catalytic in nature due to their extremely small size and high surface to volume ratio. In addition to this, CuNPs possess similar SPR properties, as that of silver nanoparticles and AuNPs. Thus, CuNPs becomes suitable candidates for development of cost-effective colorimetric sensors. Even though, many practical applications of CuNPs have been explored, colorimetric sensing based on CuNPs are rarely reported.

Major difficulty in use of CuNPs is their lower stability due to their affinity to oxidize after synthesis.[73] However, some research reports suggest synthesis of CuNPs having good stability. Literature shows that, use of effective capping agents and inert atmosphere can increase shelf life of CuNPs.

Colloidal dispersion of CuNPs having size less than 100 nm exhibits surface plasmon absorption band in visible region at around 570 nm. CuNPs solution is usually bright red in colour, but its interaction with analyte can diminish the colour and turns to yellow. In presence of dissolved oxygen, intensity of LSPR peak of CuNPs gradually reduces due to its oxidation, resulting in formation of reddish brown precipitate.

As explained in AuNPs, most of the reported sensors based on CuNPs are working via aggregation mechanism and colour change is

observed from red to yellow along with a reduction in LSPR band intensity. Removal of capping agent from surface or bond formation with analyte molecule could be the reason for aggregate formation. Generation of nanoparticles upon addition of analyte can also be used for sensing purpose. Here analytes having a reducing property reduces salt solution, leading to changes in colour. Oxidized or unreacted analyte moieties can stabilize the nanoparticles via capping.

1.2.4.4 A brief literature review on synthesis and/or colorimetric sensing application of some nanomaterials

Owing to the simplicity in synthesis, purification and functionalization of nanomaterials, sensors based on nanomaterials is a rapidly growing field. Several colorimetric sensors are developed till date making use of the properties of nanomaterials. A few of them are described below.

Using mercaptopropionic acid and homocysteine functionalised AuNPs, sensitive and selective sensing of Hg (II) ions was reported by Tan et al.[74] Interaction of Hg (II) ions with AuNPs produced colour change which was used for sensing purpose. Here, cloud point extraction was carried out in presence of 2,6-pyridinedicarboxylic acid and triton X-114 and colourless AuNPs were obtained. Red colour was produced upon interaction with Hg (II). This allowed the trace level determination of Hg (II).

Cao et al. presented a novel and sensitive colorimetric sensing method for melamine.[75] At room temperature 3,5-dihydroxybenzoic acid

induced reduction based synthesis of AuNPs was carried out. Upon interaction with melamine, colour of AuNPs changed from purple to yellowish green by H-bonding formation of DBA with melamine. Linear calibration graph was obtained in the concentration range from 1.0×10^{-5} to 1.0×10^{-9} M. Detection limit of the developed method was found to be 8.0×10^{-10} M.

A novel method for the colorimetric sensing of HCl in aqueous environment was reported by Tripathy et al..[76] Sensing is based on non-aggregation strategy using unlabeled AuNPs. Ability of chloro species for the leaching of AuNPs in presence of strong oxidizing agents is exploited here and thereby a remarkable decrease in surface plasmon resonance results. Developed strategy showed superior selectivity for HCl over common acids, salts and anions. This study entails the detection of HCl in natural water systems even at 500 ppm.

Chitosan stabilized copper nanoparticle have been synthesized by Usman and coworkers.[77] Synthesized nanoparticles were characterized using various analytical techniques such as ultraviolet visible spectroscopy, TEM, X-ray diffraction, FTIR spectroscopy and field emission SEM. Antifungal and antibacterial effects of synthesized nanoparticles was studied. By varying the concentration of chitosan used, nanoparticles having size ~ 2 – 350 nm can be synthesized by this approach.

Soomro and coworkers demonstrated a new approach for the synthesis of CuNPs using L-cysteine as protecting agent.[78] Reaction parameters was optimized by controlling experiments by noting the changes in LSPR band using UV–visible spectroscopy. Various analytical techniques

were used for the characterization of the developed CuNPs. Prepared CuNPs showed color changes from red to yellow upon interaction with Hg (II) ions. This response allows the determination of Hg (II) ions in the concentration range of 3.5×10^{-6} to 5.0×10^{-7} M with detection limit down to 4.3×10^{-8} M. Developed sensor is also applied for quantification of Hg (II) ions in river water samples.

A novel method for the large-scale production of CTAB capped CuNPs was reported by Wu et al.[79] Synthetic method was based on the reduction of cupric chloride with hydrazine in presence of CTAB solution. Various analytical techniques were used for the characterization of synthesized CuNPs. It was found that, only the concentration of hydrazine affect the size of the particles, and CTAB does not showed much influence in the size of nanoparticles. Thermogravimetric analysis revealed the formation of bilayer on the surface of CuNPs by showing two weight loss curves. These results reveal the stability of CuNPs and so this method can be used for the mass production.

Menon and coworkers reported a new sensing method for noradrenaline using silver nitrate solution in basic medium.[43] Here, dual channel sensing based on colorimetry and fluorimetry has been proposed. Formation of brown colored silver nanoparticles from silver ions upon interaction with noradrenaline entails the visual detection. Proposed linear ranges for the determination through colorimetry and fluorimetry are 1.0×10^{-6} to 6.6×10^{-8} M and 8.9×10^{-3} to 5.6×10^{-5} M respectively. Quantification of noradrenaline by developed method was also carried out successfully in artificial blood serum.

Drescher et al. developed another analytical strategy based on the in situ formation of AuNPs in eukaryotic cell cultures.[80] Studies were carried out to understand the formation process by varying the incubation medium. Different techniques such as surface-enhanced Raman scattering, laser ablation inductively coupled plasma mass spectrometry, microscopic mapping and TEM were performed to study the characteristics of gold compounds produced inside the cells. Difference in the distribution of AuNPs inside the cell implied the presence of some toxic chemicals. Authors suggested that, insitu and ex situ formation and comparison of results can be used for the sensing of these species.

1.3 Scope of present investigation

There is a perceived and increasing demand for simple, cost effective and rapid analytical tests for the determination of trace concentrations of food additives and clinically important compounds. In this regard, electrochemical and optical sensors offer promising means of analysis owing to its reliability and simplicity.

In continuation to the development of sensors for a variety of compounds in our laboratory,[81-93] present study intended to develop reliable, sensitive and cost effective methods for quantification of food additives and biomarkers. Integration of nanotechnology with sensor technology will bring significant developments in sensing field. With this point of view, nanomaterials based voltammetric, fluorescent and colorimetric sensors were developed for some food additives and important biomarkers.

Three voltammetric sensors based on gold nanoparticles, nickel nanoparticles and gold-polymer nanocomposite were developed for the

determination of food additives octyl gallate, propyl gallates and biomarker uric acid. In addition, six optical sensors were also developed in the course of study. Among the optical sensors fabricated, three of them are fluorescence sensors, in which quantum dots and nanoclusters were used as fluorescent probe for the quantification of food additives, brilliant blue FCF, quinoline yellow and biomarker glutathione. Two of the developed optical sensors were colorimetric sensor based on gold and copper nanoparticles for biomarkers such as dopamine and creatinine. The remaining one of the optical sensor is a dual channel sensor based on both fluorimetry and colorimetry for the quantification of biomarker adrenaline. Analytical figures of merit and different experimental parameters of each sensor were also studied. Practical applications of developed sensors were established by quantifying concentration of target analyte in artificial or commercially available samples and the results were compared with that of the established methods.

.....ൠ.....

Chapter 2

MATERIALS AND METHODS

Contents

A brief account of the reagents, reference methods and instruments used for the whole study is given in this chapter. Preparation of buffer solutions and artificial physiological solutions, cleaning procedure of electrodes are also discussed in detail.

2.1 Reagents

All solvents and other chemicals used for the studies were of analytical reagent grade and consumed without further purification. All aqueous solutions were prepared using Millipore water. Propyl gallate, dodecyl gallate, octyl gallate, L-cysteine, uric acid, homovanillic acid and glutathione reduced were purchased from Alpha Aesar, Heysham, England. Brilliant blue FCF, L-cysteine hydrochloride hydrate and sodium sulphide were supplied by Sigma Aldrich, Switzerland. Cadmium nitrate, ascorbic acid, citric acid, sodium chloride, tartrazine and malachite green, copper chloride, bromophenol blue, urea, ethylenediamine and L-glutamic acid

were procured from S. D. Fine Chem. Ltd., India. Glucose, fructose, sodium hydroxide, sodium phosphate and sulphuric acid were acquired from Merck specialities Private Ltd., India. Tris buffer, creatinine, aurochloric acid, β-alanine and hydrazine hydrate was obtained from Spectrochem Private Ltd., India and Dopamine, adrenaline, Noradrenaline and L-lysine was from HiMedia Laboratories Private Ltd., India. Rhodamine 6G and fluorescein was brought from Loba Chemie Private Ltd., India. L-tryptophan and L-tyrosine were obtained from Sisco Research Laboratories, India. Tissue paper (for synthesis) was brought from local market.

Food samples such as margarine, butter, sunflower oil, coconut oil, soft drinks, candies and pharmaceutical formulations such as dopamine injection and adrenaline injection used for application studies were brought from local market.

2.2 Instruments

Electrochemical measurements were carried out in PC controlled electrochemical analyzer, CH instruments, 6023D (USA). A conventional three-electrode system was used with a bare and modified glassy carbon electrode as working electrode, the reference electrode is a KCl-saturated Ag/ AgCl electrode and counter electrode is a platinum wire. ELICO, LI. 120 pH meter was used for pH measurements.

Reflection FTIR spectra were obtained on a Brucker 3000 Hyperion microscope with Vertex 80 FTIR system. Transmission FTIR spectrum was recorded on JASCO 4100 spectrometer using KBr discs. Morphology studies were conducted using scanning electron microscopy (SEM), atomic

force microscopy (AFM) and transmission electron microscopy (TEM). SEM images were obtained on a JEOL 6390 LV and AFM studies was performed on composite desktop AFM/STM-Nanosurf AG, Switzerland. TEM images were captured using JEM-2100 HRTEM.

Surface functional properties of nanoparticles were studied via XPS analysis in an X-ray photoelectron spectrophotometer, Thermo-Fischer Scientific Co., USA. Formation of nanoparticles was confirmed by XRD analysis using Bruker AXS D8 Advance XRD analyzer.

Fluorescence spectroscopic studies were carried out using JAZ-EL-200-X spectrofluorimeter and UV- visible spectra were recorded with Thermoscientific, Evolution 201, China. Particle size and zeta potential were obtained from ZetasizerNano ZS series, Malvern instruments and Nano partical, nanoparticles size analyzer, SZ-1000, HORIBA Scientific. Fluorescence lifetime was measured using a HORIBA fluorescence lifetime system (Helteapro tm, USA).

2.3 Reference methods for validation

Based on the available literature, developed methods are validated by analyzing the samples used in application study via already established analytical techniques and the procedures are detailed below.

2.3.1 Spectrophotometric estimation of gallates

The method proposed by AOAC was used for the estimation of propyl gallate (PG) and octyl gallate (OG).[94] Solutions of PG/OG were made using methanol. In a 25 mL standard flask, adequate amount of stock solution of PG/OG was added and 2.5 mL of 10% ammonium acetate solution was

added to it. Then 1 mL of ferrous sulphate was mixed with the above solution and total volume was made up to 25 mL using water. By following the same protocol, solutions having different concentrations of PG/OG were prepared, and incubated for 5 minutes. After incubation, resultant absorbance was measured at 540 nm using a UV-visible spectrophotometer. A calibration graph was plotted with absorbance vs. concentration of PG/OG. Using the above calibration graph, concentration of PG/OG in the samples was determined.

2.3.2 Folin's colorimetric determination of uric acid

Commercially available Folin's reagent (Phosphotungstate) was used for color generation. 50 µL of reagent was mixed with adequate amount of uric acid (to obtain the concentration of 1×10^{-3} to 2×10^{-5} M in 2 mL) followed by 10 µL of 0.1 M NaOH solution. Solutions were diluted to 2 mL and incubated for 30 minutes at room temperature. Absorbance at 520 nm was measured after incubation and a calibration graph was plotted by absorbance against concentration of uric acid. By knowing the absorbance of spiked physiological solutions, concentrations are obtained from calibration plot.[95]

2.3.3 Spectrophotometric determination of food colorants

Procedure proposed by AOAC was used for the spectrophotometric estimation of brilliant blue FCF (BB) and quinoline yellow FCF (QY).[96] Stock solutions of the above mentioned colorants are prepared in water followed by serial dilution to prepare standard solutions. Absorbance of each sample at corresponding wavelength of absorption (630 nm for BB and 416 nm for QY) was recorded using UV- visible spectrophotometer. A

standard linear graph was plotted with absorbance against concentration of colorant. Using standard addition method, concentration of colorant in the commercial food samples was determined.

2.3.4 Ellman's colorimetric estimation of glutathione

Yellow color generated by the reaction of glutathione (GSH) with Ellman's reagent (5,5-dithio-bis-(2-nitrobenzoic acid) = DTNB) was used for the colorimetric estimation of GSH.[97] 500 µL of 1.0×10^{-3} M solution of DTNB was mixed with suitable amount of GSH solution in a 25 mL standard flask. Total volume of the solution was made up to 25 mL using 0.2 M PBS solution of pH 7. Solution was incubated for 30 minutes and resultant absorption at 412 nm was noted and calibration graph was plotted with absorbance vs. concentration of GSH. By standard addition method, concentration of GSH in spiked - artificial saliva sample was obtained.

2.3.5 HPLC based determination of dopamine

Stock solution of dopamine (DA) was prepared in water followed by serial dilution to prepare standard solutions. 10 µL of solution was directly injected into a reversed-phase HPLC system with UV detector. Calibration graph was plotted with peak area vs. concentration of DA. Spiked physiological solutions were used for analysis after centrifugation and filtration. Concentration of DA in samples was obtained from calibration plot.[98]

2.3.6 Jeffe's reaction based spectrophotometric estimation of creatinine

Color produced by Jeffe's reaction was analyzed by spectrophotometrically and calibration graph was plotted by absorbance (at 410 nm) against concentration of creatinine (CR).[99] For this purpose, 500 µL of 3.6×10^{-2} M solution of picric acid and 250 µL of 1.4 M NaOH solution was mixed with standard solution of CR and used for analysis after 15 minutes incubation. CR in the spiked artificial physiological solutions was determined using standard addition method.

2.3.7 HPLC based determination of adrenaline

Stock solution of adrenaline (ADR) was prepared by dissolving ADR in water. Serial dilution of stock solution was carried out to prepare standard solutions. For each analysis, 10 µL of solution was injected directly into a reversed-phase HPLC system coupled with a UV detector. Calibration graph was drawn by plotting peak area vs. concentration of ADR. Spiked urine was used for analysis after centrifugation and filtration. ADR present in the samples was estimated using calibration plot.[100]

2.4 Preparation of artificial physiological solution

For application studies, artificially prepared physiological solutions were used. Procedures for the preparations are discussed below.

2.4.1 Preparation of artificial saliva

Artificial saliva samples were prepared by following Macknight - Hane and Whitford formula.[101] Due to viscosity problems; sorbitol was not

included in the preparation. Compositions of chemicals for the preparation of artificial saliva are listed in Table 2.1. Corresponding amounts was dissolved in 100 mL of water and pH of the solution was adjusted to 6.75 with concentrated KOH solution.

Table 2.1: Composition of artificial saliva in 100 mL solution.

Chemicals	Weight (mg)
Methyl-p-hydroxybenzoate	200.0
Sodium carboxymethyl cellulose	100.0
KCl	62.5
$MgCl_2.6H_2O$	5.9
$CaCl_2.2H_2O$	16.6
K_2HPO_4	80.4
KH_2PO_4	32.6

2.4.2 Preparation of synthetic urine

Artificial urine was made by dissolving 3.640 g of urea, 1.500 g of NaCl, 0.900 g of KCl and 0.960 g of Na_2PO_4 in 150 mL water. pH of the solution was adjusted within the 5.5 to 6.5 pH range using 0.1M HCl solution.[102]

2.4.3 Preparation of synthetic blood serum

Blood serum was prepared by dissolving 0.720 g of NaCl, 0.017 g of $CaCl_2$ and 0.037 g of KCl in 100 mL water. The pH of above solution was adjusted to 7.3 to 7.4 using 0.1 M NaOH solution.[103]

2.5 Preparation of buffer solutions

Buffer solutions for the electrochemical and optical studies were prepared by the procedures described below.

2.5.1 Tris buffer solution

0.5 M Tris buffer solution was used for synthesis of cadmium sulphide quantum dots and for the fluorescence studies. 0.605 g of tris(hydroxymethyl)-aminomethane was dissolved in 100 mL of water to prepare 0.5 M Tris buffer.

2.5.2 Acetate buffer solution (ABS)

ABS of desired pH was prepared by dissolving different amounts of glacial acetic acid and sodium acetate trihydrate in 100 mL of water. Amounts needed for ABS of corresponding pH is given in Table 2.2.

Table 2.2: Composition of chemicals required for preparation of ABS of various pH.

Resulting pH	Acetic acid (mL)	Sodium acetate trihydrate (g)
2	0.570	0.0024
3	0.561	0.0237
4	0.485	0.2054
5	0.205	0.8711
6	0.030	1.2885
7	0.003	1.3534
8	0.003	1.3602
9	0.003	1.3609

2.5.3 Citrate buffer solution (CBS)

Various combinations of trisodium citrate and citric acid as given in Table 2.3 were used for making CBS of different pH. Amounts for the above preparation for different pH was weighed and dissolved in 100 mL water.

Table 2.3: Compositions of chemicals desired for preparation of CBS of various pH.

Resulting pH	Citric acid monohydrate (g)	Sodium citrate trihydrate (g)
2	2.0544	0.0652
3	1.7963	0.4265
4	1.3115	1.1051
5	0.7819	1.8642
6	0.2650	2.5700
7	0.0375	2.8880
8	0.0039	2.9355
9	0.0003	2.9404

2.5.4 Phosphate buffer solution (PBS)

By dissolving various amounts of monosodium dihydrogen phosphate and disodium hydrogen phosphate, PBS of corresponding pH can be prepared. Table 2.4 details the quantity of chemicals needed for 0.1 M PBS of desired pH.

Table 2.4: Composition of chemicals necessitated for preparation of PBS of various pH.

Resulting pH	NaH_2PO_4 (g)	Na_2HPO_4 (g)
2	1.3799	0.0001
3	1.3790	0.0003
4	1.3780	0.0036
5	1.3615	0.0360
6	1.2143	0.3218
7	0.5836	1.5466
8	0.0940	2.4970
9	0.0100	2.6605
10	0.0010	2.6781

2.6 Cleaning procedure for electrodes

To obtain clean and uniform surface at each step of experiments, electrodes were cleaned by established protocol as described below.

2.6.1 Cleaning of glassy carbon electrode

Prior to use, glassy carbon electrode (GCE) was polished with 0.05 μm alumina slurries on felt pads, followed by sequential cleaning in ultrasonic bath using methanol, 1:1 HNO3, acetone and water respectively to dissolve any adsorbed alumina particles on the surface of electrode.

2.6.2 Cleaning of platinum and gold electrodes

Pt electrode (PtE) / gold electrode (GE) was cleaned by both mechanically and electrochemically. Initially the PtE/GE was polished with alumina (0.3 μm)/ water slurries on felt pads, followed by rinsing with

Millipore water. Then, sequential washing in ultrasonic bath using water, ethanol and finally with water were carried out. Followed by the mechanical cleaning, PtE / GE was electrochemically cleaned by cyclic scans from 0 to 1.5 V at a scan rate of 0.1 Vs^{-1} in 0.5 M H_2SO_4 until a stable voltammogram was obtained.

.....ꕥ.....

Chapter 3

GOLD NANOPARTICLES AND SELF-ASSEMBLED MONOLAYER BASED VOLTAMMETRIC SENSOR FOR OCTYL GALLATE

Contents

Fabrication of a voltammetric sensor for the determination of Octyl gallate (OG) is discussed in this chapter. Glassy carbon electrode (GCE) is chemically modified with gold nanoparticles (AuNPs) followed by deposition of a self-assembled monolayer of dodecane thiol (DDT). An anodic peak corresponds to the oxidation of OG was observed at a potential of 0.23 V at DDT/AuNPs/GCE by square wave voltammetry. Based on this, a novel electrochemical sensor was developed for the determination of OG in oils and fats. Linear calibration graph was obtained within the range 1.2×10^{-6} to 2.0×10^{-7} M and detection limit was found to be 8.3×10^{-9} M. The applicability of the method was demonstrated by analysing OG in commercially available food samples such as margarine, butter and sunflower oil.

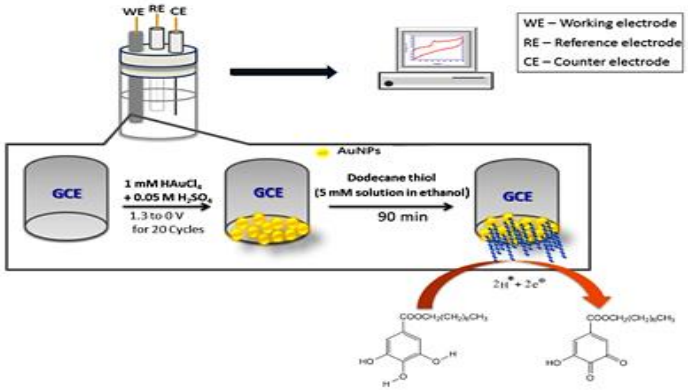

Scheme 3.1: Pictorial representation of the developed sensing strategy of OG.

3.1 Introduction

Antioxidants are a class of compounds which have the ability to prevent or slow down oxidation reactions of other substance. Due to this nature, antioxidants are widely used in food industry to prevent or retard deterioration, rancidity and/or decolouration of food stuffs against reactive oxygen species. Detrimental effects include formation of compounds like aldehydes, ketones and organic acids which yield off-flavours.[104] Octyl Gallate (OG) is an ester of gallic acid (3, 4, 5-trihydroxy benzoic acid) and n-octanol (Figure 3.1), which retard or break the rancidity and/or decolourisation of fats and oils. Therefore it is used as a preservative in food stuffs such as sunflower oil, margarine, lard etc.

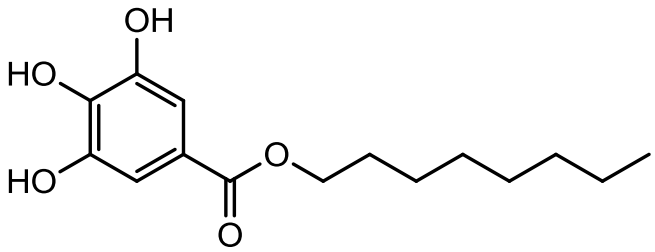

Figure 3.1: Chemical structure of OG.

Recent studies have shown that antioxidants could enter human body through the intake of food, pharmaceuticals etc. Although they are powerful in protecting product quality in food distribution, excess antioxidants added to food might produce toxicities or mutagenicities and may endanger the health of people.[105] Studies on OG have shown that, it can provoke allergic reactions, irritation to skin, repeated exposure may cause skin cracking.[106] On degradation in the intestine it gives gallic acid and octanol, of which gallic acid causes eczema, stomach problems and hyperactivity.[106] Also OG

may induce apoptosis with DNA fragmentation in hepatocytes.[107,108] Therefore the detection and determination of this antioxidant is of importance.

Recently chemically modified electrodes have been widely used in the development of electrochemical sensor because of their high sensitivity and selectivity. Self-assembled monolayer (SAM) based electrodes are widely used for the construction of sensors due to advantages such as high sensitivity, selectivity and small over potential in electrocatalytic reactions.[20,109] Instead of gold electrode, gold nanoparticles (AuNPs) coated glassy carbon electrode can be used for SAM formation. AuNPs increase the immobilized amount of thiols and enhance the Au-S bond and stability of SAM.[20,110] The aim of this work is to combine the advantages of gold nanoparticles and SAM of thiol to fabricate an electrochemical sensor for OG.

Considering the above facts, AuNPs were introduced on the surface of glassy carbon electrode (GCE) via electrodeposition to enhance the catalytic activity and a platform for SAM formation. Among the various SAM on AuNPs/GCE was tried (Table 3.1), better response with higher peak current and lower overpotential were found with dodecane thiol (DDT) modified AuNPs/GCE. So DDT/AuNPs/GCE was used for the determination of OG. Several analytical parameters were studied and optimised. Developed method was applied for the determination of OG in commercial food samples and results were compared with spectrophotometric method.

Table 3.1: Comparison of various modifications studied for determination of OG in 0.1 M ABS pH 6.

Modified electrode	Potential (V)	Current (A)
AuNPs /GCE	0.248	1.8×10^{-5}
L-cys/AuNPs/GCE	-	-
MBT/AuNPs/GCE	0.460	9.6×10^{-6}
DDT/AuNPs/GCE	0.228	2.6×10^{-5}

L-cys = L-cysteine, MBT = Mercapto benzothiazol

3.2 Experimental

3.2.1 Preparation of the SAM-AuNPs modified GCE

Prior to use, GCE was cleaned according to the procedure described in section 2.6.1. Electrodeposition of gold nanoparticles on cleaned GCE was achieved in a one compartment / three electrodes electrochemical cell with a solution containing 5.0×10^{-2} M H_2SO_4 and 1.0×10^{-3} M $HAuCl_4$. 20 cyclic scans were carried out between 1.3 to 0 V at a scan rate of 0.1V/s (Figure 3.2). During the deposition process, an oxidation peak at 1.11 V and a reduction peak at 0.79 V were obtained and peak currents were found to increase after each scan, indicating the formation of AuNPs on the surface of GCE. Then modified electrode was washed with water and allowed to dry.[111]

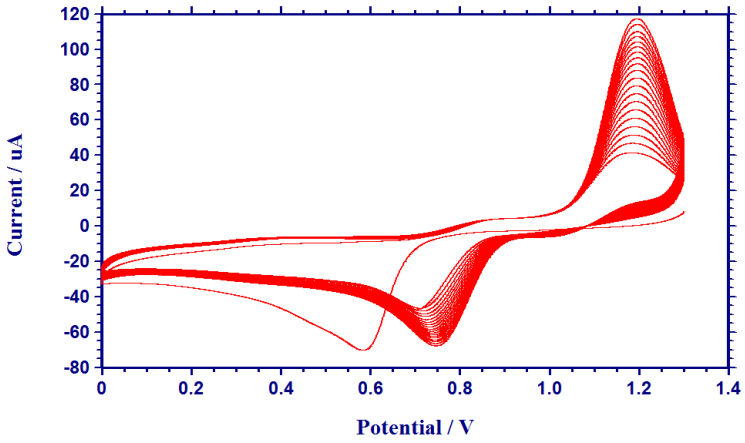

Figure 3.2: Cyclic voltammograms obtained for electrodeposition of AuNPs on GCE.

SAM of dodecane thiol (DDT) was formed on AuNPs modified GCE by soaking the electrode in 5.0×10^{-3} M ethanolic solution of DDT for 90 min at room temperature. Then DDT/AuNPs/GCE electrode was washed with water to remove physically adsorbed DDT and then dried.

3.2.2 Analytical procedure

Unless otherwise stated, a 0.1 M pH-6 acetate buffer solution (ABS) was used as supporting electrolyte for the determination of OG. Square wave voltammogram was recorded from 0.1 to 0.5 V at a potential increment of 0.004 V and amplitude of 0.025 V. The signal for the oxidation of OG was measured at a potential of 0.23 V. Since SWV gave a well-defined oxidation peak with a lower potential and higher peak current compared to CV, LSV and DPV, SWV was selected for all the experiments.

3.2.3 Real sample preparation and determination

Margarine, butter and sunflower oil samples were purchased from a local market. Five gram of sample was dissolved in suitable volume of hexane and appropriate amount of OG was added (to make spiked samples). It was then extracted four times using acetonitrile (4 × 50 mL). The acetonitrile extract was evaporated to dryness under vacuum at a temperature less than 40˚C. Then the contents were dissolved in 10 mL methanol and were used for the determination.[112,94] Besides, a spectrophotometric method was also conducted to these sample extracts as explained in section 2.3.1 for comparison.[113,114]

3.3 Results and discussion

3.3.1 Characterization of DDT/AuNPs/GCE

Physical morphology of the surface such as roughness, porosity etc. can affect the response of an electrochemical sensor, mainly in the current response.[20] Atomic force microscopy (AFM) provides information about surface morphology, roughness, molecular alignment etc. Therefore AFM technique was used to illustrate the self-assembly process of DDT on AuNPs/GCE. AFM images of bare GCE, AuNPs/GCE, DDT/AuNPs/GCE are given in Figure 3.3. From the figure, it is clear that surface morphology (roughness) is changed during modification. These observations may be due to the formation of SAM on AuNPs/GCE.

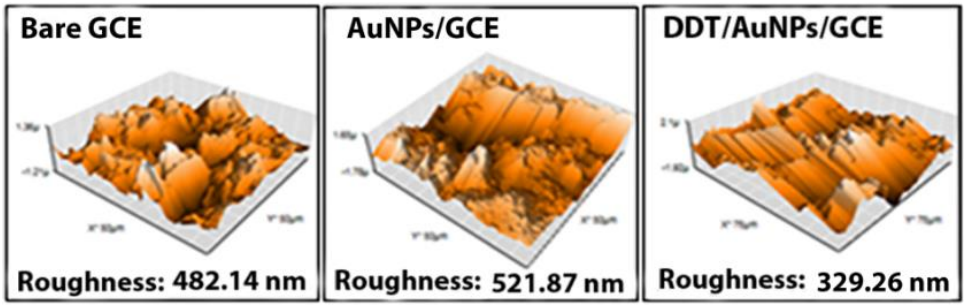

Figure 3.3: AFM images of bare and modified GCE.

Electrode modification is further confirmed through electrochemical impedance spectroscopy (EIS). This is a very effective tool for the analysis of interfacial properties of electrodes and electrolytes, and provides information about change in capacitance and resistance during modification of electrodes.[115] EIS is also suitable for the analysis of SAM formation.[116] Figure 3.4 shows the Nyquist plots of the EIS spectra of the bare and modified GCE in the presence of $[Fe(CN)_6]^{4-}$/ $[Fe(CN)_6]^{3-}$ redox couple (PBS pH-7). Here we get three semicircular curves (corresponds to the diffusion process) having different diameters. The diameter represents the magnitude of electron- transfer resistance (Rct) at the electrode surface.[115] From the figure it is clear that, modification of GCE with AuNPs, enhances the electron transfer rate (poorly defined semicircle with Rct = 96 ohm) compared to bare GCE, where electron transfer resistance is larger (Rct = 641 ohm). But SAM formation on AuNPs modified GCE gave EIS spectra with a semicircular curve with larger diameter than others, which is indicative of an increase in the electron transfer resistance (Rct = 858 ohm). However, the obtained resistance for DDT/AuNPs/GCE is small compared with other reported SAMs.[115,116] This may be due to the combined effect of AuNPs and SAM.

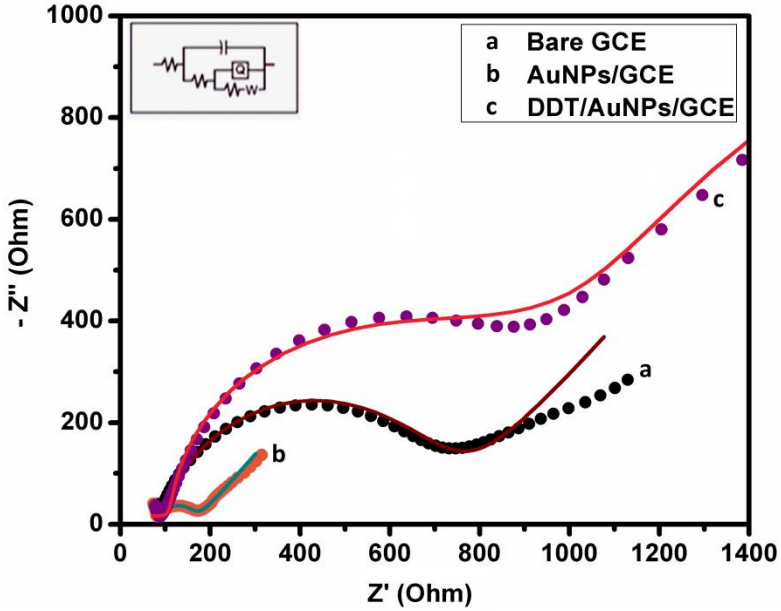

Figure 3.4: EIS of bare and modified GCE (●) obtained spectra and (−) the best fit of the corresponding circuit diagram.

The attachment of thiol on gold surface is realized through covalent bond formation.[110] The bond formation can be evaluated using FTIR measurements. Comparison of the transmission FTIR spectrum of liquid DDT (spectrum-1) with the infrared reflection spectrum of DDT/AuNPs/GCE (spectrum-2) is visualized in Figure 3.5. Compared to the FTIR spectrum-1, the band corresponding to the –SH stretching vibration mode (2584 cm^{-1}) disappeared in spectrum-2 which demonstrate that the sulphur atoms are directly bonded to gold atoms.[110] This may be due to the formation of a monolayer of DDT on the surface of AuNPs film. This result is consistent with those reported for alkane thiols adsorbed on gold surfaces.[110]

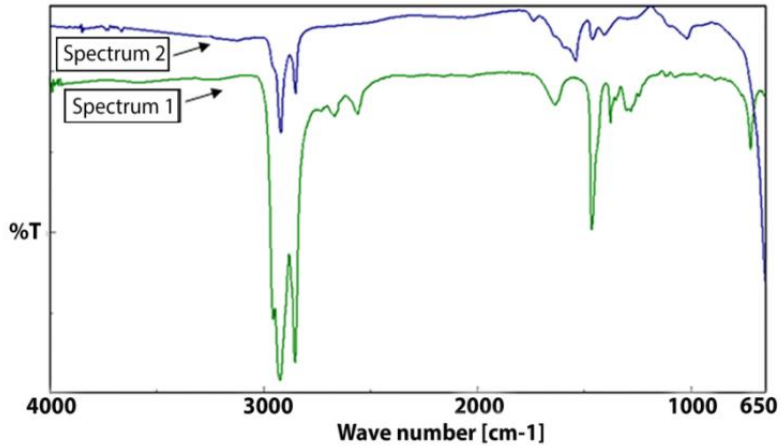

Figure 3.5: The transmission FTIR spectrum of DDT (spectrum 1) and the reflectance spectrum of DDT adsorbed on the AuNPs/GCE (spectrum 2).

3.3.2 Electrochemical behaviour of octyl gallate

Figure 3.6 illustrates square wave voltammetric (SWV) responses of 1.0×10^{-6} M OG on the surface of bare GCE and modified GCE. The response of OG at the bare GCE is weak (0.31 V potential with a peak current of 9.30×10^{-7} A) may be due to slow electron transfer, while the response is considerably improved at the AuNPs/GCE (0.25 V potential with a peak current of 1.62×10^{-6} A). In comparison to the bare GCE and AuNPs/GCE, a reduction in the over potential together with a remarkable enhancement in the peak current was observed on DDT/AuNPs/GCE (0.23 V potential with a peak current of 2.08×10^{-6} A), indicating the synergic effect of individual layers (AuNPs and DDT) on the surface of the electrode. Furthermore, the cyclic voltammetric response of OG showed an irreversible process as only an oxidation peak could be observed.

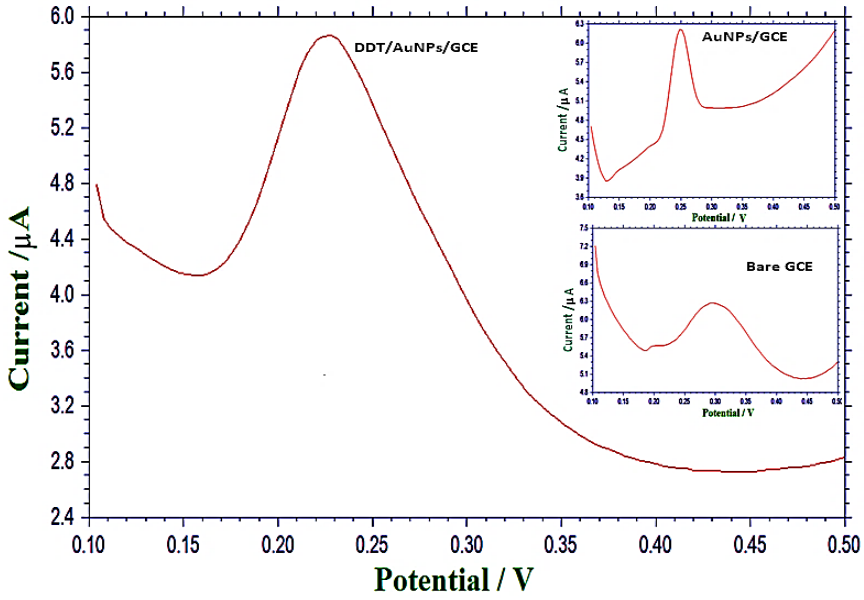

Figure 3.6: Square wave voltammogram of 1.0×10^{-6} M OG at bare and modified GCE.

3.3.3 Optimization of experimental conditions

3.3.3.1 Influence of supporting electrolyte

Choice of suitable supporting electrolyte is important since it can affect the mass transfer, kinetics and thermodynamics of electrochemical processes.[117] The electrochemical response of OG at DDT/AuNPs/GCE in different supporting electrolytes (0.1 M) such as acetate buffer, phosphate buffer, citrate buffer, HCl, NaCl and NaOH were examined by SWV. It was found that the best results were obtained with 0.1 M acetate buffer solution (ABS). Hence, 0.1 M ABS was chosen as the experimental medium.

3.3.3.2 Effect of film thickness

The influence of film thickness (of AuNPs) on the oxidation peak current of OG was studied. As shown in Figure 3.7, when the scan cycles were 20, the peak current reached its maximum value. But as the scan cycles were increased beyond 20, a decrease in current was observed. This may be due to the decreased electron transfer rate of OG with an increase in film thickness,[118] which might be associated with the decrease of surface area due to aggregation of AuNPs on the electrode surface. So scan cycles were optimized to 20 cycles.

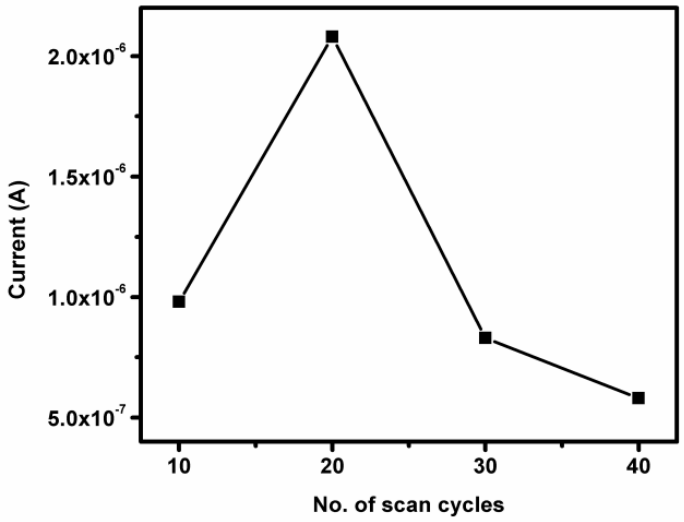

Figure 3.7: Effect of scan cycles of AuNPs deposition on the peak current of 1.0×10^{-6} M OG.

The SEM images (Figure 3.8 (a) and (b)) show the AuNPs on GCE at 20 cycles as well as in 40 cycles. The obtained particle sizes confirm the aggregation of AuNPs on GCE surface as scan cycle exceeds 20.

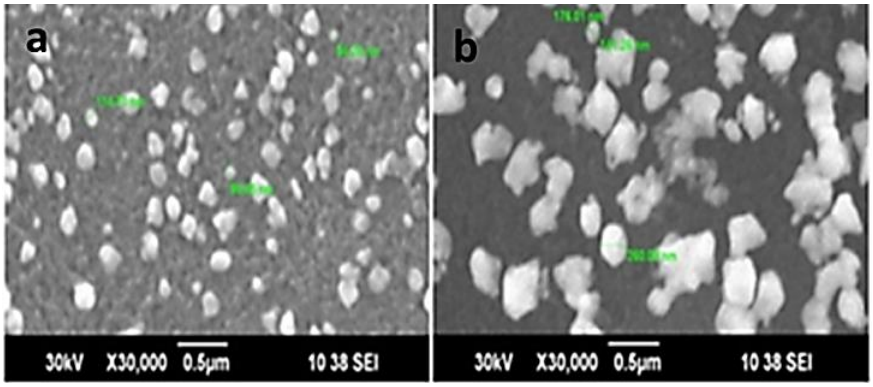

Figure 3.8: (a) SEM image of AuNPs on GCE at 20 cycles of deposition, and (b) at 40 cycles of deposition.

3.3.3.3 Effect of pH

SWV response of the DDT/AuNPs/GCE on the oxidation of 1.0×10^{-6} M OG over the pH range from 2.0 to 9.0 ABS (0.1M) was studied. By increasing the pH, the oxidation peak current increased up to pH 6.0 with decrease in oxidation potential. Further increase in pH value to 9.0 showed a decrease in oxidation peak potential as well as in peak current, and the peak disappeared after pH 9.0. Figure 3.9 (a) and (b) shows the influence of pH on peak current and potential of OG on DDT/AuNPs/GCE. To get the maximum current at lower potential, ABS (pH- 6.0) was used throughout the studies.

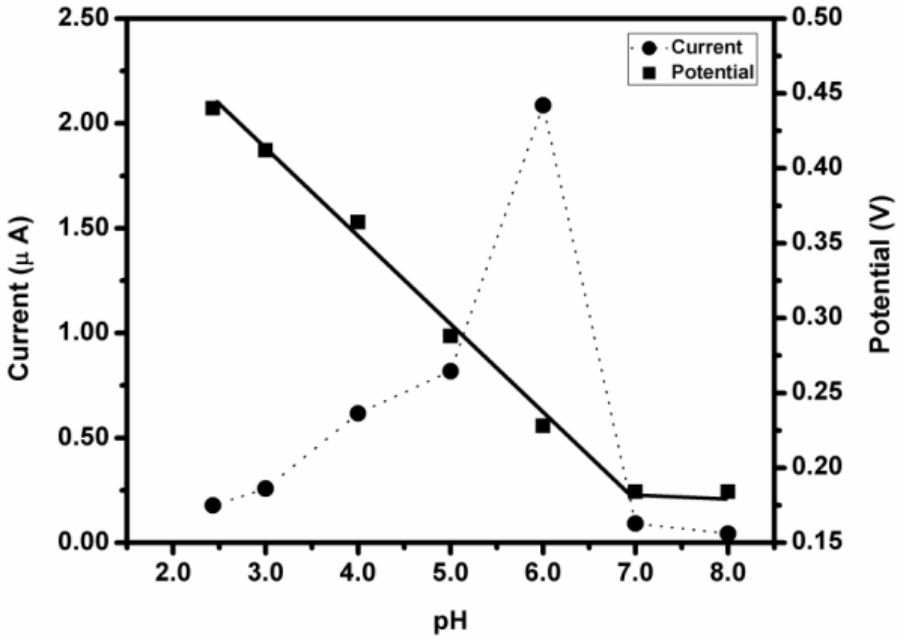

Figure 3.9: Effect of pH on peak current and potential.

3.3.4 Effect of scan rate

Effect of scan rate (ν) on the oxidation peak current of 1.0×10^{-6} M OG was studied by linear sweep voltammetry (LSV). Figure 3.10 shows the linear sweep voltammogram of 1.0×10^{-6} M OG at different scan rate in the range of 0.03 - 0.12 Vs^{-1}. When the scan rate increases from 0.03 to 0.12 Vs^{-1}, peak potential shift to higher value indicating the irreversible character of the oxidation process.[27]

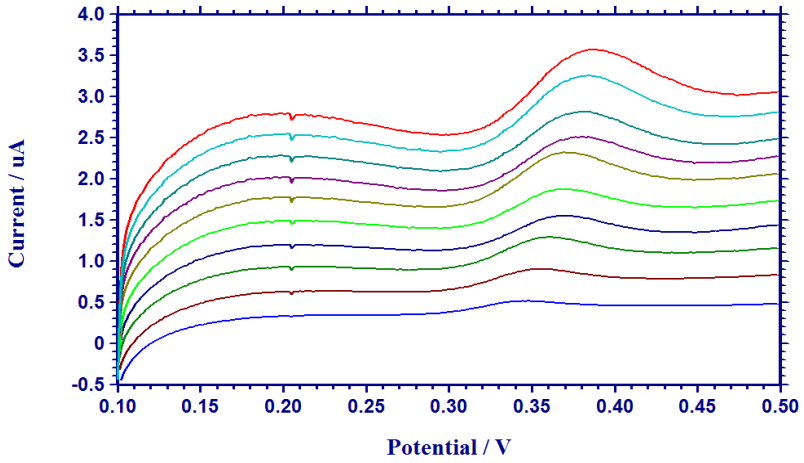

Figure 3.10: Overlay of LSVs for oxidation of OG at various scan rates.

It was found that, peak current (i_p) for oxidation of OG showed a linear relationship with square root of scan rate (Figure 3.11), which is indicative of diffusion controlled mechanism for oxidation of OG.[25] Linear correlation of ln(i_p) against ln(v) (Figure 3.12) with a slope of 0.62 (comparable to theoretical value of 0.50), confirms the diffusion controlled mechanism of oxidation.[119]

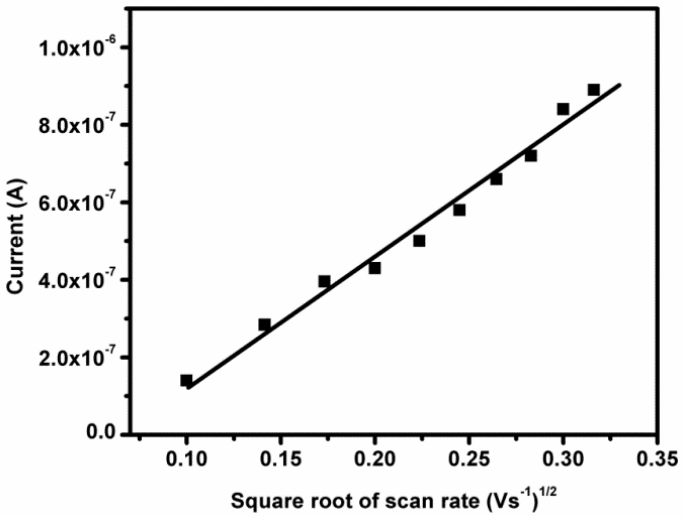

Figure 3.11: Plot of peak current versus square root of scan rate.

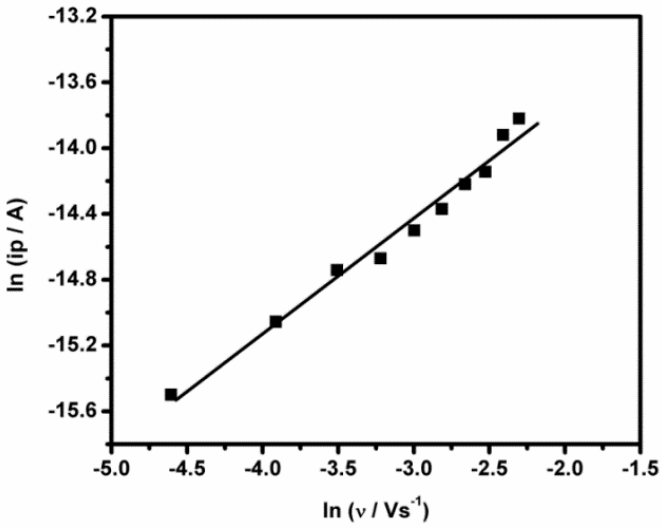

Figure 3.12: Plot of natural logarithm of peak current against natural logarithm of scan rate.

3.3.5 Determination of diffusion coefficient

Chronoamperometric analyses were conducted to estimate the value of diffusion coefficient. Obtained chronoamperograms for different concentrations (1.0×10^{-6} to 1.0×10^{-5} M) of OG are depicted in figure 3.13. Slopes obtained from the plots of electro-catalytic current (I) against $t^{-1/2}$ at different concentrations (Figure 3.14) were plotted against concentration (C) of OG (Figure 3.15), and the ensuing slope was used for the calculation of diffusion coefficient (D) according to Cottrell equation.[11]

$$\mathbf{I = nFAD^{1/2}C\pi^{-1/2}\,t^{-1/2}}$$

Hear, A is the surface area of the modified electrode, n is number of electrons involved in the reaction, F is Faraday's constant.

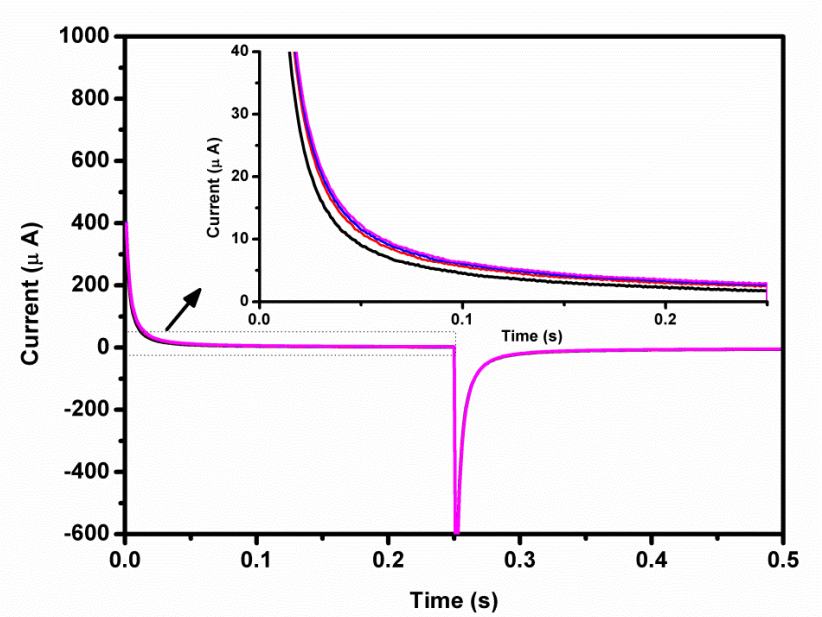

Figure 3.13: Overlay of chronoamperograms of OG at various concentrations.

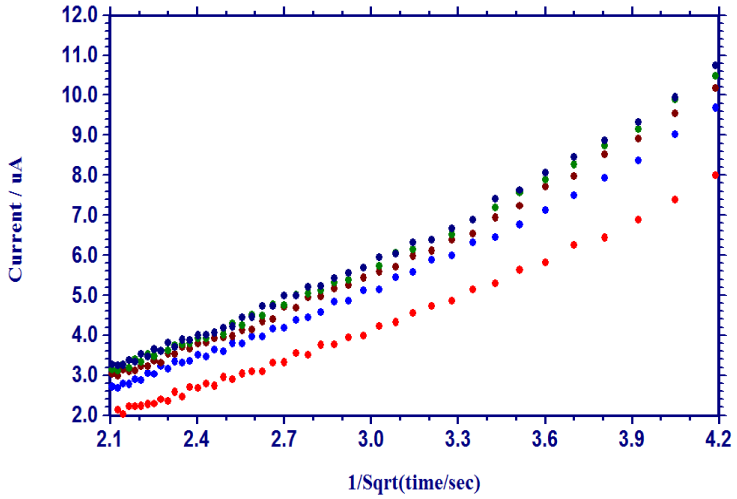

Figure 3.14: Plot of current vs. $t^{-1/2}$ derived from the chronoamperograms in Figure 3.13.

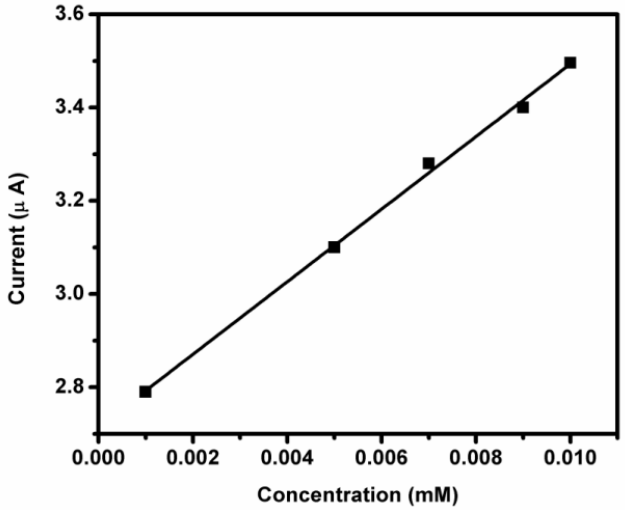

Figure 3.15: Plot of slope of (I vs $t^{-1/2}$ from Figure 3.14) against concentration of OG.

On immobilization of SAM in gold nanoparticles, negligible change in surface area will result and as the determination of surface area of SAM modified electrode is more tedious, surface area of AuNPs modified GCE was used for calculation. So, effective surface area of AuNPs/GCE was calculated using Randles – Sevcik equation for reversible systems.[120]

$$I_p = 2.69 \times 10^5 A D_R^{1/2} n^{3/2} v^{1/2} C$$

For this, CVs of 2.0×10^{-3} M $K_3[Fe(CN)_6]$ on AuNPs/GCE at different scan rates (Figure 3.16) were recorded. By substituting the obtained slope of the graph of peak current (I_p) versus square root of scan rate ($v^{1/2}$) and other quantities in Randles – Sevcik equation, effective surface area was calculated and was found to be 0.105 cm^2. By substituting the obtained surface area and other quantities in Cottrell equation, average value of D was found to be 3.82×10^{-5} cm^2 s^{-1}. The value D also supports the diffusion controlled mechanism of oxidation.

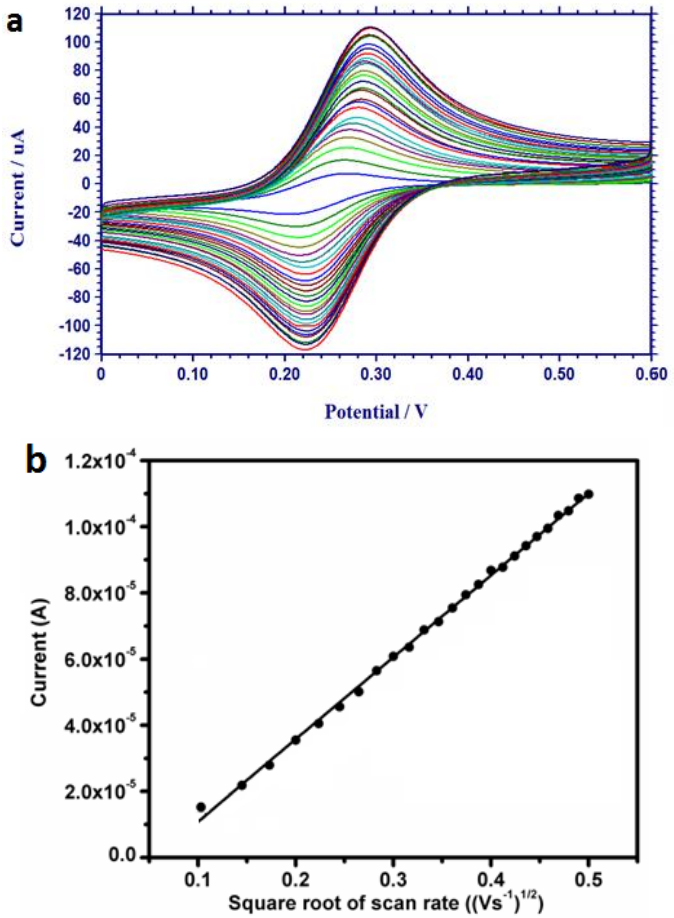

Figure 3.16: (a) Overlay of cyclic voltammograms of 2.0 × 10^{-3} M $K_3[Fe(CN)_6]$ on AuNPs/GCE at various scan rates (b) plot of peak current *vs* square root of scan rate.

3.3.6 Variation of SWV of OG with concentration

SWV responses of OG on DDT/AuNPs/GCE under optimized conditions towards different OG concentrations were analysed. Figure 3.17 represents the SWV curves of OG at different concentrations on DDT/AuNPs/GCE. It was found that the oxidation peak current of OG varies linearly with its concentration in the range of 1.2×10^{-6} to 2.0×10^{-7} M.

Figure 3.18 shows the linear fit of oxidation peak current vs concentration of OG. From the graph, a detection limit of 8.3×10^{-9} M was obtained.

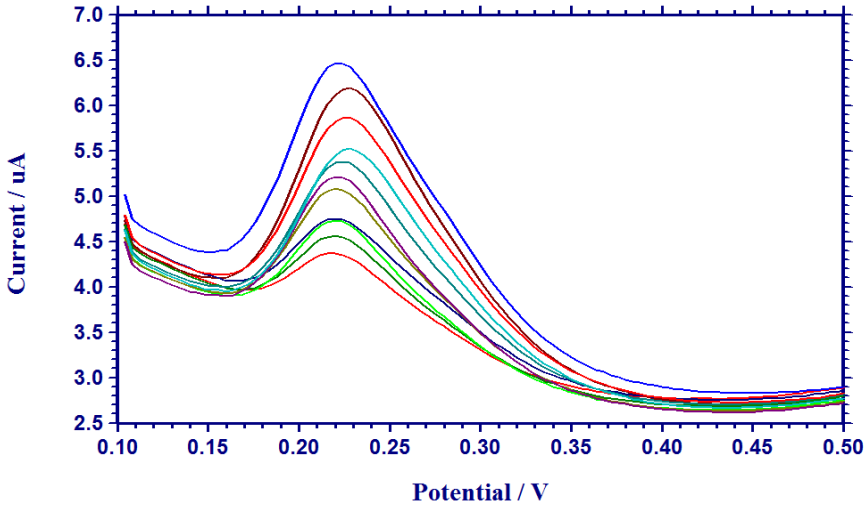

Figure 3.17: Overlay of SWVs for oxidation of OG at various concentrations.

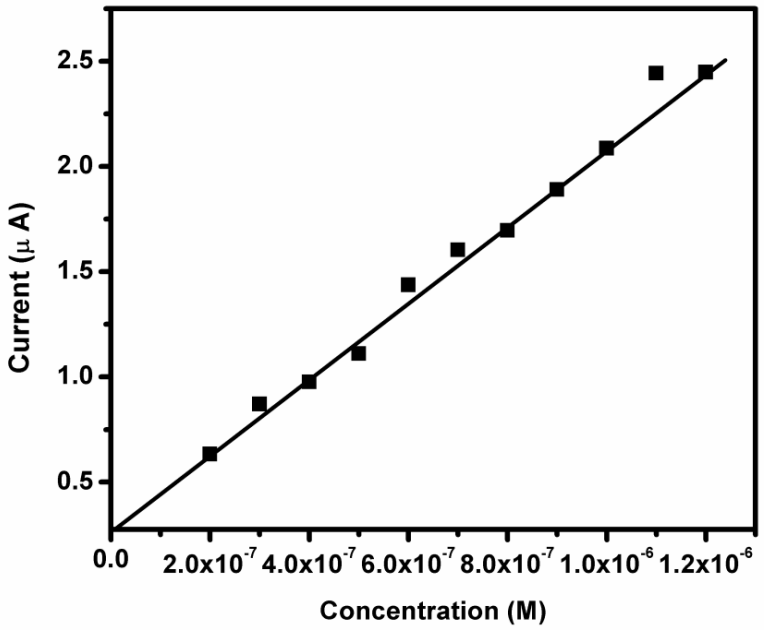

Figure 3.18: Plot of various concentrations of OG versus peak current.

Table 3.2 represents the comparison of various analytical methods for the determination of OG. Examination of Table 3.2 reveals that the limit of detection of the proposed method is far superior to the existing methods.

Table 3.2: Comparison of various analytical methods for determination of OG.

Sl. No.	Method	Linear range (M)	LOD (M)	References
1.	Flow injection Amperometry	4.6×10^{-5} to 3.5×10^{-7}	1.1×10^{-6}	121
2.	Chromatography with pulsed Amperometry	6.9×10^{-5} to 2.3×10^{-6}	2.3×10^{-6}	122
3.	Resonance light scattering detection	3.5×10^{-5} to 3.0×10^{-8}	8.0×10^{-8}	123
4.	Electro kinetic chromatography	2.0×10^{-4} to 2.0×10^{-6}	7.4×10^{-7}	124
5.	Voltammetry	1.2×10^{-6} to 2.0×10^{-7}	8.3×10^{-9}	-

3.3.7 Interference study

To determine the influences of foreign species on the determination of OG, some common co-existing substances were added with OG and changes were studied (Table 3.3). The study revealed that, even up to a 100 fold excess of acetic acid, EDTA, NaCl, Na_2SO_3 and antioxidants such as tert-butyl hydroquinone (TBHQ), PG and 10 fold excess of citric acid, DG and butylated hydroxyl anisole (BHA) did not interfere the determinations. However ascorbic acid affects the determination severely.

Table 3.3: Effect of coexistence on the determination of 1.0×10^{-6} M OG.

Coexisting species	Concentration (M)	Interference (%)
Acetic acid	1.0×10^{-4}	2.8
EDTA	1.0×10^{-4}	2.0
NaCl	1.0×10^{-4}	4.2
Na_2SO_3	1.0×10^{-4}	3.2
Tertiary butyl hydroquinone	1.0×10^{-4}	2.3
Propyl gallate	1.0×10^{-4}	1.9
Citric acid	1.0×10^{-5}	3.6
Dodecyl gallate	1.0×10^{-5}	5.8
Butylated hydroxy anisole	1.0×10^{-5}	1.4
Ascorbic acid	1.0×10^{-6}	14.1

3.3.8 Mechanism of the electro-oxidation process

The presence of anodic peak may be due to the oxidation of hydroxyl group present in OG. Number of electrons involved in the process can be calculated using the Laviron's equation.[125] The slope obtained from plot of peak potential (Ep) against ln ν (Figure 3.19) is equal to $\frac{RT}{\alpha F n_a}$, where α is the electron transfer coefficient and which is assumed to be 0.50 for irreversible process. By knowing the other quantities, the value of 'n_a' was calculated to be 2.

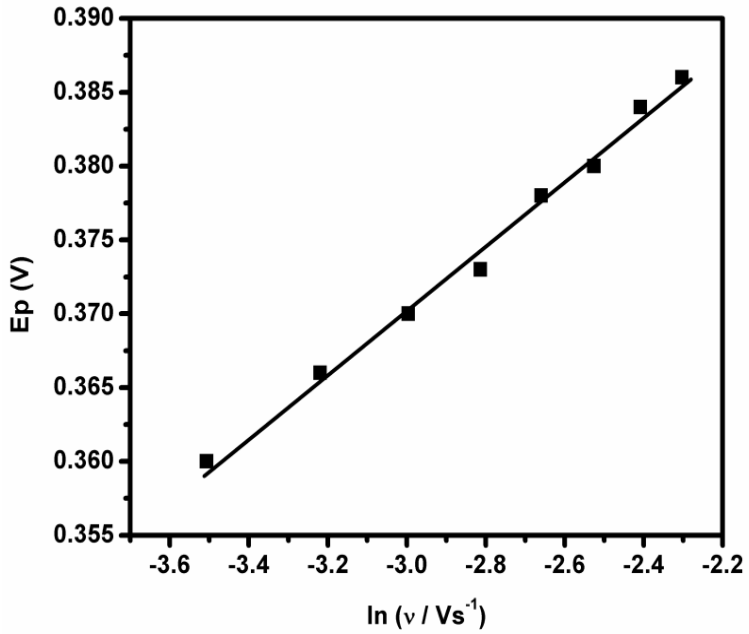

Figure 3.19: Plot of peak potential versus natural logarithm of scan rate.

The anodic peak potential showed a negative shift on increasing the pH of the solution (Figure 3.9 (b)). A slope of −0.058 V is approximately close to the theoretical value (−0.059 V), indicating that electron transfer is accompanied by an equal number of protons on the electrochemical oxidation of OG.[126] The overall reaction involves 2 H^+ and 2 e^- transfer. Gallates differ in their side chain, but the mechanistic pathways of oxidation are similar. Hence we can propose a mechanism for the oxidation of OG, similar to that reported.[27,127] The proposed mechanism is explained in Scheme 3.2.

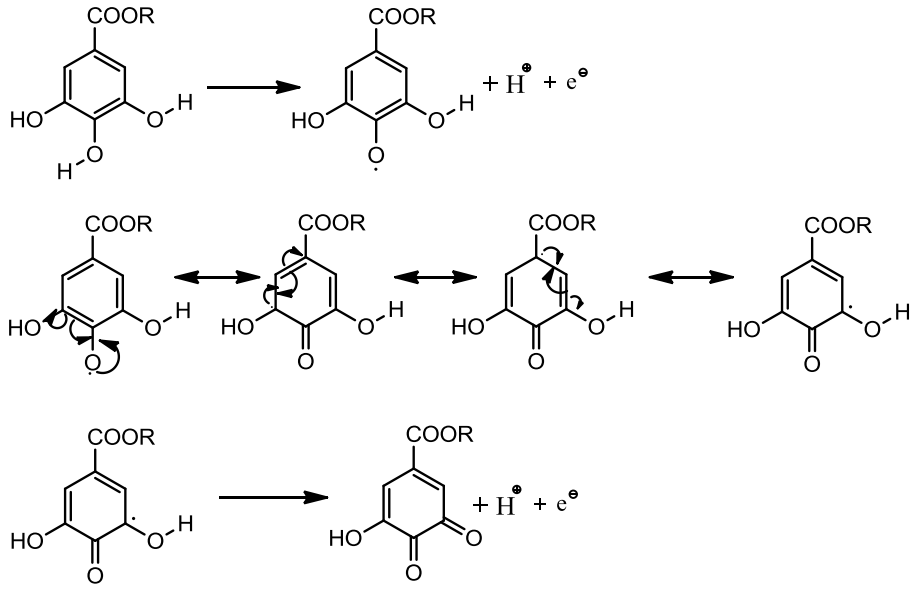

R = $CH_3(CH_2)_6CH_2$-

Scheme 3.2: Mechanism of OG oxidation.

3.3.9 Reproducibility and Repeatability

Reproducibility of the developed sensor was studied by conducting five replicate measurements on DDT/AuNPs/GCE in 1.0×10^{-6} M OG solution under optimized conditions. The relative standard deviation (RSD) was found to be ±2.2 %. Similarly the repeatability of the sensor is studied by taking five successive measurements using same electrode, RSD was found to be ±4.5%. These results show that the proposed sensor has good reproducibility and repeatability.

3.3.10 Analytical application

In order to study the performance of the proposed sensor in real sample analysis, determination of OG in three spiked food samples viz.

margarine, butter and sunflower oil were carried out. The results are given in the Table 3.4. The obtained results are in good agreement with those of spectrophotometric method.[113,114] This result reveals the accuracy and precision of the proposed sensor for the analysis of real samples.

Table 3.4: Determination of OG in food samples.

Samples	Added (M)	Spectrophotometry			Proposed method		
		Found (M)	R (%)*	RSD[a]	Found (M)	R (%)*	RSD[a]
Margarine	3.0×10^{-7} to 9.0×10^{-7}	2.9×10^{-7} to 9.0×10^{-7}	100	0.7	3.0×10^{-7} to 9.0×10^{-7}	101	0.5
Butter	3.0×10^{-7} to 9.0×10^{-7}	3.0×10^{-7} to 8.8×10^{-7}	99	1.5	2.9×10^{-7} to 8.9×10^{-7}	99	0.2
Sunflower oil	3.0×10^{-7} to 9.0×10^{-7}	3.1×10^{-7} to 8.9×10^{-7}	101	1.5	3.0×10^{-7} to 8.8×10^{-7}	99	1.5

*From five measurements, R = recovery, RSD = relative standard deviation.

3.4 Conclusions

A DDT/AuNPs/GCE was fabricated and successfully used for the determination of antioxidant OG in food stuffs. The presence of DDT and AuNPs shows a decrease in oxidation potential, enhancement in peak current, nano-molar level detection limit, reproducibility, repeatability and good recovery. The obtained results make this electrode very useful as an effective voltammetric sensor for the determination of OG in real samples.

.....ൠ.....

Chapter 4

GOLD NANOPARTICLES AND POLY(BROMOPHENOL BLUE) BASED VOLTAMMETRIC SENSOR FOR URIC ACID

Contents

This chapter details the development of a simple voltammetric sensor for direct determination of an important biomarker uric acid (UA) based on poly bromophenol blue - gold nanoparticles composite modified glassy carbon electrode. Scanning electron microscopy, atomic force microscopy and various electrochemical techniques were used for characterization of modified electrode surface. The electro-oxidation of UA in 0.1 M NaOH was excellently catalyzed by modified electrode. The anodic peak corresponding to the oxidation of UA was observed at a potential of -0.10 V by Square wave voltammetry (SWV). The oxidation peak current was increased linearly on increasing the concentration of UA in the range 1.0×10^{-3} to 2.0×10^{-5} M (R^2 = 0.994) with a limit of detection 2.2×10^{-6} M. The proposed method was effectively applied to determine Uric acid in artificial blood serum and urine samples.

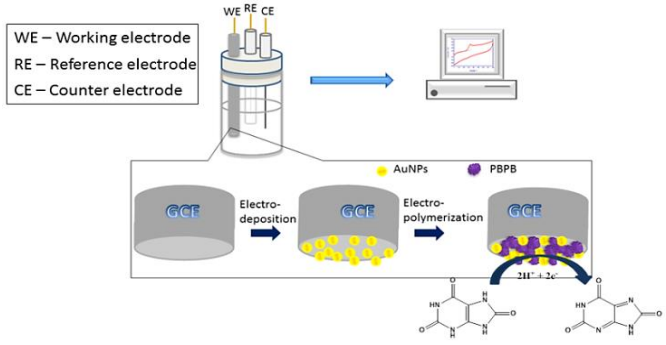

Scheme 4.1: Diagrammatic representation of sensing process.

4.1 Introduction

Rheumatologists are too busy to dig into treatment of gout, the dark shadow that falls over our senility. Increasing number of gout patients would largely be a modern phenomenon, connected to our lifestyles.[128] Gout is generally associated with higher level of uric acid (UA) in blood (Hyperuricemia), due to higher intake of dietary purine, sugar etc.[129,130] In body fluids, UA (Figure 4.1) also exists in ionic form – urate.[131] Extent of UA in body mainly depends on equilibrium between dietary purines eaten and synthesized within the body to the quantity of UA excreted.[132] In human, normal range of UA varies from 200 – 430 µmol/L for men and 140 – 360 µmol/L for women.[133] Due to the above reasons, UA analysis helps to understand functioning of kidneys, monitoring of symptoms of hyperuricemia or level of UA.

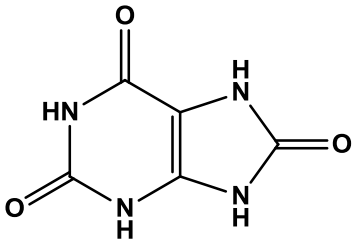

Figure 4.1: Chemical structure of UA.

This work is devoted to the development of a new voltammetric method for precise measurement of UA in biological samples. For this purpose, various chemical modifications on glassy carbon electrode (GCE) was tried (Table 4.1), among them, higher peak current and lower overpotential were found with gold nanoparticles (AuNPs) and poly(Bromophenol blue) (PBPB) modified GCE. So AuNPs/PBPB/GCE

was used for the determination of UA. The two-stage modification procedure is carried out, based on electro-deposition of AuNPs and electro-polymerization of bromophenol blue using cyclic voltammetry. Obtained composite structure enhanced the electro-catalytic activity of GCE towards the oxidation of UA (Scheme 4.1). The whole protocol has also been validated by estimating UA in physiological samples and the recoveries were compared with that of colorimetric analysis.

Table 4.1: Comparison of various modifications studied for determination of UA in 0.1 M PBS pH 7.

Modified electrode	Potential (V)	Current (A)
PPABSA/GCE	0.39	6.30×10^{-6}
PMG/GCE	0.26	3.75×10^{-6}
AuNPs/GCE	-0.10	1.73×10^{-6}
PBPB/GCE	0.21	6.45×10^{-6}
PBPB/AuNPs/GCE	0.18	1.16×10^{-5}

PPABSA= poly(p-aminobenzene sulphonic acid), PMG = poly(malachite green)

4.2 Experimental

4.2.1 Fabrication of PBPB-AuNPs modified GCE

Prior to use, the GCE was cleaned according to the procedure described in section 2.6.1. Electrodeposition of AuNPs on cleaned GCE was achieved in an electrochemical cell with three electrode system in a solution containing 5.0×10^{-2} M H_2SO_4 and 1.0×10^{-3} M $HAuCl_4$ prepared in water. Twenty cyclic scans were carried out between 0 to 1.30 V at a scan rate of

0.10 V/s (Figure 4.2).[111] During the deposition process, an oxidation peak at 1.15 V and a reduction peak at 0.77 V were obtained and peak currents were increased after each scan, indicating the formation of AuNPs on the surface of GCE. The modified electrode was washed with water and allowed to dry.

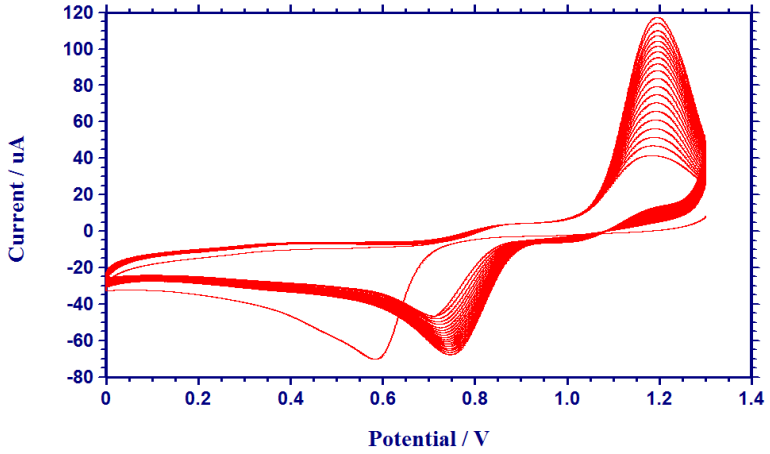

Figure 4.2: Cyclic voltammograms obtained for electrodeposition of AuNPs on GCE.

AuNPs/GCE was further modified with a polymer film of bromophenol blue (BPB) using a previously reported procedure.[134] The AuNPs/GCE was dipped in a 5.0×10^{-4} M solution of BPB in 0.1 M phosphate buffer of pH 6.0, and potential scanned between -1.00 to 1.80 V for 10 cycles at a scan rate of 0.10 V/s (Figure 4.3). Obtained oxidation peak at 0.74 V, corresponding to the oxidation of hydroxyl group of BPB and the reversible reduction peak at 0.14 V imply the formation of polymer film on the surface of AuNPs/GCE. Modified electrode was washed with water and dried in air.

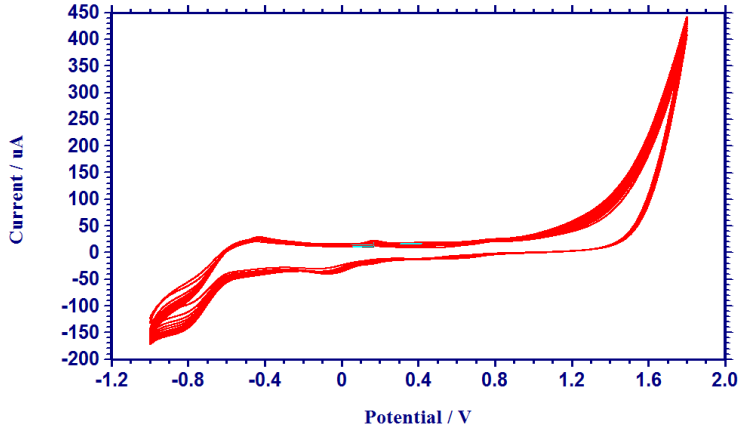

Figure 4.3: Cyclic voltammograms obtained for electropolymerisation of BPB on GCE.

4.2.2 Experimental procedure

Square wave voltammograms were recorded from – 0.40 to 0.30 V (potential increment of 0.004 V and amplitude of 0.025 V) in 0.1 M NaOH solution. The oxidation signal of UA was measured at a potential of -0.08 V. SWV showed a well-defined oxidation peak with lower potential and higher peak current compared to CV, DPV and LSV. Hence, SWV was selected for all the experiments unless otherwise stated.

Impedimetric measurements were carried out in 5 mM $K_3[Fe(CN)_6]$ in 1 M KCl. Impedance spectra were recorded over a frequency range from 100 kHz to 1 Hz with an amplitude of 0.005 V. The measurements were performed at formal redox potential of $[Fe(CN)_6]^{3-}$ and obtained spectra were fitted using ZSimpWin software (version 3.21, Michigan, USA).

4.2.3 Measurement of UA in artificial biological samples

Artificial blood serum and urine samples were prepared as discussed in section 2.4. Prepared samples were spiked with UA solution within the linear range of proposed method and used for further analysis. Amount of UA was estimated from linear calibration graph. Besides, Folin's colorimetric test[95] was also conducted according to the procedure described in section 2.3.2 and the obtained results were compared with that of the developed method.

4.3 Results and discussion

4.3.1 Characterization of PBPB/AuNPs/GCE

AFM and SEM analyses were carried out to study the changes occurred at electrode surface prior to and after modification. AFM images of bare GCE, AuNPs/GCE and PBPB/AuNPs/GCE are shown in Figure 4.4. From the Figure, it is evident that morphology of electrode surface is changed during modification. Alteration in magnitude of area roughness (23.86 nm, 37.01 nm, 108.98 nm and 45.26 nm for bare GCE, AuNPs/GCE, $PBPB_{(10\ cycles)}$/AuNPs/GCE and $PBPB_{(20\ cycles)}$/AuNPs/GCE respectively) represents changes during modification.

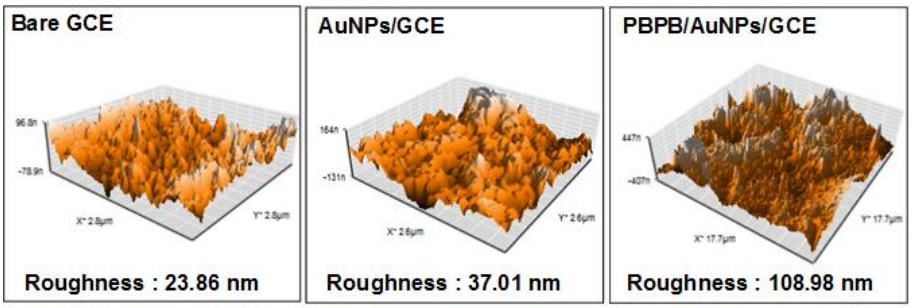

Figure 4.4: AFM images of bare and modified GCE.

SEM images (Figure 4.5) also supports findings obtained from AFM studies. From the Figure, smooth and uniform surface of bare GCE can be envisaged and this uniform surface was changed to rough and porous upon deposition of AuNPs (white colored particles) and film of PBPB (gray colored sheets). These observations confirm the successive modification of GCE surface.

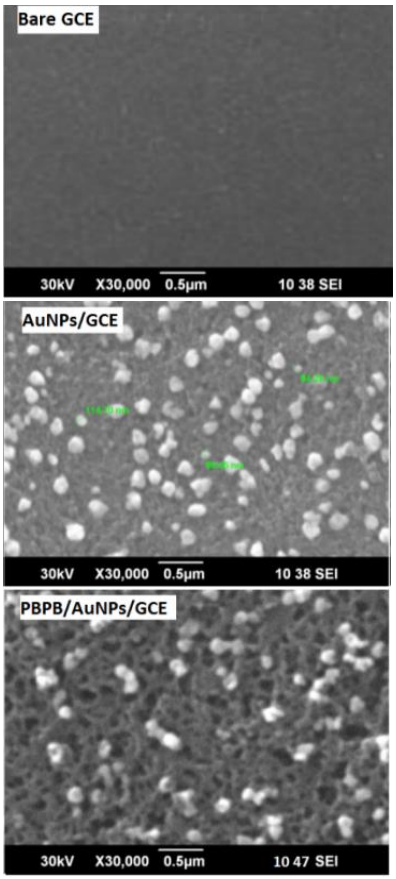

Figure 4.5: SEM images of bare and modified GCE.

In electrochemical impedance spectroscopic (EIS) measurements (Figure 4.6), after modification, diameter of semicircle was decreased noticeably (R_{ct} = 248.9 ohm) in comparison to bare GCE (R_{ct} = 641.1 ohm),

indicating that AuNPs/PBPB composite layer could facilitate electron transfer of $[Fe(CN)_6]^{3-/4-}$. Thus, EIS studies proved that, electro-catalytic capacity of the GCE was largely improved upon modification.

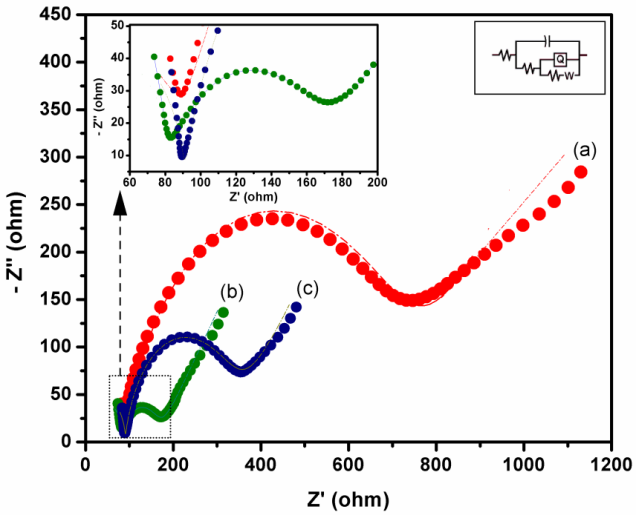

Figure 4.6: Electrochemical impedance spectra of (a) bare, (b) AuNPs and (c) PBPB/AuNPs modified GCE. (●) found spectra and (-) the best fit of the equivalent circuit diagram.

As additional evidence for the effective modification, effective surface area of bare and modified GCE were calculated using Randles – Sevcik equation for reversible systems.[120]

$$I_p = 2.69 \times 10^5 A D_R^{1/2} n^{3/2} \nu^{1/2} C$$

By recording CV's of 2.0×10^{-3} M $K_3[Fe(CN)_6]$ on bare GCE (Figure 4.7) and modified GCE (Figure 4.8) at different scan rates and using the obtained slope of the graph I_p vs $\nu^{1/2}$, effective surface area of the electrodes were calculated. Effective surface area of bare GCE and PBPB/AuNPs/GCE were found to be 0.078 to 0.096 cm^2 respectively. Increased effective surface

area of GCE after the electrochemical treatments clearly shows the successive modification of electrode surface.

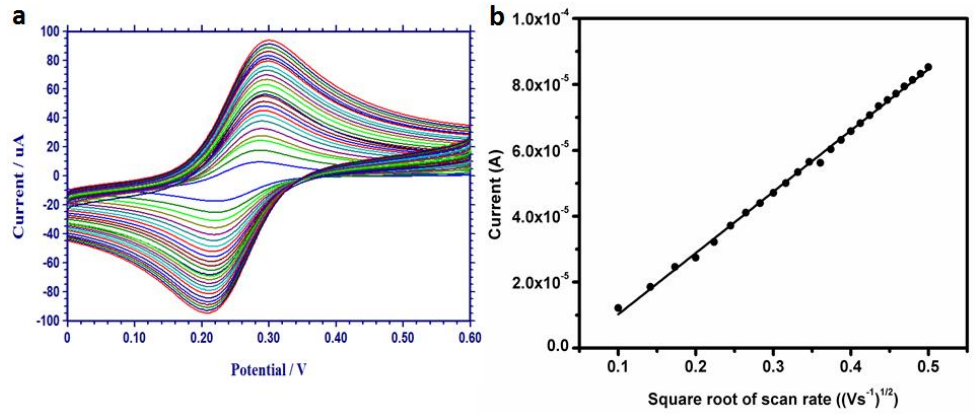

Figure 4.7: (a) Overlay of cyclic voltammograms of 2.0 × 10^{-3} M $K_3[Fe(CN)_6]$ on bare GCE at various scan rates (b) plot of peak current *vs* square root of scan rate.

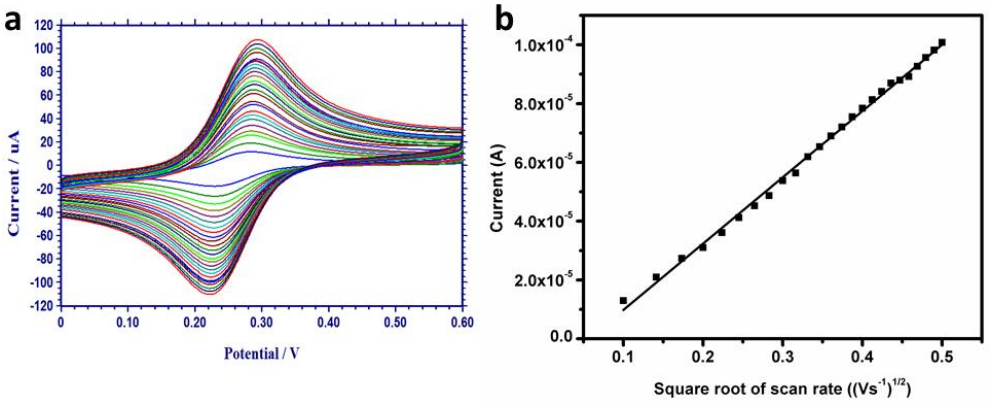

Figure 4.8: (a) Overlay of cyclic voltammograms of 2.0 × 10^{-3} M $K_3[Fe(CN)_6]$ on PBPB/AuNPs/GCE at various scan rates (b) plot of peak current *vs* square root of scan rate.

4.3.2 Electrochemical behavior of Uric acid

Figure 4.9 shows overlay of square wave voltammetric (SWV) responses of 1.0×10^{-3} M UA on surface of bare GCE and modified GCE. At bare GCE, UA gave an anodic peak at a potential of 0.52 V with a peak current of 5.3×10^{-7}A. This weak response may be due to slow electron transfer, while an improved response is obtained at PBPB/AuNPs/GCE with a drastic reduction in the overpotential and significant enhancement (~25 times) in the peak current (-0.080 V potential with a peak current of 1.37×10^{-5} A). This may be due to the synergic effect of AuNPs and polymer layer on the surface of the electrode. Moreover, cyclic voltammetric response of UA showed only one (anodic) peak - corresponding to an irreversible oxidation process.[27]

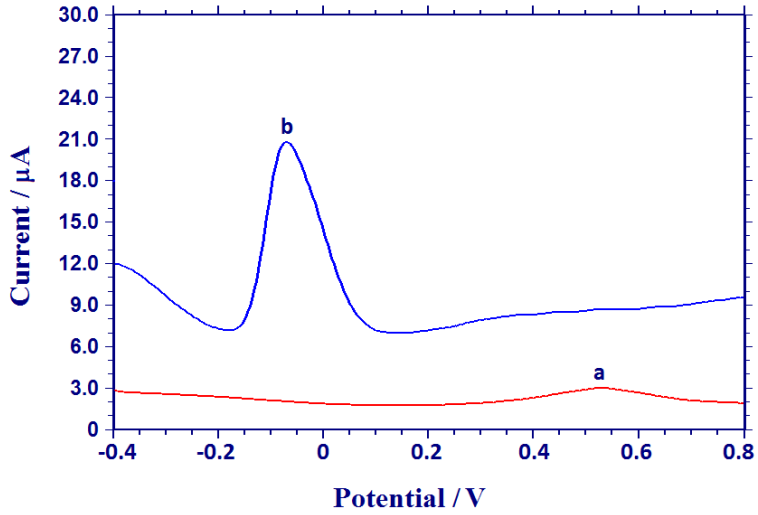

Figure 4.9: Overlay of SWVs of 1.0×10^{-3}M UA at (a) bare and (b) PBPB/AuNPs/GCE.

4.3.3 Optimization of experimental conditions

4.3.3.1 Influence of supporting electrolyte

Selection of suitable supporting electrolyte is significant since it can affect the mass transfer kinetics and thermodynamics of electrochemical processes.[117] The electrochemical response of UA at PBPB/AuNPs/GCE in different supporting electrolytes (0.1 M) such as acetate buffer, phosphate buffer, citrate buffer, NaOH, NaCl and HCl were studied. The lowest oxidation potential was attained for 0.1 M NaOH and hence it was chosen as the supporting electrolyte.

4.3.3.2 Number of cycles for electrode modification

The number of scan cycles of electro-deposition/electro-polymerization is proportional to the thickness of composite film. Influence of film thickness (AuNPs - PBPB composite) on the oxidation peak current of 1.0×10^{-4} M UA was examined by varying the scan cycles of electrodeposition. On increasing the scan cycles of electrodeposition of AuNPs, an increase in peak current was observed and maximum value was obtained at 20 cycles (Figure 4.10). Further increase in scan cycles results in a decrease in peak current. This may be due to the decreased electron transfer rate by the decrease in active surface area, which might be associated with aggregation of AuNPs on electrode surface.[118] The thickness of polymer film, suited for the quantification of UA was optimized by varying the number of cycles of polymerization. The maximum peak current was obtained when the number of cycles of polymerization was 10 (Figure 4.11).

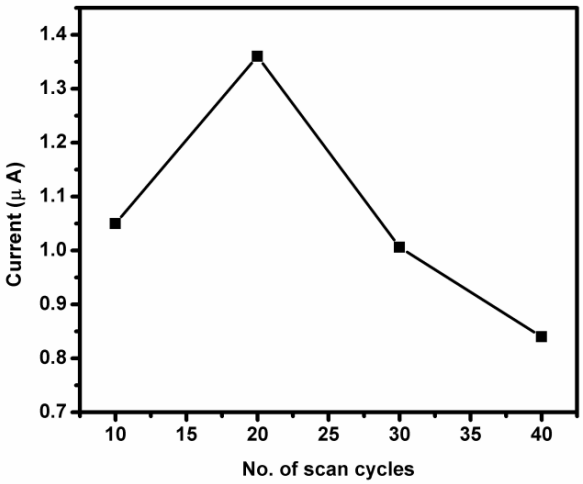

Figure 4.10: Influence of number of cycles of electro-deposition of AuNPs on GCE in the determination of 1.0×10^{-4} M UA.

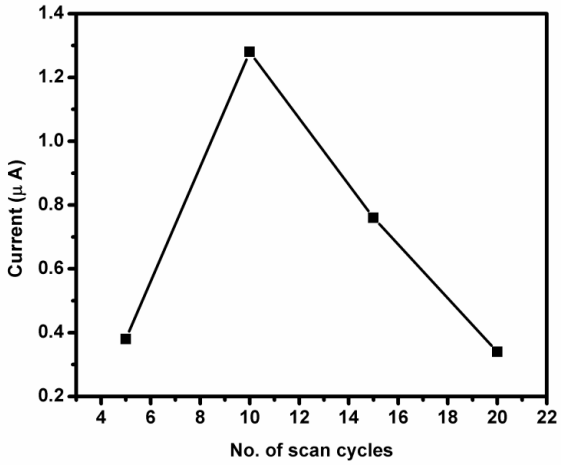

Figure 4.11: Influence of number of cycles of electro-polymerization of BPB on GCE in the determination of 1.0×10^{-4} M UA.

Beyond 10 cycles, the peak current decreases. The increase in film thickness (Figure 4.12 (a and b)) may reduce the approach of electrons from electrode surface to the bulk. So scan cycles for the deposition of AuNPs and for the polymerization were optimized to 20 and 10 cycles respectively.

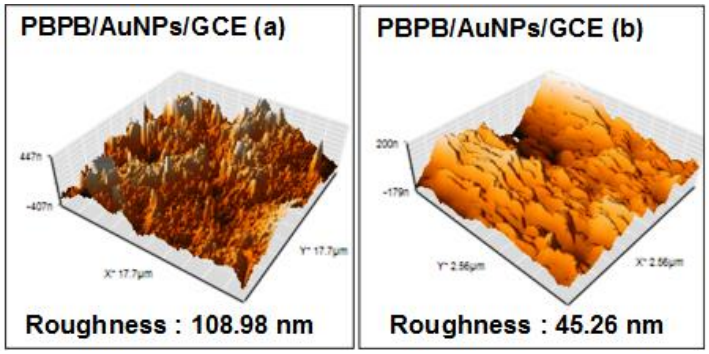

Figure 4.12: AFM images of PBPB modified AuNPs/GCE, (a) at 10 cycles of polymerization and (b) at 20 cycles.

4.3.4 Effect of scan rate on the electrode process

Variation of oxidation peak parameters with scan rate (ν) in linear sweep voltammetric (LSV) mode was studied. Oxidation peak of UA showed a positive shift on increase in scan rate from 0.01 to 0.15 V/s, which confirms the irreversible character of oxidation process.[117] Figure 4.13 represents linear sweep voltammogram of 3.0×10^{-4} M UA at various scan rates (0.01 – 0.15 V/s) and figure 4.14 shows relationship of square root of scan rate with peak current (i_p).

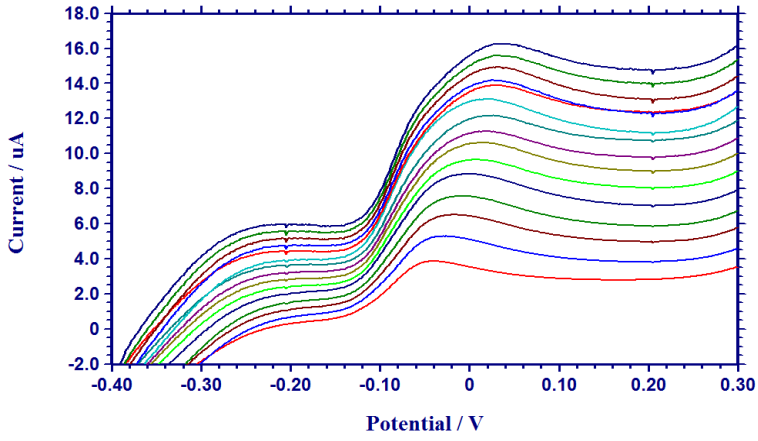

Figure 4.13: Overlay of LSVs for oxidation of UA at different scan rates.

This linear relationship endorses diffusion controlled mechanism for oxidation of UA.[25, 135] Moreover, plot of ln i_p vs. ln ν (Figure 4.15) is found to be linear with a slope of 0.503 which is very close to theoretical value of 0.50 for a diffusion controlled process.[119] These results confirm that the electro oxidation process is diffusion controlled.

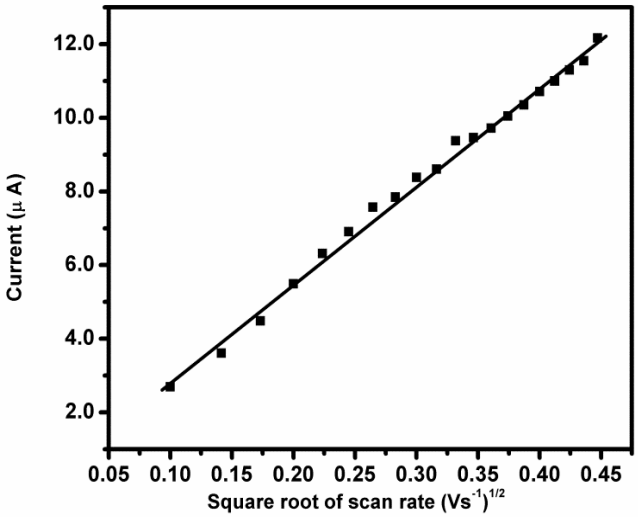

Figure 4.14: Plot of peak current vs. square root of scan rate.

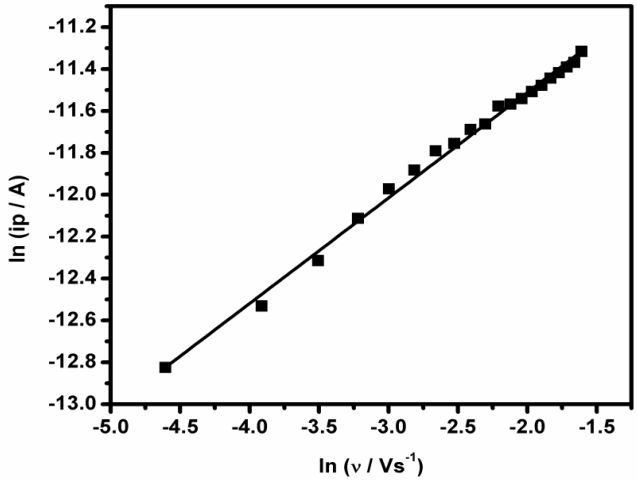

Figure 4.15: Plot of logarithm of peak current vs. logarithm of scan rate.

4.3.5 Calculation of diffusion coefficient

It is believed that charge transfer through electroactive polymer film occurs by electron hopping process.[136] This process was overseen by the Fick's laws of diffusion for a variety of polymer films and find out that the charge transfer was mostly diffusion-controlled at polymer/solution interface.[136] Chronoamperometric studies were conducted to estimate value of diffusion coefficient. Chronoamperograms obtained for various concentrations (1.0×10^{-4} to 8.0×10^{-4} M) of UA are depicted in figure 4.16.

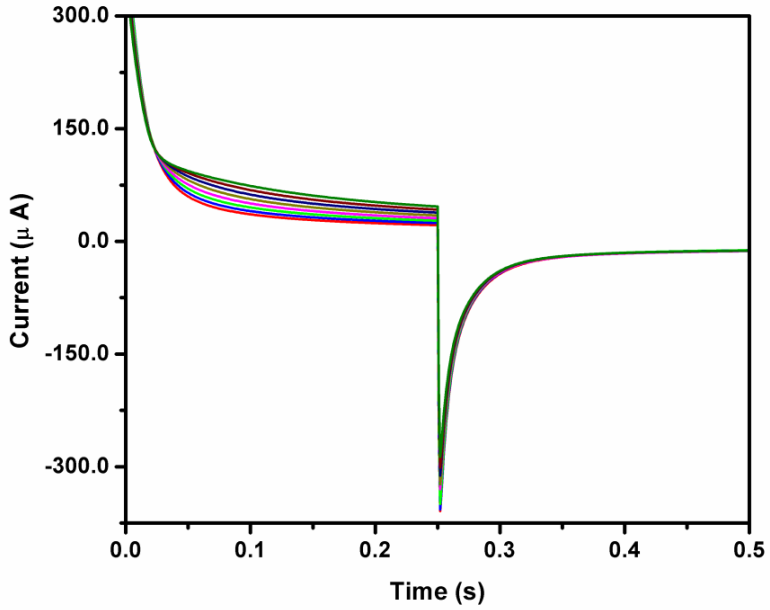

Figure 4.16: Overlay of chronoamperograms of UA at various concentrations.

Cottrellian behaviour was obtained in the plot of electrocatalytic current vs $t^{-1/2}$, which reveals that the current is controlled by diffusion of UA from bulk solution to the surface of PBPB/AuNPs/GCE (Figure 4.17).

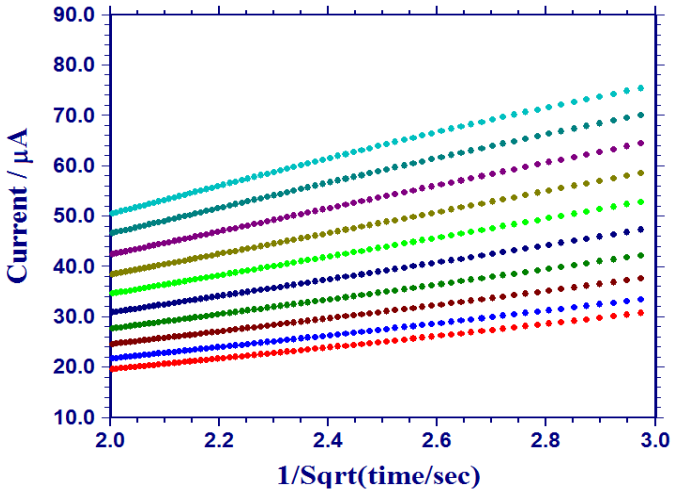

Figure 4.17: Plot of peak current vs. $t^{-1/2}$ derived from the chronoamperograms of UA of figure 4.16.

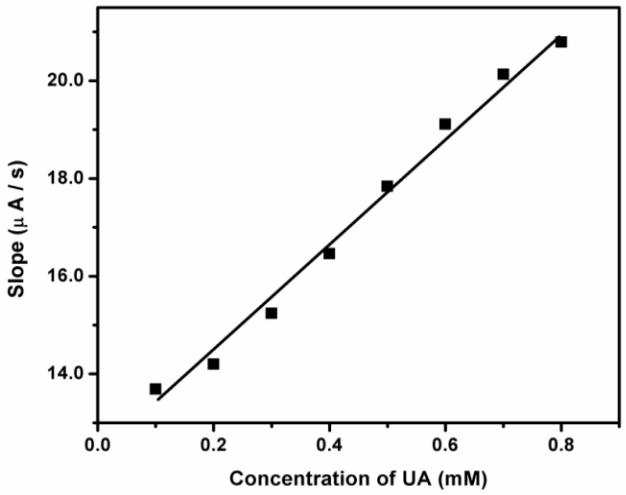

Figure 4.18: Plot of slope of (I vs $t^{-1/2}$) against concentration of UA.

The resulting slope of the plot of 'slopes of above mentioned straight lines vs concentration (C) of UA' (Figure 4.18) was used for the calculation of diffusion coefficient (D) using Cottrell equation.[11]

$$\mathbf{I = nFAD^{1/2}C\pi^{-1/2}t^{-1/2}}$$

Here 'A' is the effective surface area of the electrode (0.0968 cm^2) and the value of D was estimated to be 1.33×10^{-6} cm^2/s.

4.3.6 Determination of UA

Under optimized conditions, SWV responses of different concentrations of UA at PBPB/AuNPs/GCE were studied. Figure 4.19 represents the square wave voltammograms of various concentrations of UA on PBPB/AuNPs/GCE. It is found that the oxidation peak current of UA increases linearly with its concentration in a range of 1.0×10^{-3} M to 2.0×10^{-5} M (Figure 4.20). Limit of detection and limit of quantification were calculated to be 2.2×10^{-6} M and 7.5×10^{-6} M respectively.

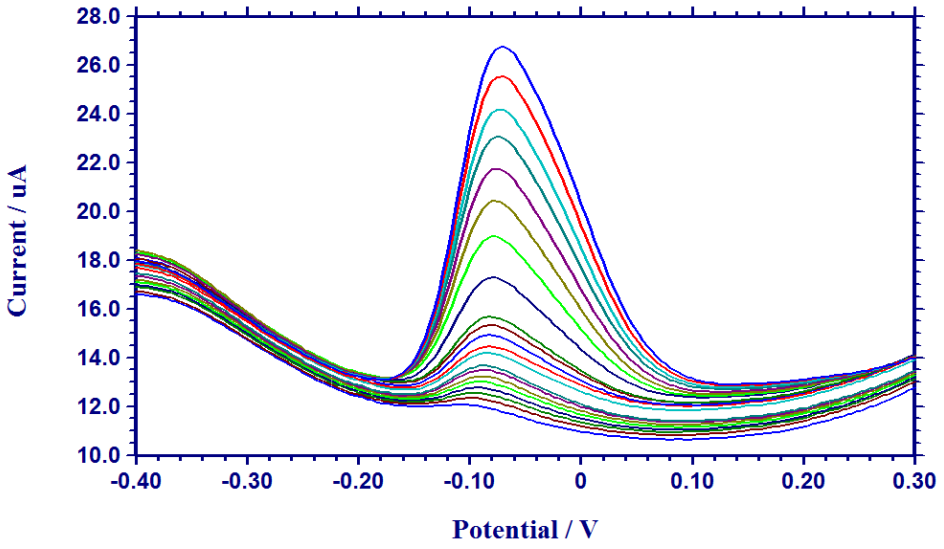

Figure 4.19: Overlay of SWVs for oxidation of UA at various concentrations.

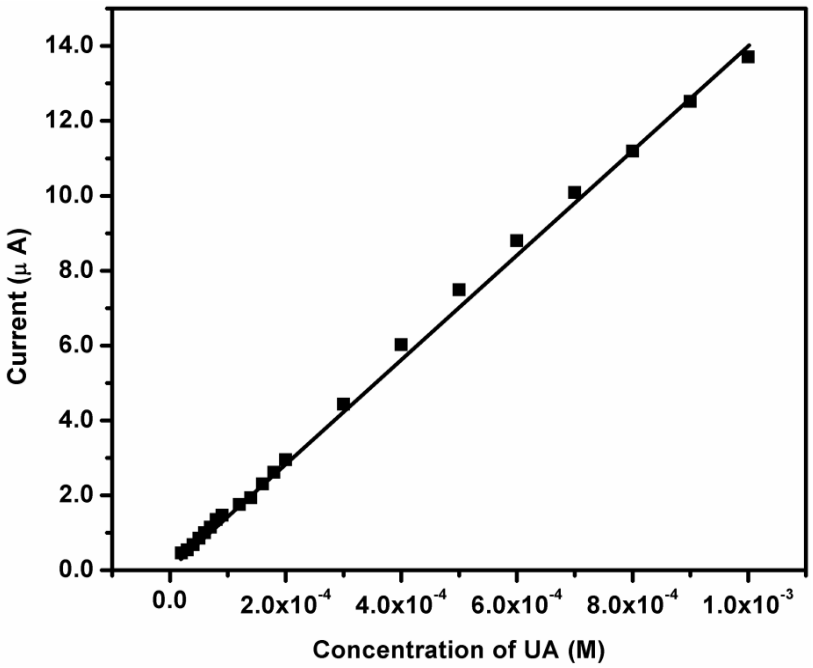

Figure 4.20: Plot of peak current vs. concentration of UA.

Table 4.2 represents the comparison of a number of recent electrochemical sensors for the determination of UA. From Table 4.2, it is clear that, overpotential of the proposed sensor is far superior to existing sensors. Additionally, compared with the previous literatures, the PBPB/AuNPs nanocomposite is easy to prepare and control by in situ deposition / polymerization method.

Table 4.2: Comparison of analytical parameters of proposed sensor with reported voltammetric sensors for UA determination.

Sl. No.	Sensing element	Potential (V)	Linear range (M)	LOD (M)	References
1	Bare CPE	0.64	1.0×10^{-4} to 1.0×10^{-5}	5.6×10^{-6}	137
2	Poly-2,6-Diaminopyridine/CNT/GCE	0.32	2.2×10^{-4} to 4.1×10^{-6}	7.0×10^{-7}	138
3	GCE/GO/polypyrrole/Poly tetraphenyl porphyrin	0.34	2.0×10^{-4} to 5.0×10^{-6}	1.1×10^{-6}	30
4	PdNPs/CM/GCE	0.30	1.3×10^{-5} to 3.2×10^{-6}	6.6×10^{-7}	31
5	Hemin-Reduced GO/GCE	0.41	5.0×10^{-6} to 5.0×10^{-7}	1.7×10^{-7}	139
6	Poly(L-leucine)/DNA/GCE	0.55	1.0×10^{-4} to 5.0×10^{-7}	2.0×10^{-7}	140
7	MWCNT/SPE	0.18	1.0×10^{-4} to 1.0×10^{-6}	-	141
8	CdTe/CPE	0.30	1.4×10^{-3} to 7.5×10^{-6}	2.0×10^{-6}	32
9	GO/ImAS/GCE	0.28	4.0×10^{-4} to 2.0×10^{-5}	5.0×10^{-6}	142
10	PBPB/AuNPs/GCE	-0.10	1.0×10^{-3} to 2.0×10^{-5}	2.2×10^{-6}	Present work

CPE : Carbon paste electrode, GO : Graphene Oxide, PdNPs : Palladium nanoparticles, CNT : Carbon nanotubes, SPE : Screen printed electrode, MWCNT : Multi walled carbon nanotube.

4.3.7 Influence of possible coexisting species

For a sensor to be useful for real time analysis, it should be selective towards a particular analyte ie., the possible coexisting species should produce minimal effect on the signal. To determine effects of foreign species on the determination of 2.0×10^{-5} M UA, some common co-existing substances (which usually show interference) were added with UA and signal changes were studied (Table 4.3). The obtained results show that, only ascorbic acid interferes when present in the same concentration as UA and Dopamine, Norepinephrine, Epinephrine, Creatinine and Homovanilic acid does not make any interference even up to a 100 fold excess concentration.

Table 4.3: Effect of coexistence on the determination of 2.0×10^{-5} M UA.

Coexisting species	Concentration (M)	Interference (%)
Dopamine	2.0×10^{-3}	2.7
Adrenaline	2.0×10^{-3}	0.2
Noradrenaline	2.0×10^{-3}	1.0
Creatinine	2.0×10^{-3}	1.6
Homovanilic acid	2.0×10^{-3}	0.2
Ascorbic acid	2.0×10^{-5}	38.3

4.3.8 Possible mechanism of the electro-oxidation process

The number of electrons involved in the oxidation process was calculated to ascertain the mechanism. For this, charge transfer coefficient α_a to be calculated. According to the latest considerations of IUPAC,[143]

$$\alpha_a = \left(\frac{RT}{F}\right) \cdot \left(\frac{d\ln|j|}{dE}\right)$$

where α_a is the anodic charge transfer coefficient, j is current density, *F*, *R*, and *T* have their usual significance. The term ($d\ln|j|/dE$) is the slope of plot ($ln|j|$ *vs E*) (Figure 4.21). By knowing other quantities, value of 'α_a' was calculated to be 0.51, which is in hand with theoretical value, 0.50.[32]

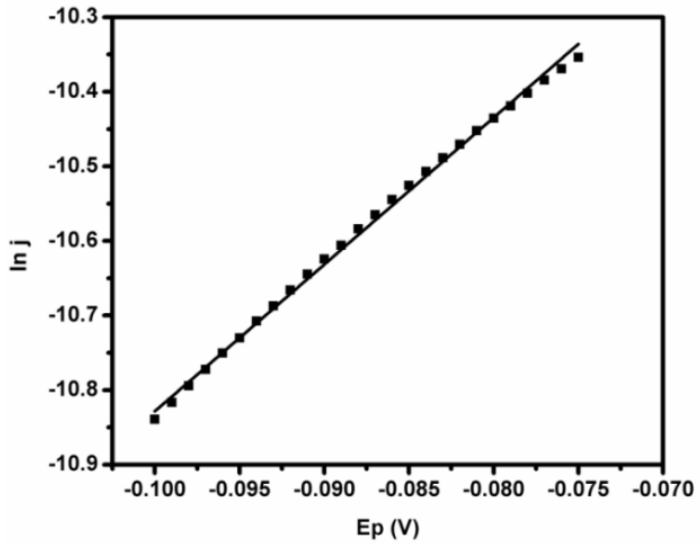

Figure 4.21: Plot of natural logarithm of current density against peak potential.

According to Bard and Faulkner,[11] n and α_a can be related as,

$$(1 - \alpha_a)n = \frac{47.7}{\left(E_P - E_{p_{1/2}}\right)}$$

Where, n is number of electrons involved, E_P and $E_{P1/2}$ are potential and half peak potentials respectively. Substituting the known quantities, number of electrons is calculated to be 2.04, which is in agreement with that of earlier report (~ 2).[138] The proposed mechanism is given in scheme 4.2.

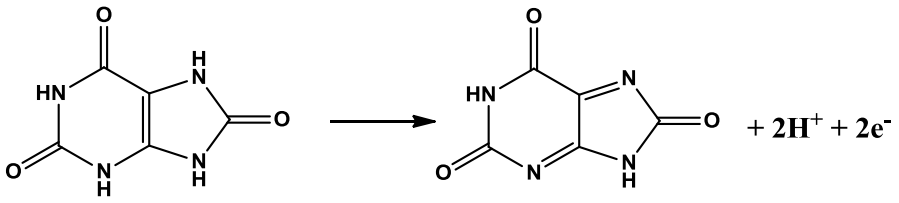

Scheme 4.2: Mechanism of electrooxidation of UA.

4.3.9 Repeatability, reproducibility and stability

The repeatability of the sensor is tested by taking five consecutive measurements using same PBPB/AuNPs/GCE electrode in 2.0×10^{-5} M UA solution under optimized conditions. The relative standard deviation (RSD) was calculated to be ± 3.8 %. Similarly, reproducibility of the developed sensor was studied by performing five replicate measurements using five different PBPB/AuNPs/GCE electrodes and RSD was calculated to be ± 2.4 %. Moreover, on analysis of stability of PBPB/AuNPs/GCE, anodic peak current for UA remains unchanged up to three days. Hence, the proposed sensing strategy is precise and liable for determination of UA.

4.3.10 Application studies

Determination of UA in artificial blood serum and urine samples were carried out in order to evaluate the utility of developed sensor in real sample analysis. In order to validate the proposed method, Folin's colourimetric test[95] was conducted and the results are given in Table 4.4. The recoveries of proposed method are in good agreement with those of reference and this establishes the feasibility of the developed sensor for real samples analysis.

Table 4.4: Determination of UA in artificial biological samples

Samples	Added (M)	Proposed method			Folin's colorimetry		
		Found (M)	R (%)[a]	RSD[a]	Found (M)	R (%)[a]	RSD[a]
Urine	2.00×10^{-5} to 1.00×10^{-3}	2.05×10^{-5} to 9.87×10^{-4}	100	2.1	2.08×10^{-5} to 9.90×10^{-4}	101	1.9
Blood serum	2.00×10^{-5} to 1.00×10^{-3}	2.04×10^{-5} to 9.90×10^{-4}	100	0.5	2.05×10^{-5} to 9.80×10^{-4}	100	2.2

[a]From six measurements, R = recovery, RSD= relative standard deviation

4.4 Conclusions

A PBPB/AuNPs/GCE was fabricated and found to have better electron transport and catalytic efficiency towards the oxidation of uric acid compared to the bare GCE. The presence of PBPB and AuNPs shows a decrease in oxidation potential, enhancement in peak current, micro-molar level detection limit, reproducibility, repeatability and good recovery. The modified electrode was successfully used for the determination of UA in artificial blood serum and urine samples. The obtained results proved the proposed electrode as an effective voltammetric sensor for determination of UA in physiological solutions.

.....ꕥ.....

Chapter 5

NICKEL NANOPARTICLES BASED VOLTAMMETRIC SENSOR FOR PROPYL GALLATE

Contents

This chapter comprises of the fabrication of a voltammetric sensor for the synthetic phenolic antioxidant - propyl gallate (PG). The present study proposes the development of a cost-effective voltammetric sensor for PG using nickel nanoparticles (NiNPs). As proof-of-concept, the surface of glassy carbon electrode were coated with nickel nanoparticles via electrodeposition and used for the determination of PG. Using the signal amplification strategy, PG as low as 5.8×10^{-8} M could be detected. Under optimized experimental conditions, two linear ranges could be observed from 1.0×10^{-3} M to 4.0×10^{-4} M and 3.0×10^{-4} M to 2.0×10^{-6} M. Developed method was used for the quantification of PG in commercial food samples and the results were in agreement with those obtained from standard spectrophotometric method.

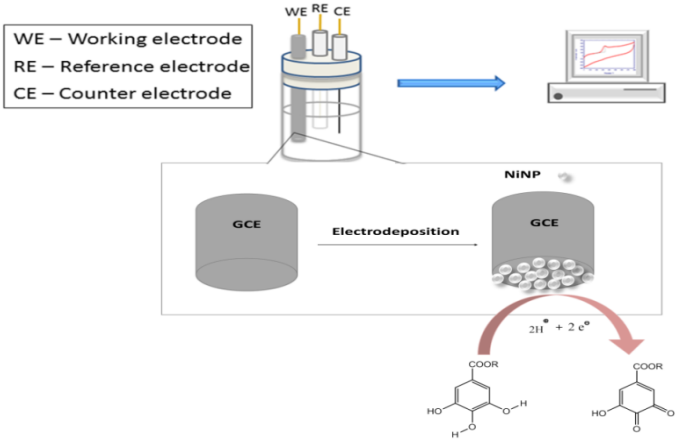

Scheme 5.1: Diagrammatic representation of sensing process.

5.1 Introduction

Propyl gallate (PG) is a commonly used synthetic phenolic antioxidant in food products to prevent rancidity, and discoloration caused by oxidation.[144] Among the various phenolic antioxidants available, PG (Figure 5.1) is widely used due to its special characteristics such as high performance, stability and wide availability.

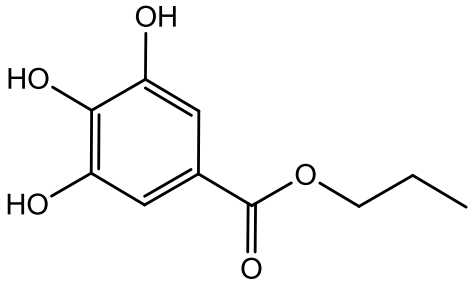

Figure 5.1: Chemical structure of PG.

PG is usually added in food stuffs such as edible oils, margarine, lard, food concentrates etc.[28] Even though antioxidants protect the food products from damage, excess use of these products can result in potential health problems.[145,146] As per the international organization JECFA (Joint FAO/WHO Expert Committee on Food Additives) the permissible intake of PG on a daily basis is 0 – 2.5 mg kg^{-1} of body weight.[147] Studies show that, PG can cause health problems such as irritation of stomach and skin, allergic reactions that constrict breathing.[148] PG is degraded in intestine to gallic acid and propanol, and the gallic acid can cause eczema and hyperactivity.[149] It can also cause liver and kidney problems.[150] Studies on rats have shown that propyl gallate may cause cancer.[150] Therefore the

detection and/or determination of this antioxidant in food products is important.

Based on the above facts, this work was targeted to develop a cost effective voltammetric sensor for the selective and sensitive determination of PG using a modified glassy carbon electrode (GCE). Among the various chemical modifications on GCE studied (Table 5.1), higher peak current with lower overpotential was established with nickel nanoparticles (NiNPs) modified GCE. So NiNPs/GCE was selected for the quantification of PG. The suitability of the present method was established for the determination of PG in food products.

Table 5.1: Comparison of a number of modifications studied for determination of 1.0×10^{-4} M PG in 0.1 M PBS pH 8.

Modified electrode	Potential (V)	Current (A)
Fe_3O_4NPs/GCE	-	-
ZrO_3NPs/GCE	-	-
AuNPs/GCE	0.50	1.73×10^{-6}
PtNPs/GCE	0.61	4.50×10^{-7}
NiNPs/GCE	0.09	3.67×10^{-6}

5.2 Experimental

5.2.1 Preparation of NiNPs modified GCE

Before modification, GCE was cleaned according to the procedure detailed under section 2.6.1. Potentiostatic deposition of NiNPs on cleaned GCE was carried out (Figure 5.2) from 0.2 M solution of $NiSO_4$ containing 1 M H_2SO_4 by applying a potential of −1.25 V for 1000 s.[29] Modified

electrode was washed twice with double distilled water and dried in a flow of N_2 gas.

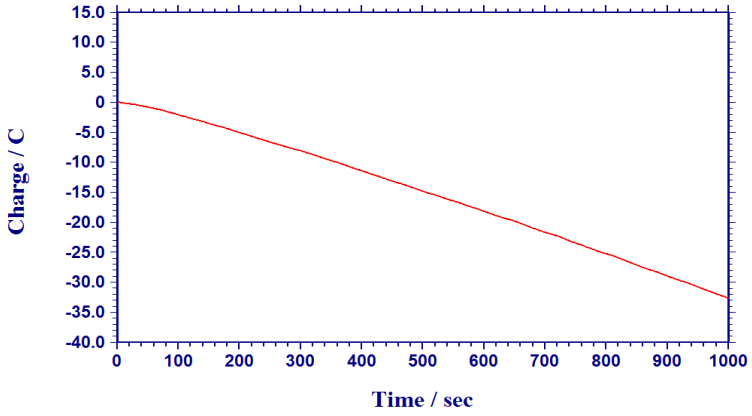

Figure 5.2: Electrodeposition of NiNPs on GCE using bulk electrolysis.

5.2.2 Experimental procedure

Unless otherwise stated, 0.1 M phosphate buffer solution (PBS) of pH 8.0 was used as the supporting electrolyte. Electrode was activated by 20 cyclic scans between −0.40 to 0.30 V in PBS 8.0. Then a suitable amount of PG was added (to obtain 1.0×10^{-3} M to 2.0×10^{-6} M) and differential pulse voltammogram (DPV) was recorded from −0.40 V to 0.30 V with pulse amplitude of 0.50 V, pulse width of 0.2 s, pulse period of 0.5 s and a potential step of 0.004 V. Signal for the oxidation of PG was measured at a potential of -0.10 V.

Electrochemical impedance spectroscopic studies were carried out in 5.0×10^{-3} M $K_3[Fe(CN)_6]$ containing 1.0 M KCl over a frequency range from 100 kHz to 1 Hz with an amplitude of 0.005 V, at formal redox potential of $[Fe(CN)_6]^{3-}$. Obtained spectra were fitted using ZSimpWin software (version 3.21, Michigan, USA).

5.2.3 Sample preparation and determination

Sunflower oil, coconut oil and Margarine samples were procured from a local market. Five grams of the sample was dissolved in appropriate volume of hexane (60 mL), and suitable amount of PG was spiked in it. PG was then extracted five times using acetonitrile (5 × 40 mL). Acetonitrile extract was evaporated to dryness in vacuum at less than 40 °C. Then, the residue was dissolved in 10 mL methanol and 100 µL aliquot of this sample solution was used for the determination.[94,112] Furthermore, a spectrophotometric method[94] was also conducted to each sample extract using the procedure described under section 2.3.1 for comparison.

5.3 Results and Discussion

5.3.1 Characterization of NiNPs/GCE

Modified electrode surface was characterized using scanning electron microscopy (SEM), atomic force microscopy (AFM) and electrochemical impedance spectroscopy (EIS). Figure 5.3 (a, b) displays the SEM images of bare and NiNPs modified GCE, where white colored particles represent the deposited NiNPs.

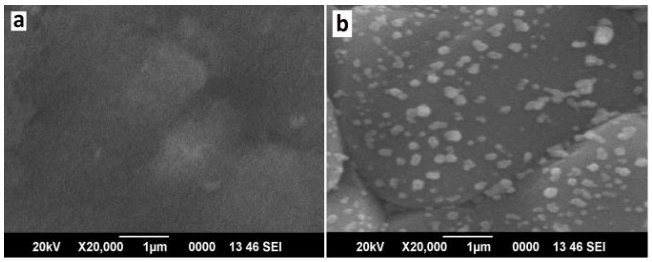

Figure 5.3: SEM images of (a) bare GCE and (b) NiNPs/GCE.

AFM images (Figure 5.4 (b, c)) also supports the observations about surface morphology of bare and modified electrode, which implies the

change in surface roughness (area roughness) during modification. From these images it could be clearly seen that NiNPs are well fixed and dispersed uniformly on the surface of GCE.

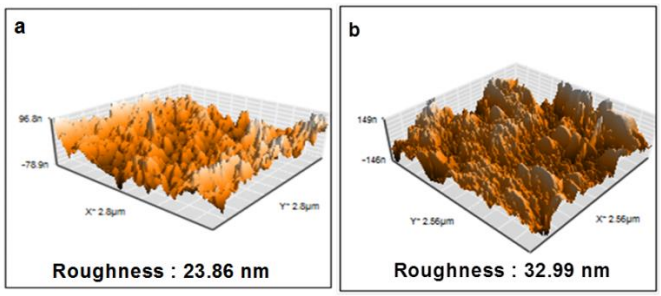

Figure 5.4: AFM images of (a) bare GCE and (b) NiNPs/GCE.

Figure 5.5 shows the Nyquist plots of bare GCE (a) and NiNPs/GCE (b) in presence of $[Fe(CN)_6]^{4-}/[Fe(CN)_6]^{3-}$ redox couple (in 0.1 M KCl). Compared to bare GCE (electron transfer resistance, Rct = 641.1 ohm), NiNPs/GCE shows a very small semicircle (Rct = 85.9 ohm) at the high frequency region indicating its enhanced electron transfer properties.[28]

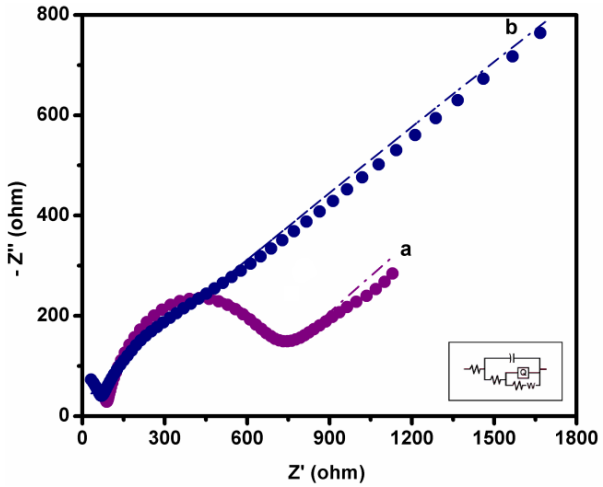

Figure 5.5: Nyquist plots of (a) bare GCE and (b) NiNPs/GCE, (●) obtained spectra and (-) the best fit of the equivalent circuit diagram.

Effective modification of GCE was further evidenced by surface area calculation using Randles – Sevcik equation for reversible systems.[120]

$$I_p = 2.69 \times 10^5 A D_R^{1/2} n^{3/2} \nu^{1/2} C$$

CVs of 2.0×10^{-3} M $K_3[Fe(CN)_6]$ on bare GCE (Figure 5.6) and modified GCE (Figure 5.7) at different scan rates were recorded. By substituting the slope of the graph of peak current (I_p) against square root of scan rate ($\nu^{1/2}$) and other quantities such as diffusion coefficient (D), concentration (C) and number of electrons (n) in Randles – Sevcik equation, effective surface area of the electrodes were calculated. The obtained surface area of bare GCE and PBPB/AuNPs/GCE were found to be 0.078 and 0.152 cm^2 respectively. Enhancement in effective surface area of GCE after electrodeposition clearly shows the modified electrode surface.

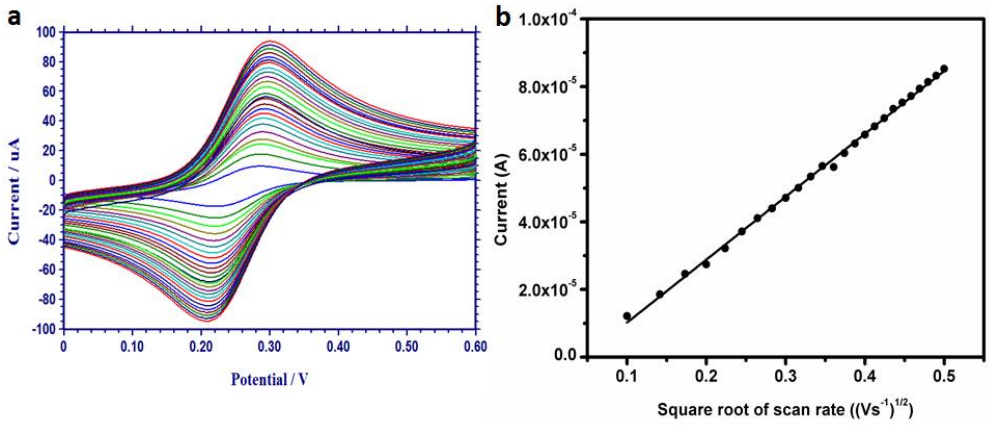

Figure 5.6: (a) Overlay of cyclic voltammograms of 2.0×10^{-3} M $K_3[Fe(CN)_6]$ on bare GCE at various scan rates (b) plot of peak current *vs* square root of scan rate.

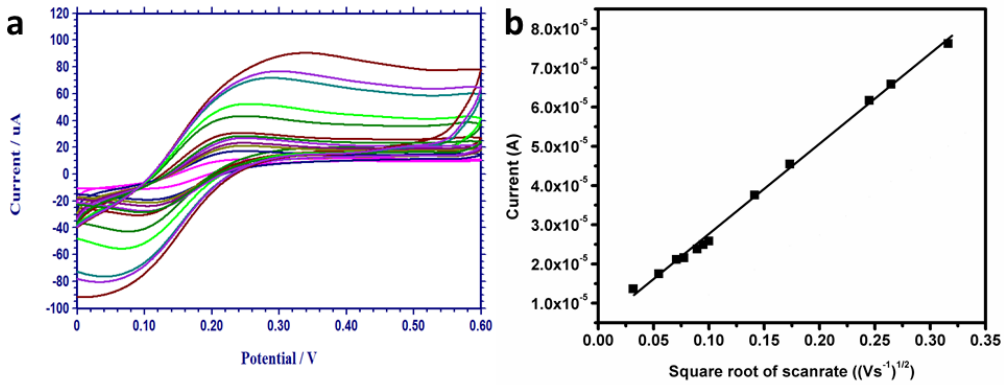

Figure 5.7: (a) Overlay of cyclic voltammograms of 2.0×10^{-3} M $K_3[Fe(CN)_6]$ on NiNPs/GCE at various scan rates (b) plot of peak current *vs* square root of scan rate.

5.3.2 Electrochemical behavior of PG

Since DPV showed a more defined oxidation peak with a higher peak current and lower peak potential compared to cyclic voltammetry (CV), linear sweep voltammetry (LSV) and square wave voltammetry (SWV), DPV was chosen for all the experiments. Figure 5.8 shows a comparison of the DPV of PG on bare GCE (a = 1.0×10^{-5} M, c =1.0×10^{-4} M) and NiNPs/GCE (b = 1.0×10^{-5} M, d = 1.0×10^{-4} M), in 0.1 M PBS (pH 8.0). At lower concentration (1.0×10^{-5} M), no response was obtained at bare GCE (a) whereas, an oxidation peak at 0.09 V (b) was obtained at NiNPs/GCE. At higher concentration (1.0×10^{-4} M), bare electrode also showed an oxidation peak at 0.19 V with 4.0×10^{-6} A current (c). But the oxidation of PG at modified electrode produced a better electrochemical response (d) compared to bare GCE. For NiNPs/GCE, a remarkable decrease (~ 50 %) in over potential and significant increase (~ 61%) in peak current was observed. All these results elucidate that oxidation of PG can be effectively catalyzed by

the modifier NiNPs. In the CV, only an oxidation peak was observed that represents an irreversible process of oxidation.

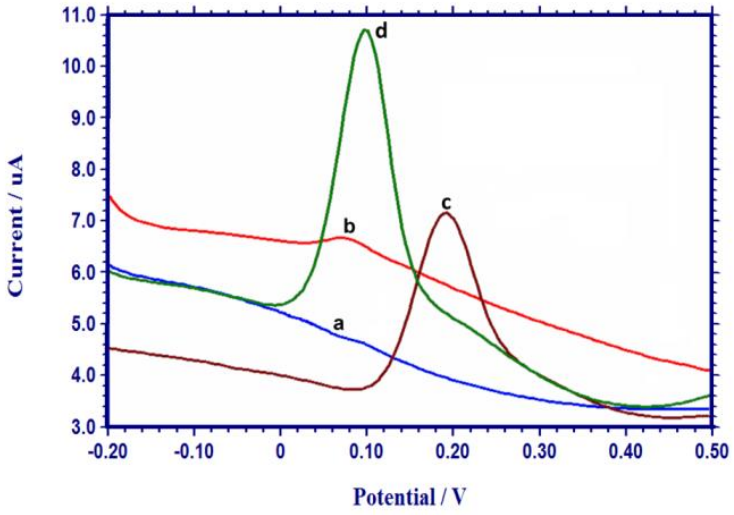

Figure 5.8: Overlay of DPVs of PG at bare GCE (a = 1.0×10^{-5}M, c = 1.0×10^{-4}M) and NiNPs/GCE (b = 1.0×10^{-5}M, d = 1.0×10^{-4}M).

5.3.3 Optimization of experimental conditions

5.3.3.1 Selection of supporting electrolyte

Oxidation process of PG in various electrolytes (0.1 M) such as acetate buffer, citrate buffer, phosphate buffer, hydrochloric acid, sulphuric acid and sodium hydroxide were studied. PBS was selected as the supporting electrolyte as it gave the lowest oxidation potential with a high current.

5.3.3.2 pH of the supporting electrolyte

Effect of pH of (0.1 M) PBS on oxidation of PG (1.0×10^{-5} M) was studied by recording DPV at different pH (4.0 to 9.0). On increasing the pH from 4.0 to 8.0, oxidation peak current increases with decrease in oxidation

potential and beyond pH 8.0, peak current decreases (Figure 5.9). Thus, pH 8.0 was selected as the optimum pH for the analysis.

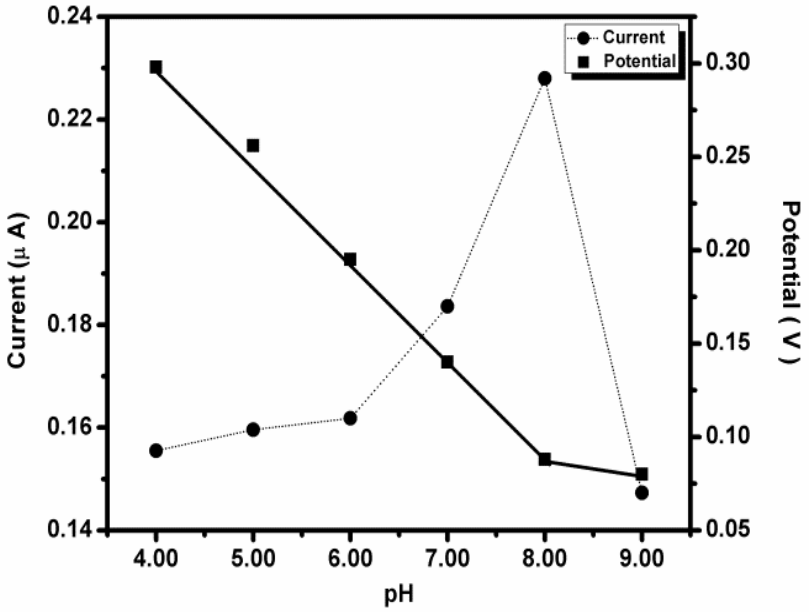

Figure 5.9: Effect of pH of supporting electrolyte (0.1 M PBS) on the oxidation peak current and peak potential of PG.

5.3.3.3 Optimization of time for electrodeposition

In order to optimize the time for electrodeposition of the modifier NiNPs, GCE is modified by potentiostatic electrolysis at various time intervals (30 s to 1000 s) and used for the quantification of PG. It was observed that when the time interval increases up to 400 s oxidation peak current increases, and remains almost same beyond 400 s (up to 1000 s). But upon repeated use (3 to 6 runs) of the modified electrode, oxidation peak current decreases rapidly if the deposition time was 400 s. This may be due to the detachment of NiNPs from the electrode surface. This problem can be overcome when GCE is modified with a 1000 s deposition. Modification at

1000 s allows the determination up to 12 times. Therefore, the optimal time for electrodeposition was taken as 1000 s.

5.3.4 Effect of scan rate

Effect of scan rate (ν) on electro-oxidation of PG (5.0×10^{-5} M), in 0.1 M PBS (pH 8.0) on NiNPs/GCE was studied by linear sweep voltammetry (LSV). The results revealed that when the scan rate is increased from 0.01 to 0.20 V/ s, the oxidation peak of PG showed a positive shift (Figure 5.10), which endorses that the oxidation process is irreversible in nature.[27] Figure 5.11 displays the relationship of square root of ν with peak current (i_p). This linear relationship authenticates the diffusion controlled mechanism of oxidation.[25,135]

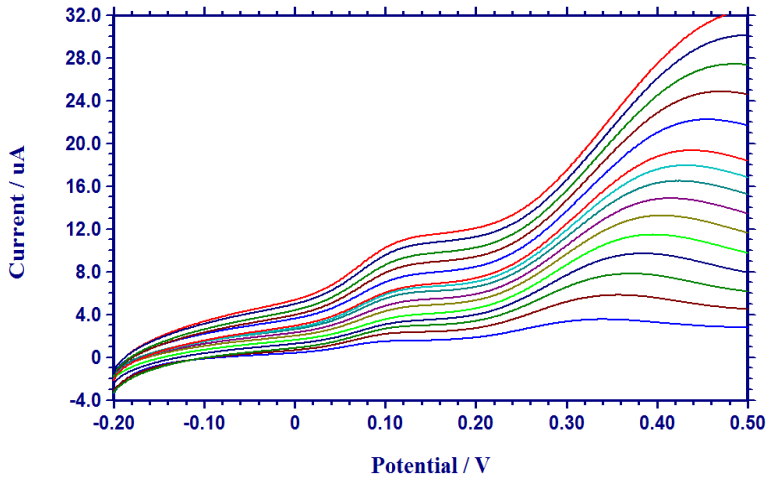

Figure 5.10: Overlay of LSVs of PG oxidation at different scan rates.

Also, plot of ln ν with ln i_p (Figure 5.12) is found to be linear with a slope of 0.48 which is around the theoretical value of 0.50 for a diffusion controlled process.[119] All these results endorse that the oxidation of PG on the surface of NiNPs/GCE was diffusion controlled.

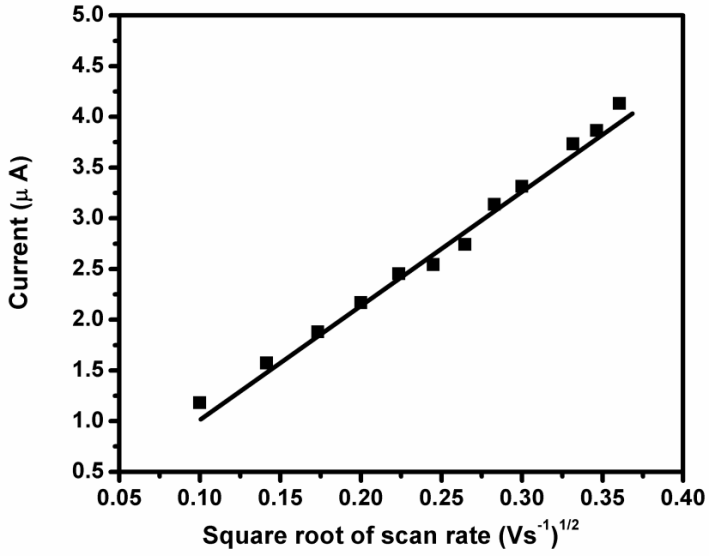

Figure 5.11: Plot of oxidation peak current vs. square root of scan rate.

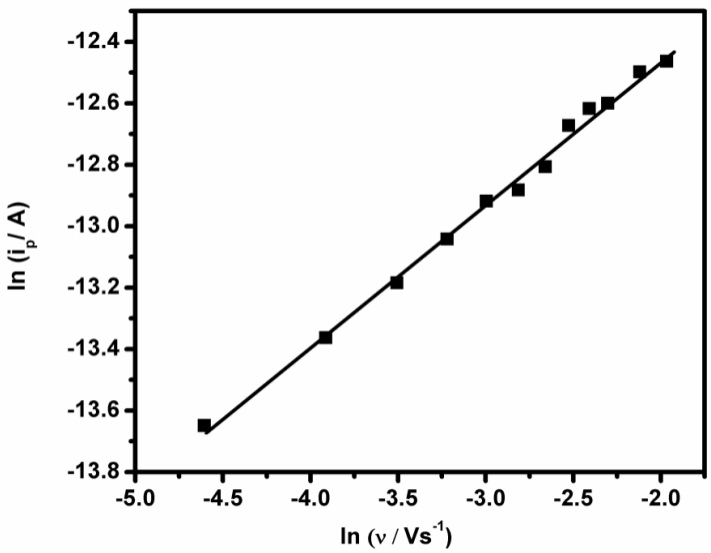

Figure 5.12: Plot of logarithm of peak current vs. logarithm of scan rate.

5.3.5 Determination of diffusion coefficient

Chronoamperometric technique was employed to estimate the value of diffusion coefficient. Obtained chronoamperograms for various concentrations (2.0×10^{-6} to 1.0×10^{-4} M) of PG are represented in figure 5.13.

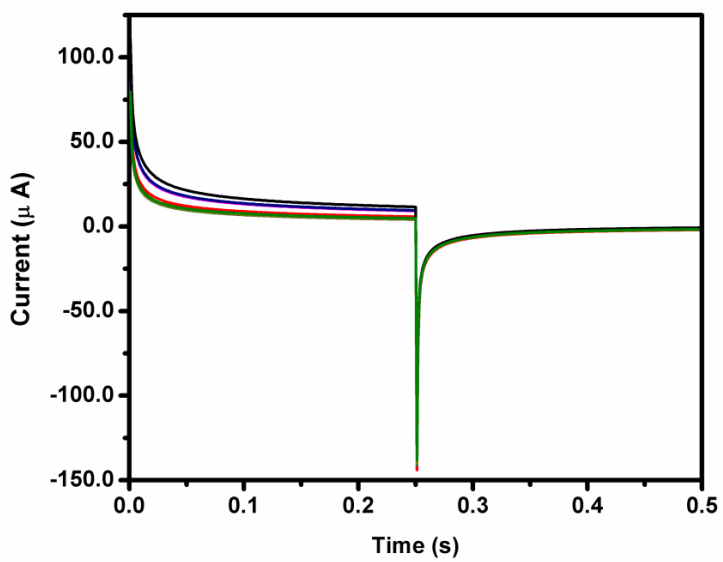

Figure 5.13: Overlay of chronoamperograms of PG at different concentrations.

Slopes of the plots of electrocatalytic current (I) vs $t^{-1/2}$ at different concentrations (Figure 5.14) were plotted against concentration (C) of PG (Figure 5.15), and the resulting slope was used for the calculation of diffusion coefficient (D) according to Cottrell equation.[11]

$$\mathbf{I = nFAD^{1/2}C\pi^{-1/2}t^{-1/2}}$$

By substituting the calculated surface area and other quantities in the above equation, average value of D was found to be 1.94×10^{-6} cm^2 s^{-1} which

is comparable with the previous report (2.30×10^{-6} cm^2 s^{-1}).[2] The value D also supports the diffusion controlled mechanism of oxidation.

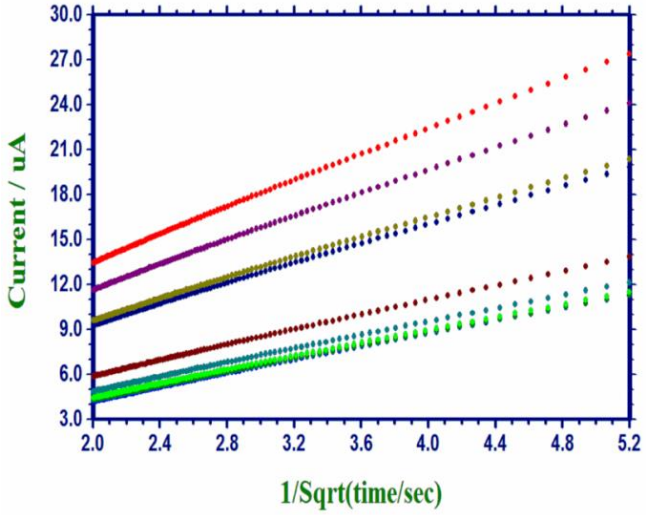

Figure 5.14: Plot of peak current vs. $t^{-1/2}$ derived from the chronoamperograms in Fig. 5.13.

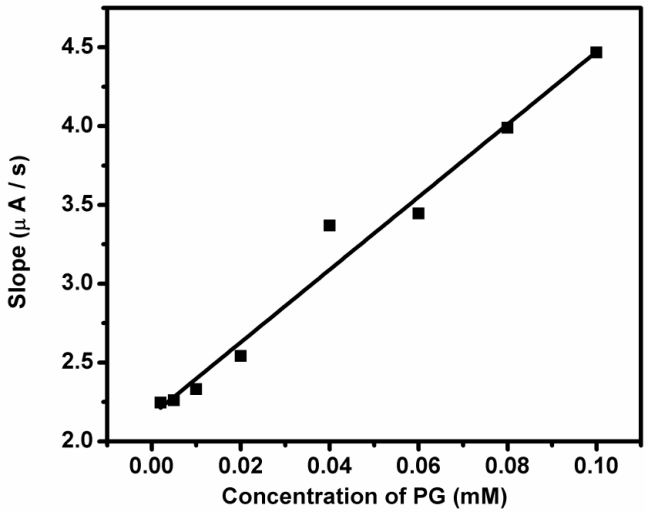

Figure 5.15: Plot of slope of (I vs $t^{-1/2}$ from Figure 5.14) against concentration of PG.

5.3.6 Concentration study and linear range

DPV responses of various concentrations of PG at NiNPs/GCE were studied under optimized experimental conditions (Figure 5.16). A gradual increase in peak current with concentration of PG was observed. Within the range 1.0×10^{-3} M to 4.0×10^{-4} M, oxidation peak current and concentration follows a linear relationship according to the equation $I_p\,(A) = 0.0064C\,(M) + 4.0\times10^{-6}$ (R^2 = 0.987) where as in the concentration range 3.0×10^{-4} M to 2.0×10^{-6} M variation occurs as per the equation $I_p\,(A) = 0.0162\,C\,(M) - 7.0\times10^{-8}$ (R^2 = 0.999) (Figure 5.17). The decrease in slope at higher concentration range may be due to the decrease in active sites / catalytic sites per analyte molecule. Limit of detection and limit of quantification for the method were calculated to be 5.85×10^{-8} M and 1.95×10^{-7} M respectively.

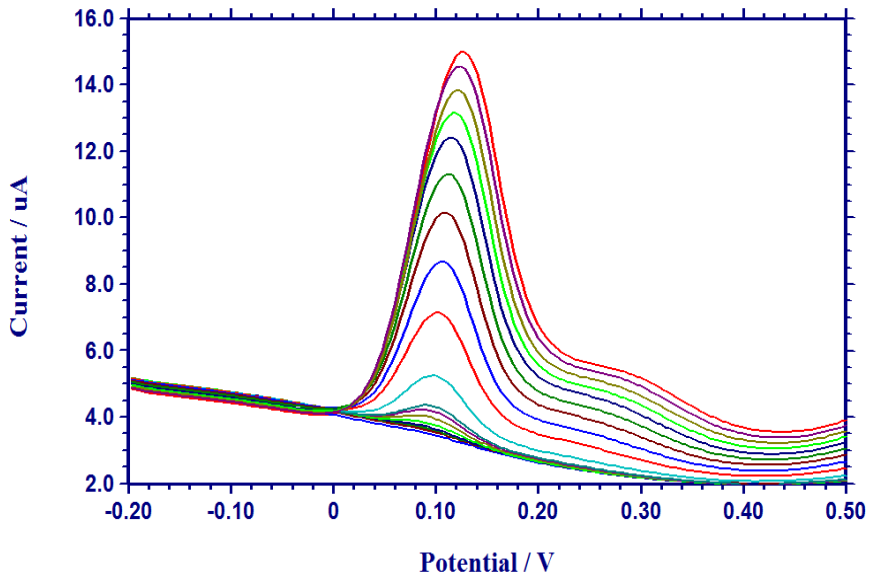

Figure 5.16: Overlay of DPVs for the oxidation of PG at various concentrations.

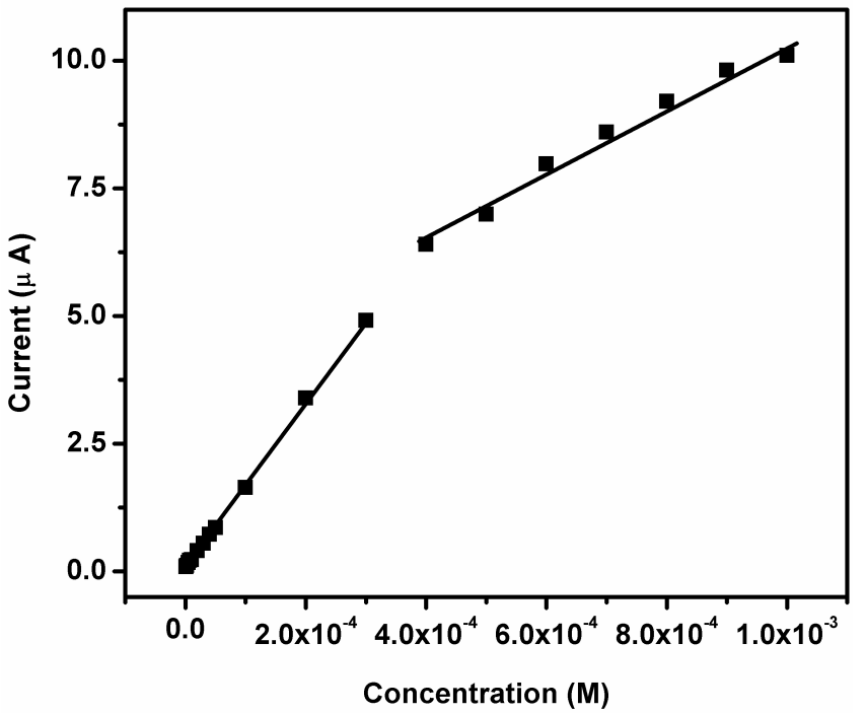

Figure 5.17: Plot of peak current vs. concentration of PG.

Performance of the proposed sensor was compared with other reported sensors in Table 5.2. From the table, it is observed that detection limit and overpotential of the proposed sensor is better than the existing sensors. Moreover, NiNPs are easy to prepare and controlled by in situ deposition method. They are cost effective electrode modifier while compared to noble metals like gold and platinum.

Table 5.2: Comparison of proposed sensor with existing PG sensors.

Electrode	Peak potential (V)	Linear range (M)	LOD (M)	References
GCE	0.59	0.70×10^{-3} to 4.71×10^{-6}	2.54×10^{-6}	151
NiPcTs/Ppy/Pt	0.55	4.00×10^{-3} to 4.00×10^{-4}	7.23×10^{-6}	152
P3MT/CFMEs	0.44	1.00×10^{-5} to 1.00×10^{-6}	4.00×10^{-7}	153
MWNT/GE	0.18	1.00×10^{-4} to 1.00×10^{-5}	6.30×10^{-7}	135
AuNP/PPABSA/ GCE	0.10	1.00×10^{-4} to 9.00×10^{-6}	1.90×10^{-7}	28
NiNPs/GCE	0.08	1.00×10^{-3} to 4.00×10^{-4} and 3.00×10^{-4} to 2.00×10^{-6}	5.85×10^{-8}	-

LOD - limit of detection, Pt/Ppy/NiPcTs - Platinum/polypyrrole electrode modified with tetrasulfonate nickel (II) phthalocyanine complex, P3MT/CFMEs - poly(3-methylthiophene) /cylindrical carbon fiber microelectrodes, MWNT- multiwalled carbon nanotube, GE- gold electrode, AuNP – Gold nanoparticles, PPABSA – Poly(p-aminobenzene sulfonic acid)

5.3.7 Interference study

Effect of coexisting species on the electro-oxidation of PG (3.0×10^{-5} M) on NiNPs/GCE was studied (Table 5.3). The results showed that, octyl gallate, butylated hydroxyl toluene, NaCl, Na_2SO_3, CH_3COOH and EDTA has no influence (signal change below 5%) on the determination of PG even at 100 fold excess concentration. However, citric acid, butylated hydroxyl anisole and ascorbic acid interferes the determination severely.

Table 5.3: Effect of coexistence on the determination of 3.0×10^{-5} M PG.

Coexisting species	Concentration (M)	Interference (%)
Acetic acid	3.0×10^{-3}	0.5
EDTA	3.0×10^{-3}	2.5
Sodium sulphite	3.0×10^{-3}	0.4
Sodium chloride	3.0×10^{-3}	1.8
Octyl gallate	3.0×10^{-3}	3.7
Butylated hydroxytoluene	3.0×10^{-3}	0.4
Butylated hydroxyanisole	3.0×10^{-5}	18.2
Citric acid	3.0×10^{-5}	14.1
Ascorbic acid	3.0×10^{-5}	21.9

5.3.8 Mechanism of the electro-oxidation process

Calculation of number of electrons participated in the oxidation process helps to establish the mechanism. For this, anodic charge transfer coefficient α_a is determined. According to the latest reports of IUPAC,[143]

$$\boldsymbol{\alpha_a = \left(\frac{RT}{F}\right) \cdot \left(\frac{d\ln|j|}{dE}\right)}$$

where j represents current density, R is universal gas constant, F is Faraday's constant, and T is the temperature in Kelvin. The term ($d\ln|j|/dE$) is slope of the plot $\ln|j|$ vs. E (Figure 5.18). By substituting other quantities, value of 'α_a' was calculated to be 0.51, which is in agreement with that of theoretical value, 0.50.[143]

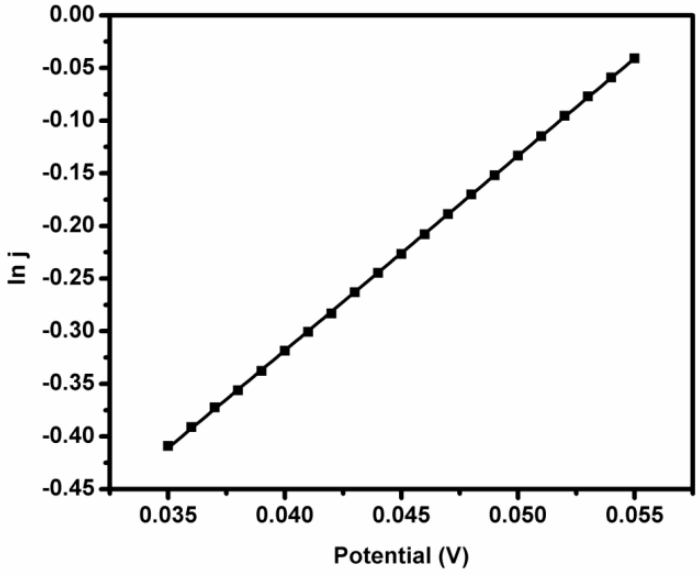

Figure 5.18: Plot of natural logarithm of current density vs. peak potential.

According to Bard and Faulkner, number of electrons (n) participated in the oxidation reaction and α_a can be related as,[11]

$$(1 - \alpha_a)n = \frac{47.7}{\left(E_P - E_{p_{1/2}}\right)}$$

Where, E_p and $E_{p1/2}$ are potential and half peak potentials respectively. Number of electrons is calculated to be 1.97, which is in agreement with that of earlier report (~2).[27,28] It indicates that the mechanism of oxidation of PG is similar to that of substituted phenols involving two electrons.[153] Moreover, the plot of oxidation potential vs pH exhibited a negative shift on increasing the pH from 4.0 to 8.0 (Figure 5.9). Relationship between the oxidation potential and pH of PBS was linear with regression equation, $E_p(V) = -0.0557\ pH + 0.5311$ ($R^2 = 0.996$) . The obtained slope is

approximately near to the theoretical value (0.057 V/pH),[118] indicating that electron transfer is followed by an equal number of protons (2 H^+ and 2 e^-) on the electro - oxidation of PG. The proposed mechanism is shown in scheme 5.2.

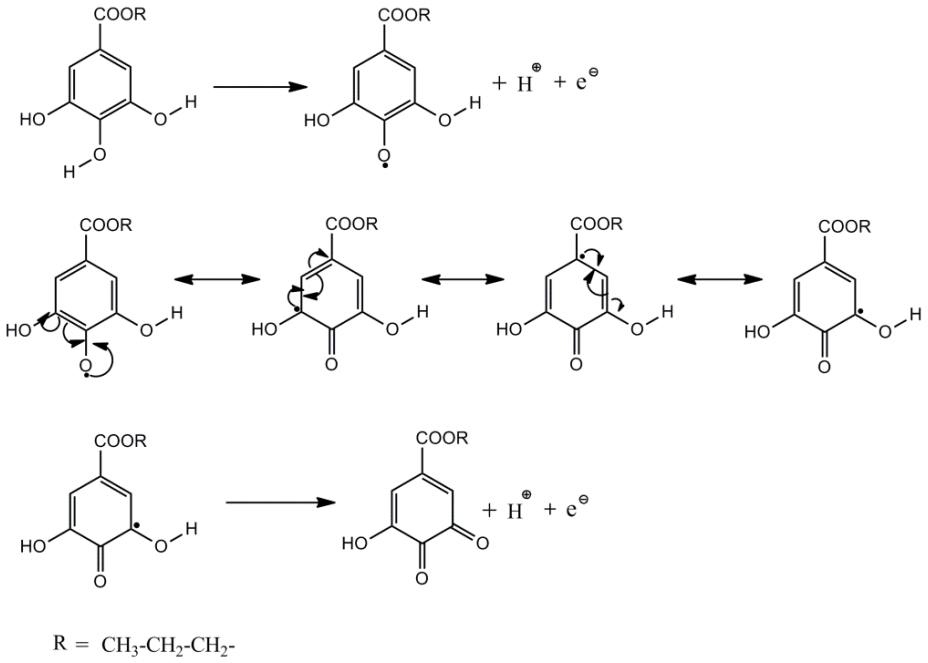

Scheme 5.2: Mechanism of electro-oxidation of PG.

5.3.9 Reproducibility, repeatability and stability

Reproducibility of proposed sensor was studied by carrying out five replicate measurements using five different NiNPs/GCE electrodes in 2.0×10^{-6} M PG solution under optimized conditions. The relative standard deviation (RSD) was calculated to be ± 0.2%. Likewise, repeatability of the sensor is verified by taking five repeated measurements using same NiNPs/GCE electrode and RSD was calculated to be ± 3.5%. The RSD values indicated that proposed sensor has good reproducibility and

repeatability. In addition, the response of PG at NiNPs/GCE did not show any difference even two days after modification, indicates the stability of NiNPs/GCE. Therefore the proposed method is precise and consistent for the determination of PG.

5.3.10 Application studies

To validate the performance of the proposed sensor in real samples, NiNPs/GCE was used for the quantification of PG in spiked food samples, such as coconut oil, sunflower oil and margarine (Table 5.4). The obtained recoveries are in good concordance with those of standard spectrophotometric method.[94] These results reveal the reliability of developed sensor for the determination of PG in food stuffs.

5.4 Conclusions

A novel voltammetric sensor for the quantification of PG was developed using the advantageous characteristics of NiNPs. Studies on modified electrode showed that the oxidation peak current increases by approximately 61% and peak potential decreases by approximately 50% in comparison to the bare GCE, thus increasing the sensitivity of the developed method. This is one of the sensitive methods for the determination of PG with the lowest over potential compared with previously reported electrochemical methods.[28,135,151-153] Furthermore, the proposed sensor was employed for the analysis of PG in real food samples and results were found to be satisfactory. Moreover, the proposed method was validated by comparing the results obtained using standard spectrophotometric method. The proposed sensor has great potential for wide applications in the field of food analysis.

Table 5.4: Determination of PG in food samples.

Samples	Proposed method				Spectrophotometric method			
	Added (M)	Found (M)	R (%)[a]	RSD (%)[a]	Added (M)	Found (M)	R (%)[a]	RSD (%)[a]
Coconut oil	2.00×10^{-6} to 1.00×10^{-4}	2.08×10^{-6} to 9.50×10^{-5}	101	3.3	8.00×10^{-6} to 1.00×10^{-4}	7.98×10^{-6} to 1.00×10^{-4}	100	1.3
Sunflower oil	2.00×10^{-6} to 1.00×10^{-4}	2.01×10^{-6} to 9.95×10^{-5}	98	1.9	8.00×10^{-6} to 1.00×10^{-4}	8.13×10^{-6} to 9.94×10^{-5}	100	1.1
Margarine	2.00×10^{-6} to 1.00×10^{-4}	2.11×10^{-6} to 9.75×10^{-5}	99	3.4	8.00×10^{-6} to 1.00×10^{-4}	8.13×10^{-6} to 9.99×10^{-5}	100	2.2

a From five measurements, RSD relative standard deviation

Chapter 6

CADMIUM SULPHIDE QUANTUM DOTS BASED FLUORESCENT SENSOR FOR BRILLIANT BLUE FCF

Contents

This chapter explains the development of a fluorescent sensor based on L-cysteine capped cadmium sulphide quantum dots for the determination of Brilliant blue FCF (BB) (in 0.5 M Tris buffer solution of pH 9.5) over other synthetic food colorants. Addition of BB into quantum dot solution induces the quenching of fluorescence. Quenching mechanism was studied using various analytical techniques which evidently points to the inner filter effect (IFE). The developed sensor exhibited a linear concentration range of 4.00×10^{-5} to 4.50×10^{-6} M and limit of detection 3.50×10^{-7} M. The developed sensing strategy is simple and flexible due to less laborious synthetic procedure. More importantly, the proposed sensor exhibit sensitive responses toward BB in food samples such as sports drink and candies, demonstrating its potential in food analysis.

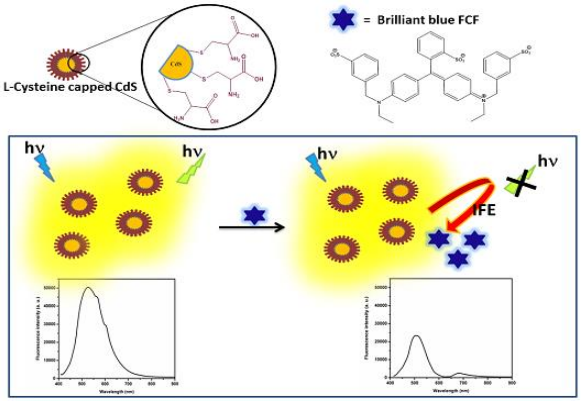

Scheme 6.1: Diagrammatic representation of the sensing of BB using L-cys-CdS.

6.1 Introduction

Food habits have changed a lot today so that attractiveness and taste has over ruled the nutritional value of food products. This changing consumer interests have made food industries to introduce additives that can impart flavours and colour. Synthetic colorants are added to food products to make them more appealing.[118,155] These colorants do not contribute any nutritional value but it lead to significant health problems, which points towards the need for its analysis.[156,157]

Brilliant blue FCF (BB) is a blue food colorant commonly used in sports drink, candies, jellies etc. BB a triarylmethane derivative, is chemically disodium 3-[N-ethyl-N-[4-[[4-[N-ethyl-N-(3-sulfonatobenzyl)-amino] phenyl] (2-sulfonatophenyl) methylene] - 2, 5-cyclohexadiene-1-ylidene] ammoniomethyl] benzenesulfonate. Due to the extensive π-conjugated structure, BB shows high colour intensity among the triarylmethane class and makes it a common food colorant. Even though BB is allowed as a food colorant, its uses can cause several health problems. Studies on BB have shown that, it can provoke allergic reactions, asthma, cancer, hyperactivity, insomnia, urticarial etc.[158] Also it can disrupt cell metabolism when it enters the blood stream.[158] The acceptable daily intake proposed by Joint FAO/WHO Expert Committee on Food Additives (JECFA) and Scientific Committee for Food (SCF) is 6 mg/Kg bw/day.[159]

Due to the importance of BB sensing, this work is aimed to develop a fluorescent sensing strategy using L-cysteine capped CdS (L-cys-CdS) quantum dots as fluorophores and inner filter effect (IFE) of BB as the mechanism of quenching. In IFE, radiative energy transfer arises when the

absorption spectrum of absorber overlaps with the excitation and/or emission spectrum of the fluorophore, converting the absorption to the corresponding fluorescence signal.[91] The developed sensor was also applied for determination of BB through real sample analysis.

6.2 Experimental

6.2.1 Synthesis of L-cysteine capped CdS quantum dots

L-cysteine capped CdS quantum dots were synthesized as per the reported procedure.[160] 100 mL of 1mM solution of L-cysteine hydrochloride hydrate was prepared in water and then purged with N_2 gas for half an hour. Using 0.5 M Tris solution, pH of the solution was adjusted to 9.0. Then 0.5 mM solution of $Cd(NO_3)_2$ was dropped slowly in to the mixed solution (in a molar ratio L-cys / Cd of 2:1) and allowed to react for half an hour. Finally 10 mL of 0.5 mM solution of Na_2S was dropped slowly in to the vortex of solution to reach a molar ratio of S/Cd of 1:1. Obtained solution was sealed and incubated at 47^oC in water bath for 2 hours. The unreacted sulphide was removed using N_2 gas. A bright yellowish green colloid was obtained.

6.2.2 Analytical procedure

The fluorescence spectra were recorded at λ_{ex}/ λ_{em} = 400 / 528 nm. The CdS probe solution was taken in a quartz cuvette and required amount of BB solution (to obtain 4.00×10^{-5} to 4.50×10^{-6} M) was added and made up to a total volume of 2 mL by adding appropriate amount of 0.5 M Tris buffer (pH 9.5) and the resultant spectra were recorded. The quenching of fluorescence intensity was noted as a ratio I_0 / I, where I_0 and I are the found fluorescence intensities in the absence and presence of BB.

6.2.3 Analysis of food samples

Sports drink (Gatorade sports drink blue bolt flavor) sample was used directly (100 µL) without extraction. BB in candies (Tic Tac mintensity) was extracted using water. 5g of candies were taken, washed with 5 mL of water, the resultant solution was collected and repeated the same procedure till the extract become colourless. The extract was then evaporated to dryness followed by dissolving the residue in 10 mL water, and 100 µL of this extract was used for further analysis.[161,162] Concentration of BB was estimated using standard addition method and a spectrophotometric method[96] was also conducted as per the procedure described in section 2.3.3 for comparison.

6.3 Results and discussion

6.3.1 Characterization of synthesized L-cysteine capped Cadmium sulphide

Synthesized probe (L-cys-CdS) was characterized by transmission electron microscopy (TEM), dynamic light scattering analysis (DLS), Fourier transform infrared (FTIR), UV-visible and fluorescence spectroscopy. From TEM image it is clear that, the particles are spherical, well dispersed and has an average size of 6 nm (Figure 6.1). From DLS studies, the hydrodynamic volume was found to be 17.8 nm (Figure 6.2).

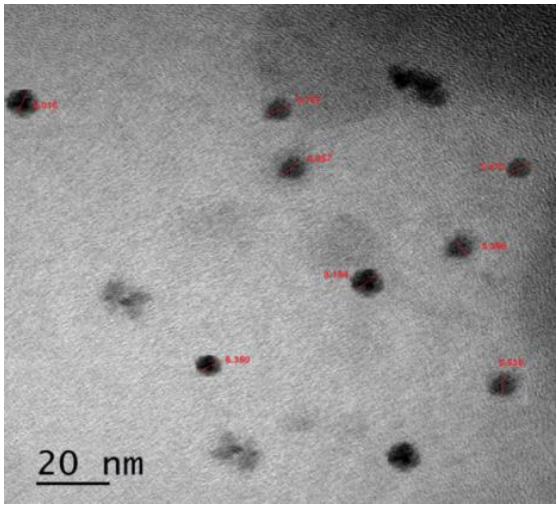

Figure 6.1: TEM image of synthesized L-cys-CdS QDs.

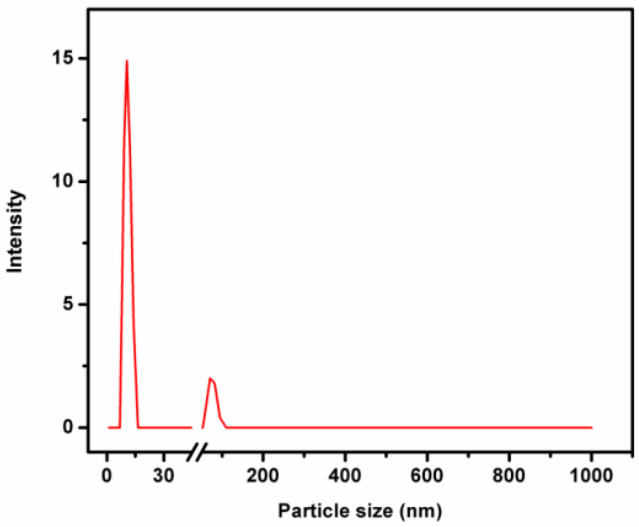

Figure 6.2: DLS spectrum of L-cys-CdS QDs.

The absorption spectrum of L-cys-CdS showed a weak broad absorption in the UV range with maximum absorbance at 375 nm (Figure 6.3a). Upon excitation at 400 nm, the fluorescence spectrum of L-cys-CdS showed a broad emission centred at 528 nm (Figure 6.3b). The broad

emission corresponds to the trap state emission from surface trap states of CdS QDs.[163]

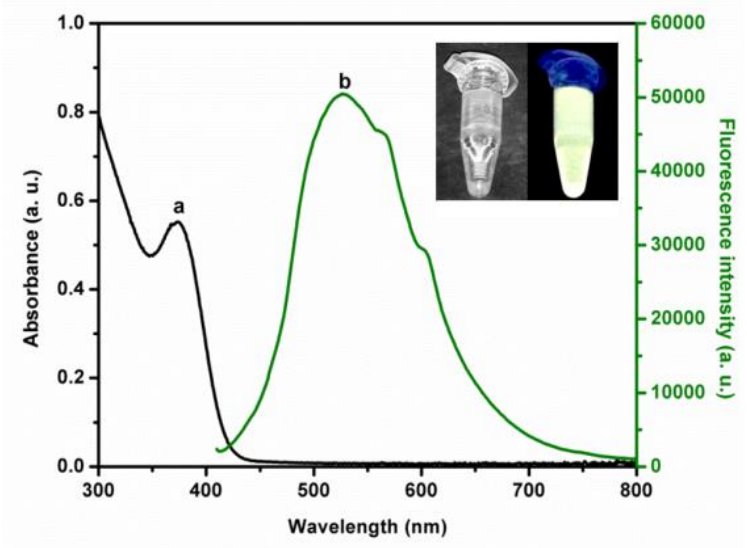

Figure 6.3: (a) Absorption and (b) emission spectrum of synthesized L-cys-CdS QDs. Inset depicts the photograph of probe kept under white light and UV light.

IR spectroscopic analysis reveals the effective capping of L-cysteine on the surface of synthesized probe. While comparing the FTIR spectrum of L-cysteine and L-cys-CdS, the band corresponding to the -SH stretching vibration (λ = 2558 nm) was absent in probe (Figure 6.4). This observation indicates the covalent bond formation between L-cysteine and Cd atoms on the surface of QDs.[164] These points to the effective capping of L-cysteine on the surface of synthesized QDs.

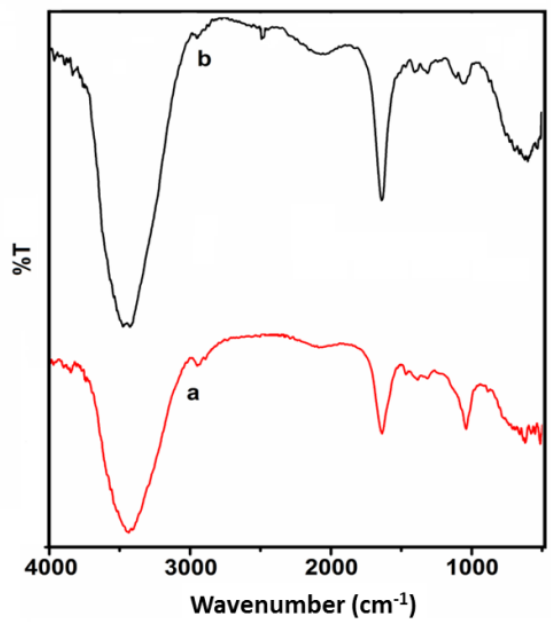

Figure 6.4: FTIR spectra of (a) L-cys-CdS QDs and (b) L-cysteine.

By taking Rhodamine 6G (quantum yield of 95 %) as reference material, quantum yield of the synthesized QDs was calculated from its absorption and emission spectra at different concentrations.[165] The integral fluorescence intensities (IFI) of different concentrations of Rhodamine 6G (Rh) and L-cys-CdS were measured, then plotted vs absorbance. Figure 6.5 and Figure 6.6 shows the corresponding plots of IFI vs. absorbance of rhodamine 6G and L-cys-CdS respectively. The resulting slopes were used to calculate the quantum yield using the following equation.

$$\phi_{CdS} = \phi_{Rh} \times \frac{\mu_{CdS}}{\mu_{Rh}} \times \left(\frac{\eta_{CdS}}{\eta_{Rh}}\right)^2$$

Where ϕ_{CdS} is the quantum yield of synthesized L-cys-CdS and ϕ_{Rh} is the quantum yield of Rh. μ_{CdS} and μ_{Rh} represents the slopes of the plot of IFI vs

absorbance of L-cys-CdS and Rh respectively. η_{CdS} and η_{Rh} denotes the refractive indices of the solutions of fluorescent probe and standard.The quantum yield was found to be 35.5%.

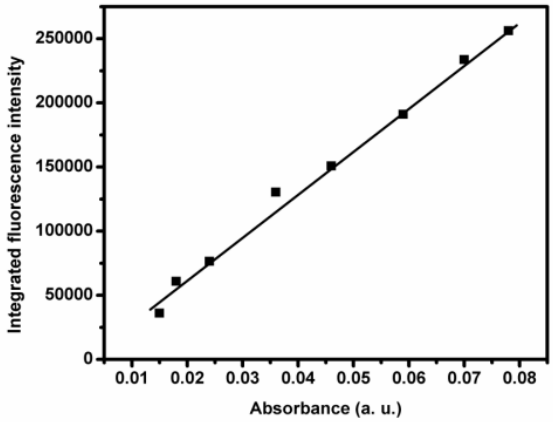

Figure 6.5: Plot of integrated fluorescence intensity against absorbance of different concentrations of rhodamine 6G.

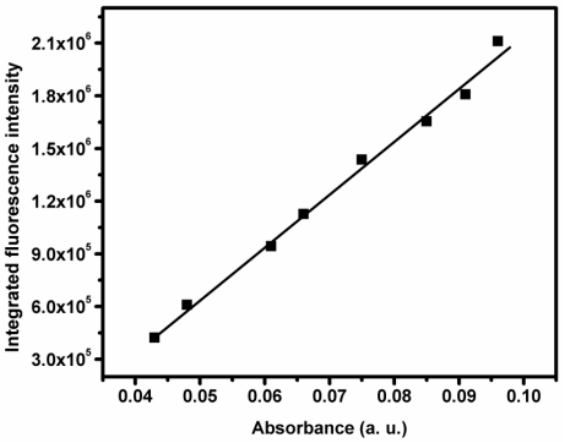

Figure 6.6: Plot of integrated fluorescence intensity against absorbance of different concentrations of L-cys-CdS.

The synthesized L-cys-CdS QDs were found to be stable for about 4 months, when stored at 4^{o}C.

6.3.2 Optimization of experimental parameters

6.3.2.1 Effect of buffer

Since Tris buffer solution was used in synthesis, it is used for dilution as well. On dilution, fluorescence intensity decreases. The amount of solvent was fixed to obtain the fluorescence intensity ~50000 a. u., which is used throughout the studies.

6.3.2.2 Effect of irradiation time on fluorescence intensity

Change in fluorescence intensity with time was studied by irradiating the probe solution in absence and presence of BB respectively. The L-cys-CdS solution gave stable fluorescence signal up to 14 min. Upon addition of BB, the fluorescence intensity of the probe quenched and became stable suddenly (Figure 6.7), which eliminates the time consuming incubation step, necessitate by many of the existing method for food analysis.

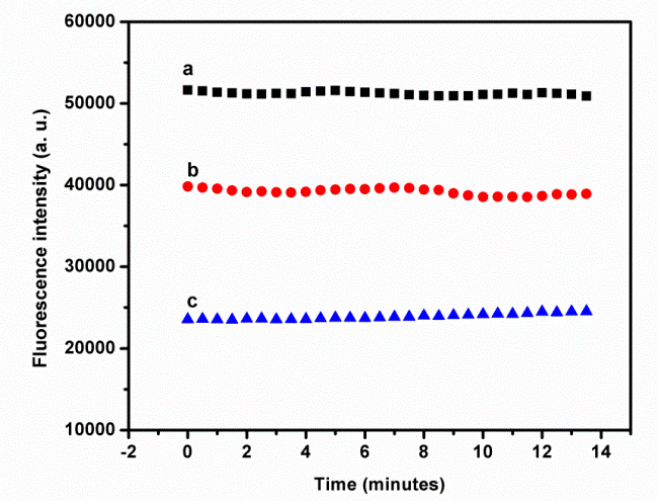

Figure 6.7: Effect of time on the fluorescence intensity of (a) L-cys-CdS and (b) L-cys-CdS + 1.5×10^{-5} M BB, (c) L-cys-CdS+ 4.5×10^{-5} M BB.

6.3.3 Performance of the sensor

6.3.3.1 Effect of concentration

On increasing the concentration of BB, a steady decrease in the intensity as well as a change in shape of the fluorescence signal was observed (Figure 6.8).

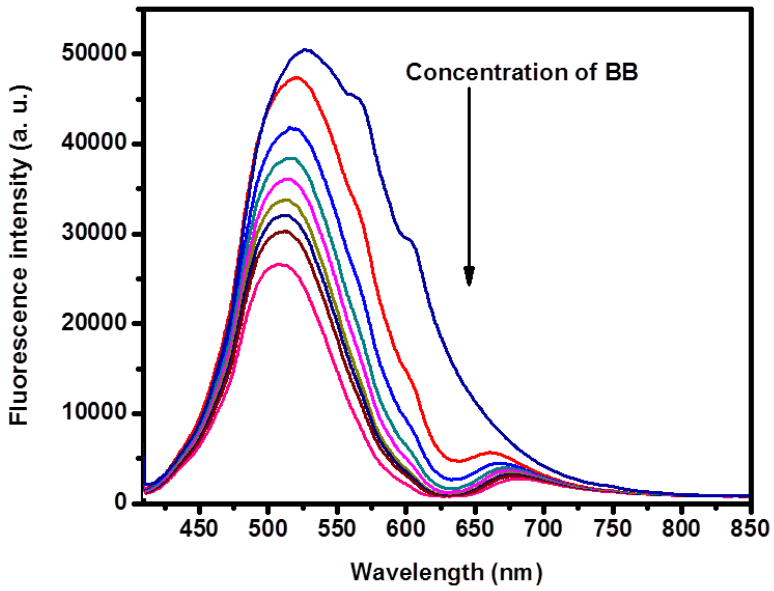

Figure 6.8: Effect of concentration of BB on the fluorescence intensity of L-cys-CdS.

A calibration graph was plotted with concentration of BB against I_0/I, and it was found to be linear in the range 4.00×10^{-5} to 4.50×10^{-6} M (Figure 6.9). The limit of detection and limit of quantification were calculated using formulae '3S/ m' and '10S / m' respectively, where 'S' is the standard deviation and 'm', the slope of calibration graph. The limit of detection and limit of quantification were found to be 1.73×10^{-7} M and 6.01×10^{-7} M. The

relative standard deviation for the determination of 4.50×10^{-6} M BB was 1.6 % (n = 5).

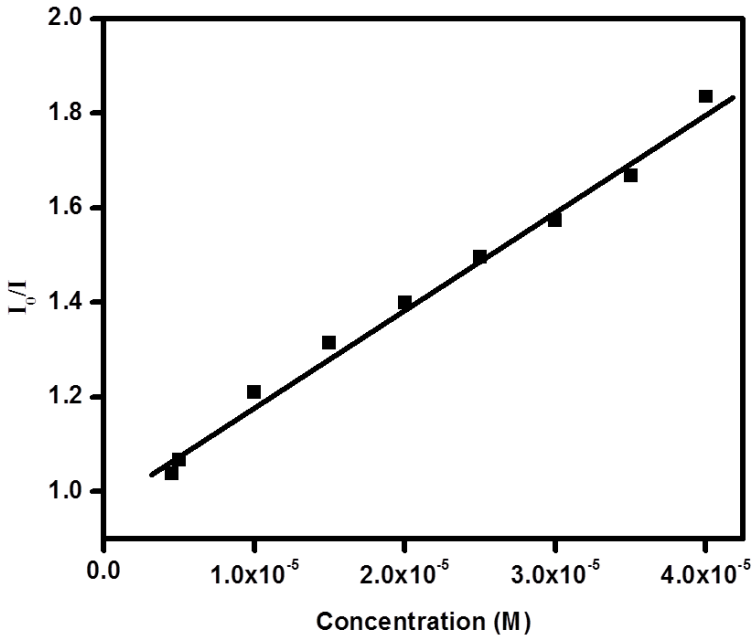

Figure 6.9: Linear calibration graph between the ratio of fluorescence intensities and concentrations of BB.

Analytical parameters of the recently reported works concerning the quantification of BB and that of developed method are described in Table 6.1. Examination of the table reveals that while the developed sensor possesses comparable sensing performance to that of existing sensors, it is superior to the existing ones in terms of simplicity and selectivity.

Table 6.1: Analytical parameters of the proposed method and existing methods for determination of BB.

Sl. No.	Method	Linear range (M)	LOD (M)	References
1.	Cathodic stripping voltammetry	1.00×10^{-7} to 1.00×10^{-8}	1.91×10^{-9}	166
2.	LC-MS	1.51×10^{-9} to 1.63×10^{-10}	-	167
3.	Solid-state ECL	5.00×10^{-7} to 1.00×10^{-7}	5.70×10^{-8}	168
4.	Spectrophotometry	1.89×10^{-7} to 1.89×10^{-9}	4.28×10^{-10}	169
5.	Fluorimetry	4.00×10^{-5} to 4.50×10^{-6}	3.50×10^{-7}	-

ECL: electrochemiluminescence

6.3.3.2 Selectivity and interference studies

One of the most significant properties of a sensor is its selectivity. To study the selectivity of the probe, different species (2.5×10^{-5} M) that are either structurally similar or coexisting or same coloured substances were taken and their effect on the fluorescence intensity of probe was studied.

Figure 6.10 shows the changes in fluorescence spectra of L-cys-CdS that occurred after the separate addition of BB, Brilliant Cresyl blue (another blue coloured dye), Malachite green (trimethane aryl class compound), and coexisting species such as Tartrazine, ascorbic acid, glucose, fructose, Saccharin and sodium chloride. From the figure it is clear that, variations in fluorescence intensity of L-cys-CdS in the presence of BB were strikingly larger than that of others. These results point out that the proposed assay had high selectivity for BB and has potential in the practical detection of BB in food samples.

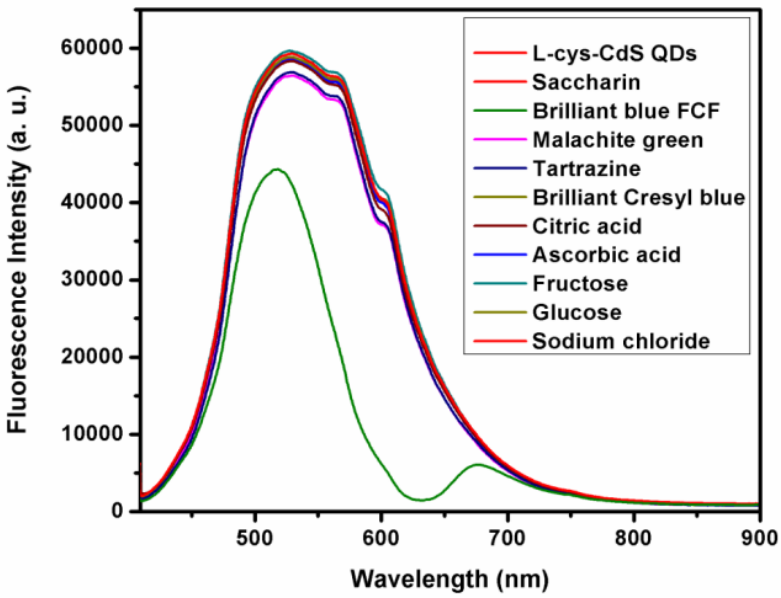

Figure 6.10: Effect of various substances (2.5×10^{-5} M) on the fluorescence spectrum of L-cys-CdS in Tris buffer solution.

Effect of concentration of above mentioned coexisting species in the fluorescence signal of QDs in presence of BB (5.0×10^{-6} M) was also studied (Table 6.2). Only Tartrazine showed significant interference (above 5%) in the fluorescence signal when it was present in above 2 fold excess concentration of BB. Ascorbic acid, glucose, fructose, saccharin and sodium chloride didn't show any interference even up to 100 fold excess concentration of BB.

Table 6.2: Effect of coexistence on the determination of 5.0×10^{-6} M BB.

Coexisting species	Concentration (M)	Interference (%)
Fructose	5.0×10^{-4}	2.4
Glucose	5.0×10^{-4}	1.0
Ascorbic acid	5.0×10^{-4}	4.5
Sodium chloride	5.0×10^{-4}	0.8
Saccharin	5.0×10^{-4}	1.9
Citric acid	5.0×10^{-4}	1.6
Tartrazine	1.0×10^{-5}	5.4

6.3.4 Mechanism of quenching

It can be seen from figure 6.8 that the fluorescence intensity of L-cys-CdS is effectively quenched by BB. Quenching of fluorescence is mainly due to ground state or excited state interactions / energy transfer between probe and analyte. To study the mechanism, UV–vis absorption spectroscopy and fluorescence emission spectra were studied. While considering the absorption spectrum of BB and emission spectrum of L-cys-CdS (Figure 6.11), an excellent overlapping can be observed. UV–vis absorption spectra of 1.0×10^{-5} M BB in the absence (a) and presence (b) of L-cys-CdS (Figure 6.12) were also recorded. No observable variation in the absorption band of BB was noticed, which further point out that no complex has formed between BB and L-cys-CdS.[40,170] Hence the possible mechanism may be FRET or IFE.

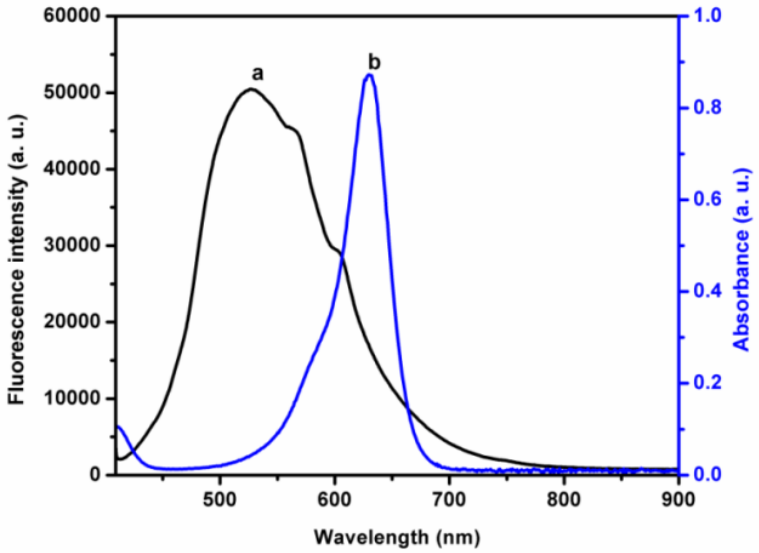

Figure 6.11: An overlay of (a) fluorescence spectrum of L-cys-CdS and (b) absorption spectrum of BB.

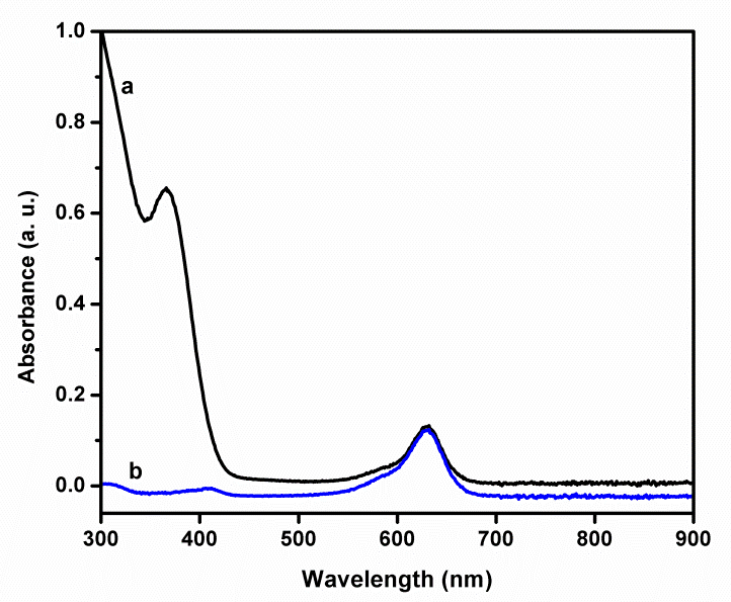

Figure 6.12: Absorption spectra of 1.0 × 10^{-5} M BB in the presence (a) and absence (b) of L-cys-CdS.

To further clarify the mechanism, zeta potential analysis of L-cys-CdS (Figure 6.13) and BB (Figure 6.14) in Tris buffer solution was carried out. Since both L-cys-CdS and BB were negatively charged (-30.5 mV and -9.2 mV respectively), BB could not be adsorbed on the surface of L-cys-CdS via electrostatic interaction.[171] Hence the distance between QDs and BB should be greater than 10 nm, ensuring the fact that no electrostatic attraction-induced FRET donor-accepter assemblies are formed.[171,172]

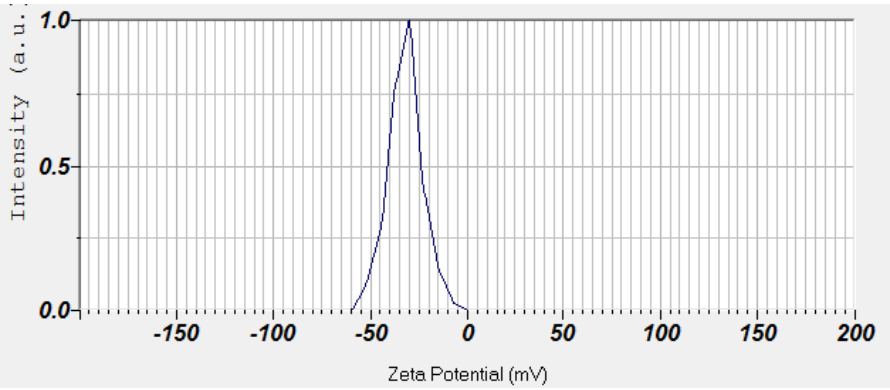

Figure 6.13: Zeta potential analysis of L-cys-CdS.

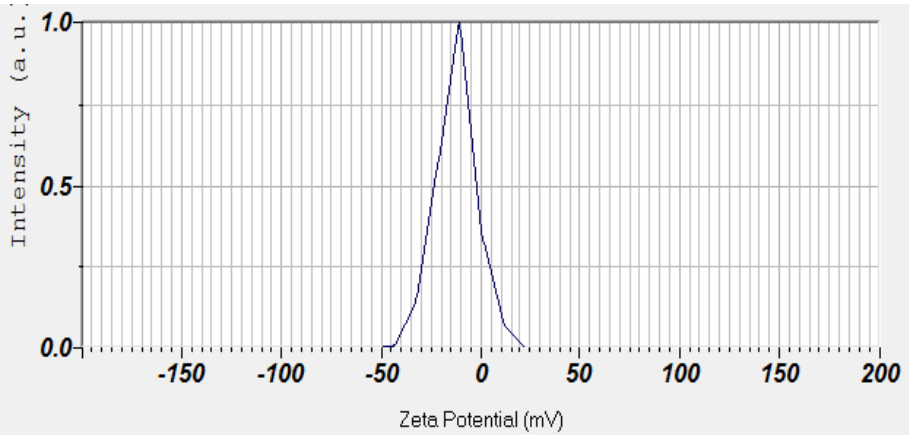

Figure 6.14: Zeta potential analysis of BB.

Since IFE do not affect the excitation lifetime, a study on fluorescence lifetime will help again to confirm the mechanism.[40] As shown in figure 6.15, the fluorescence decay curve of L-cys-CdS has no significant change (other than that due to possible instrumental errors) in the absence and presence of BB (lifetime of L-cys-CdS was 9.20×10^{-9} s, lifetime of L-cys-CdS + BB was 8.96×10^{-9} s), which confirmed that no FRET process has occurred. In addition to this, the emission spectrum of L-cys-CdS shows a change in shape together with quenching, upon addition of BB which further proves the mechanism as IFE.[91, 173, 174]

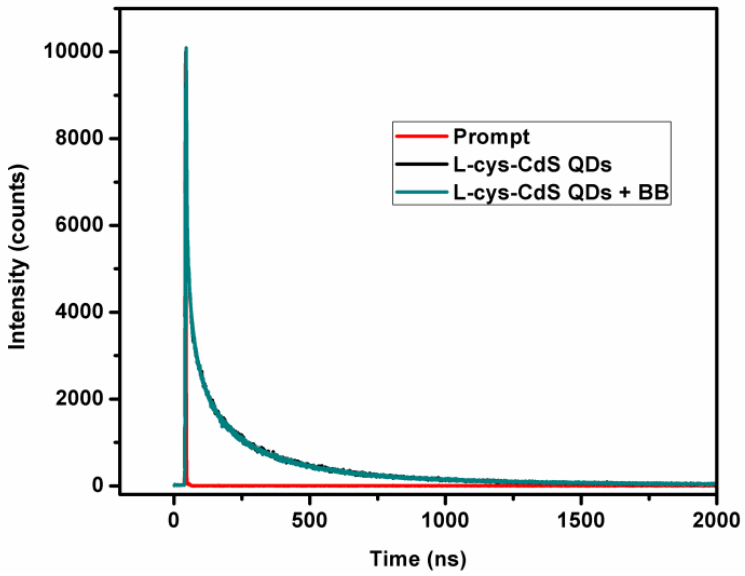

Figure 6.15: Fluorescence decay curves of L-cys-CdS in absence and presence of 1.0×10^{-5} M BB.

6.3.5 Application studies

In order to study the utility of the proposed sensor for real sample analysis, determination of BB in sports drink (Gatorade sports drink blue bolt flavor) and candies (Tic Tac mintensity) were carried out.

Concentration of BB was determined by standard addition method. The concentration of BB in sports drink and candies were found to be 3.19×10^{-6} M and 3.93×10^{-6} M respectively. Spectrophotometric analysis[96] was also used to determine the concentrations of BB. The obtained results (concentration of BB in soft drink and candies were 2.84×10^{-6} M and 3.82×10^{-6} M respectively) are in good agreement with those of proposed fluorescence assay and it reveals the effectiveness of the developed sensor for real samples.

6.4 Conclusions

A sensitive fluorescence sensor has been developed for the determination of Brilliant blue FCF in food products. The developed sensor shows below micro-molar level detection limit, good reproducibility and repeatability. The assay response was linear in the concentration range of 4.00×10^{-5} M to 4.50×10^{-6} M with a detection limit of 3.50×10^{-7} M. The developed method has been applied for the determination of BB in food products. Due to its simplicity, good sensitivity and selectivity, this sensor can be used for practical applications.

.....ഠോര.....

Chapter 7

COPPER NANOCLUSTERS BASED FLUORESCENT SENSOR FOR QUINOLINE YELLOW

Contents

This chapter details the development of a fluorescence sensing strategy for quinoline yellow (QY), a widely used artificial food colorant. Studies show that, L-cysteine stabilized copper nanoclusters (L-cys-CuNCs) can function as a fluorescence sensor by selectively sensing QY among other yellow colorants, giving a detection limit as low as 1.11×10^{-7} M. Several experimental parameters such as supporting medium, pH of the medium and reaction time were studied and optimized. Developed sensor exhibits a linear concentration range between 5.50×10^{-6} to 2.00×10^{-7} M. The developed fluorescence assay was successfully applied for testing of commercial samples, thereby making this sensing strategy significant for quality control of food stuffs.

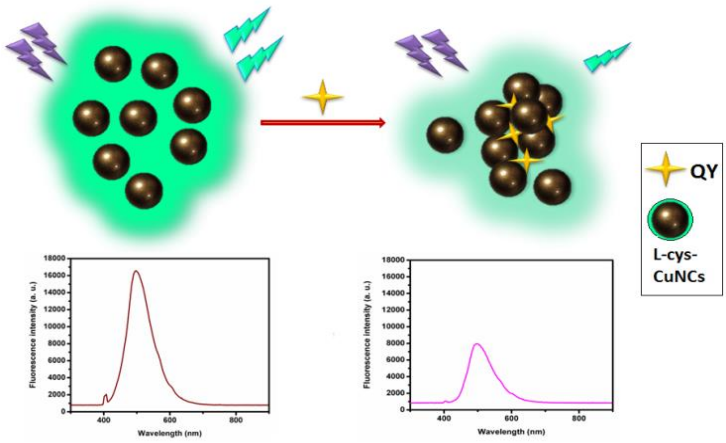

Scheme 7.1: Pictorial representation of fluorescence sensing of QY.

7.1 Introduction

Food manufacturing industry target their consumers especially children by imparting attractive flavor, appearance and taste, than focusing on nutritious value of sustenance items. Food industry achieves this by introducing additives that can grant flavors and shading. [155,118] Most of these colorants may not contribute any nutritional value,[155,118] yet it predisposes consumers huge medical issues which makes the focus of researches towards its base level of inclusion and its detailed examination.

Quinoline yellow (C_{18} H_{13} N $O_{5/8/11}$ $S_{1/2/3}$ $Na_{1/2/3}$ = QY) is generally utilized as an artificial colorant to provide a greenish - yellow shading to sustenance items. It is usually added to products like juices, candies or sorbet. QY also known as D and C yellow 10, is allowed in medications and cosmetics but is banned as a food additive in countries like Canada and the US.[175] Whereas in the European Union and Australia, QY is allowed in refreshments and is utilized as a part of nourishments like sauces, decorations and coatings. Similar to all other artificial food colorants, QY may likely to cause hyperactivity in kids. There are chances of causing hypersensitivity in individuals who are allergenic to aspirin.[176] QY also interfere with the stability of DNA by causing chromosome breakages.[158] On the premise of above studies, the European food safety authority has reduced the acceptable permissible intake of QY from 10 mg to 0.5 mg/kg of body weight.[177]

Accordingly present study is intendent to develop a simple and economic strategy for the determination of artificial food color QY using L-cysteine stabilized copper nanoclusters (L-cys-CuNCs) as fluorophores.

Several experimental parameters for developed sensor were studied and optimized. Developed sensor was applied successfully to real sample analysis.

7.2 Experimental

7.2.1 Synthesis of L-cysteine stabilized copper nanoclusters

Copper nanoclusters (CuNCs) stabilized by L-cysteine was synthesized by minor modification of reported procedure.[178] 175 mg of L-cysteine was dissolved in 5 mL of 0.4 M NaOH solution by sonication. Then, 500 µL of 1.00×10^{-3} M solution of $CuSO_4$ was mixed with above solution and kept undisturbed for 30 minutes. After incubation, the solution having a slight yellow colour was reacted for 4 hours at 55°C. The obtained dark yellow solution was then filtered, dialyzed and stored at 4°C in an amber colored bottle and is stable up to 5 months when stored under refrigeration.

7.2.2 Analytical Procedure

100 µL of L-cys-CuNCs solution was taken in a quartz cuvette and adequate amount of QY solution was added in to the solution so as to get concentration in the range 5.50×10^{-6} to 2.00×10^{-7} M and made up to a total volume of 2 mL by adding appropriate volume of 0.1 M phosphate buffer (pH 6). The resultant fluorescence spectra were recorded at $\lambda ex/ \lambda em$ = 400 / 495 nm. The ratiometric quenching of fluorescence intensity (I_0/I) was noted, where I_0 and I represents fluorescence intensities of the probe in the absence and presence of QY.

7.2.3 Analysis of QY in sugar candies and soft drink samples

5 g of powdered candies were taken and dissolved in 10 mL of water; the resultant solution was centrifuged and filtered to separate the undissolved contents. 100 μL of this extract was used for further analysis.[96] After spiking with QY, soft drink samples were analyzed and recoveries were calculated. Using standard addition method, concentrations of QY in samples were estimated. The results obtained were compared with that of spectrophotometric method[96] conducted as detailed in section 2.3.3.

7.3 Results and discussion

7.3.1 Characterization of Synthesized L-Cysteine stabilized copper nanoclusters

Synthesized CuNCs was characterized using UV-visible spectroscopy, fluorescence spectroscopy, TEM, FTIR spectroscopy, zeta potential and dynamic light scattering analyses. The synthesized nanoclusters gave an absorption peak at 385 nm (in UV-visible spectrum) and a strong blue emission centered at 495 nm (in fluorescence spectroscopic analysis with λex = 400 nm) (Figure 7.1). Particle size of these clusters was obtained through TEM imaging (Figure 7.2) and was found to have an average size of 2.3 nm.

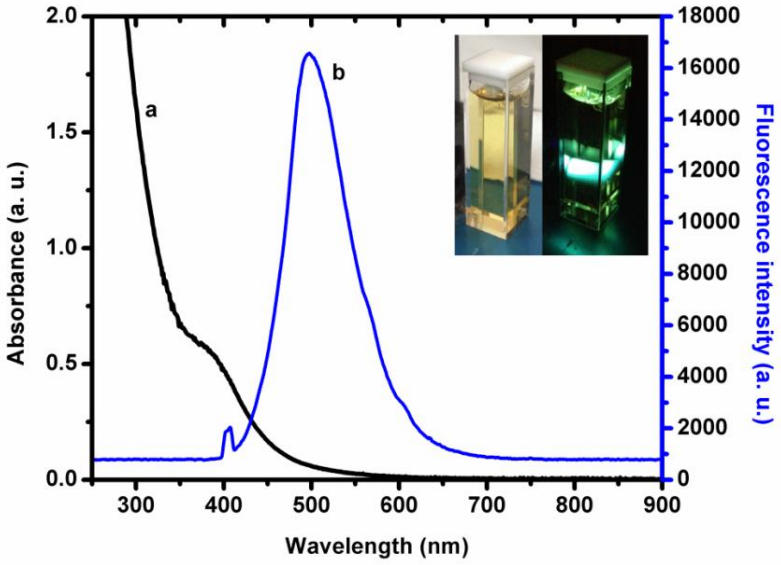

Figure 7.1: (a) Absorption and (b) emission spectra of L-cys-CuNCs. Inset shows the photograph of probe kept under normal light and in UV light.

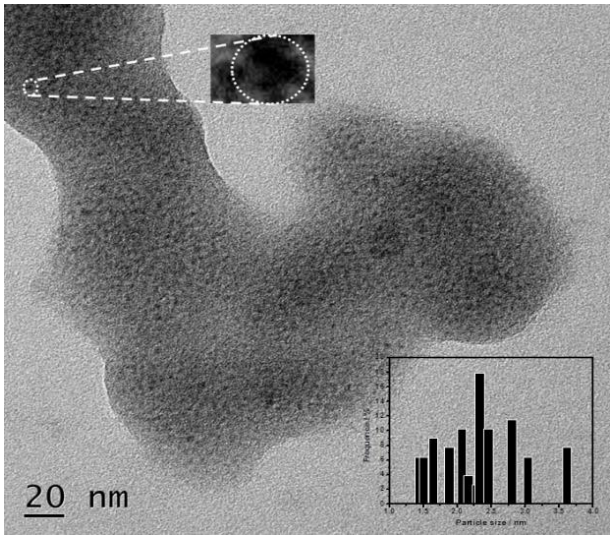

Figure 7.2: TEM image of L-cys-CuNCs. Inset depicts the histogram of particle size.

Hydrodynamic diameter of L-cys-CuNCs was obtained as 2.8 nm using dynamic light scattering analysis (Figure 7.3) which is in agreement with the particle size obtained using TEM analysis.

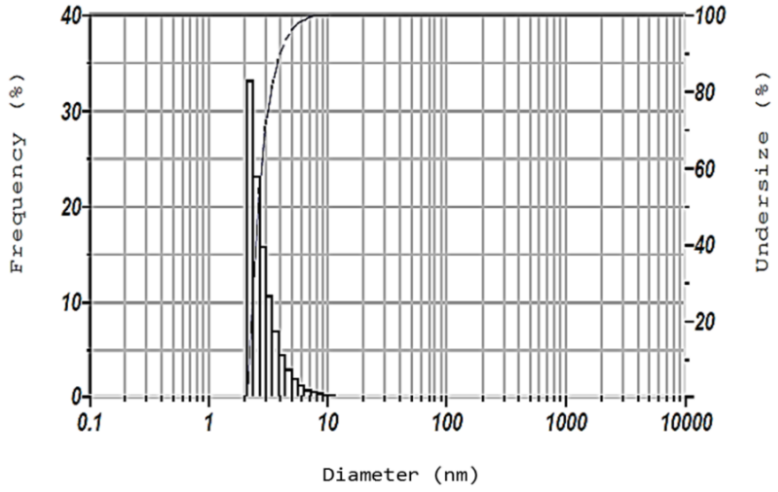

Figure 7.3: DLS analysis of L-cys-CuNCs.

In addition to this, in the zeta potential analysis (Figure 7.4), L-cys-CuNCs gave a higher zeta potential value of -14.7mV, which shows that these particles are highly stable.[179]

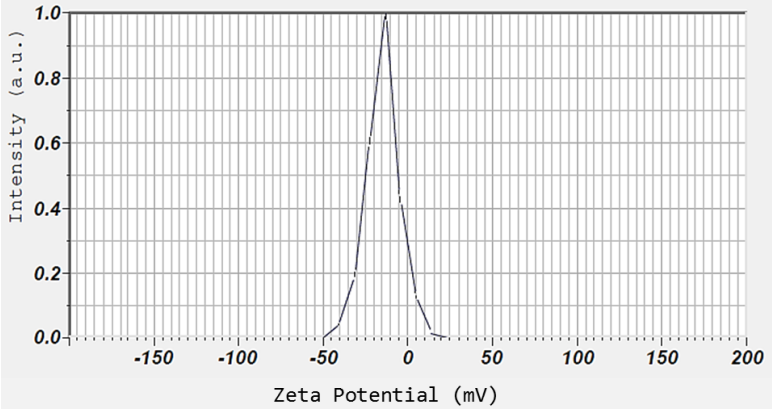

Figure 7.4: Zeta potential analysis of L-cys-CuNCs.

FTIR analysis shows excellent capping of L-cysteine on the surface of CuNCs. Upon comparing the IR spectra of L-cysteine and L-cys-CuNCs, the band corresponding to -SH stretching vibration (ν = 2558 cm^{-1}) was absent in probe (Figure 7.5), indicates formation of covalent bond between sulphur atoms in L-cysteine and Cu atoms on surface of nanoclusters (NCs).[180] These data point to the effective capping of L-cysteine on the surface of synthesized NCs.

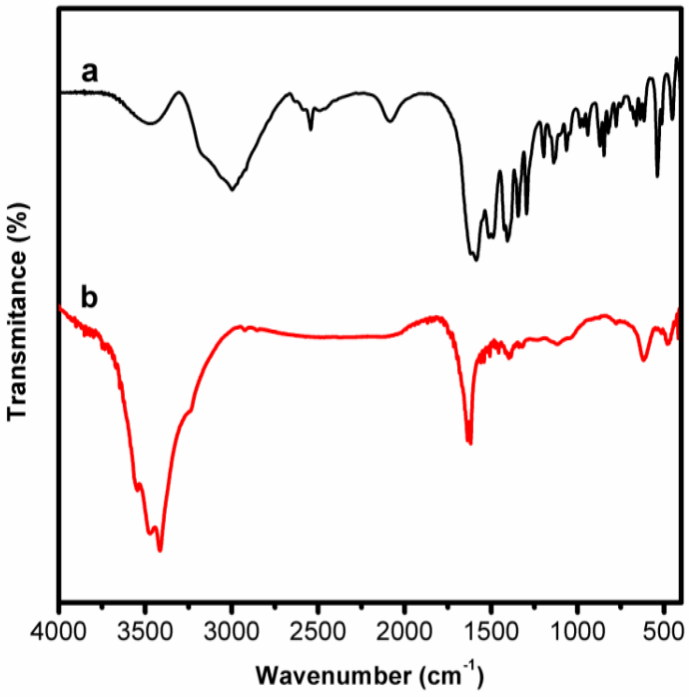

Figure 7.5: FTIR spectrum of (a) L-cysteine and (b) L-cys-CuNCs.

Using Rhodamine 6G (quantum yield of 95 %) as reference material, quantum yield of synthesized CuNCs was calculated from its absorption and emission spectra at different concentrations.[165] Figure 7.6 shows the plot of integrated fluorescence intensity against absorbance of L-cys-CuNCs at

various concentrations. Using the slope of above graph, quantum yield was calculated to be 0.37 %. Overall results showed that, the synthesized CuNCs can be used as a sensing element for fluorescence sensor.

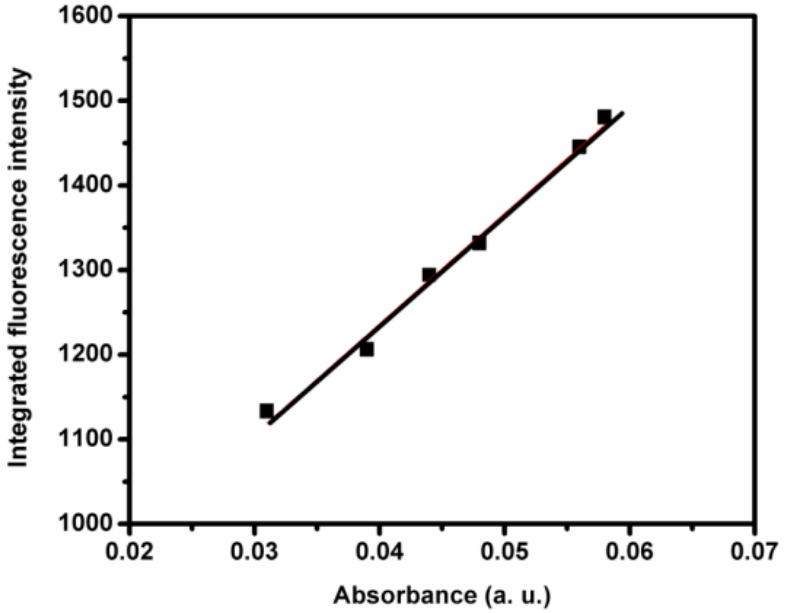

Figure 7.6: Plot of integrated fluorescence intensity against absorbance of various concentrations of L-cys-CuNCs.

7.3.2 Optimization of Experimental Parameters

7.3.2.1 Selection of Buffer

Fluorescence intensities of L-cys-CuNCs before (I_0) and after the addition of QY (I) were measured in different buffer solutions viz., phosphate (PBS), citrate, acetate buffer solutions of 0.1 M concentration and the I_0/I was calculated (Table 7.1). PBS gave a higher value for I_0/I and was chosen as medium for further studies.

Table 7.1: Effect of the medium in the fluorescence signal of CuNCs alone and in presence of QY.

Buffer	I_0	I	I_0/I
ABS 7	15009.16	10978.95	1.36
PBS 7	15141.00	10956.26	1.38
CBS 7	16475.99	14233.87	1.15

7.3.2.2 Effect of pH

The pH of the medium can affect the sensing characteristics. PBS having different pH (2 to 9) were used as the sensing medium and better result (higher value of I_0/I) was observed for pH of 6 (Table 7.2), hence PBS of pH 6 was selected.

Table 7.2: Effect of pH of PBS in the fluorescence signal of CuNCs alone and in presence of QY.

Buffer	I_0	I	I_0/I
2	7869.53	5829.66	1.34
3	14822.43	11864.57	1.24
4	14389.26	12181.86	1.18
5	14637.43	10826.85	1.35
6	14611.76	10232.53	1.42
7	15141.00	10956.26	1.38
8	9911.73	9150.94	1.08
9	11365.68	8286.93	1.37

7.3.2.3 Effect of irradiation time on fluorescence intensity

Photo stability of probe with and without QY is evaluated by irradiating solution continuously and L-cys-CuNCs solution gave stable fluorescence signal up to 23 minutes in the absence of QY. In presence of QY, fluorescence signal quenched and became stable quickly within 30 seconds and retained its stability up to 23 minutes (Figure 7.7). This fast response reduces the time consuming incubation step which is a common and inevitable part of most of the present day analytical strategies for evaluation of food quality.

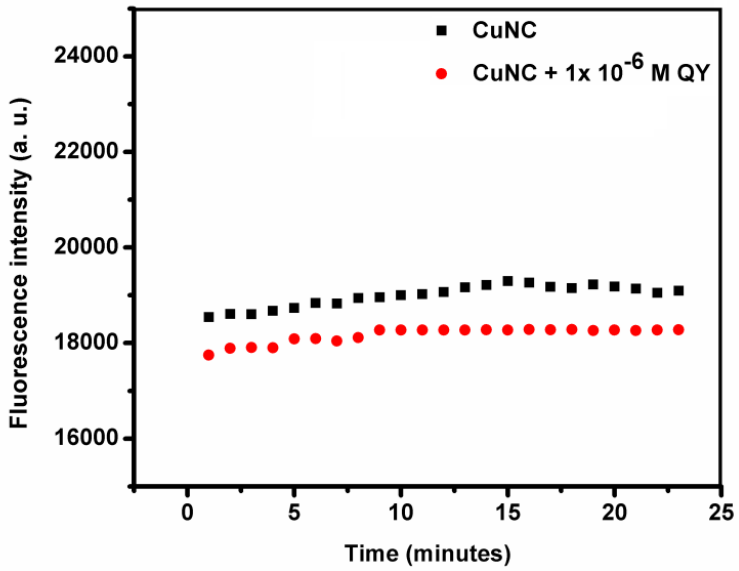

Figure 7.7: Effect of time on the fluorescence intensity of L-cys-CuNCs with and without QY.

7.3.3 Performance of Sensor

7.3.3.1 Effect of Concentration

Upon increasing concentration of QY, a considerable reduction in intensity of fluorescence signal was observed (Figure 7.8). A calibration graph was plotted with ratio of fluorescence intensities (I_0/I) versus concentration of QY.

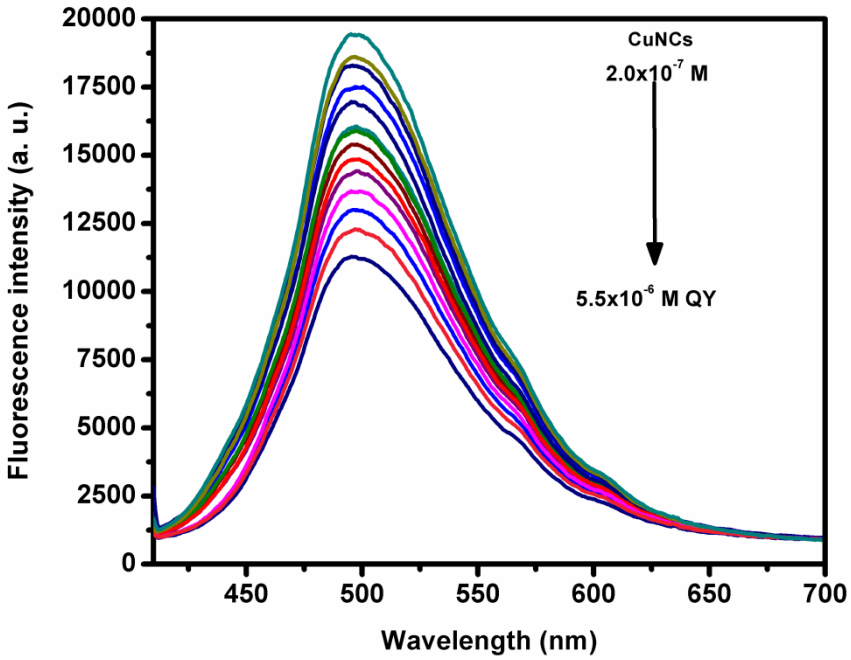

Figure 7.8: Effect of concentration of QY on the fluorescence intensity of L-cys-CuNCs.

The plot of the ratio of fluorescence intensities (I_0/I) against the concentration of QY was found to be linear relationship in the range of 5.50×10^{-6} M to 2.00×10^{-7} M (Figure 7.9), which follows the Stern- Volmer equation:

$$\frac{I_0}{I} = 1 + K_{SV}[C]$$

Here [C] is the concentration of QY and the slope K_{SV} was found to be 7.9×10^4 M^{-1}. Limit of detection (LOD) was calculated using the formula '3S/m', where 'S' and 'm' are the standard deviation and slope of the calibration graph respectively[181] and LOD was found to be 1.11×10^{-7} M. Lower value of relative standard deviation (RSD) (0.77% (n = 5)) for the quantification of 2.00×10^{-7} M QY reveals good reproducibility of sensor.

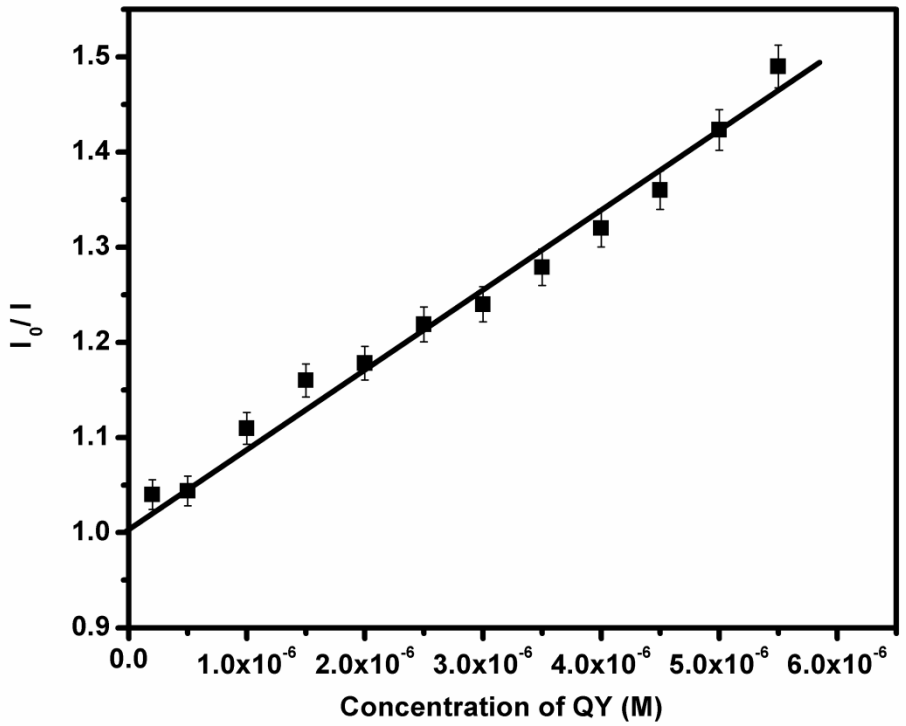

Figure 7.9: Linear calibration graph between I_0/I and concentrations of QY.

Table 7.3 shows the comparison of different analytical techniques for quantification of QY. A close examination of Table 7.3 reveals that the performance of proposed sensor is comparable with existing analytical methods.

Table 7.3: Analytical parameters of the proposed method and existing methods for determination of QY.

Sl. No.	Method	Linear range (M)	LOD (M)	Reference
1.	Digital image analysis	5.23×10^{-4} - 6.28×10^{-5}	1.68×10^{-5}	182
2.	LC-MS	1.46×10^{-7} - 2.09×10^{-8}	1.04×10^{-8}	183
3.	Voltammetry	1.00×10^{-6} - 5.00×10^{-8}	2.70×10^{-8}	184
4.	HPLC	6.28×10^{-6} - 1.04×10^{-6}	9.21×10^{-8}	185
5.	Spectrophotometry	-	3.35×10^{-7}	186
6.	Fluorimetry	9.50×10^{-6} - 2.00×10^{-7}	1.11×10^{-7}	-

7.3.3.2 Selectivity of proposed sensor

One of the significant properties of an ideal sensor is its selectivity towards target species.[187] To check the selectivity of developed sensor, various species having concentration of 1.00×10^{-6} M that are either coexisting with QY in real samples or having a yellow color were used and their effect on fluorescence intensity of L-cys-CuNCs was studied. Figure 7.10 shows changes in fluorescence spectra of L-cys-CuNCs which occur upon addition of QY, sunset yellow, tartrazine, citric acid, acetic acid, ascorbic acid, glucose, fructose, NaCl and saccharin respectively. L-cys-CuNCs showed excellent selectivity towards QY by giving a high value of I_0/I.

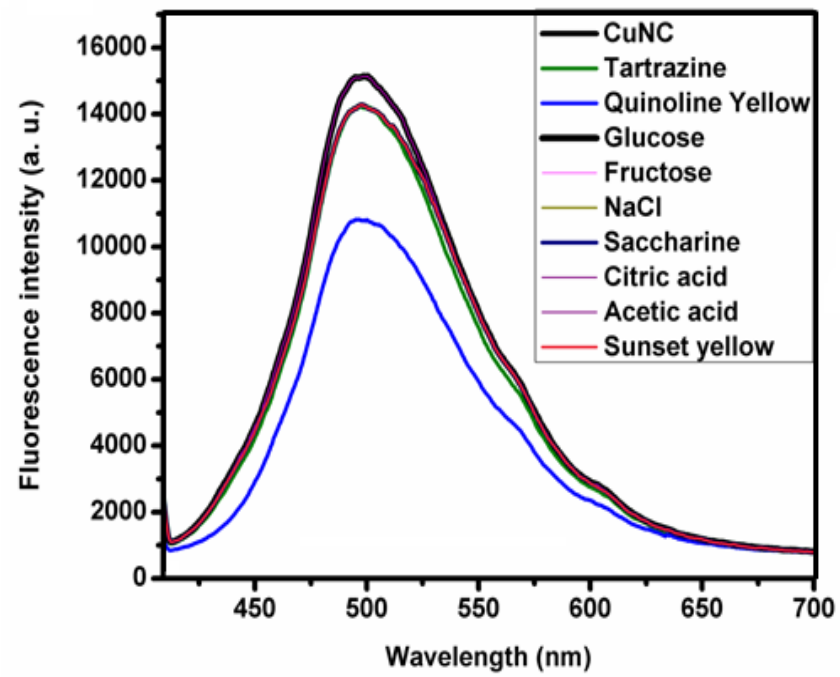

Figure 7.10: selectivity of L-cys-CuNCs towards various analytes.

Possible interference caused by the above mentioned species was also studied by measuring quenching efficiency of QY in presence of different concentrations of similar colored or coexisting species (Table 7.4). Similar colored compounds such as sunset yellow and tartrazine produced negligible interference when present at a 1:1 concentration with QY. Other foreign species did not interfere with the analysis even in presence of up to 100 fold excess concentration.

Table 7.4: Effect of coexisting species on fluorescence quenching of QY.

Analyte	Concentration (M)	Signal change (%)
Saccharin	1.00×10^{-4}	0.2
Sodium chloride	1.00×10^{-4}	1.0
Glucose	1.00×10^{-4}	0.1
Fructose	1.00×10^{-4}	1.2
Ascorbic acid	1.00×10^{-4}	1.3
Acetic acid	1.00×10^{-4}	0.1
Citric acid	1.00×10^{-4}	4.3
Sunset yellow	1.00×10^{-6}	6.8
Tartrazine	1.00×10^{-6}	7.4

7.3.4 Investigation on sensing mechanism

Reduction in the fluorescence intensity of L-cys-CuNCs upon addition of QY clearly indicates the existence of an interaction between probe and analyte. To ascertain type of quenching, lifetime, TEM, DLS and UV – visible spectroscopic analyses were carried out in the absence and presence of QY. A negligible change in lifetime measurement of L-cys-CuNCs (before 1.58 ns and after addition 1.50 ns) was observed (Figure 7.11), suggesting the possibility for a static quenching by means of ground state interactions.[35]

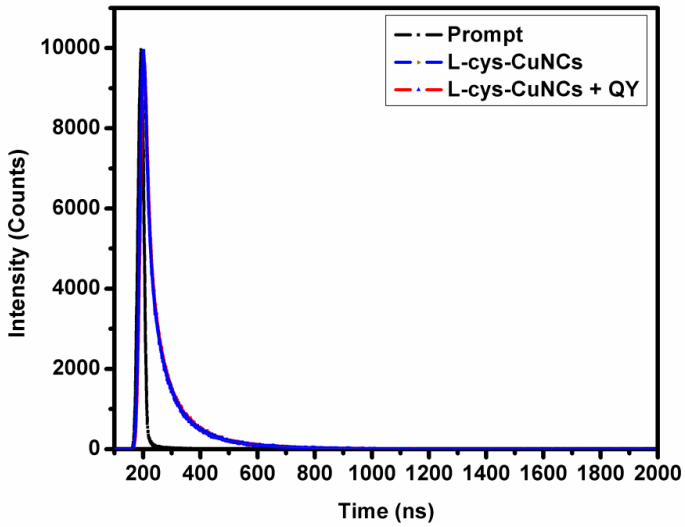

Figure 7.11: Fluorescence decay curves of probe and probe + QY.

In the UV-visible spectral analysis (Figure 7.12), appearance of a new peak at ~ 420 nm was observed after 30 seconds of mixing which ruled out the possibility of inner filter effect,[187] consequently 'the formation' implying of a complex between the probe and analyte.[188]

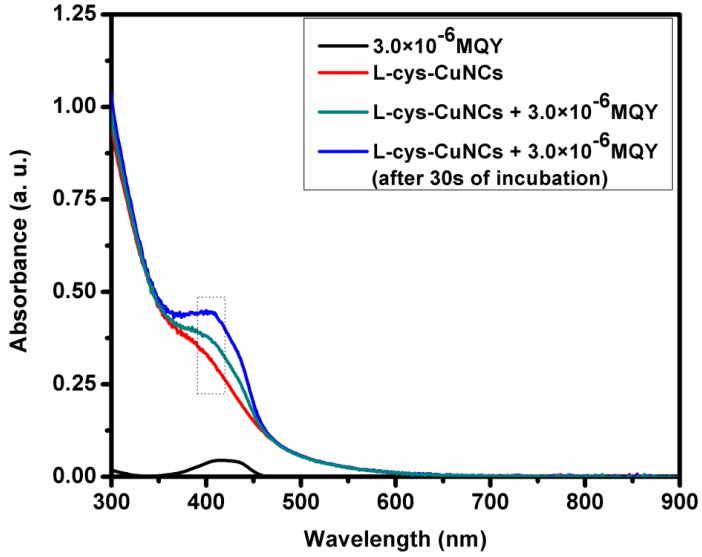

Figure 7.12: Absorption spectra of probe with and without QY.

Additionally, there was a large increase in hydrodynamic diameter from 2.8 nm to 18.3 nm after the addition of QY clearly indicate aggregation of particles (Figure 7.13). Also, visualization of aggregates in TEM image of L-cys-CuNCs in presence of QY (Figure 7.14) confirms the proposed mechanism.

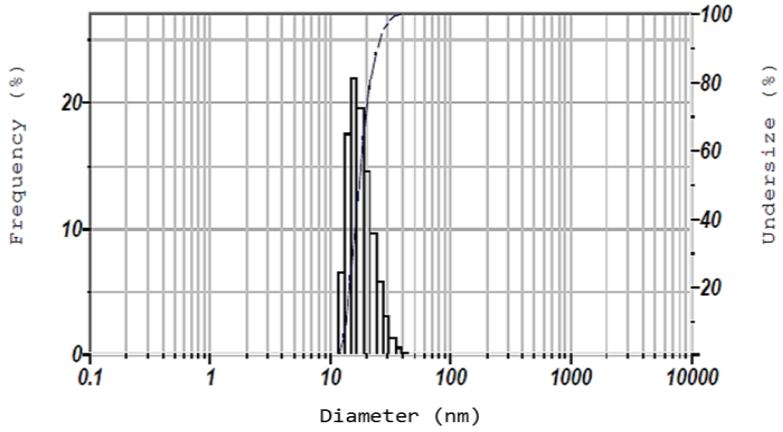

Figure 7.13: DLS analysis of L-cys-CuNCs in presence of QY.

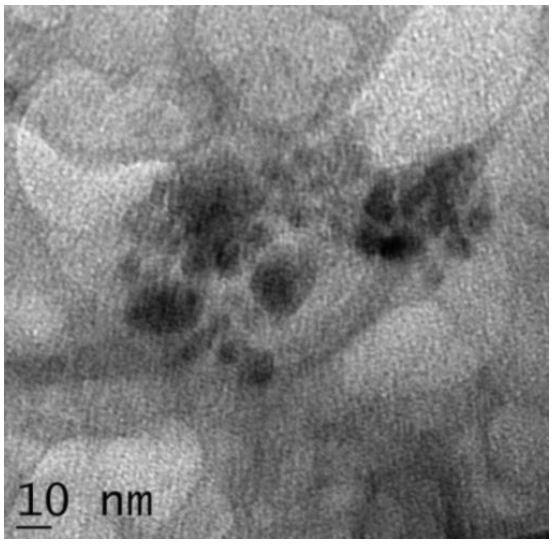

Figure 7.14: TEM image of L-cys-CuNCs in presence of QY.

7.3.5 Determination of QY from food samples

To prove the effectiveness of developed fluorescence assay in real sample analysis, determination of QY in candies and soft drink were carried out. Concentration of QY was estimated using standard addition method and spectrophotometric method was employed for comparison.[96] Table 7.5 represents the concentrations of QY obtained from proposed and standard method. From the table, it is clear that, results obtained from spectrophotometry are in good agreement with those of proposed assay and it reveals practical utility of the developed sensor for real sample analysis.

Table 7.5: Estimation of QY in food samples by proposed and reference methods.

Samples	Spiked concentration (M)	Proposed method		Spectrophotometric method	
		Found[a] (M)	Recovery[a] (%)	Found[a] (M)	Recovery[a] (%)
Candy 1	-	6.96×10^{-7}	-	7.35×10^{-7}	-
Candy 2	-	1.96×10^{-6}	-	1.90×10^{-6}	-
Soft drink	2.00×10^{-6}	2.03×10^{-6}	102	1.98×10^{-6}	99

[a] = average of three replicates

7.4 Conclusions

A new fluorescence assay for QY has been developed and it shows good reproducibility and effectiveness towards estimating the concentration of QY in food samples. The developed method is simple and cost effective compared to present existing methods for QY determination. Proposed sensor exhibited good working linear ranges between 9.50×10^{-6} and 2.00×10^{-7} M with a detection limit of 1.11×10^{-7} M for determining the concentration of QY in phosphate buffer. Developed method was

successfully applied for determination of QY in commercial food product samples and thus can find huge potential in food quality control.

.....ꕥ.....

Chapter 8

SYNTHESIS OF CARBON DOTS AND APPLICATION AS A FLUORESCENT SENSOR FOR GLUTATHIONE

Contents

Development of a novel, cost - effective synthetic strategy for carbon dots and its application as a fluorescent sensor is explained in this chapter. Tissue paper was chosen as the carbon source for the 'green one pot' synthesis of ethylenediamine passivated carbon dots (EDA-CDs). The master antioxidant - glutathione (GSH) could induce quenching of the fluorescence intensity of EDA-CDs through aggregation, resulting from their surface interactions. Based on this, a novel fluorescence sensor was fabricated for the determination of GSH in body fluids. A linear calibration graph was obtained in the range of 6.0×10^{-7} to 5.0×10^{-8} M with a detection limit of 1.74×10^{-9} M. The developed sensor was successfully used for the determination of GSH in artificial saliva samples.

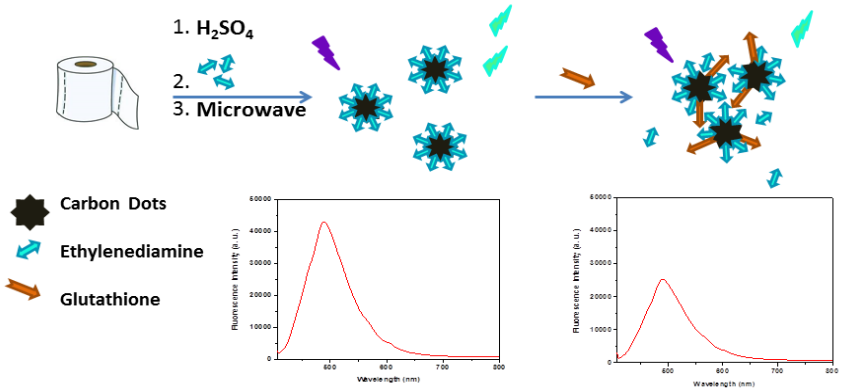

Scheme 8.1: Diagram illustrating the synthesis of EDA-CDs and application as fluorescent sensor for GSH.

8.1 Introduction

Antioxidants are present in all body fluids and tissues, which protect our body from endogenously formed free radicals. Their body levels are governed by the balance between the degrees of production and clearance. Dietary derived components (non- protein thiols and uric acid) and superoxide dismutase, catalase, the glutathione redox cycling enzymes, glutathione peroxidase and glutathione reductase and glutathione can act as biological antioxidants.[189- 192] The development of analytical tools for the determination of antioxidants in biological systems is significant in view of changing life styles.

Glutathione (γ-glutamyl-cysteinyl-glycine; GSH) is a tripeptide composed of three amino acids viz., cysteine, glutamic acid and glycine. It is found at millimolar levels in cells and at micromolar levels in biological fluids.[193] GSH plays an important role in limiting the pathogenesis of many syndromes, such as psoriasis, liver damage, cancer and heart problems.[194, 195] In addition, its crucial role in delaying the process of aging by reducing oxidative stress signifies its importance in the human system. Thus, GSH is indispensable for life, and the analysis of glutathione levels is significant for the early diagnosis of many diseases.

In recent years, fluorescence spectrometry has been evolving as a promising tool for GSH determination[196 -198] due to its simplicity, high sensitivity and cost effectiveness.[199]

Carbon quantum dots or carbon dots (CDs) are a special class of carbon nanomaterials with sizes of less than 10 nm. Due to special properties, such as high (aqueous) solubility, chemical inertness and high

resistance to photo bleaching in comparison with traditional semiconductor quantum dots and organic dyes,[51] CDs was chosen as the fluorescent probe for this study.

Currently, various methods like chemical ablation,[200] electrochemical carbonization,[201] Laser ablation,[202] microware irradiation[203] and hydrothermal/solvothermal treatment[204] have been used for the synthesis of CDs. Among these, microwave irradiation technique stands out due to its advantages, like increased reaction rates, uniform heating, improved product yields, broad dynamic temperature range and environment friendly nature.[205] However, no reports have been found concerning the green synthesis of CDs from low - cost tissue paper (cellulose) as the carbon source.

This chapter describes the development of a novel green method for the synthesis of ethylenediamine (EDA) passivated carbon dots from tissue paper; and it was successfully used for the determination of GSH in artificial saliva samples.

8.2 Experimental

8.2.1 Synthesis of ethylenediamine passivated CDs

A new cost - effective and simple 'one - pot green' synthesis of ethylenediamine passivated CDs (EDA-CDs) using cellulose as the carbon source is reported here. In the proposed method, microwave irradiation is carried out to speed up the reaction. Surface passivation is necessary for a higher fluorescence intensity.[206] Since ethylenediamine is an effective

passivating agent for CDs, it was chosen in the proposed method. Passivation with EDA enhances the fluorescence intensity of CDs.

One gram of tissue paper was taken in a 100 mL beaker and mixed vigorously with 1 mL of con. H_2SO_4. The obtained gel - like material was mixed with 3 mL of EDA. When the mixture stopped giving out fumes, it was irradiated in a domestic microwave oven at 800 W power for 4 minutes. The product was collected after cooling and dissolved in 25 mL of deionized water (Figure 8.1). The solution was filtered and centrifuged at 400 rpm and the supernatant solution was taken for further studies. The obtained EDA-CDs were further purified by dialysis. The removal of sulphate ions was confirmed by using $BaCl_2$ solution. The obtained probe solution was diluted to adjust the absorbance below 1 a.u.

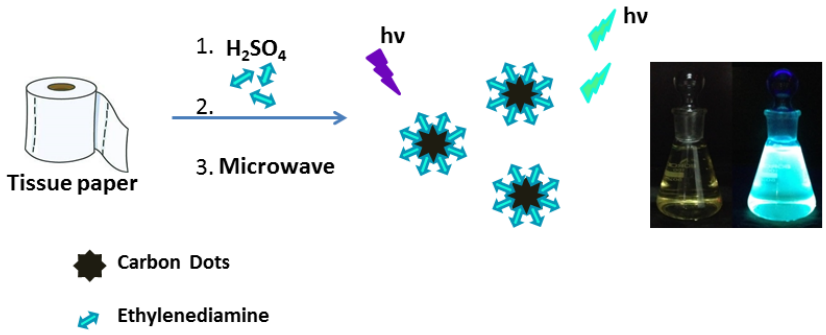

Figure 8.1: Pictorial representation of synthetic strategy of EDA-CDs. Inset: photograph of EDA-CDs under normal light and UV light.

8.2.2 UV-Vis and fluorescence studies

Absorption (UV-Vis) spectrum was obtained by glancing over the sample in a wavelength range from 200 to 900 nm. Emission (fluorescence) spectrum was measured at λ_{ex}/ λ_{em} = 400 / 520 nm. To the EDA-CDs

solution (0.03 mL of diluted probe solution) taken in a 1 cm × 1 cm quartz cuvette, the required amount of GSH (0.12 mL to 0.01 mL of 1.00×10^{-5} M) was added for respective sampling and the total volume was made up to 2 mL by adding an appropriate amount of water so that the concentration of GSH in the resultant solution would be from 6.0×10^{-7} M to 5.0×10^{-8} M. Studies were conducted after 5 minutes of incubation. The relative quenching of the fluorescence intensity was denoted by (I_0 / I), where I and I_0 are the fluorescence intensities obtained with and without GSH respectively.

8.2.3 Measurement of GSH in artificial saliva samples

Artificial saliva samples were prepared by following the procedure described in section 2.4.1. Saliva samples were spiked with a GSH solution to obtain concentration within the dynamic range (6.0×10^{-7} M to 5.0×10^{-8} M) of the proposed method. Samples containing GSH were used for further analysis, and the amount of GSH was estimated from the linear calibration graph. For comparison, the concentrations of GSH in artificial saliva samples were also determined using Ellman's colorimetric test[97] as described in section 2.3.4.

8.3 Results and discussion

8.3.1 Optimized conditions for the synthesis of EDA-CDs

Amount of passivating agent and time required for microwave irradiation for the synthesis of EDA-CDs from 1 g of tissue paper were optimized as discussed below.

8.3.1.1 Amount of passivating agent

By varying the amount of EDA, CDs were synthesized and its stability and fluorescence intensity were studied. From 0.5 mL to 3 mL of EDA, fluorescence intensity increases and become almost constant thereafter (Figure 8.2). So 3 mL of EDA was chosen as the optimal volume for the synthesis.

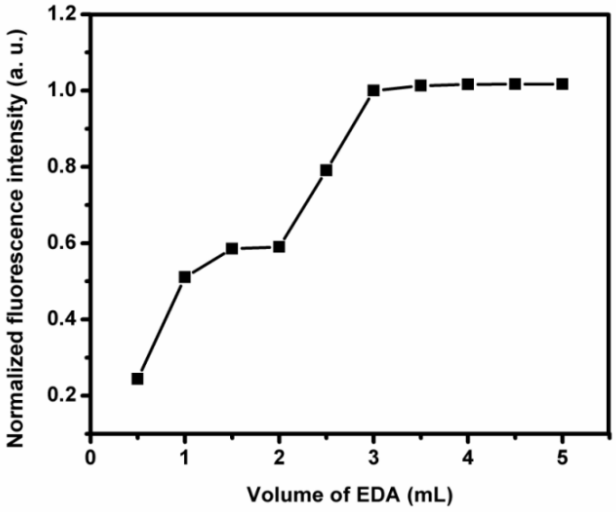

Figure 8.2: Effect on the fluorescence intensity of CDs synthesised by different volume of EDA.

8.3.1.2 Microwave irradiation time required for the formation of CDs

Irradiation time of microwave for the synthesis of CDs from 1 g of tissue paper and 3 mL EDA was optimized by varying the time period from 1 to 6 minutes. A remarkable increase in fluorescence intensity of CDs was observed as the reagent was irradiated under microwave up to 4 minutes and intensity become constant after 4 minutes of irradiation (Figure 8.3). So the time period required for the synthesis was optimized to be 4 minutes.

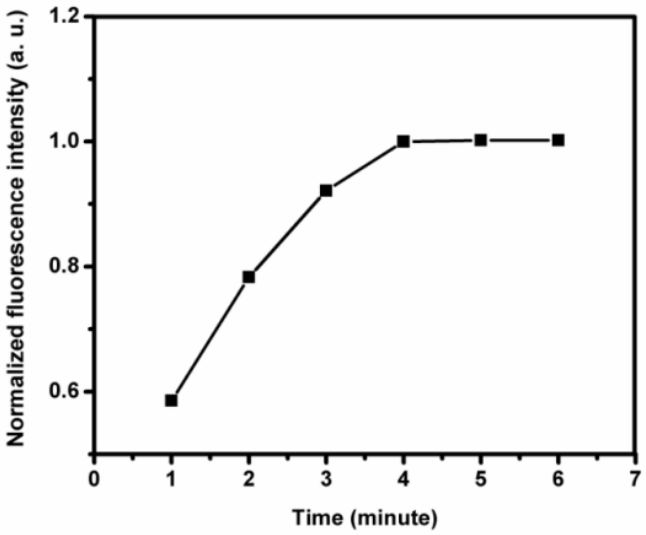

Figure 8.3: Effect on the fluorescence intensity of EDA-CDs synthesised by irradiation of microwave at different time intervals.

8.3.2 Characteristics of ethylenediamine passivated CDs

The synthesized EDA-CDs were characterized by UV/vis absorption, fluorescence spectroscopy, dynamic light scattering analysis (DLS) and transmission electron microscopy (TEM). The UV/vis absorption spectrum of CDs exhibited a broad peak with maximum absorption at 335 nm (Figure 8.4). In the emission spectrum (excitation wavelength 400 nm), an intense peak centered at 490 nm was observed (Figure 8.5).

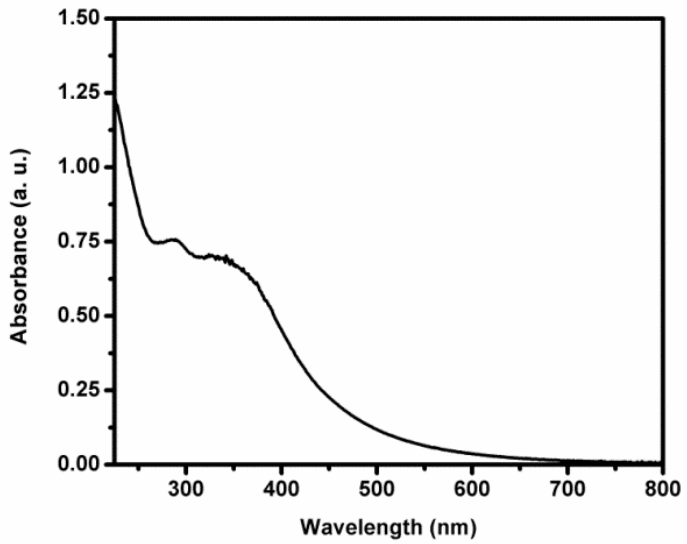

Figure 8.4: Absorption spectrum of synthesized EDA-CDs.

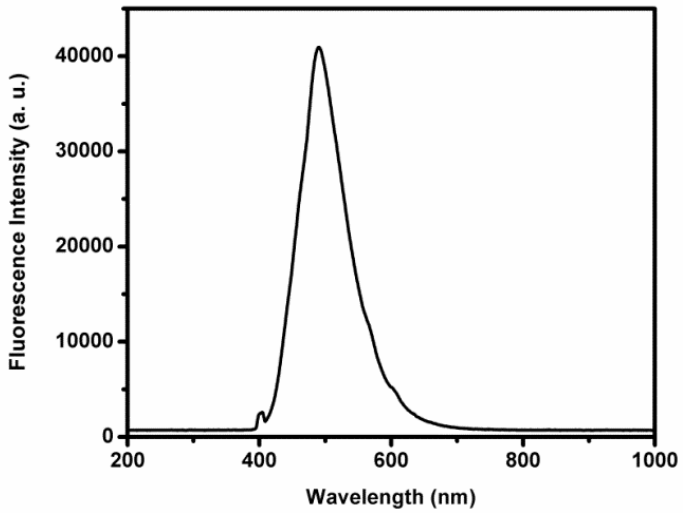

Figure 8.5: Emission spectrum of synthesized EDA-CDs.

The fluorescence intensity of EDA-CDs was enhanced around 20 times to that of bare CDs (without passivation) (Figure 8.6). This may be due to the effective surface passivation of EDA on the surface of the CDs.[207]

The obtained broad spectrum indicates the presence of a large number of surface defects.[163] Under UV irradiation, the pale - yellow colored solution of EDA-CDs showed a bright blue fluorescence (Inset of figure 8.1).

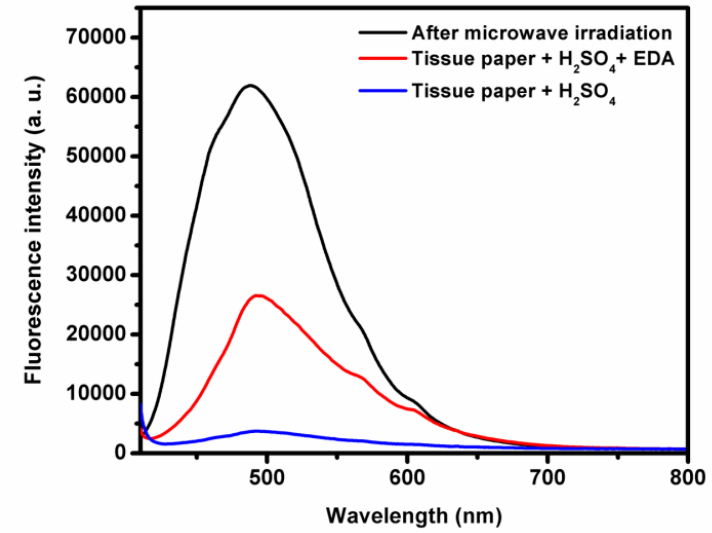

Figure 8.6: Fluorescence spectra of (a) bare CDs (b) EDA passivated CDs.

TEM image indicates that the synthesized EDA-CDs were spherical and well dispersed, and had an average diameter of 4.2 nm (Figure 8.7). The lattice spacing determined from HRTEM image was found to be 0.35 nm (inset of figure 8.7); this may be due to the formation of some graphene QDs (for graphene QDs, lattice spacing was 0.34 nm). Hydrodynamic diameter obtained from DLS analysis was ~7.40 nm (Figure 8.8). The observed fluorescence lifetime of EDA-CDs was 2.98×10^{-9} seconds.

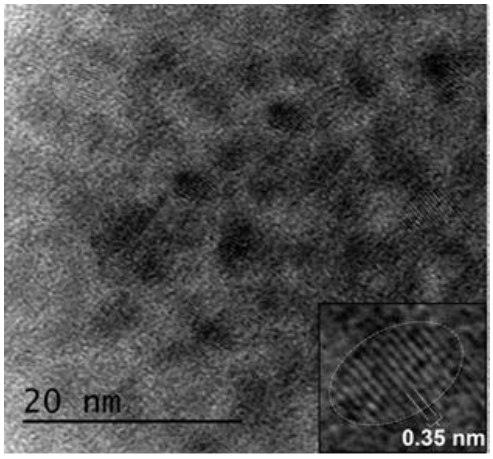

Figure 8.7: TEM images of EDA-CDs. Inset: lattice spacing of one particle.

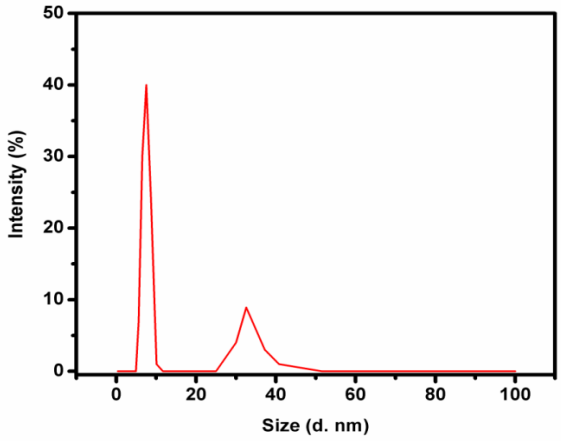

Figure 8.8: DLS spectrum of EDA-CDs.

Taking fluorescein (Fl) as the standard (with a fluorescence quantum yield of 93.0 %), the quantum yield of the EDA-CDs was determined from its absorption and emission spectra at different concentrations.[202] The integral fluorescence intensities (IFI) of various concentrations of Fl and EDA-CDs were measured and plotted against absorbance. Figure 8.9 and Figure 8.10 shows the resultant plots of IFI vs. absorbance of Fl and EDA-CDs respectively.

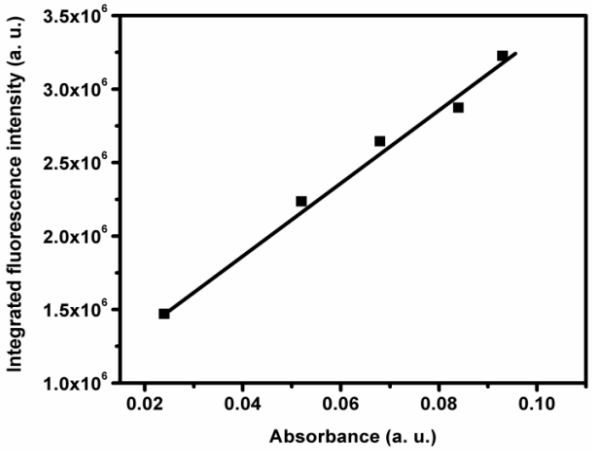

Figure 8.9: Plot of integrated fluorescence intensity against absorbance of different concentrations of fluorescein.

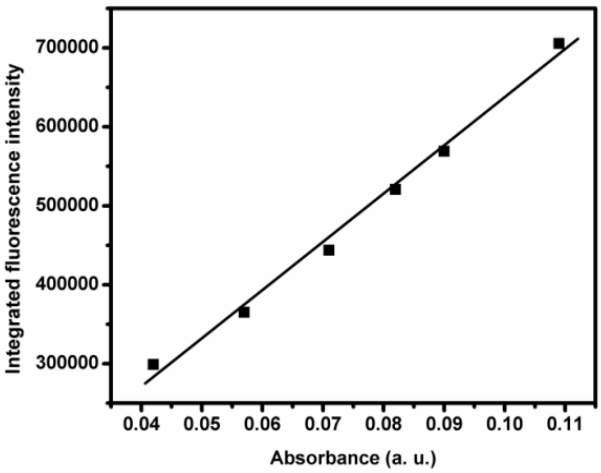

Figure 8.10: Plot of integrated fluorescence intensity against absorbance of different concentrations of EDA-CDs.

Using the obtained slopes in the following equation, quantum yield was calculated.

$$\Phi_{CDs} = \Phi_{Fl} \times \frac{\mu_{CDs}}{\mu_{Fl}} \times \left(\frac{\eta_{CDs}}{\eta_{Fl}}\right)^2$$

Where ϕ_{CDs} is the quantum yield of EDA-CDs and ϕ_{Fl} is the quantum yield of Fl. μ_{CDs} and μ_{Fl} represents the slopes of the plot of IFI vs absorbance of EDA-CDs and Fl respectively. η_{CDs} and η_{Fl} denotes the refractive indices of the solutions of fluorescent probe and standard. Quantum yield was calculated to be 23.6 %.

8.3.3 Optimized conditions for sensing application

Stability of the probe in different media, towards photo-bleaching and time required for the completion of interaction of probe and analyte were optimized as detailed below.

8.3.3.1 Effect of the medium

To select a suitable medium for studies, the emission properties (stability and intensity) of the probe were studied in different media, such as acetate buffer, citrate buffer, phosphate buffer and water. Since the cell environment is always buffered at approximately pH 7, buffers with pH 7 were used for the studies. Table 8.1 represents the normalized fluorescence intensity and the stability of EDA-CDs in different media studied. The best result was obtained in water and hence water was chosen as the solvent for the analysis.

Table 8.1: Effect of the medium in the fluorescence signal of EDA-CDs.

Studied medium	Normalized fluorescence intensity (a. u.)	Stability (minutes)
Acetate buffer	0.5921	3.5
Citrate buffer	0.4852	8.0
Phosphate buffer	0.1934	9.5
Water	1	20.0

8.3.3.2 Effect of time on the fluorescence intensity

Under the illumination conditions, irreversible destruction of the fluorescent probe could be taken place, which could result in a decrease in fluorescence intensity. A study on the variation of fluorescence intensity with time revealed that the fluorescence intensity of EDA-CDs was stable up to 20 minutes. Upon addition of GSH, fluorescence signal attained stability after 5 minutes and remained stable up to 18 minutes (Figure 8.11). Further measurements were also made after 5 minutes of mixing.

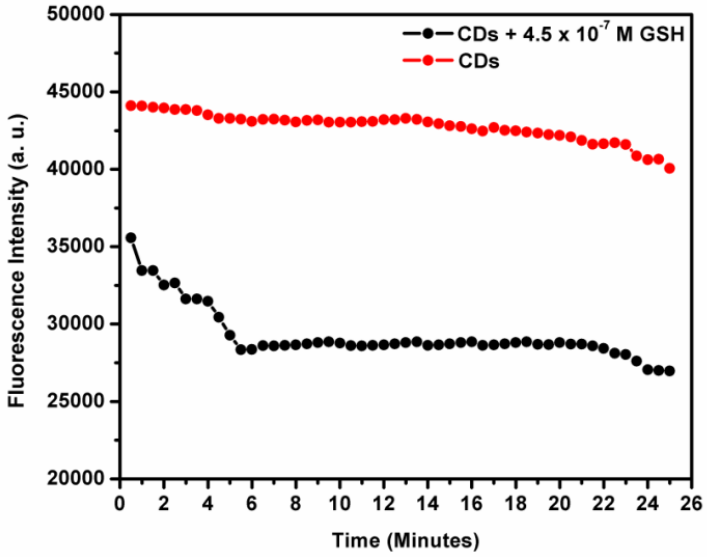

Figure 8.11: Effect of time on fluorescence intensity of EDA-CDs alone and in presence of GSH.

8.3.4 Effect of foreign species

A significant property of a good sensor is its selectivity towards a particular species. Among various biological molecules (5.00×10^{-7} M) studied, such as β-Alanine, L-Glycine, L-Glutamic acid, L-Tyrosine, L-

Cysteine, L-Histidine, L-Lysine, L-Tryptophan, Uric acid and GSH, only GSH effectively quench the fluorescence of EDA-CDs (Figure 8.12).

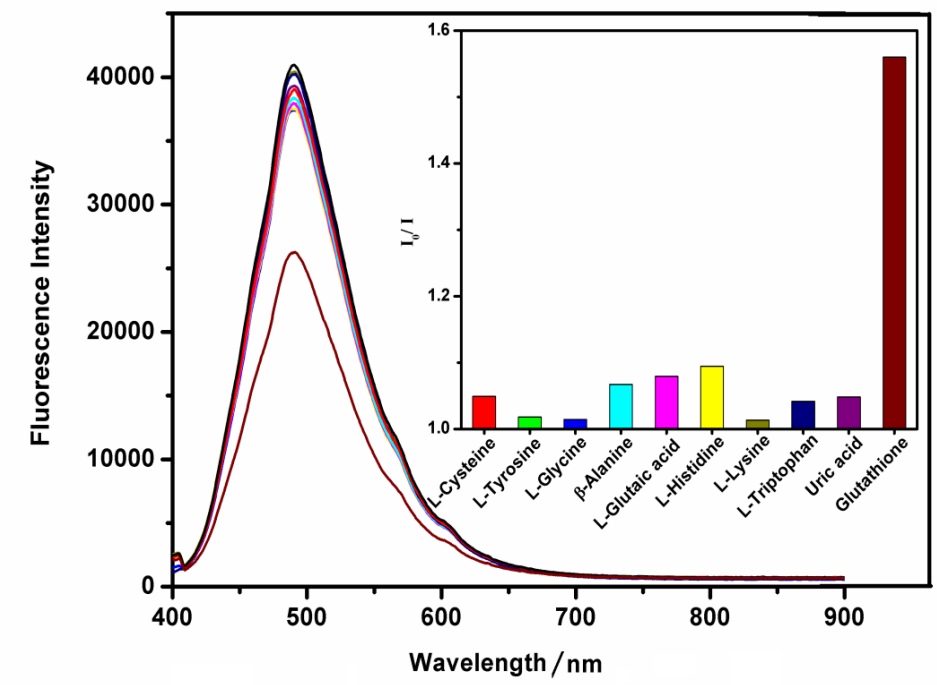

Figure 8.12: Selectivity of the probe towards different species.

Influence of concentration of above mentioned species in the fluorescence signal of EDA-CDs in presence of GSH (1.5×10^{-7} M) was also studied (Table 8.2). β-Alanine, L-Glycine, L-Glutamic acid, L-Tyrosine, L-Lysine and uric acid didn't show any interference even up to 100 fold excess concentration of GSH. However, L-Cysteine, L-Histidine and L-Tryptophan showed significant signal changes (above 5%) when present above 50 fold excess concentration (7.5×10^{-6} M).

Table 8.2: Effect of coexistence on the determination of 1.5×10^{-7} M GSH.

Coexisting species	Concentration (M)	Interference (%)
β-Alanine	1.5×10^{-5}	4.4
L-Glycine	1.5×10^{-5}	4.0
L-Glutamic acid	1.5×10^{-5}	3.1
L-Tyrosine	1.5×10^{-5}	1.9
L-Cysteine	1.5×10^{-5}	6.3
L-Histidine	1.5×10^{-5}	6.0
L-Lysine	1.5×10^{-5}	1.2
L-Tryptophan	1.5×10^{-5}	7.0
Uric acid	1.5×10^{-5}	4.2

8.3.5 Fluorescence quenching of EDA-CDs by GSH

Fluorescence intensity of EDA-CDs was quenched by the addition of GSH. A dramatic decrease in the fluorescence intensity of the probe was observed with increasing concentration of GSH (Figure 8.13). A plot of the ratio of fluorescence intensities (I_0/I) against the concentration of GSH shows a linear relationship (Figure 8.14) in the range of 6.0×10^{-7} to 5.0×10^{-8} M ($R^2 = 0.998$), which follows the Stern- Volmer equation:

$$\frac{I_0}{I} = 1 + K_{SV}[C]$$

Here I and I_0 represent the fluorescence intensities of EDA-CDs with and without GSH; [C] is the concentration of GSH and the slope K_{SV} was found to be 1.32×10^{6} M^{-1}. The limit of detection and the limit of quantification were calculated to be 1.74×10^{-9} M and 5.82×10^{-9} M respectively. The relative standard deviation for the determination of 5.0×10^{-8} M GSH was 3.8 % (n = 5).

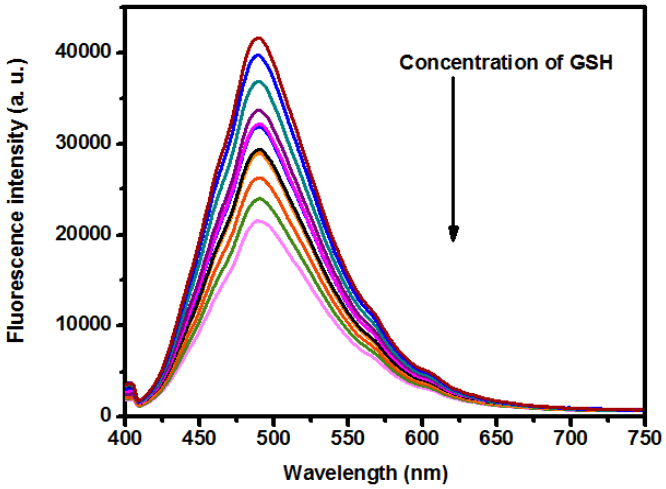

Figure 8.13: Emission spectra of EDA-CDs in presence of various concentrations of GSH.

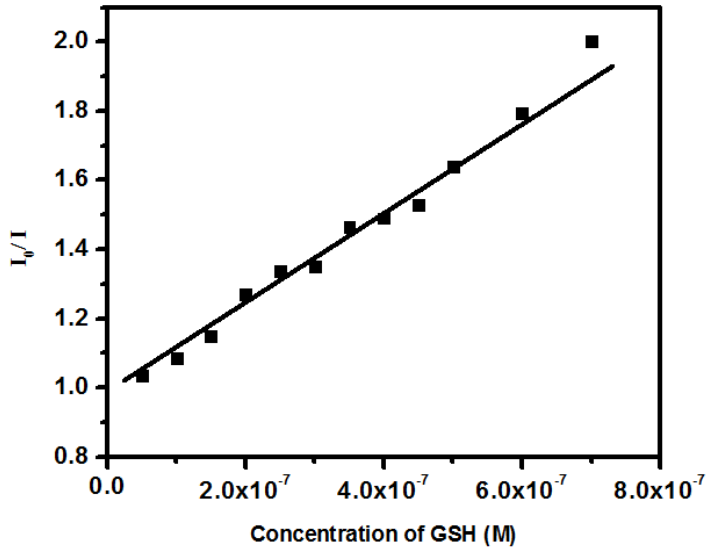

Figure 8.14: Linear calibration graph between the ratio of fluorescence intensities and concentration of GSH.

Table 8.3 represents a comparison of various fluorescence sensors for the quantification of GSH; it reveals that the proposed sensor exhibited superior sensing performance compared with other reports.

Table 8.3: Comparison of the proposed sensor with other fluorescence sensors.

Fluorescent probe used	Linear range (M)	LOD (M)	Reference
Dopamine-modified QDs	0 to 1.0×10^{-2}	Not given	22
MnO_2 modified UCNPs	Not given	9.0×10^{-7}	23
R6G-QDs conjugate	8.0×10^{-7} to 5.0×10^{-8}	1.5×10^{-8}	24
AuNCs + Hg^{2+}	0 to 2.5×10^{-4}	9.4×10^{-9}	25
PEI-capped AgNCs	6.0×10^{-6} to 5.0×10^{-7}	3.8×10^{-7}	8
AuNPs + CQDs	Not given	5.0×10^{-8}	9
CdTe QDs	4.1×10^{-5} to 2.6×10^{-6}	1.6×10^{-9}	10
EDA-CDs	6.0×10^{-7} to 5.0×10^{-8}	1.7×10^{-9}	-

8.3.6 Mechanism of quenching

Figure 8.15 shows the absorption spectrum of (a) GSH, (b) EDA-CDs and (c) EDA-CDs in the presence of GSH. From the figure, it is clear that GSH did not have any absorption in the studied wavelength range. The decrease in the absorbance value of CDs upon the addition of GSH indicates the ground state interactions of analyte (GSH) with probe (EDA-CDs).

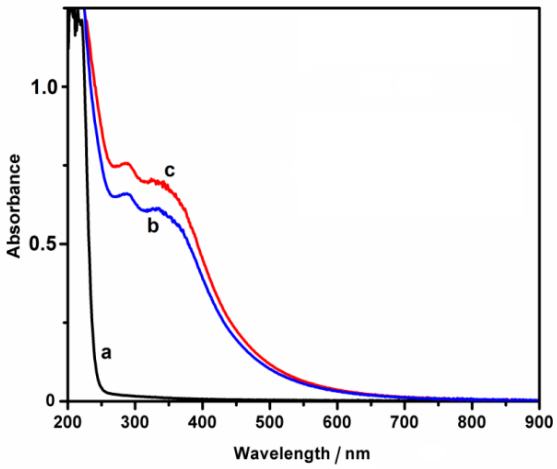

Figure 8.15: UV-visible absorption spectra of (a) GSH, (b) EDA-CDs and (c) EDA-CDs in presence of GSH.

To confirm the ground state interactions, fluorescence lifetime measurements were carried out (Figure 8.16). Fluorescence lifetime of EDA-CDs before and after addition of GSH was found to be almost similar (2.98×10^{-9} s and 3.08×10^{-9} s), which ruled out the probability of excited state interactions and points to the ground state interactions.

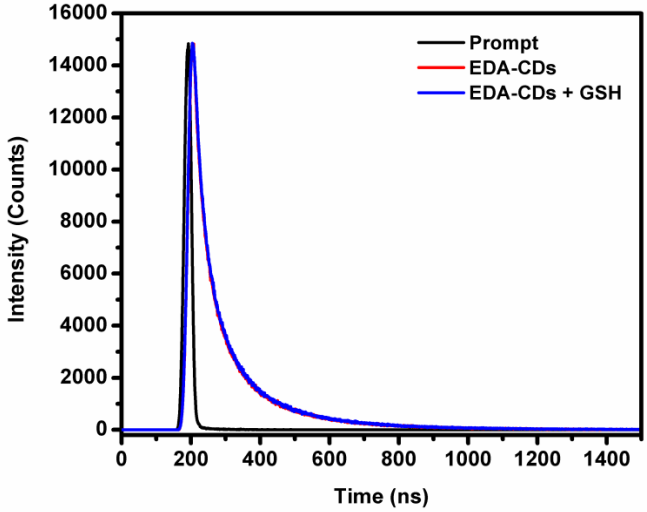

Figure 8.16: Fluorescence decay curves of EDA-CDs alone and in presence of 1.00×10^{-5} M GSH.

Assigned reasons for the fluorescence of CDs are the quantum effect,[45, 212] defects and surface states.[213] Therefore, a change in electron density on the surface may alter the fluorescence intensity of QDs. Accordingly, the fluorescence intensity of QDs may increase in the presence of a Lewis base and a decrease in the presence of a Lewis acid.[214-216] The observed quenching of fluorescence intensity of EDA-CDs in the presence of GSH may be due to the Lewis acid nature of the thiol group in GSH. The hydrophilic thiols decrease the fluorescence intensity by replacing the amine species from the surface of the QDs.[217,218] Here, the replacement of ethylene

diamine molecules may have occurred by the addition of GSH, which is evident from FTIR. ie, the –SH stretching band (~2540 cm^{-1}) in the GSH is vanished when it was mixed with EDA-CDs (Figure 8.17). This result is attributed to the formation of 'surface' – sulphur bonds.

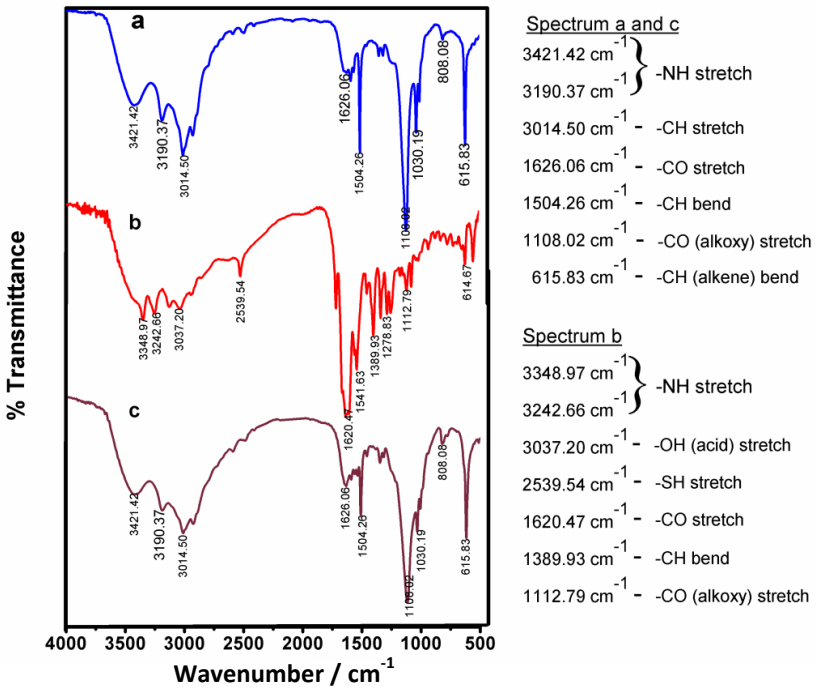

Figure 8.17: FTIR spectra of (a) EDA-CDs, (b) GSH and (c) EDA-CDs in presence of GSH.

Analysis of zeta potential gives information about stability of the colloidal system (probe) as well as its surface effects.[179] Higher value of the zeta potential indicates the stability of the system, a decrease in zeta potential value will results in aggregation of particles.[179] To study the changes in the surface of EDA-CDs upon the addition of GSH, the zeta potential analysis was carried out. Zeta potential value of EDA-CDs obtained before and after the addition of GSH is in support of the proposed

mechanism. Zeta potential of EDA-CDs was -18.9 mV (Figure 8.18), and that of EDA-CDs + GSH was -8.2 mV (Figure 8.19). This decrease in the magnitude of zeta potential is indicative of surface effects, like the replacement of ethylenediamine by GSH. Due to a reduction in the surface charges, the CDs come closer and become aggregated.

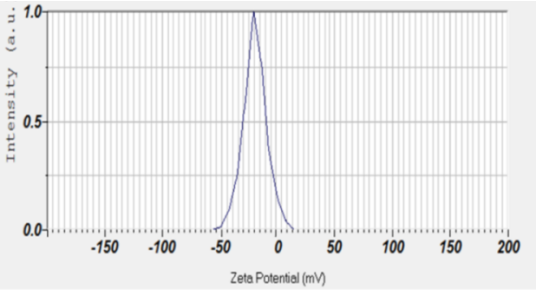

Figure 8.18: Zeta potential analysis of EDA-CDs.

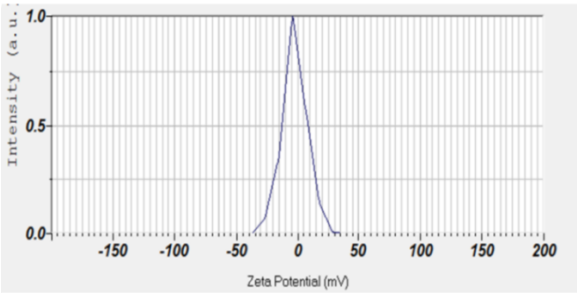

Figure 8.19: Zeta potential analysis of EDA-CDs in presence of GSH.

Hydrodynamic diameter (from DLS analysis) obtained after the addition of GSH (Figure 8.20) was much higher (228.4 nm) than that of the probe (7.4 nm) (Figure 8.8). This is also evident from the TEM images, where particles (CDs) are aggregated after the addition of GSH (Figure 8.21). These observations further confirm the proposed mechanism. The delay in the attainment of stability of the fluorescence signal upon the addition of GSH may also be due to the time lag for aggregation.

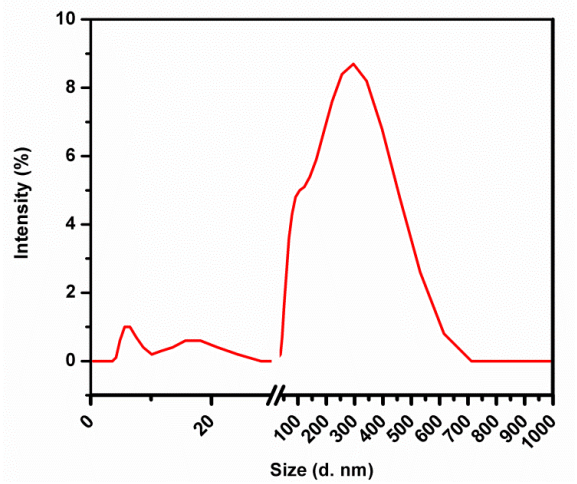

Figure 8.20: DLS spectrum of EDA-CDs in presence of GSH.

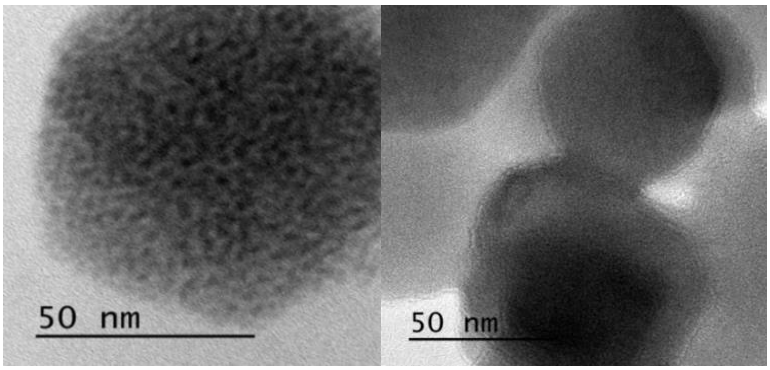

Figure 8.21: TEM images of EDA-CDs (a) before and (b) after the addition of GSH.

8.3.7 Application of the sensor for saliva analysis

Determination of GSH was carried out in artificially prepared saliva samples spiked with GSH. For a comparison, a colorimetric method has been carried out using Ellmann's reagent[97]; the observed results are presented in Table 8.4. The obtained recoveries are in good agreement with those of the colorimetric method. This proves the applicability of the developed sensor towards real sample analysis.

Table 8.4: Determination of GSH in artificial saliva samples.

Samples	Proposed method				Colorimetric method			
	Added (M)	Found (M)	R %[a]	RSD	Added (M)	Found (M)	R %[a]	RSD
Saliva 1	5.00×10^{-8} to 2.50×10^{-7}	5.04×10^{-8} to 2.53×10^{-7}	100	4.1	3.00×10^{-6} to 5.00×10^{-6}	2.96×10^{-6} to 5.06×10^{-6}	101	3.0
Saliva 2	5.00×10^{-8} to 2.50×10^{-7}	4.86×10^{-8} to 2.51×10^{-7}	100	2.0	3.00×10^{-6} to 5.00×10^{-6}	2.93×10^{-6} to 5.09×10^{-6}	101	3.2

a. Five replicates, R= recovery

8.4 Conclusions

A "green one – pot" method for the preparation of ethylenediamine passivated carbon quantum dots from tissue paper has been developed and successfully used for the determination of Glutathione. Under the optimum conditions, the linear dynamic range was 6.0×10^{-7} to 5.0×10^{-8} M. The quenching of fluorescence of EDA-CDs upon the addition of GSH allowed for determination as low as 1.74×10^{-9} M. Changes in the surface passivating groups can be a possible mechanism for quenching of the fluorescence. The proposed method was successfully applied to spiked artificial saliva samples; the recoveries are in good agreement with the standard colorimetric method.

.....ꕥ.....

Chapter 9

GOLD NANOPARTICLES BASED COLORIMETRIC SENSOR FOR DOPAMINE

Contents

This chapter explains the development of a simple colorimetric sensor for quantification of dopamine (DA) based on anti-aggregation of citrate capped gold nanoparticles. In presence of DA, the color of aggregated gold nanoparticles (AuNPs) solution changes from blue to greenish black with a shift in surface plasmon band. Sensing mechanism includes the formation of a poly-dopamine layer on the surface of AuNPs in alkaline medium, which in turn disperse the aggregated AuNPs. Results show that ratio of absorbance of AuNPs to concentration of DA was linear in the range 1.85×10^{-4} to 5.85×10^{-6} M (R^2 = 0.99) with a detection limit of 1.67×10^{-6} M. Proposed sensor was successfully applied for determination of DA in artificial urine and pharmaceutical formulation (injection). Obtained results are in good agreement with the results of HPLC method.

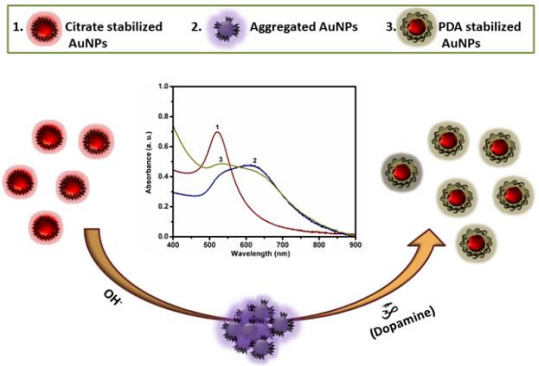

Scheme 9.1: Pictorial representation of the formation of PDA coated AuNPs and corresponding spectral changes.

9.1 Introduction

Colorimetric sensors have attracted significant attention in clinical diagnosis due to ease of detection and simple instrumentation.[219] A major class among gold nanoparticles (AuNPs) based colorimetric sensors works via the principle of aggregation induced color change.[220] Sensing mechanisms in most of AuNPs based colorimetric systems are aggregation together with a shift in surface plasmon absorption band to higher wavelength.[221] Additionally, resultant color change is easily detectable, stable, bio compatible and is easy to perform. Thus, colorimetric sensors based on AuNPs find wide applications.[222-224]

A major disadvantage of above mentioned method is its lower selectivity - because, when AuNPs aggregates, color of solution change from red to blue.[225] In several cases most of coexisting compounds will aggregate the citrate capped AuNPs and may provide false positive results (usually same color change),[226] which lead to inaccuracy in determination process. This can be overcome by using the method aggregated to anti-aggregated state or dissolution. Based on this, few colorimetric sensing methods have been developed in recent years.[227-229] In conjunction to above facts, we have developed a sensing system for dopamine (DA) based on anti-aggregation of AuNPs.

DA is an important neurotransmitter belonging to catecholamine and phenyl ethylamine family.[230] DA is an active participant in metabolism of cardiovascular, renal and central nervous system and is also involved in hormonal balance.[163] It has been considered as a biomarker for several neurological diseases viz, Parkinson's disease, schizophrenia, Alzheimer's

disease and Huntington's disease.[163] Therefore, development for highly selective and simple sensors for the quantification of DA is warranted.

In basic medium, DA oxidizes in to corresponding aminochrome which then polymerizes and poly-dopamine (PDA) or a type of melanin is formed.[231,232] Moreover, presence of concentrated alkali decreases the colloidal stability of citrate stabilized AuNPs by forming aggregates.[233] Also, PDA can act as a stabilizing agent for gold nanoparticles due to formation of a coating around it.[234] Considering the above facts, alkali can be used as an aggregating agent for AuNPs and increased pH of solution will help to form PDA. Newly formed PDA will stabilize the aggregated AuNPs and results in dissolution of aggregates in to single nanoparticles. In view of these, a selective and simple colorimetric sensor is developed for quantification of DA in physiological samples utilizing citrate stabilized gold nanoparticles as color indicator.

9.2 Experimental

9.2.1 Preparation of citrate stabilized AuNPs

Colloidal gold nanoparticles was synthesized by the citrate reduction and used for present study.[235] About 12.50 mL (1.00×10^{-2} M) solution of sodium citrate was added quickly to a boiled solution (237.5 mL of 2.67×10^{-4} M) of $HAuCl_4$ under vigorous stirring. Vortex solution was boiled and stirred for 30 minutes. The ensuing ruby red colored solution was cooled to room temperature, filtered and stored at 4°C in an amber colored bottle until use.

9.2.2 Experimental procedure

AuNPs solution (1.5 mL) with 40 μL of 2.0 M NaOH was taken in a quartz cuvette (10 mm × 10 mm) and various amount of DA in the range from 1.85×10^{-4} to 5.85×10^{-6} M was added and total volume was made up to 2 mL using appropriate amount of water. After an incubation period of 12 minutes, UV – visible absorption spectra were recorded against a blank (NaOH solution). Ratio between absorbance of peaks at λ_{max} 528 nm (A_0) and 610 nm (A) was noted as $\Delta A = A_0 / A$.

9.2.3 Analysis of clinical samples

To access the validity, analysis of DA was carried out in spiked urine and commercial DA injection samples. As described in section 2.4.2 in chapter 2, artificial urine is prepared and suitable amount of DA was spiked. Commercial injection sample was used after 10 times dilution with water. Concentrations of DA in these samples were determined by standard addition method. To validate the developed method, HPLC analysis[98] was also carried out. Procedure for the HPLC analysis is also detailed in section 2.3.5 of chapter 2.

9.3 Results and discussion

9.3.1 Characterization of citrate capped AuNPs

Characterization of synthesized AuNPs was carried out using various techniques such as UV – visible absorption spectroscopy, transmission electron microscopy (TEM), dynamic light scattering (DLS) and zeta potential analysis. In UV – visible absorption spectrum (Figure 9.1a), synthesized AuNPs showed an absorption peak with maximum absorbance

at 523 nm. As evidenced from TEM images (Figure 9.2a), synthesized particles have a particle size of around 14.02 nm, which implies that the size of synthesized particles was in nanometer scale.

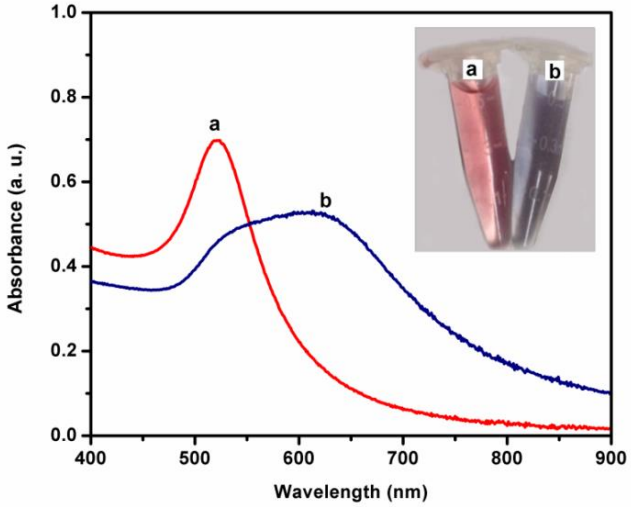

Figure 9.1: UV-visible absorption spectra of (a) citrate stabilized AuNPs and (b) aggregated AuNPs after NaOH addition. Inset shows the corresponding colour change of (a) and (b).

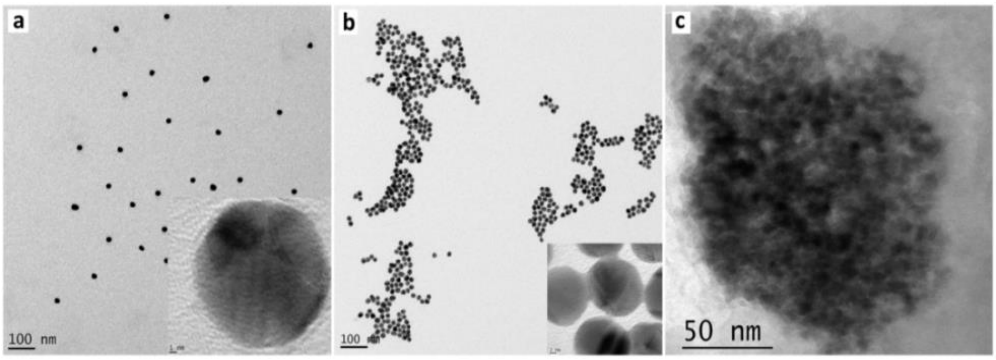

Figure 9.2: TEM images of (a) citrate stabilized AuNPs, (b) AuNPs after the addition of 1.00×10^{-2} M NaOH and (c) AuNPs after the addition of 4.00×10^{-2}M.

DLS analysis also confirms the above observation, in which the hydrodynamic diameter is recorded is 27.8 nm (Figure 9.3a). Zeta potential analysis reveals the good stability of AuNPs with a zeta potential of -62 mV which in turn supports the nanoparticle formation (Figure 9.4a).

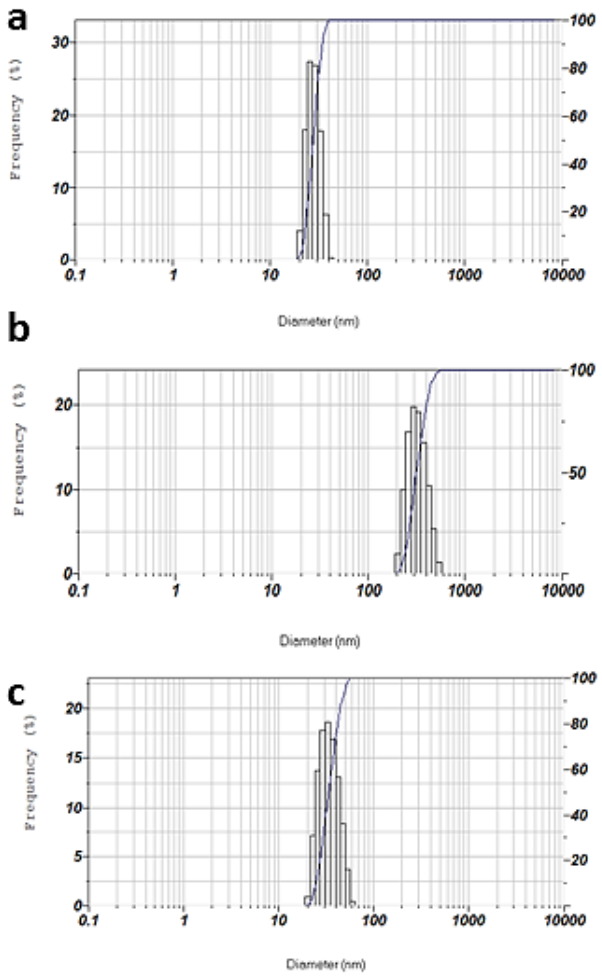

Figure 9.3: DLS analysis of (a) citrate stabilized AuNPs, (b) aggregated AuNPs in presence of NaOH and (c) after the addition of DA to aggregated AuNPs.

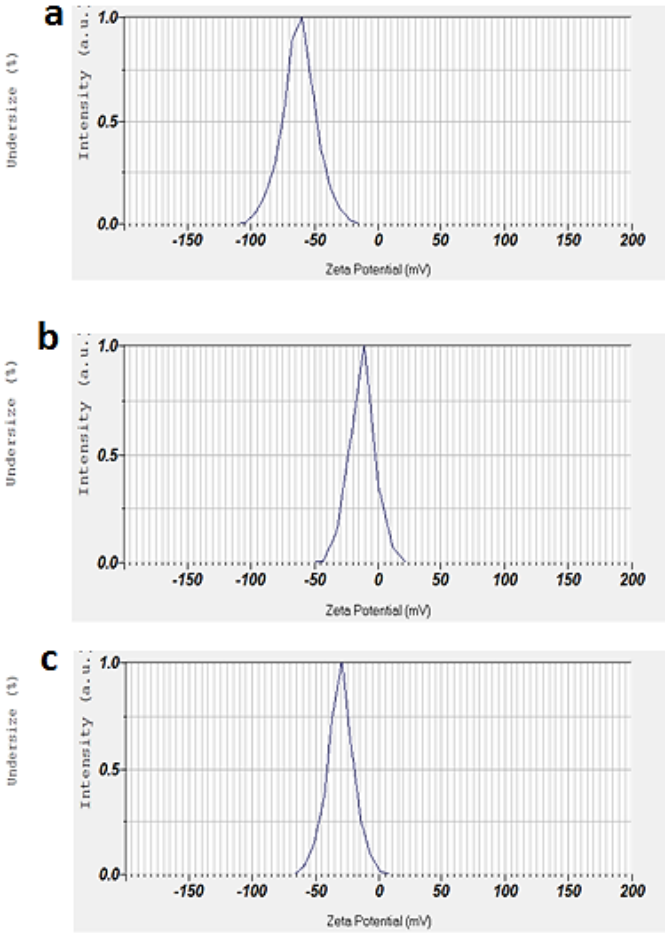

Figure 9.4: Zeta potential analysis of (a) citrate stabilized AuNPs, (b) aggregated AuNPs in presence of NaOH and (c) after the addition of DA to aggregated AuNPs.

9.3.2 Evidences for proposed mechanism

Stability of the as-synthesized AuNPs can be ascribed to the excellent capping of citrate moieties. According to latest studies, two types of citrates are present in the surface of the particles, one is directly bonded to surface and other is known as dangling citrates – linked to the former via hydrogen

bonding and Vander-walls interactions.[236] The dangling groups cause the stability of nanoparticle by rendering it from aggregation. In presence of higher amounts of OH^- hydrogen abstraction from –COOH group takes place thereby detachment of dangling citrate moiety occurs. This process decreases the stability of nanoparticle and they get aggregated. Zeta potential analysis reveals that as-synthesized AuNPs has a zeta potential of -62 mV, which is reduced to -12.8 mV upon addition of NaOH (Fig. 9.4a & b).

In the aggregated state, there is a shift in absorption maximum to a longer wavelength (~ 610 nm). Additionally, there is a considerable reduction in the absorbance at shorter wavelength band (523 nm) (Fig. 9.1b). The spectrophotometric change is accompanied by a red to blue color change, which is similar to reported systems for gold nanoparticles (Fig. 9.1 inset).[221] DLS and TEM analysis also strengthens the obtained results from zeta potential analysis because, the hydrodynamic diameter and particle size of as-synthesized AuNPs were 27.8 nm and 14.02 nm respectively, which has changed into 329.2 nm (Fig. 9.3b) and ~ 170.3 nm (Fig. 9.2 b & c) respectively upon mixing with NaOH. These results imply that AuNPs get aggregated upon the incorporation of OH^-.

Presence of OH^- group is an important factor in this study, because it induces the formation of aggregated AuNPs and make the reaction medium highly alkaline. In basic solutions DA oxidizes in to corresponding aminochrome which further combines with other DA molecules and polymer form of DA will be formed.[231,232] In the present study, the produced PDA stabilizes the aggregated AuNPs. By this way, anti-aggregation results

in increase of absorption at 528 nm and reduction of absorption at 610 nm. From TEM images (Fig. 9.5a), anti-aggregation can be easily visualized, where the 'new' AuNPs has an average size ~ 23.4 nm, which shows the increased size of particle in comparison to as-synthesized state. When higher concentration of DA is added, formed PDA layer on surface of AuNPs can be visualized from high resolution TEM image (Fig. 9.5b), which is in agreement with earlier report.[234] DLS analysis (Fig. 9.3c) also strengthens the observations from TEM, where, obtained hydrodynamic diameter was slightly greater than the as-synthesized one (33.8 nm). Zeta potential also increased upon addition of DA up to – 30.5 mV (Fig. 9.4c), which shows the increased stability and anti-aggregation mechanism.

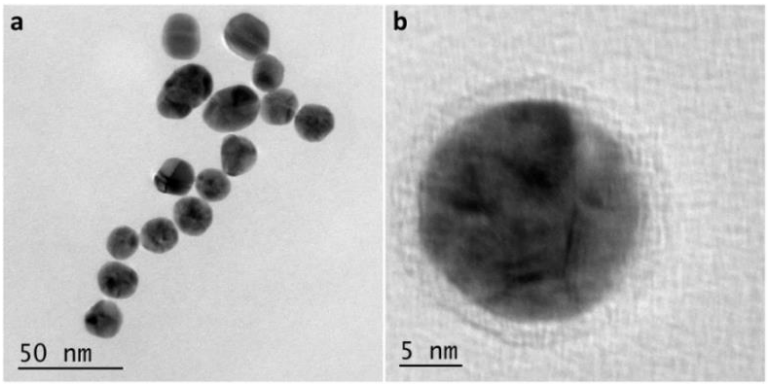

Figure 9.5: (a) TEM image of PDA stabilized AuNPs, (b) HRTEM image of PDA stabilized AuNPs.

Further evidence in PDA formation on surface of AuNPs was obtained from analysis of XPS spectra (Fig. 9.6 and 9.7). In the de-convoluted spectrum of as-synthesized AuNPs (Figure 9.6), C 1s peak can be fitted with four components: peak at 284.6 eV is assigned to adventitious carbon, peaks at 285.4 and 285.7 eV is related to C-H / C-OH bonds, peak at 288.3 eV is

ascribed to C(= O)O bond.[237,238] The O1s peak can be fitted with 5 components: peaks at 530 eV and 530.6 eV attributed to O–Au and O–H bonds respectively. Similarly, peaks at 531 eV and 531.6 eV ascribed to oxygen atoms in the carboxyl group and peak at 532 eV is related to C-O-H bond.[238] This is in accordance with reported values.[239] After addition of DA, sample is centrifuged and residue is washed and re-dispersed in water and used for further analysis. New peaks are generated for carbon at 283.4 eV (C - NH_2), 285.9 eV (C – N) and for oxygen at 530.2 eV (O - Au), 531 eV (O-(CO)) and 532.7 eV (O-C) respectively, corresponding to PDA.[239-242]

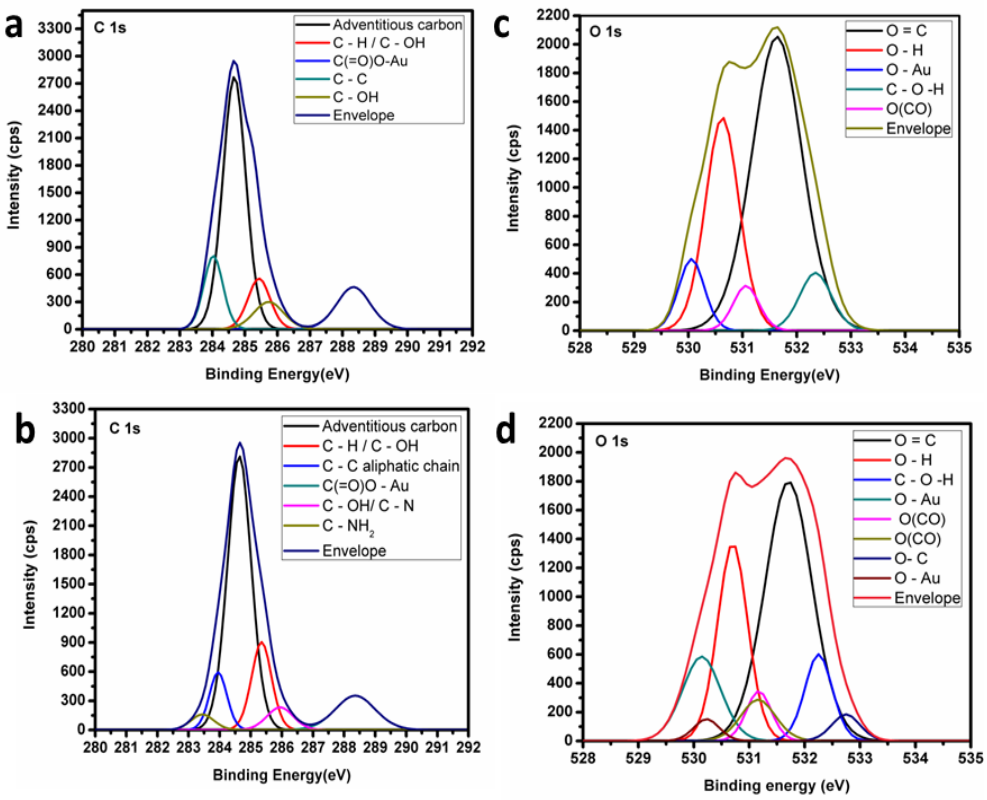

Figure 9.6: De-convoluted XPS spectrum of (a) and (c) represents C1s and O1s of citrate stabilized AuNPs and (b) and (d) for C1s and O1s of PDA stabilized AuNPs.

In addition to this, presence of nitrogen atoms is also found from XPS spectrum (Figure 9.7). Representative de-convoluted spectra of N 1s region, shows peaks at 398.4 eV, 398.6 eV (=NR), 398.9 eV, 399.2 eV (C-N-C), 399.4 eV (N-C=O), 399.9 eV (RNH_2) corresponding to PDA.[243,244] These results confirm the capping / adsorption of PDA on the surface of AuNPs.

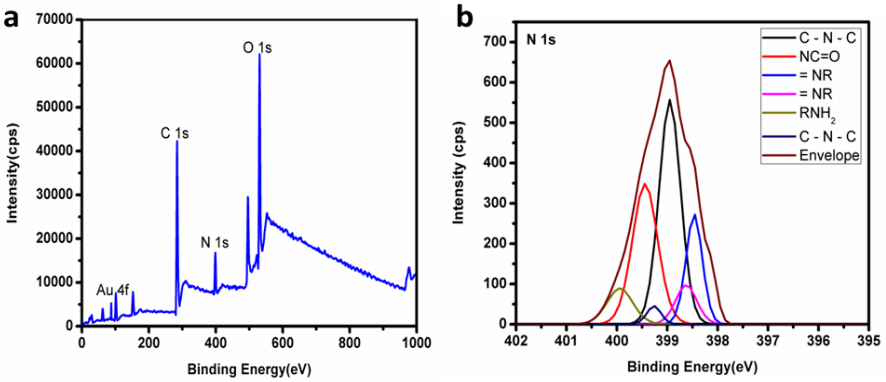

Figure 9.7: (a) Survey XPS spectrum of PDA stabilized AuNPs and (b) De-convoluted XPS spectrum of N1s of PDA stabilized AuNPs.

9.3.3 Optimization of experimental parameters

Choice of an appropriate medium for the studies is an important parameter that can influence the sensing characteristics. Therefore absorption of AuNPs and aggregated AuNPs were studied in phosphate buffer, citrate buffer, acetate buffer and water. Preeminent result was found in water and it was chosen as reaction medium.

Time required for completion of reaction (PDA capped AuNPs formation) was ascertained by measuring the absorbance at every 30 seconds, up to 20 minutes. It was found that, upon addition of DA (5.33×10^{-6} M), absorption signal attained stability after 12 minutes (Fig. 9.8).

Accordingly, further measurements were also done after 12 minutes of incubation.

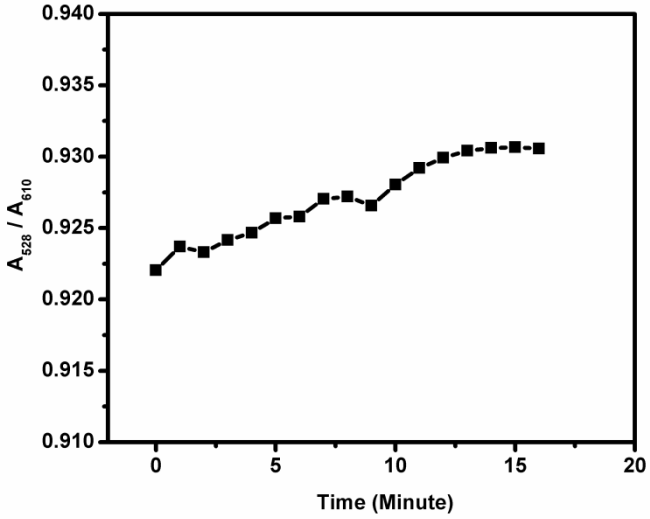

Figure 9.8: Effect of time on the formation of PDA stabilized AuNPs.

9.3.4 Effect of coexisting species

A good sensor selectively senses a particular analyte.[245] In case of colorimetric sensors, change in color is necessary upon addition of analyte of interest. Among various biologically important molecules viz. homovanillic acid, creatinine, uric acid, ascorbic acid, glutathione, noradrenaline, adrenaline and DA were studied (Fig. 9.9), only DA effectively produces a change in color together with change in UV – visible spectral profile. Table 9.1 shows effect of coexistence of the above species on the determination of DA. Evaluation of the table reveals that, homovanillic acid, creatinine, uric acid, ascorbic acid and glutathione did not affect the determination up to 100 times of the concentration of DA.

However, noradrenaline and adrenaline showed significant signal change (above 5%) when they were present above 10 fold excess concentration.

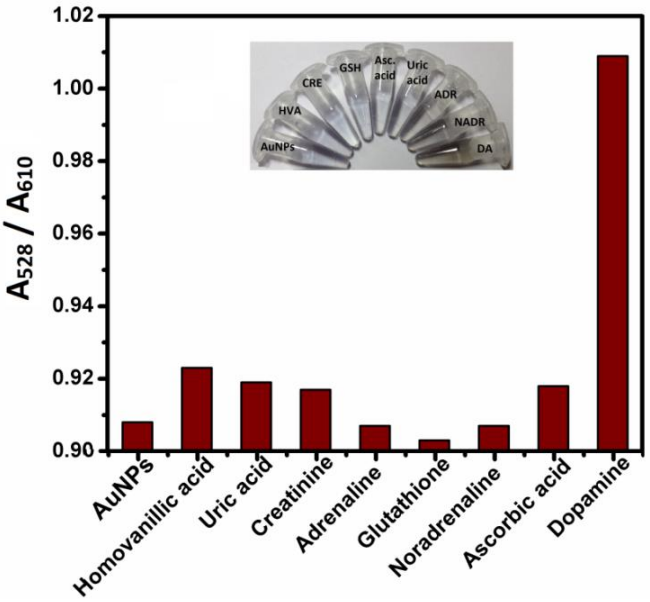

Figure 9.9: Selectivity of NaOH mediated AuNPs aggregates towards various biologically important species.

Table 9.1: Interference caused by coexisting species on the determination of 5.85×10^{-6} M DA.

Analyte	Concentration (M)	Signal change (%)
Homovanillic acid	5.85×10^{-4}	1.82
Creatinine	5.85×10^{-4}	1.7
Uric acid	5.85×10^{-4}	3.6
Ascorbic acid	5.85×10^{-4}	3.9
Glutathione	5.85×10^{-4}	1.4
Noradrenaline	5.85×10^{-6}	1.4
Adrenaline	5.85×10^{-6}	3.0

9.3.5 Analytical performance of the colorimetric assay

Upon addition of NaOH solution, AuNPs showed a shift in absorption maximum from 523 to 610 nm. On gradual addition of DA, absorption at 610 nm decreases with a significant increase in absorption at 528 nm. Along with the spectral changes, a change in color of the solution from blue to greenish black can also be observed (Figure 9.10). This allows the visible detection of DA by naked eye.

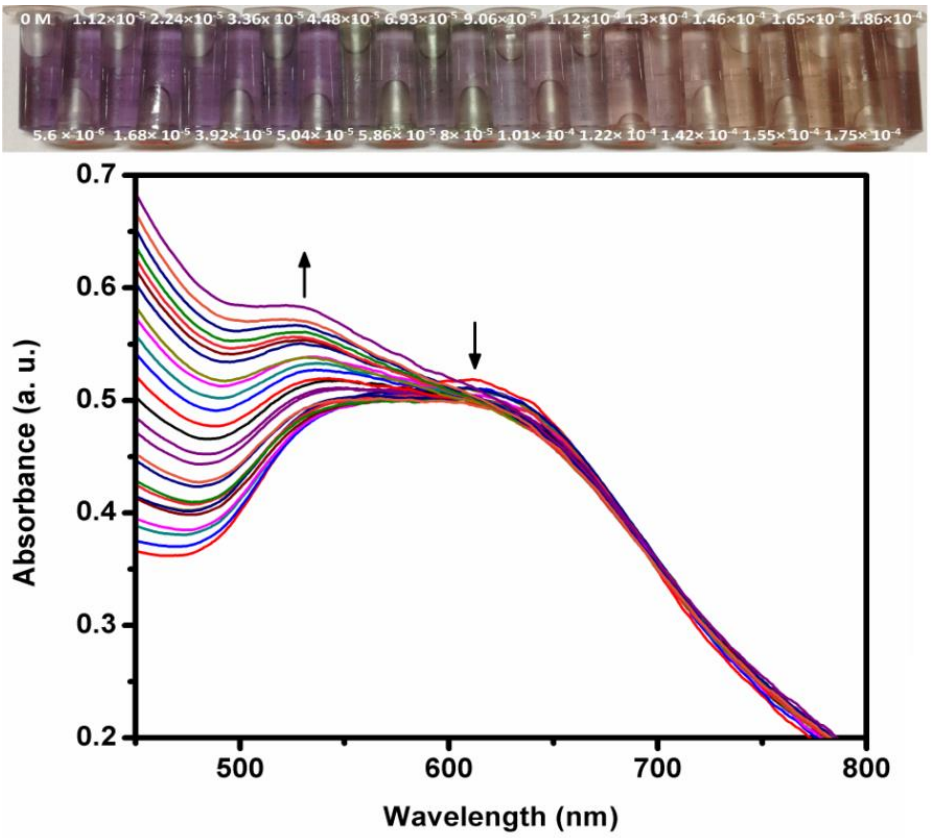

Figure 9.10: Effect of concentration of DA on UV-visible absorption spectrum of NaOH mediated AuNPs aggregates and the observed colour changes (above the graph).

A plot of ratio of absorbance A_{528}/A_{610} against concentration of DA depicts a linear relationship in the range from 1.85×10^{-4} to 5.85×10^{-6} M (R^2 = 0.99) with a detection limit of 1.67×10^{-6} M (Figure 9.11). The relative standard deviation for the determination of 5.85×10^{-6} M DA was 4.5% (n = 4).

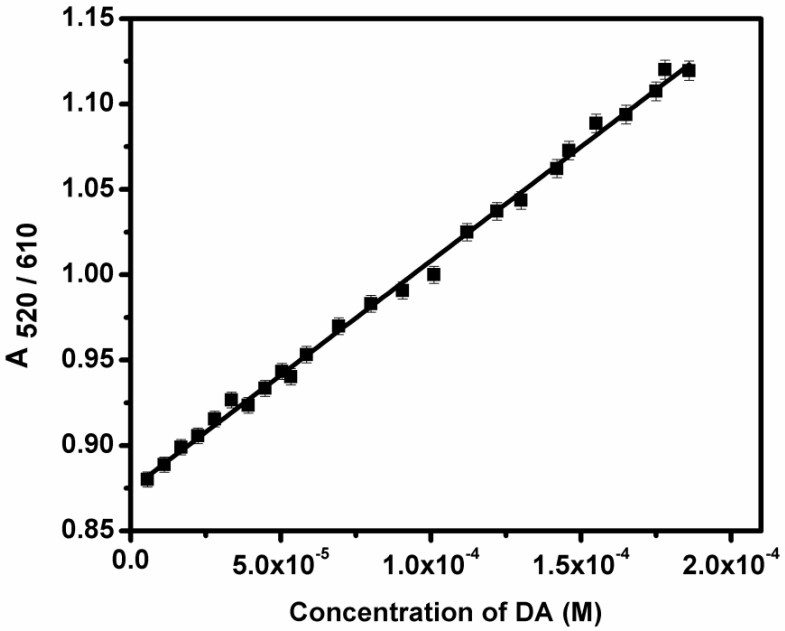

Figure 9.11: Linear calibration graph of ratio of absorbance vs. concentration of DA.

Comparison of the developed assay with previous colorimetric techniques is represented in Table 9.2 and the results reveals that the proposed assay is simple to perform and the sensing performance was comparable with other reported methods.

Table 9.2: Comparison of proposed method with gold nanomaterials based recent colorimetric methods for DA determination.

Probe used	Linear range (M)	LOD (M)	RT (min)	Reference
CTAB-AuNPs + TGA	1.0×10^{-6} to 5.0×10^{-9}	3.3×10^{-8}	30	246
MBA-DSP-AuNPs	1.8×10^{-7} to 5.0×10^{-9}	5.0×10^{-8}	5	247
AHMP-AuNPs	1.1×10^{-6} to 2.0×10^{-7}	7.0×10^{-8}	30	248
Melamine - AuNPs	3.3×10^{-3} to 3.3×10^{-8}	3.3×10^{-8}	-	249
Aptamer + AuNPs	5.4×10^{-6} to 5.4×10^{-7}	3.6×10^{-7}	5	250
AuNRs + Ag+	1.2×10^{-5} to 2.0×10^{-7}	4.7×10^{-8}	25	251
AuNPs + NaOH	1.8×10^{-4} to 5.8×10^{-6}	1.6×10^{-6}	12	-

MBA= 4-mercaptophenyl boronic acid, DSP = dithiobis (succinimidylpropionate), AuNRs = gold nanorods. RT = Reaction time.

9.3.6 Determination of DA in Urine sample and pharmaceutical formulation

Application studies of developed sensor were carried out in pharmaceutical formulations and artificial urine samples. Concentrations were determined by standard addition method and the obtained results are represented in Table 9.3. Recoveries of spiked concentrations are in good agreement with the standard HPLC – UV method. Also the determined concentration of DA from pharmaceutical formulation was comparable with that of declared in the sample bottle. This proves the feasibility of the developed method for real sample analysis.

Table 9.3: Results obtained from application of proposed method in artificial urine and commercial injection samples.

	Proposed method				HPLC – UV method			
	Added (M)	Found[a] (M)	R[a] (%)	RSD[a] (%)	Added (M)	Found[a] (M)	R[a] (%)	RSD[a] (%)
Urine	1.00×10^{-5}	1.035×10^{-5}	104	2.4	2.10×10^{-7}	2.16×10^{-7}	103	1.1

[a] average of three replicates, R = recovery, RSD = Relative standard deviation.

Sample	Declared amount (mg / 5 mL)	Found (mg / 5 mL)	RSD[a] (%)
Sterile dopamine concentrate IP (Ciron Drugs and Pharmaceuticals, India)	200	208	1.0

[a] average of three replicates

9.4 Conclusions

A simple colorimetric approach for the determination of DA using aggregated AuNPs through a poly-dopamine assisted anti–aggregation procedure is presented here. UV – visible spectroscopy, TEM, DLS, zeta potential analysis and XPS results have demonstrated the anti-aggregation mechanism. Under optimal conditions, linear dynamic range was observed from 1.85×10^{-4} to 5.85×10^{-6} M with a detection limit of 1.67×10^{-6} M. Proposed method was successfully applied for determination of DA in real samples. Therefore, the proposed strategy may offer a new approach for developing low cost and simple sensor for detection of DA in biological samples and for a wide range of applications including clinical diagnostics.

.....ഠോര.....

Chapter 10

COPPER NANOPARTICLES BASED COLORIMETRIC SENSOR FOR CREATININE

Contents

Copper nanoparticles based colorimetric sensing of the renal biomarker - creatinine (CR) is described in this chapter. L-cysteine stabilized copper nanoparticles (L-cys-CuNPs) exhibited selective and sensitive interaction with CR. Utilizing this interaction, a colourimetric sensor has been developed based on the reduction in LSPR intensity as monitored by a UV–visible spectrophotometer. The developed sensor exhibited a linear dynamic range of 5.33×10^{-6} to 3.33×10^{-7} M and detection limit of 4.54×10^{-10} M. The sensor was successfully applied for quantification of CR in artificial serum and urine samples. Agreement of the recovery values of the developed method to that of Jeffe's colorimetric method reveals the potential of the developed method for rapid and on-site determination of CR in physiological samples.

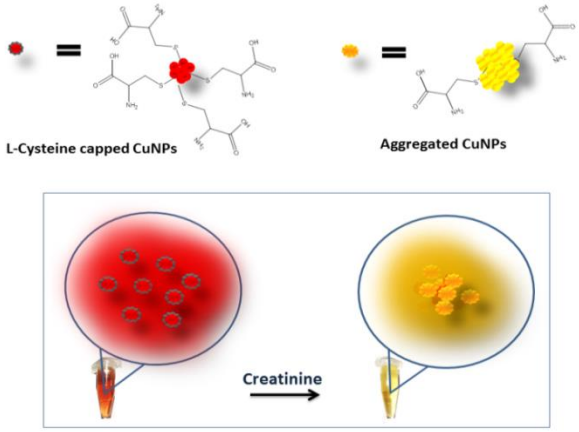

Scheme 10.1: Diagrammatic representation of sensing of CR using L-cys-CuNPs.

10.1 Introduction

Kidneys are one of the important chemical factories in our body, which regulates blood pressure, remove waste products of metabolism and maintain the water balance and composition of electrolytes in blood.[252] Generally functioning of kidneys is studied by observing the levels of blood urea nitrogen, creatinine clearance and also by glomerular filtration rate, the flow rate of filtered fluid through the kidney.[253] Hence, research on breakdown products such as urea and creatinine (CR) (2-amino-1-methyl-5H-imidazol-4-one) can explore the biological effects and functions of kidneys.[254] Additionally, concentrations of the above species can also reveal the muscular and thyroid functions.[255]

CR is the end product of creatine metabolism.[254] It is produced by body and is filtered from bloodstream by kidneys in relatively constant amounts every day.[254] Normal physiological concentration in blood is 0.9 to 1.3 mg/dL in men and 0.6 to 1.1 mg/dL in women, but it can exceed from these levels in certain pathological conditions.[256] In contrast to urea, the concentration of CR in body fluids is not influenced by protein intake, so the level of CR serves as a more reliable indicator of renal function.[257] Hence, quantification of CR is an important area of research in science, especially in the fields of clinical biochemistry and medicine.[258,259]

Generally, colorimetric methods are easy to perform and can easily detect the presence of analyte. Most common colorimetric determination methods used for CR are Jaffé's reaction[99] and the enzymic colorimetric method.[260] But these methods are limited with respect to selectivity or time-consuming complicated procedure (enzyme linked).

By utilizing the advantages of copper nanoparticles (CuNPs) a simple and cost effective colourimetric technique for the determination of CR was developed and is explained in this chapter. Compared to noble metal nanoparticles such as gold and silver, CuNPs are considered to be cost effective and are more catalytic in nature because of the extremely small size and high surface to volume ratio.[261] Developed assay was successfully applied for the determination of CR in artificial blood serum and urine samples. Moreover, the proposed method may serve as an ideal test for clinicopathological investigations associated with renal function.

10.2 Experimental

10.2.1 Synthesis of L-cysteine stabilized CuNPs

L-cysteine stabilized CuNPs were synthesized as per the reported procedure.[78] 3.0 mL of 3.0×10^{-3} M solution of $CuCl_2$ was diluted to 80.0 mL using water and mixed with 2.0 mL of 1.0×10^{-2} M L-cysteine solution. Then, 10.0 mL of 0.1 M hydrazine hydrate was dropped slowly in to the mixed solution. Obtained solution was sealed and reacted for 90 minutes. Finally a dark red colloid was obtained, which was stored at 4 ºC until use. The synthesized CuNPs is stable and gave reproducible results up to 4 months when it was stored in refrigerator.

10.2.2 Analytical procedure

L-cys-CuNPs solution was taken in a quartz cuvette and aliquots of CR (to obtain 5.33×10^{-6} to 3.33×10^{-7}M) were added and the total volume was made up to 3 mL by adding appropriate amount of water. After 7 minutes incubation at room temperature, the UV – visible spectra were

recorded at λ_{max} 563 nm. Difference in absorbance was noted as $\Delta A = A_0 - A$, where A_0 and A are the absorbance of L-cys-CuNPs in the absence and presence of CR.

10.2.3 Analysis of physiological samples

Artificial serum and urine samples were prepared as explained in section 2.4. Spiked samples were prepared onsite by mixing 10 to 50 μL of 1.0×10^{-4} M solution of CR with 100 μL of artificial sample solution. Then 1.5 mL of L-cys-CuNPs was added to the mixture and total volume was made up to 3 mL by adding water (final concentrations were within the linear range of proposed method). Standard addition method was used for the determination of the concentration. As discussed in section 2.3.6 Jeffe's reaction[99] based spectrometric method was also conducted for comparative purpose.

10.3 Results and Discussion

10.3.1 Characterization of the synthesized L-cys-CuNPs

Synthesized L-cys-CuNPs were characterized using various techniques such as transmission electron microscopy (TEM), Energy-dispersive X-ray spectroscopy (EDX), dynamic light scattering (DLS), zeta potential analysis and UV – visible absorption spectroscopy. From TEM images (Figure 10.1), it is clear that the synthesized particles have a particle size of around 14.02 nm. Lattice fringes can be seen at HRTEM image (inset of figure 10.1) indicative of the crystalline nature of nanoparticles.

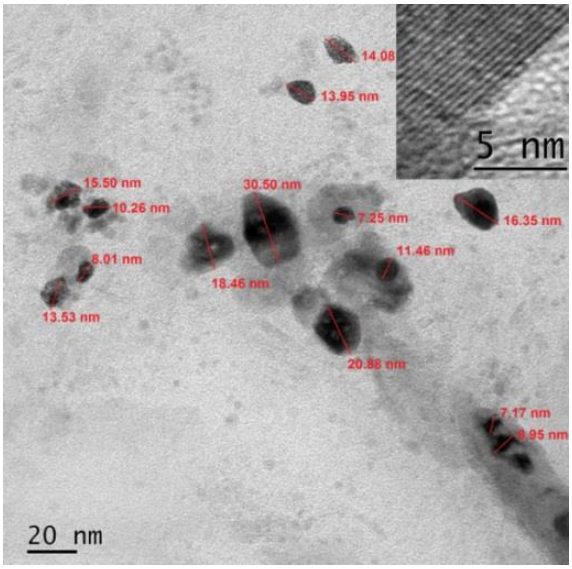

Figure 10.1: TEM images of L-cys-CuNPs, inset: lattice spacing of one particle.

Hydrodynamic diameter obtained from DLS analysis is 30.6 nm (Figure 10.2) also supports the observation from TEM. Zeta potential measurement (Figure 10.3) shows the high surface charge of -52 mV, revealing excellent stability of CuNPs in solution.

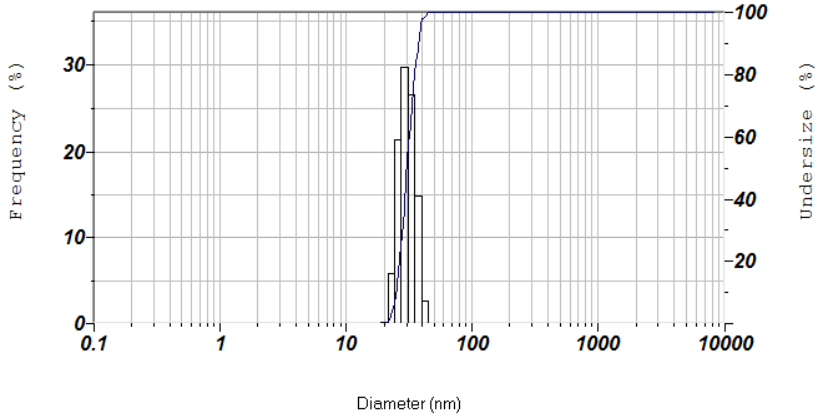

Figure 10.2: DLS spectrum of L-cys-CuNPs.

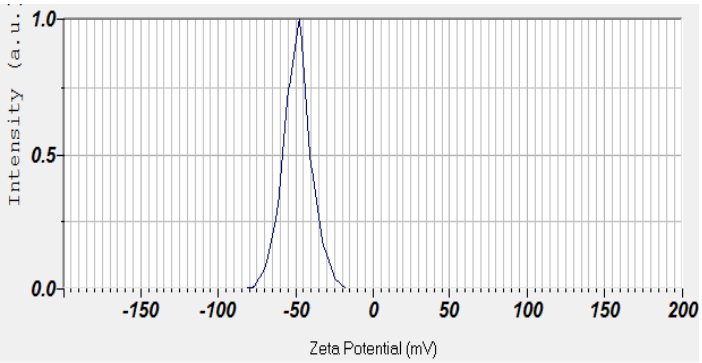

Figure 10.3: Zeta potential measurement of L-cys-CuNPs.

In UV – visible absorption spectrum (Figure 10.4), L-cys-CuNPs showed an absorption peak with maximum absorbance at 563 nm. Observed absorption peak is due to localized surface plasmon resonance (LSPR) of l-cys-CuNPs,[73,78] which is narrow in shape confirming the crystalline nature and uniform distribution of particles in the solution.

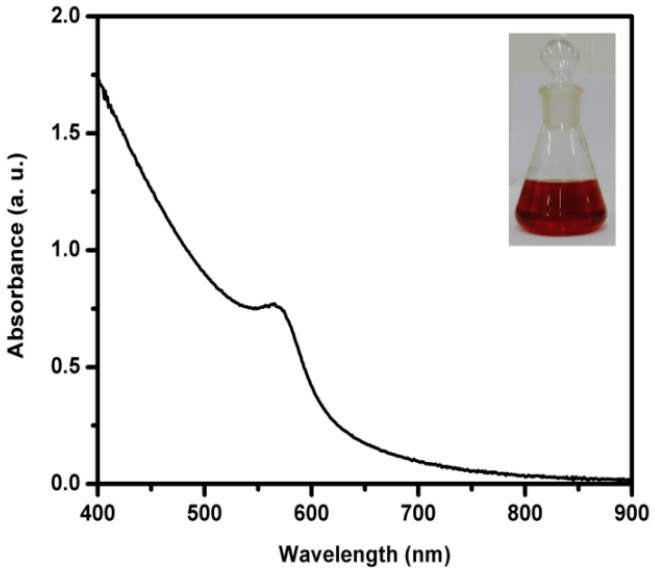

Figure 10.4: UV-visible absorption spectrum of L-cys-CuNPs, inset: as-synthesized L-cys-CuNPs in visible light.

Composition of CuNPs was further probed by EDX analysis. Figure 10.5 shows the EDX pattern of selected area in SEM image of CuNPs coated on a glass plate, which indicates the presence of copper, carbon, nitrogen, sulphur and oxygen. The small amount of oxygen in comparison with copper denotes the formation of metallic copper and lower concentration of copper oxides.

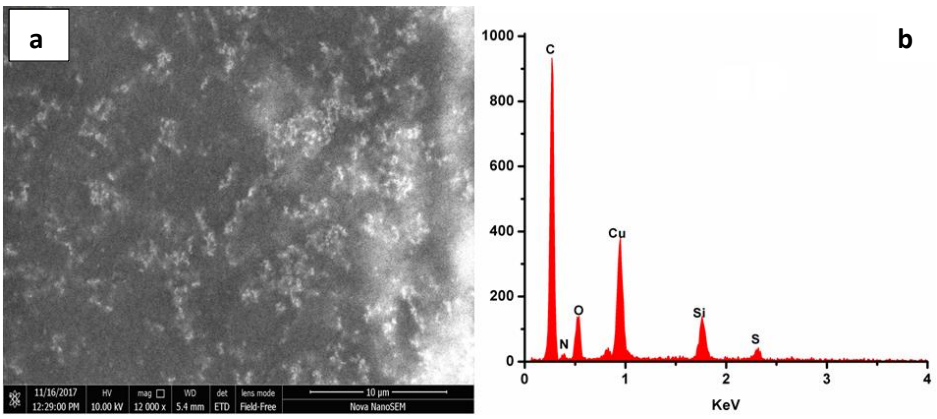

Figure 10.5: (a) SEM images of L-cys-CuNPs coated on a glass plate, (b) corresponding EDX spectrum of the area shown in SEM image.

10.3.2 Optimization of experimental parameters

To select an appropriate medium for the studies, absorption of L-cys-CuNPs were studied in phosphate buffer, citrate buffer, acetate buffer and water (Table 10.1). The best result such as better stability and higher absorbance were obtained in water, hence further studies were done in water.

Table 10.1: Effect of medium on the absorption signal of L-cys-CuNPs.

Studied medium	Absorbance (a. u.)	Stability (minutes)
ABS 7	0.61	15.5
CBS 7	0.57	12.0
PBS 7	0.56	10.5
Water	0.65	25.0

Time required for the completion of reaction was ascertained by measuring the absorbance at every 30 seconds, up to 25 minutes. It was found that, upon addition of CR (5.33×10^{-6} M), the absorption signal attained stability after 7 minutes and retains to 25 minutes (Figure 10.6), accordingly, further measurements were also done after 7 minutes of mixing.

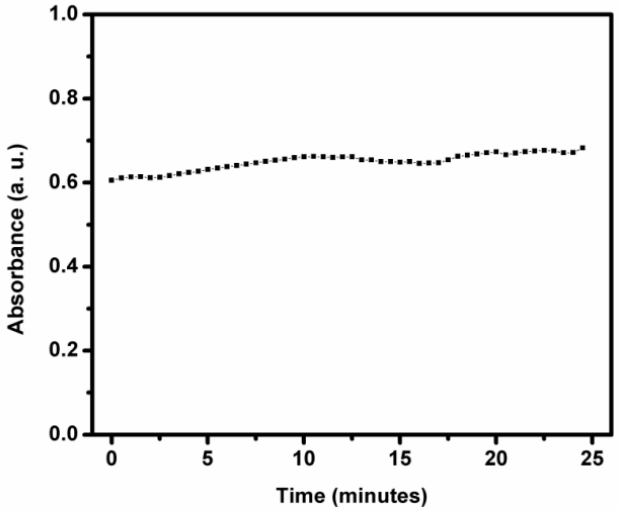

Figure 10.6: Effect of time on absorbance of L-cys-CuNPs in presence of CR.

10.3.3 Effect of coexisting species

An important property of a sensor is its selectivity towards a particular species. Among various biologically imperative molecules (1.4×10^{-6} M) studied, such as dopamine, ascorbic acid, glucose, uric acid, sodium chloride, potassium chloride, urea, albumin, creatine and CR, only CR effectively change the absorbance of L-cys-CuNPs together with a colour change from red to yellow (Figure 10.7).

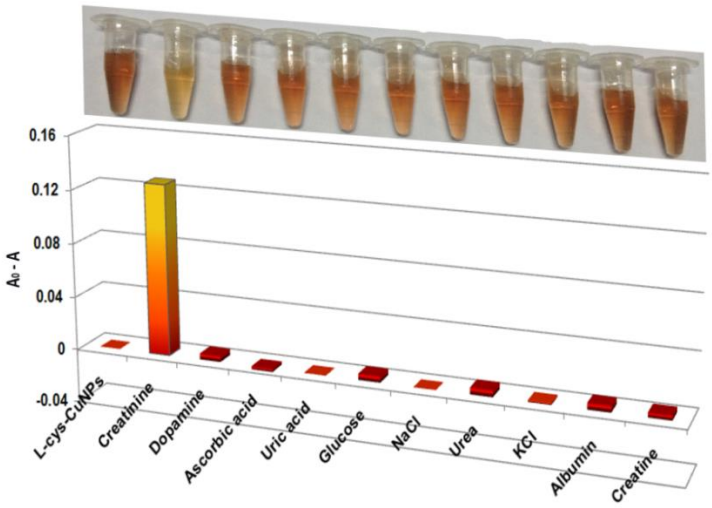

Figure 10.7: Selectivity of L-cys-CuNPs towards creatinine, inset: observed colour change after the addition of 2.66×10^{-6} M of each analyte.

Impact of concentration of above stated species in the absorption signal of L-cys-CuNPs containing CR (1.5×10^{-6} M) was also studied (Table 10.2). Dopamine, ascorbic acid, glucose, uric acid, sodium chloride, potassium chloride didn't showed any interference even up to 100 fold excess concentration of CR. However, urea, albumin and creatine showed significant signal changes (above 5%) when present above 20 fold excess concentration (3.00×10^{-5} M).

Table 10.2: Effect of coexistence on the determination of 1.5×10^{-6} M CR.

Coexisting species	Concentration (M)	Interference (%)
Dopamine	1.5×10^{-4}	3.6
Ascorbic acid	1.5×10^{-4}	1.3
Glucose	1.5×10^{-4}	3.8
Uric acid	1.5×10^{-4}	0.3
Sodium chloride	1.5×10^{-4}	1.3
Potassium chloride	1.5×10^{-4}	2.3
Urea	3.0×10^{-5}	1.8
Albumin	3.0×10^{-5}	1.6
Creatine	3.0×10^{-5}	1.0

10.3.4 Analytical performance of the colorimetric assay

It was found that presence of CR makes a color change of L-cys-CuNPs from red to yellow that can be easily detected by naked eye (Inset of figure 10.8). Additionally, gradual decrease in the intensity of LSPR band of probe (absorbance) was observed with increase in concentration of CR (Figure 10.8). A plot of the difference in absorbance (A_0-A) against the concentration of CR shows a linear relationship in the range of 5.33×10^{-6} to 3.33×10^{-7} M (R^2 = 0.98) (Figure 10.9). The limit of detection and limit of quantification were calculated to be 4.54×10^{-10} M and 1.51×10^{-9} M respectively. Relative standard deviation for the determination of 3.33×10^{-7} M CR was 3.6 % (n = 5).

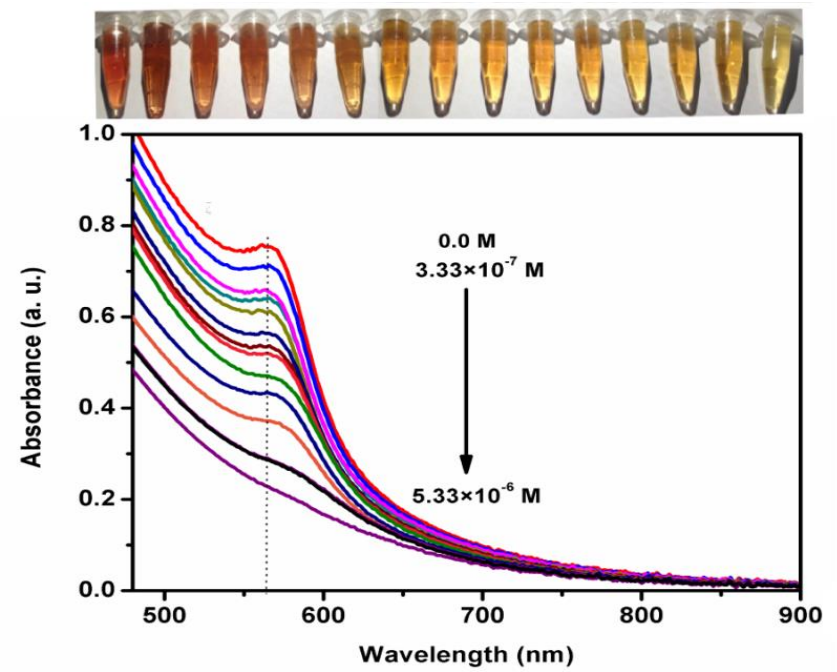

Figure 10.8: Effect of concentration of creatinine on the absorption spectrum of L-cys-CuNPs and the observed colour change (left to right) is depicted in inset.

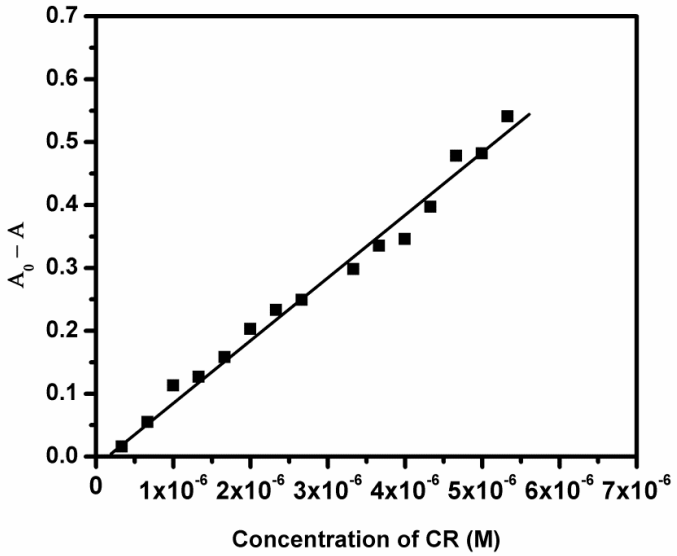

Figure 10.9: Linear dynamic range of creatinine.

Table 10.3 represents a comparison of various spectrophotometric techniques for the quantification of CR; it reveals that the proposed sensor is superior with respect to cost effectiveness and has comparable sensing performance with other methods.

Table 10.3: Comparison of proposed colorimetric sensor with previously reported sensors.

Probe used	Linear range (M)	LOD (M)	Reference
Metol + $CuSO_4$	6.20×10^{-4} to 4.40×10^{-6}	1.45×10^{-7}	262
PA + biacetyl + naphthol	2.65×10^{-4} to 1.76×10^{-5}	-	263
TMB + $CuSO_4$ + DP	2.65×10^{-2} to 8.84×10^{-4}	-	264
PA stabilized AgNPs	1.00×10^{-6} to 1.00×10^{-8}	8.40×10^{-9}	255
AuNPs + Adenosine + Ag^{+}	1.40×10^{-6} to 2.00×10^{-7}	1.27×10^{-8}	265
TDAA –AgNPs	1.00×10^{-6} to 1.00×10^{-8}	3.00×10^{-9}	266
L-cys-CuNPs	5.33×10^{-6} to 3.33×10^{-7}	4.54×10^{-10}	-

Metol = p-methylaminophenol sulfate, PA = Picric acid, TMB = 3,3',5,5'-tetramethyl benzidine, DP = diisopropylbenzene dihydroperoxide, TDAA = 2,2-thiodiacetic acid

10.3.5 Mechanism of sensing

Upon interaction of L-cys-CuNPs with CR, a reduction in the absorption of L-cys-CuNPs was observed along with a color change from red to yellow (Figure 10.8).This change in spectral profile in presence of CR may be due to aggregation of L-cys-CuNPs within the solution.[78] TEM analysis reveals that aggregation of the particles occurs only after the exposure of CR. From figure 10.1, average particle size of L-cys-CuNPs was 14.02 nm, while particle size was increased about 16 times after the addition of CR (Figure 10.10).

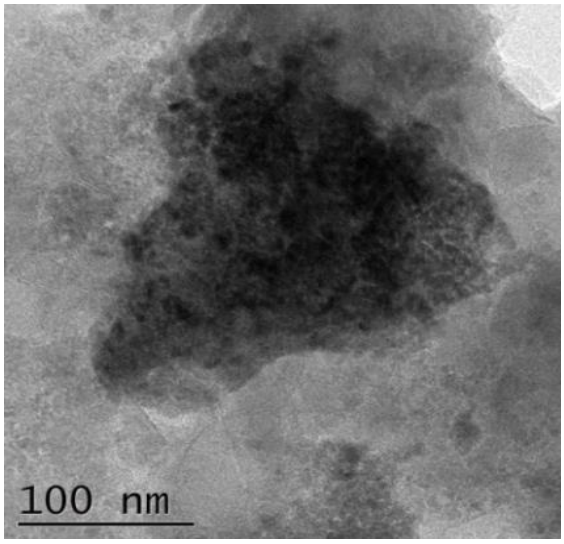

Figure 10.10: TEM images of L-cys-CuNPs in presence of CR.

DLS studies further strengthen the findings from TEM, ie, the hydrodynamic diameter of L-cys-CuNPs was increased after the addition of CR from 30.6 nm to 296.7 nm (Figure 10.11). Thus, such 'growth' accounts for the observed change (decreased intensity and shape) in LSPR band of L-cys-CuNPs.[78]

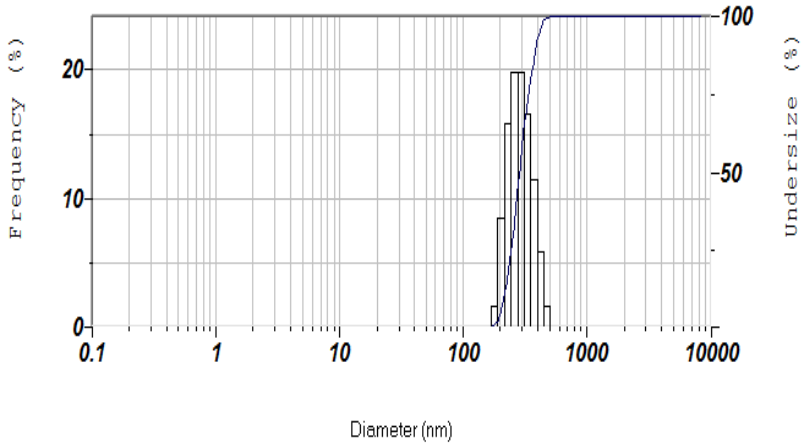

Figure 10.11: DLS spectrum of L-cys-CuNPs in presence of CR.

According to the Mie theory, when small nanoparticles aggregate, SPR band intensity will be largely reduced due to incapability of the aggregates in producing surface plasmons.[78,267] Before the addition of CR, L-cys-CuNPs have a zeta potential of -52 mV, this high value refers to high stability[179] and excellent capping of L-cysteine on the surface of CuNPs. Upon addition of CR, zeta potential was lowered (-16 mV) implying the reduced stability of CuNPs (Figure 10.12).

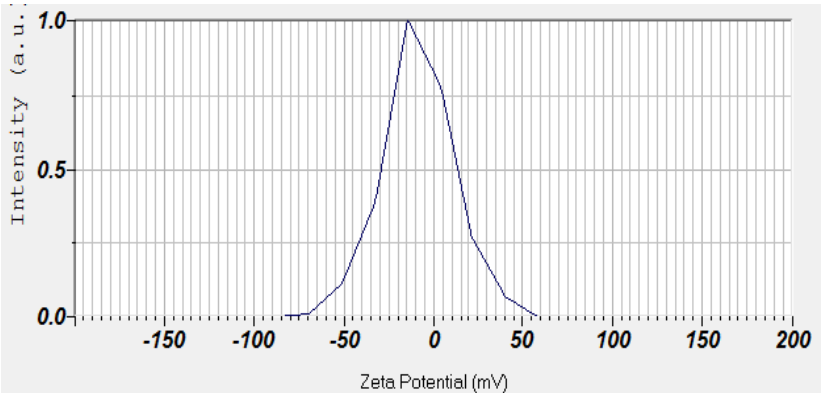

Figure 10.12: Zeta potential analysis of L-cys-CuNPs in presence of CR.

From IR spectroscopic analyses (Figure 10.13), it is clear that the disappearance of –SH stretching band in L-cysteine, when it is capped on CuNPs is due to 'S-Cu' bond formation. By virtue of the cage like structure of CR, it can easily form three hydrogen bonds with L-cysteine, which may lead to the detachment of capped L-cysteine from the surface of CuNPs.[268] Reappearance of '–SH' stretching band in the FTIR spectrum of L-cys-CuNPs upon addition of CR[25] confirms the detachment of capped L-cysteine from the surface of CuNPs. Therefore, the observed aggregation may be due to fusion of un-stabilized CuNPs.[78]

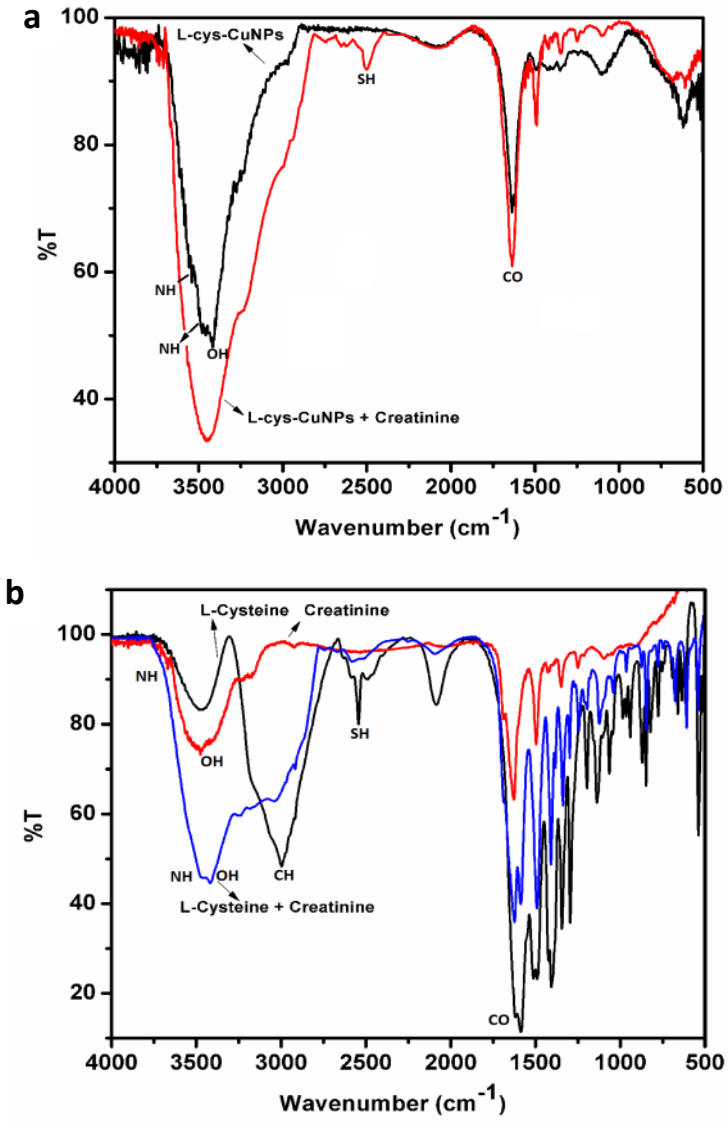

Figure 10.13: (a) FTIR spectrum of L-cys-CuNPs in the presence and absence of CR and (b) shows the FTIR spectrum of L-cysteine, CR and L - cysteine + CR.

Thus, excess of CR would offer a very little opportunity to L-cysteine to bind with the surface of CuNPs, leading to complete conversion of small sized nanoparticles to large sized aggregates in solution. Based on the above

observations, the proposed mechanism for aggregation of particles is presented in Scheme 10.2.

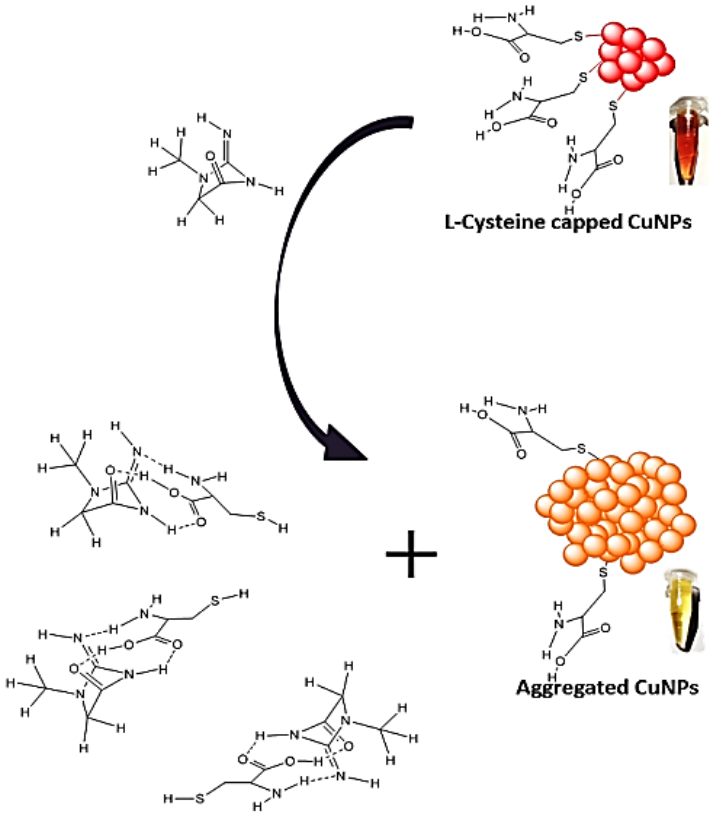

Scheme 10.2: Representation of aggregation induced mechanism of sensing.

10.3.6 Application studies

Since the developed method finds application in physiological solutions, determination of CR in spiked - artificial blood serum and urine samples were carried out. For comparison, the colorimetric method – Jeffe's reaction[99] has also been carried out using picric acid and the results are presented in Table 10.4. From table 10.4, it is clear that, the recoveries are in good agreement with those of Jeffe's method.

Table 10.4: Determination of CR in artificial blood serum and urine samples.

Samples	Added (M)	Proposed method			Standard method		
		Found (M)	R (%)[a]	RSD (%)[a]	Found (M)	R (%)[a]	RSD (%)[a]
Blood serum	3.33×10^{-7} to 1.65×10^{-6}	3.44×10^{-7} to 1.63×10^{-6}	99	3.0	3.51×10^{-7} to 1.64×10^{-6}	100	2.7
Urine	3.33×10^{-7} to 1.65×10^{-6}	3.26×10^{-7} to 1.65×10^{-6}	100	2.0	3.45×10^{-7} to 1.64×10^{-6}	101	2.2

a From five measurements, R = recovery, RSD = relative standard deviation

10.4 Conclusions

L-cysteine stabilized CuNPs were used for the quantification of renal bio-marker, creatinine, based on change in LSPR band of the colloidal solution. Under optimum conditions, linear dynamic range was 5.33×10^{-6} to 3.33×10^{-7} M and detection limit was 4.54×10^{-10} M. Successful application of the developed sensor in spiked artificial serum and urine samples, based on colorimetric and naked eye examination proves its potential in physiological and clinical investigations. In comparison to the existing sensors based on noble metal nanoparticles, the developed sensor stands out due to its cost effective nature.

.....ꕥ.....

Chapter 11

DUAL CHANNEL OPTICAL SENSOR FOR ADRENALINE BASED ON INSITU FORMATION OF COPPER NANOPARTICLES

Contents

This chapter describes development of a dual channel sensor for adrenaline (ADR) based on insitu formation of copper nanoparticles (CuNPs). The proposed sensor works via both fluorimetry and spectrophotometry. Visual detection was also enabled by colour change of solution from pale blue to reddish brown. Here $CuCl_2$ solution is used as probe to simplify method and was function as excellent fluorimetric as well as colorimetric ADR sensor. Fabricated sensor is very simple, selective and reproducible in nature. Proposed sensor works fluorimetrically in linear range of 3.00×10^{-5} to 5.00×10^{-7} M and spectrophotometrically in linear range of 5.00×10^{-4} to 2.00×10^{-5} M. Artificial urine and commercial pharmaceutical formulations were successfully analyzed as samples for estimation of ADR by developed dual channel sensor.

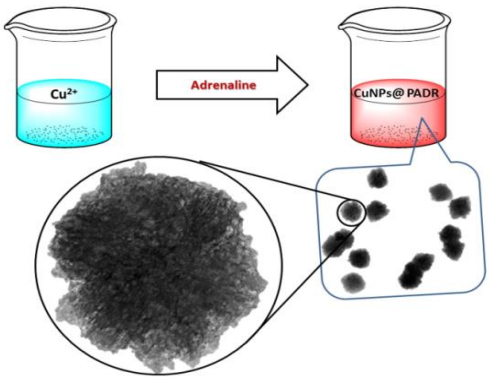

Scheme 11.1: Pictorial representation of sensing process.

11.1 Introduction

Adrenaline (ADR), a hormone that is secreted during emergency conditions, regulates important body functions viz., blood pressure, respiratory rate etc.[269] It belongs to the catechol amine family of neurotransmitters like dopamine and noradrenaline.[270] ADR is used during treatment of type I allergic reactions, including anaphylaxis.[271] Determining the levels of ADR in body fluids is clinically significant for early diagnosis of Parkinson's disease, extracranial cancer in children and hypertension etc.[269]

Though several analytical techniques were developed in recent years for detection and determination of ADR,[270,272-274] most of them have complicated procedures like sample derivatization and are either time consuming or expensive, which limit their use for routine analysis. These limitations can be overcome by a dual channel sensor, which sense in both way and give sensitive outcomes. Best example for this type of sensor is the dual channel sensor with fluorimetric and colorimetric readout.

In dual channel sensing based on fluorescence and colorimetry, a significant change in fluorescence along with a colour change is required on incorporation of analyte to probe solution. The change in fluorescence signal produced may either by quenching or enhancement via analyte interaction. By incorporating the unusual optical properties of nanoparticles, several sensors are reported so far.[272,275,276] However, most of the reports are based on expensive gold nanoparticles. Furthermore, nanoparticles have to be synthesized prior to use. Only a few approaches are devoted in the 'insitu' formation method for this type of sensing.[43,80,277,278]

Thus, in the proposed work, we report a novel sensing strategy for ADR via colorimetric as well as fluorimetric readouts based on insitu formation of copper nanoparticles from $CuCl_2$ solution. Even though CuNPs is less expensive, surface plasmon properties of these nanoparticles is less explored compared to gold and silver nanoparticles. Hence, the objective of the proposed work was to develop dual channel optical sensor based on CuNPs for determination of ADR. Further, the proposed work is simple and cost effective and can be successfully applied for clinical analysis.

11.2 Experimental

11.2.1 Analytical procedure

0.1 M solution of $CuCl_2$ was used as probe for analysis. 40 µL of the above solution (to obtain final concentration of 2.00×10^{-2} M) was mixed with 1 mL of 0.1 M NaCl solution followed by adding adequate amount of ADR solution. Final volume of mixture was made up to 2 mL by adding appropriate amount of water. After incubating for 30 minutes, the mixture was transferred to quartz cuvette and resultant fluorescence and UV-visible absorption spectra were recorded.

11.2.2 Analysis of samples

Artificially prepared urine and commercially available injection samples were used for application studies. Artificial urine was prepared by the procedure given in section 2.4.2 of chapter 2 and suitable amount of ADR is spiked to it and 100 µL of it was used for analysis. In each step of analysis, 40 µL of $CuCl_2$ is mixed with 100 µL of urine sample, 1 mL of 0.1 M NaCl and a suitable amount of standard solution of ADR (for standard addition

method). The volume was made up to 2 mL and after incubation, resultant spectra were studied. For validation, HPLC determination[100] was also carried out using the procedure discussed in section 2.3.7. In case of pharmaceutical formulation, diluted sample was used instead of urine sample. Standard addition method was also used and recovery was compared with the declared amount in sample.

11.3 Results and discussion

11.3.1 Optimization of experimental parameters

By analyzing UV-visible spectrum of probe and analyte, various parameters were studied and optimized.

11.3.1.1 Selectivity of metal salt

Since ADR can reduce the metal salt and change colour of the solution, few metal salt solutions such as $FeCl_3$, $MgCl_2$, $CdCl_2$, $BaCl_2$, $ZnCl_2$, $NiCl_2$ were also studied to confirm selectivity of ADR towards Cu^{2+} ions. 1.00×10^{-4} M solution of ADR is added to each of the metal salt solution (5.00×10^{-2} M) and resultant spectra were recorded. Figure 11.1 depicts the difference in absorbance before and after the addition of ADR. It is clear from the figure that, $CuCl_2$ solution provided best result among the salts under study.

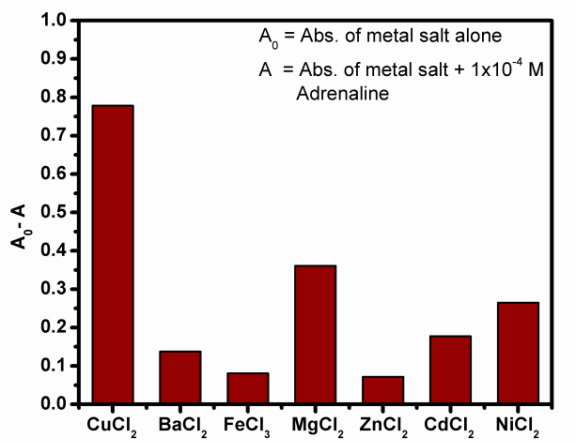

Figure 11.1: Selective oxidation of adrenaline among various metal salt solutions.

11.3.1.2 Selection of copper salt

To obtain fast response from the developed sensor, selection of suitable copper salt is very critical, because, it determines formation of NPs. For this purpose, different copper salts such as $CuSO_4$, $CuCl_2$, $Cu(COO)_2$ and $Cu(NO_3)_2$ were selected and used for analysis. Compared to others, $CuCl_2$ gave the best response (Figure 11.2) and was selected as the probe for analysis.

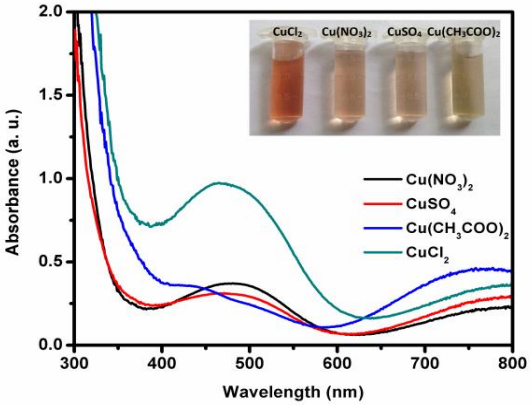

Figure 11.2: Reaction of adrenaline in various copper salts.

11.3.1.3 Selection of supporting ionic medium

A suitable supporting medium is needed for analysis and hence performances of various ionic media (0.1 M) were evaluated. NaCl solution was selected as supporting solution since it gave better results (maximum absorbance) among the various solutions studied (NaCl, KCl, H_2SO_4, Na_2SO_4, HCl, HNO_3 and buffer solutions such as phosphate, acetate, citrate of pH of 7) (Figure 11.3).

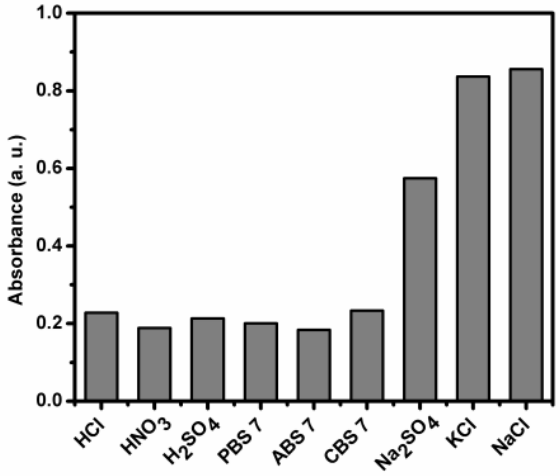

Figure 11.3: Selectivity of reaction medium for adrenaline and $CuCl_2$.

11.3.1.4 Concentration of Cu (II) solution

The minimum amount of Cu (II) required for maximum sensitivity for a solution of 5.00×10^{-4} M ADR was determined (Figure 11.4) and found that, for the studied concentration of ADR, 2.00×10^{-2} M Cu (II) was required.

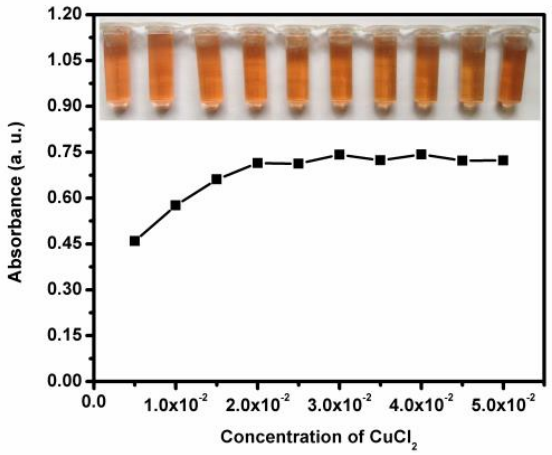

Figure 11.4: Optimization of concentration of probe for adrenaline sensing.

11.3.1.5 Incubation time

Since the present study deals with insitu formation of nanoparticles, an incubation step is necessary. Although the reaction was completed after 20 minutes of time, an additional period of 10 minutes was given to obtain a stable state and further studies were carried out after this time period. Thus, incubation time was optimized as 30 minutes.

11.3.2 Calibration graph and limit of detection

Upon addition of ADR, an emission peak was generated at 538 nm and a new absorption peak at 464 nm. On increasing the concentration, increase in both fluorescence intensity (Figure 11.5) as well as absorbance (Figure 11.7) were observed. No further increase in fluorescence intensity was observed after 3.00×10^{-5} M addition under optimized conditions. Calibration graph was plotted by noting fluorescence intensity/absorbance against concentration of ADR. The calibration plot for fluorimetry was found linear (Figure 11.6) in the range of 3.00×10^{-5} to 5.00×10^{-7} M (R^2 = 0.987) and the limit of detection (LOD) was found to be 2.00×10^{-7} M.

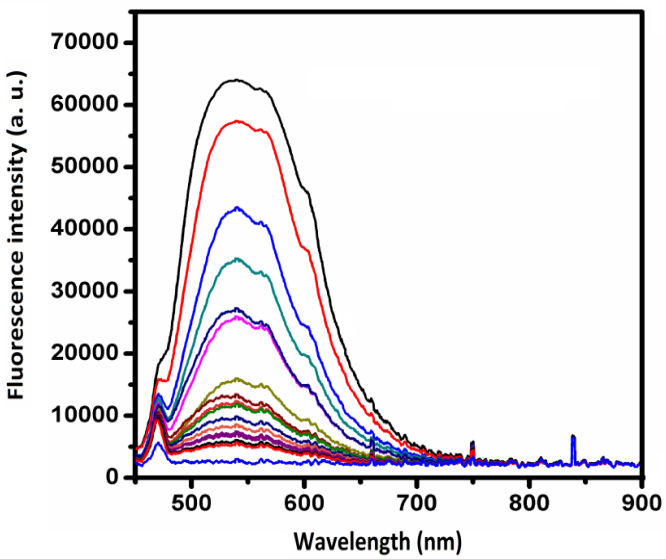

Figure 11.5: Overlay of fluorescence spectra of Melanine coated CuNPs resulting from the reaction of $CuCl_2$ and various concentrations of ADR.

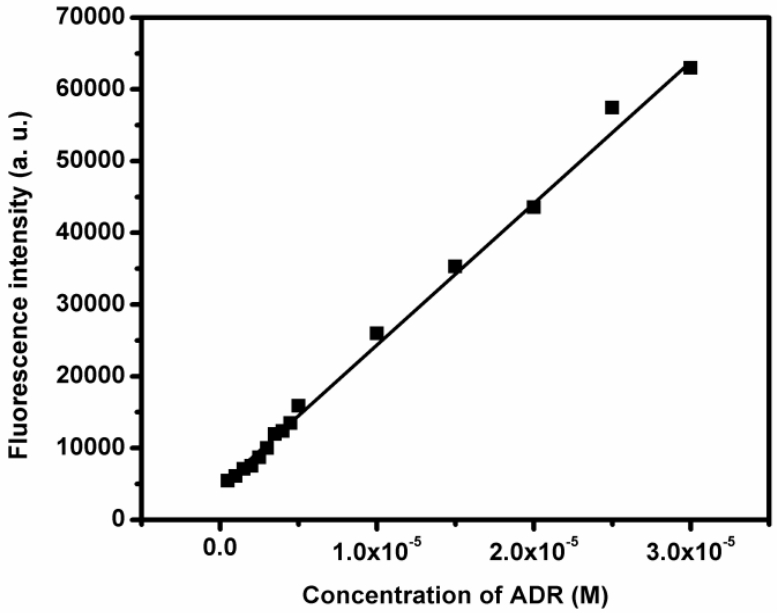

Figure 11.6: Calibration plot of fluorescence intensity vs. concentration of ADR.

Moreover, on increasing the concentration beyond 3.00×10^{-5} M, color of the solution was changed from pale blue to reddish brown (Figure 11.7). Absorbance value also showed a linear dependence (Figure 11.8) to concentration range from 5.00×10^{-4} to 2.00×10^{-5} M (R^2 = 0.988). LOD for spectrophotometry was found to be 1.00×10^{-5} M. Hence, using same strategy, determination of ADR can be carried out via both spectrophotometry and fluorimetry. Additionally colour change of solution entails the visual detection.

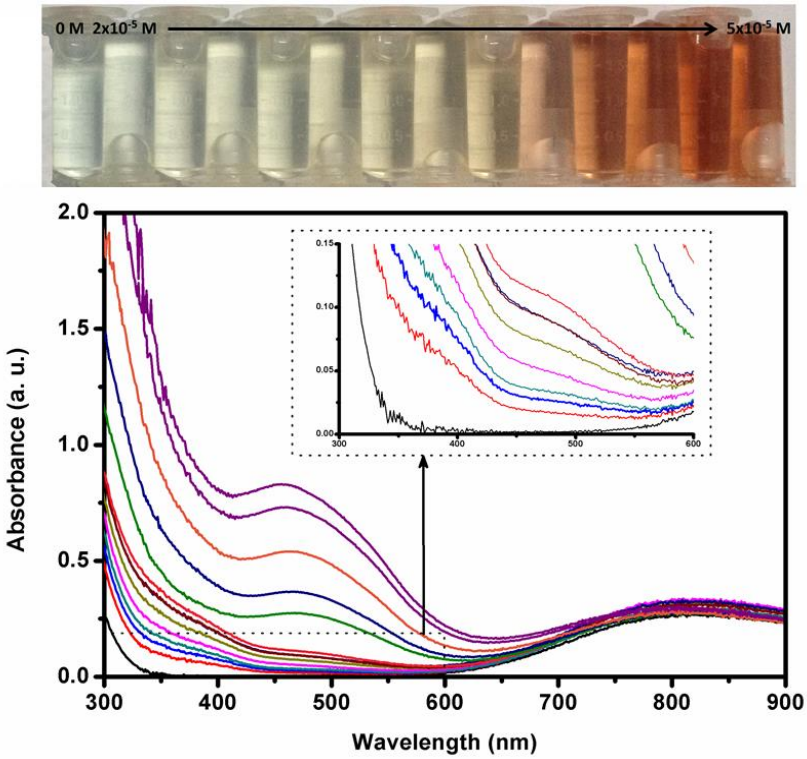

Figure 11.7: Overlay of absorption spectra of melanine coated CuNPs generated by the reaction of $CuCl_2$ with various concentrations of ADR. Corresponding color changes of the solutions are shown on the top.

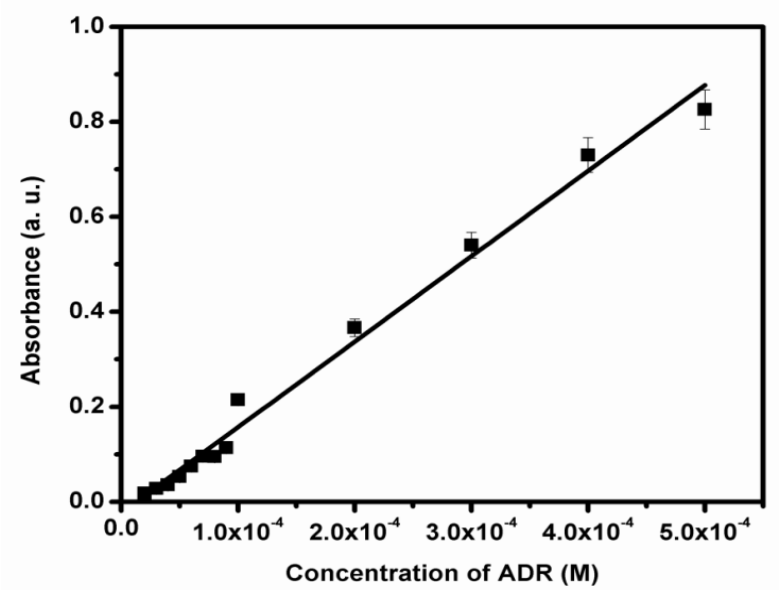

Figure 11.8: calibration graph of absorbance vs. concentration of ADR.

Performance of developed method was compared with existing analytical methods (Table 11.1) and results shows that, the developed method is comparable in sensing parameters and superior in its sensing approach and cost effective nature.

Table 11.1: Comparison of developed sensor with recently reported methods.

Method	Probe used	Linear range (M)	LOD (M)	Reference
Fluorimetry	GQDs	2.0×10^{-4} to 1.0×10^{-6}	1.0×10^{-6}	14
Amperometry	Laccase-OE	1.0×10^{-4} to 3.0×10^{-6}	3.0×10^{-6}	15
Voltammetry	DSNPs-GCE	1.6×10^{-4} to 2.6×10^{-5}	4.0×10^{-7}	16
Spectrophotometry	$AgNO_3$	6.5×10^{-6} to 5.5×10^{-6}	1.3×10^{-6}	17
Spectrophotometry	Iodic acid	7.8×10^{-4} to 6.2×10^{-6}	4.1×10^{-6}	18
Proposed method	$CuCl_2$	$^{F}3.0\times10^{-5}$ to 5.0×10^{-7} $^{C}5.0\times10^{-4}$ to 2.0×10^{-5}	$^{F}2.0\times10^{-7}$ $^{C}1.0\times10^{-5}$	-

GQDs = Graphene quantum dots, OE = oxygen electrode, DSNPs = , LOD = Limit of detection, F = Fluorimetry, C = Colorimetry

11.3.3 Selectivity of dual channel assay

Selectivity of probe towards determination of ADR can be proved by analyzing the interaction with usual coexisting species separately and in presence of ADR. The results are presented in Figure 11.9. Larger value of absorbance shows highly selective nature of sensor towards ADR. Additionally, fluorescence intensity of ADR is highest among coexisting species studied. Also, effective color change is only produced by ADR.

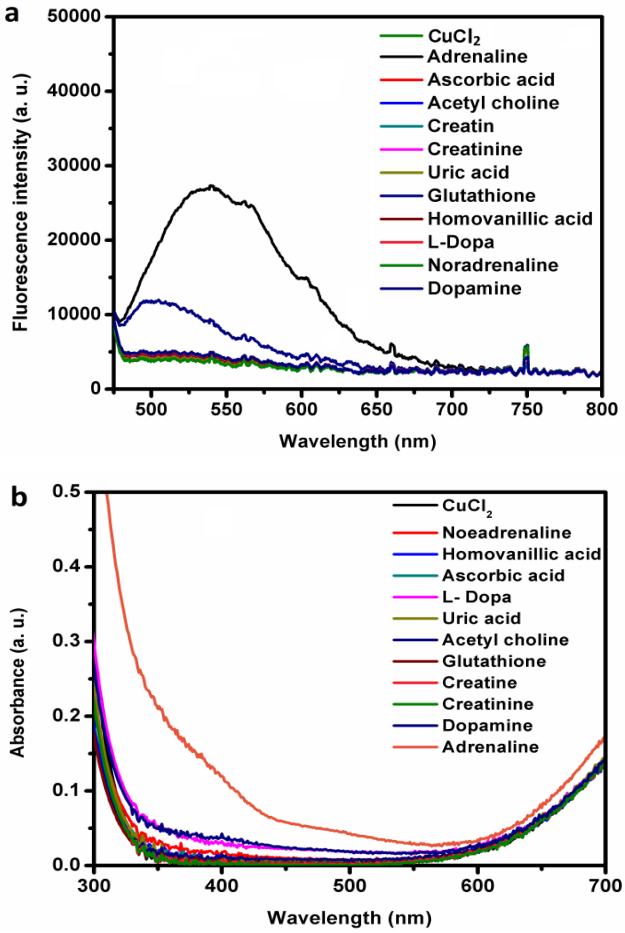

Figure 11.9: Selectivity of $CuCl_2$ towards ADR over various biologically important species in (a) emission and (b) absorption spectra.

The interference study also shows that even up to 100 times concentration of acetyl choline, creatine, creatinine, homovanillic acid and glutathione did not have any effect on either absorbance or emission intensity of the system. However, dopamine and noradrenaline showed interference with ADR at concentration of 1:1 in both cases. While, L-Dopa and uric acid did not show interference even up to 10fold excess concentrations in emission intensity, they exhibited interference in absorption intensity at 1:1 concentration with ADR. Percentage signal changes obtained in interference studies are represented in Table 11.2.

Table 11.2: Results obtained from interference studies.

	Fluorimetry (ADR 1.00×10^{-6} M)		**Colorimetry (ADR 2.00×10^{-5} M)**	
Species	**Concentration (M)**	**Signal change (%)**	**Concentration (M)**	**Signal change (%)**
Acetyl choline	1.00×10^{-4}	1.0	2.00×10^{-4}	3.4
Creatine	1.00×10^{-4}	0.1	2.00×10^{-4}	3.6
Creatinine	1.00×10^{-4}	3.1	2.00×10^{-4}	2.7
Glutathione	1.00×10^{-4}	4.8	2.00×10^{-4}	5.0
Homovanilic acid	1.00×10^{-4}	0.1	2.00×10^{-4}	2.3
L- Dopa	1.00×10^{-5}	0.7	2.00×10^{-5}	7.4
Uric acid	1.00×10^{-5}	1.5	2.00×10^{-5}	9.5
Dopamine	1.00×10^{-6}	3.9	2.00×10^{-5}	15.8
Noradrenaline	1.00×10^{-6}	6.3	2.00×10^{-5}	39.7

11.3.4 Mechanism of sensing

Reducing properties of catechol amines were studied in detail during the last century.[284] During oxidation, an aminochrome is produced initially

and it polymerizes into melanine like polymer. Also, oxidizing property of Cu^{2+} on adrenaline was established by Harrison in 1963.[285] Here oxidation of ADR via Cu^{2+} reduction produces melanine coated CuNPs. Evidences for support of above mechanism were achieved from several analytical techniques such as UV-visible spectroscopy, TEM, emission spectroscopy, X ray diffraction analysis and dynamic light scattering analysis.

After the reaction of ADR with probe, a new peak at ~464 nm is observed in the UV-visible spectrum, that implies the formation of CuNPs with a lower particle sizes than usual (having absorption at ~560 nm).[286] Also the characteristic wavelength of absorption for copper nanoclusters is at lower wavelength (250 – 350 nm),[287] so the newly generated absorption peak indicates the intermediate properties of the insitu formed particles with that of nanoclusters and usual CuNPs. TEM images clearly show the formation of flower like particles (Figure 11.10) and a close observation of the particle revealed the incorporated CuNPs inside the cage like structures (Figure 11.11 a). The obtained CuNPs has a particle sizes around 4.7 nm, which is very near to the size of nanocluster. In high resolution TEM, fringes can be observed with a 'd' spacing of 2.1 Å (Figure 11.11 b) implying the formation of CuNPs.[288] On increasing the concentration of ADR, more and more particles were generated and they tend to aggregate at concentrations above 1.00×10^{-5} M (Figure 11.12).

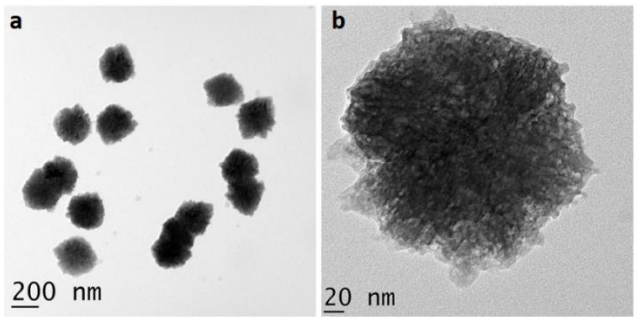

Figure 11.10: (a) TEM images of in situ formed melamine coated CuNPs and (b) cage like structure on a closer observation of one particle.

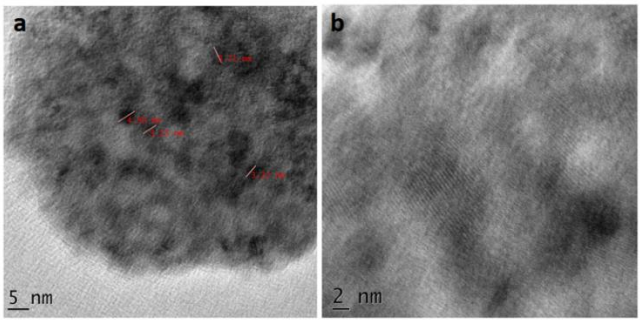

Figure 11.11: (a) TEM image of in situ formed CuNPs inside the cage like particle and (b) HRTEM image showing fringes.

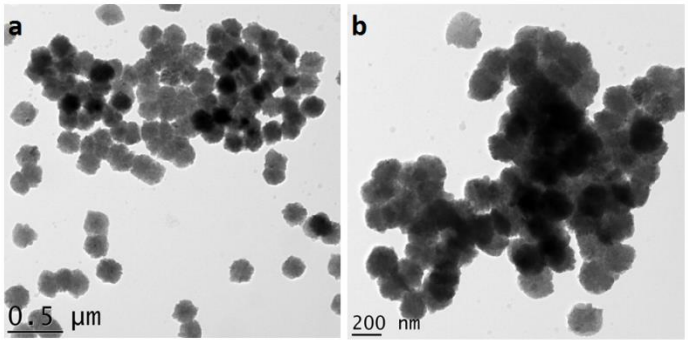

Figure 11.12: (a) TEM image of in situ formed melanine coated CuNPs at higher concentrations of ADR and (b) aggregation of insitu formed particles at higher concentrations of ADR.

DLS measurement denotes formation of particles with a hydrodynamic diameter of 253.9 nm by addition of ADR (Figure 11.13). Additionally, a stable blue fluorescence is observed at emission maximum of ~ 538 nm.

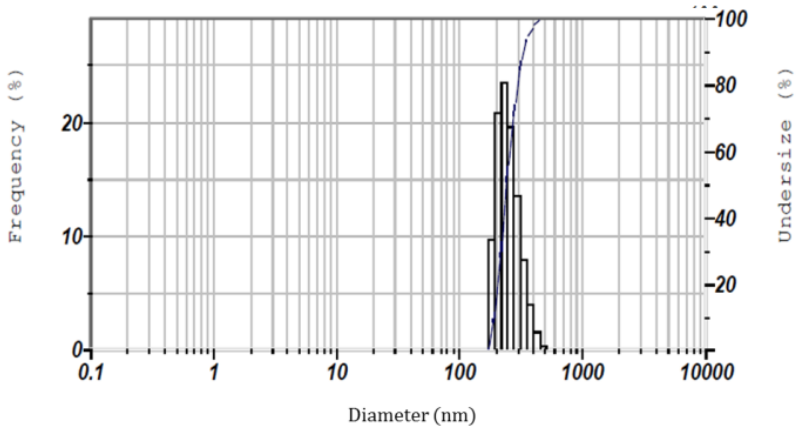

Figure 11.13: DLS analysis of insitu formed CuNPs.

Formation of CuNPs is further confirmed by XRD analysis (Figure 11.14). Characteristic peaks corresponding to the reflection of (111), (200) and (220) planes were obtained for the probe after addition of ADR.[289] Also, obtained XRD pattern is compared with that of probe, and it shows the above mentioned peaks were generated only after the reaction with ADR, confirms the CuNPs formation.

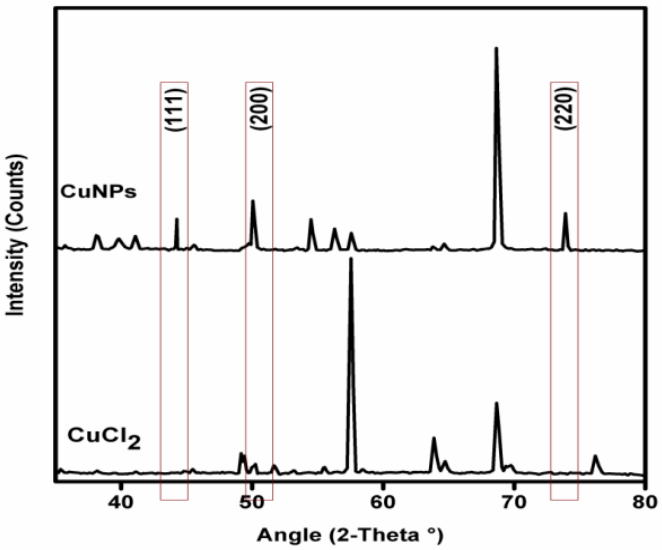

Figure 11.14: XRD pattern of $CuCl_2$ and insitu formed CuNPs upon addition of ADR.

Since both oxidation of ADR and formation of CuNPs produce the reddish brown colour, a visible change from pale blue color to reddish brown can be observed. This color change entails colorimetric sensing of ADR. Moreover, generation of fluorescence after the addition of ADR can be used for fluorimetric estimation. This stable fluorescence signal is due to metal enhanced effect of CuNPs,[44] because plasmonic nanoparticles can interacts with fluorophores and there by enhance its fluorescence.[42] Here the insitu formed CuNPs is wrapped by insitu formed melanine which makes an effective interaction between metal and fluorophore. This combined effect has shown a new path for a dual channel sensing strategy.

11.3.5 Application studies in samples

Using standard addition method, concentration of ADR was estimated from commercial pharmaceutical formulation and spiked artificial urine

samples. Recovery of spiked concentration is compared with recovery obtained from standard HPLC - UV method[100] (Table 11.3). The obtained concentrations of pharmaceutical sample were compared with the declared amount (Table 11.4). Evaluation of Table 11.3 and 11.4 reveals the effectiveness of proposed assay for real sample estimation.

Table 11.3: Results obtained from application of proposed method and reference method in artificial urine.

Proposed method				HPLC – UV method			
Added (M)	**Found[a] (M)**	**R[a] (%)**	**RSD[a] (%)**	**Added (M)**	**Found[a] (M)**	**R[a] (%)**	**RSD[a] (%)**
5.00×10^{-7} to 2.00×10^{-5}	4.94×10^{-7} to 1.97×10^{-5}	99	0.7	2.00×10^{-6} to 2.00×10^{-5}	2.02×10^{-6} to 2.00×10^{-5}	100	0.8

[a] = average of three replicates, R = recovery, RSD = Relative standard deviation.

Table 11.4: Results of application studies conducted in commercial injection samples.

Sample and brand name	Declared amount (mg / mL)	Found (mg / mL)	RSD[a] (%)
Adrenaline injection IP (Ciron Drugs and Pharmaceuticals Pvt. Ltd., India)	1	1 (Fluorimetry)	5.0
		1 (Spectrophotometry)	3.1

[a] average of three replicates

11.4 Conclusions

A simple and cost effective dual channel sensing strategy was developed using insitu formed CuNPs. Experimental parameters viz., concentration of $CuCl_2$, supporting ionic medium, incubation time etc. were studied and optimized. Sensing was based on fluorescence and absorption studies together with visual color detection. Developed assay has a detection limit of 2.00×10^{-7} M by fluorimetry and 1.00×10^{-5} M by colorimetry. Based on evidences obtained from analyses, mechanism of sensing was proposed as insitu formation of CuNPs. The proposed assay was applied in pharmaceutical formulations and artificial urine samples. The method was validated using HPLC – UV method.

.....ഠാര.....

Chapter 12

SUMMARY

Contents

Objectives of the present work, summary and future prospective of the work done are discussed in this chapter.

12.1 Objectives of the present work

12.1.1 Development of nanomaterials based electrochemical sensors

1. Fabrication of chemically modified electrodes using nanomaterials such as nanoparticles and polymer-nano composite.

2. Characterization of modified electrode using scanning electron microscopy, atomic force microscopy, cyclic voltammetry and electrochemical impedance spectroscopy.

3. Optimization of various experimental parameters of the fabrication of sensors.

4. Determination of analytical figures of merit of developed sensors.

5. Prediction of a plausible mechanism for oxidation of analyte at electrode surface.

6. Carry out application studies in spiked food or artificial physiological samples.

7. Validation of the results obtained from application study with that of existing methods.

12.1.2 Development of fluorescent sensors based on quantum dots and nanoclusters

1. Synthesis of nanostructured fluorescent probes such as quantum dots and nanoclusters.

2. Characterization of synthesized fluorescent probes by transmission electron microscopy, UV-Vis absorption spectroscopy, dynamic light scattering and zeta potential analyses.

3. Development of fluorescent sensors for food additives and biomarkers using synthesized fluorescent probes.

4. Study of fluorescence quenching/enhancement mechanism, based on the interaction between fluorophore and analyte.

5. Carry out application studies in food and artificial physiological samples.

6. Validating the results from application studies with that of existing methods.

12.1.3 Development of colorimetric sensors based on nanoparticles

1. Synthesis of nanoparticles for colorimetric sensing applications.
2. Characterization of synthesized nanoparticles by transmission electron microscopy, UV-Vis absorption spectroscopy, Energy dispersive x-ray spectroscopy, dynamic light scattering and zeta potential analysis.
3. Development of colorimetric sensors for biomarkers.
4. Study of mechanism behind the sensing process using various analytical techniques.
5. Carry out application studies in artificial physiological samples and pharmaceutical formulations.
6. Validating the results from application studies with that of existing methods.

12.2 Summary of the work done

In the present work, nine chemical sensors including three electrochemical and six optical sensors (colorimetric and fluorescence sensor) were developed for the quantification of food additives and biomarkers. Salient features of developed sensors are explained below.

Type of sensor developed	Analyte	Sensing probe	Linear range (M)	LOD (M)
Electrochemical sensor	1. Octyl gallate	DDT/AuNPs/ GCE	1.2×10^{-6} - 2.0×10^{-7}	8.3×10^{-9}
	2. Uric acid	PBPB/AuNPs/ GCE	1.0×10^{-3} - 2.0×10^{-5}	2.2×10^{-6}
	3. Propyl gallate	NiNPs/GCE	1.0×10^{-3} - 4.0×10^{-4} and 3.0×10^{-4} - 2.0×10^{-6}	5.8×10^{-8}
Fluorimetric sensor	4. Brilliant blue FCF	L-cys-CdS	4.0×10^{-5} - 4.5×10^{-6}	3.5×10^{-7}
	5. Quinoline yellow	L-cys-CuNCs	5.5×10^{-6} - 2.0×10^{-7}	1.1×10^{-7}
	6. Glutathione	EDA-CDs	6.0×10^{-7} - 5.0×10^{-8}	1.7×10^{-9}
Colorimetric sensor	7. Dopamine	Citrate-AuNPs	1.8×10^{-4} - 5.8×10^{-6}	1.6×10^{-6}
	8. Creatinine	L-cys-CuNPs	5.3×10^{-6} - 3.3×10^{-7}	4.5×10^{-10}
[F] Fluorimetric and [C]Colorimetric sensor	9. Adrenaline	$CuCl_2$	[F] 3.0×10^{-5} - 5.0×10^{-7} [C] 5.0×10^{-4} - 2.0×10^{-5}	[F] 2.0×10^{-7} [C] 1.0×10^{-5}

12.3 Future prospective

Sensor technology have become a powerful tool of analysis since it offers promising applications in fields of quality control, clinical diagnosis, pharmaceutical analysis, environmental monitoring, defence and industrial manufacturing process. Using an inter-disciplinary approach, current researchers are focused to develop sensors for in-vivo use relating various branches of science viz., physics, chemistry, life science, electronics etc. For the effective use, developed sensor devices must be portable, cheap and reliable. Commercialization of developed devices has the potential to address challenges associated with several fields. Thus, innovations in the field of sensors will help to achieve significant progress for improving quality of life.

.....ꕥ.....

References

1. S. Bankim, S. Ashwini, *Electrochim. Acta*, **55,** 8638 (2010).
2. J. Wang, *Analytical Electrochemistry,* Wiley - VCH, USA, 107 (2000).
3. J. L. Hardcastle, G. G. Murcot, R. G. Compton, *Electroanalysis*, **12,** 559 (2000).
4. J. A. Plambeck, *Electroanalytical Chemistry: Basic Principles and Applications*, John Wiley and Sons Inc., New York, 69 (1982).
5. J. Mendham, R. C. Denney, J. D. Barnes, M. J. K. Thomas, *Vogel's Textbook of Quantitative Chemical Analysis,* 6th edn., Pearson Education Ltd., Singapore (2000).
6. P. M. S. Monk, *Fundamentals of Eletroanalytical Chemistry*, Wiley, Chichester (2001).
7. F. A. Settle, *Handbook of Instrumental Techniques for Analytical Chemistry*, Prentice Hall PTR, 720 (1997).
8. D. Grieshaber, R. MacKenzie, J. Vörös, E. Reimhu, *Sensors*, **8**, 1400 (2008).
9. Z. Galus, *Fundamentals of Electrochemical Analysis*, Ellis Horwood Ltd., England, 25 (1976).
10. F. Patolsky, M. Zayats, E. Katz, I. Willner, *Anal. Chem.*, **71**, 3171 (1999).
11. A. J. Bard, L. Faulkner, *Electrochemical Methods: Fundamentals and Applications*, 2nd Edn., Wiley, New York (2001).
12. L. Mirmoghtadaie, A. A. Ensafi, M. Kadivar, M. Shahedi, M. R. Ganjali, *Int. J. Electrochem. Soc*., **8**, 3755 (2013).
13. D. C. Tiwari, R. Jain, S. Sharma, *J. Sci. Ind. Res.*, **66**, 1011 (2007).
14. P. R. Moses, L. Wier, R. W. Murray, *Anal. Chem.*, **47,** 1882 (1975).

15. R. A. Durst, A. J. Baumner, R. W. Murray, R. P. Buck, C. P. Andrieux, *Pure Appl. Chem.*, **69,** 1317 (1997).

16. A. Ambrosi, *The application of nanomaterials in electrochemical sensors and biosensors*, Ph. D. Thesis, Dublin City University, Republic of Ireland, 2 (2007).

17. H. Zhou, X. Gan, T. Liu, Q. L. Yang, G. X. Li, *J. Biochem. Biophys. Methods*, **64**, 38 (2005).

18. J. B. Broderick, M. J. Natan, T. V. O'Halloran, R. P. Van Duyne, *Biochemistry*, **32**, 13771 (1993).

19. C. Yongli, Z. Xiufang, G. Yandao, Z. Nanming, Z. Tingying, S. Xinqi, *J. Colloid Interface Sci.*, **214**, , 38 (1999).

20. A. Galal, N. F. Atta, E. H. El – Ads, *Talanta*, **93**, 264 (2012).

21. A. S. Duwez, *J. Electron. Spetrosc. Relat. Phenom.*, **134**, 97 (2004).

22. A. Ulman, *Chem. Rev.*, **96**, 1533 (1996).

23. N. J. Ronkainen, S. L. Okon, *Materials*, **7**, 4669-4709 (2014).

24. P. Yang, W. Wei, C. Tao, J. Zeng, *Bull. Environ. Contam. Toxicol.*, **79**, 5 (2007).

25. T. Jos, A. R. Jose, U. Sivasankaran, K. Girish Kumar, *J. Electrochem. Soc.*, **162,** B94 (2015).

26. G. Zhang, P. He, W. Feng, S. Ding, J. Chen, L. Li, H. He, S. Zhang, F. Dong, *J. Electroanal. Chem.*, **760**, 24 (2016).

27. A. E. Vikraman, Z. Rasheed, L. Rajith, L. A. Lonappan, K. Girish Kumar, *Food Anal. Methods*, **6**, 775 (2013).

28. S. T. Cyriac, D. Thomas, A. E. Vikraman, K. Girish Kumar, *J. Electrochem. Soc.*, **163**, B683 (2016).

29. H. Guo, Z. Huang,Y Zheng, S. Weng, *Int. J. Electrochem. Sci.*, **10**, 10703 (2015).

30. H. Dai, N. Wang, D. Wang, X. Zhang, H. Ma, M. Lin, *Microchim. Acta*, **183**, 3053 (2016).

31. S. Mukdasai, U. Crowley, M. Pravda, X. He, E. P. Nesterenko, P. N. Nesterenko, B. Paull, S. Srijaranai, J. D. Glennon, E. Moore, *Sens. Actuators, B*, **218**, 280 (2015).

32. H. Beitollahi, M. Hamzavi, M. T. Mahani, M. Shanesaz, H. K. Maleh, *Electroanalysis*, **27**, 524 (2015).

33. R. J. Herrick, *Introduction to DWDM technology*, Wiley - IEEE, New York (2000).

34. M. Papini, *Infrared Phys.* **34**, 607 (1993).

35. J. R. Lakowicz, *Principles of Fluorescence Spectroscopy*, Kluwer Academic and Plenum Publishers, New York (2000).

36. M. Abramowitz, *Jablonski Energy Diagram*, http://micro.magnet.fsu.edu/primer/java/jablonski/lightandcolor/index.html (Accessed 01 January 2018).

37. E. Ringe, J. Zhang, M. R. Langille, K. Sohn, C. Cobley, L. Au, Y. Xia, C. A. Mirkin, J. Huang, L. D. Marks, R. P. Van Duyne, *Mater. Res. Soc. Symp. Proc.*, **1208,** O10 (2009).

38. V. K. Kandimalla, *Influence of Metal Nanoparticles on Fluorescence Properties*, Ph. D. Thesis, Eastern Michigan University, Michigan, 371 (2010).

39. G. Weber, D. M. Hercules, *Fluorescence and Phosphorescence Analysis. Principles and Applications*, Interscience Publishers (J. Wiley & Sons), New York (1966).

40. X. Cao, F. Shen, M. Zhang, C. Sun, *Sens. Actuators, B*, **202**, 1175 (2014).

41. M. Hosseini, H. Khabbaz, A. S. Dezfoli, M. R. Ganjali, M. Dadmehr, *Spectrochim. Acta, Part A*, **136**, 1962 (2015).

42. K. Jia, X. Zhou, L. Pan, L. Yuan, P. Wang, C. Wu, Y. Huang, X. Liu, *RSC Adv.*, **5**, 71652 (2015).

43. S. Menon, A. R. Jose, S. Jesny, K. Girish Kumar, *Anal. Methods*, **8**, 5801 (2016).

44. S. Zhuo, M. Shao, L. Cheng, R. Que, D. D. D. Ma, S. T. Lee, *Front. Optoelectron. China*, **4**, 114 (2011).

45. H. Li, X. He, Z. Kang, H. Huang, Y. Liu, J. Liu, S. Lian, C. H. A. Tsang, X. Yang, S. T. Lee, *Angew. Chem. Int. Ed.*, **49**, 4430 (2010).

46. K. Dalei, *Synthesis and characterization of cadmium sulphide nanoparticles and its utilization in removal of cadmium from aqueous solution*, MSc. Dissertation, National Institute of Technology, Rourkela, India (2014).

47. P. A. Kurian, C. Vijayan, K. Sathiyamoorthy, C. S. Sandeep, R. Philip, *Nanoscale Research Letters*, **2**, 561 (2007).

48. V. Colvin, M. Schlamp, A. Alivisatos, *Nature*, **370**, 354 (1994).

49. S. Y. Lim, W. Shen, Z. Gao, *Chem. Soc. Rev.*, **44**, 362 (2015).

50. X. Xu, R. Ray, Y. Gu, H. J. Ploehn, L. Gearheart, K. Raker, W.A. Scrivens, *J. Am. Chem. Soc.*, **126,** 12736 (2004).

51. Y. Wang, A. Hu, *J. Mater. Chem., C*, **2**, 6921 (2014).

52. Y. Z. Lu, W. Chen, *Chem. Soc. Rev.*, **41**, 3594 (2012).

53. H. Zhang, X. Huang, L. Li, G. W. Zhang, I. Hussain, Z. Li, B. Tan, *Chem. Commun.*, **48**, 567 (2012).

54. C. I. Richards, S. Choi, J. C. Hsaing, Y. Antoku, *J. Am. Chem. Soc.*, **130,** 5038 (2008).

55. Y. Z. Lu, W. T. Wei, W. Chen, *Chin. Sci. Bull.*, **57**, 41 (2012).

56. Y. Shi, S. Luo, X. Ji, F. Liu, X. Chen, Y. Huang, L. Dong, L. Wang, *Dalton Trans.*, **46**, 14251 (2017).

57. M. J. Barthel, I. Angeloni, A. Petrelli, T. Avellini, A. Scarpellini, G. Bertoni, A. Armirotti, I. Moreels, T. Pellegrino, *ACS Nano*, **9**, 11886 (2015).

58. M. Zhao, L. Sun, R. M. Crooks, *J. Am. Chem. Soc.*, **120**, 4877 (1998).

59. G. L. Wang, H. J. Jiao, X. Y. Zhu, Y. M. Dong, Z. J. Li, *Talanta,* **93,** 398 (2012).

60. W. Tedsana, T. Tuntulani, W. Ngeontae, *Anal. Chim. Acta*, **783,** 65 (2013).

61. M. Liu, L. Xu, W. Cheng, Y. Zeng, Z. Yan, *Spectrochim. Acta, Part A*, **70,** 1198 (2008).

62. H. Xu, X. Yang, G. Li, C. Zhao, X. Liao, *J. Agric. Food Chem.,* **63**, 6707 (2015).

63. Y. Yuan, X. Zhao, M. Qiao, J. Zhu, S. Liu, J. Yang, X. Hu, *Spectrochim. Acta, Part A*, **167**, 106 (2016).

64. Y. Zou, F. Yan, L. Dai, Y. Luo, Y. Fu, N. Yang, J. Wun, L. Chen, *Carbon*, **77,** 1148 (2014).

65. N. K. Das, S. Ghosh, A. Priya, S. Datta, S. Mukherjee, *J. Phys. Chem. C*, **119**, 24657 (2015).

66. Y. Wanga, T. Chena, Q. Zhuanga, N. Yongnian, *Talanta,* **179**, 409 (2018).

67. R. Ghosh, A. K. Sahoo, S. S. Ghosh, A. Paul, A. Chattopadhyay, *ACS Appl. Mater. Interfaces,* **6**, 3822 (2014).

68. A. Lobnik, M. Turel, Š. K. Urek. Optical Chemical Sensors: Design and Applications, Advances in Chemical Sensors, Prof. Wen Wang (Ed.), In Tech Open, London (2012).

69. J. P. Chinta, *Sens. Actuators, B*, **248**, 733 (2017).

70. U. Kreibig, M. Vollmer, *Optical properties of metal clusters*, Springer, Verlag, Berlin (1995).

71. V. Amendola, *Synthesis of gold and silver nanoparticles for photonic applications*, Ph. D. Thesis, University of Padua, Italy, 15 (2008).

72. S. K. Ghosh, T. Pal, *Chem. Rev.*, **107**, 4797 (2007).

73. A. Hatamie, B. Zargar, A. Jalali, *Talanta*, **121**, 234 (2014).

74. Z. Tan, J. Liu, R. Liu, Y. Yin, G. Jiang, *Chem. Commun*., **2009**, 7030 (2009).

75. Q. Cao, H. Zhao, Y. He, X. Li, L. Zeng, N. Ding, J. Wang, J. Yang, G. Wang, *Biosens. Bioelectron.*, **25**, 2680 (2010).

76. S. K. Tripathy, J. Y. Woo, C. S. Han, *Anal. Chem.*, **83**, 9206 (2011).

77. M. S. Usman, M. E. El Zowalaty, K. Shameli, N. Zainuddin, M. Salama, N. A. Ibrahim, *Int. J. Nanomedicine,* **8**, 4467 (2013).

78. R. A. Soomro, A. Nafady, Sirajuddin, N. Memon, T. H. Sherazi, N. H. Kalwar, *Talanta*, **130**, 415 (2014).

79. S. H. Wu, D. H. Chen, *J. Colloid Interface Sci.*, **273**, 165 (2004).

80. D. Drescher, H. Traub, T. Büchner, N. Jakubowski, J. Kneipp, *Nanoscale*, **9**, 11647 (2017).

81. S. Chandran, L. A. Lonappan, D. Thomas, T. Jos, K. Girish Kumar, *Food Anal. Methods*, **7,** 741 (2014).

82. S. Jesny, S. Menon, K. Girish Kumar, *RSC Adv*., **6**, 75741 (2016).

83. D. Thomas, A. E. Vikraman, T. Jos, K. Girish Kumar, *LWT Food Sci. Technol*., **63**, 1294 (2015).

84. T. Jos, L. Lonappan, Z. Rasheed, A. E. Vikraman, K. Girish Kumar, *Electrochem. Lett.*, **3**, B23 (2014).

85. S. Jesny, K. Girish Kumar, *Electroanalysis*, **27**, 1828 (2017).

86. D. Thomas, Z. Rasheed, S. Jesny, K. Girish Kumar, *J. Food Sci. Technol*., **52**, 6719 (2015).

87. S. Jesny, Z. Rasheed, K. Girish Kumar, *Ionics*, **23,** 1533 (2017).

88. A. E. Vikraman, A. R. Jose, M. Jacob, K. Girish Kumar, *Anal. Methods,* **7**, 6791 (2015).

89. R. Leena, A. K. Jissy, K. Girish Kumar, A. Datta, *J. Phys. Chem. C*, **115**, 21858 (2011).

90. S. Jesny, K. Girish Kumar, *J. Electroanal. Chem.*, **801**, 153 (2017).

91. A. R. Jose, U. Sivasankaran, S. Menon, K. Girish Kumar, *Anal. Methods*, **8**, 5701 (2016).

92. A. Thomas, U. Sivasankaran, K. Girish Kumar, *Spectrochim. Acta A*, **188**, 113 (2018).

93. A. R. Jose, A. E. Vikraman, K. Girish Kumar, *New J. Chem.*, **41**, 10828 (2017).

94. AOAC, *Official methods of analysis of the Association of Official Analytical Chemists*, 15th Edn., K. Helrich, Editor, Arlington, Virginia, 1140 (1990).

95. O. Folin, W. Denis, *J. Biol. Chem.*, **13**, 469 (1912-13).

96. AOAC, *Official Methods of Analysis of the Association of Official Analytical Chemists*, 15th Edn., K. Helrich, Editor, Arlington, Virginia, 1125 (1990).

97. J. Sedlak, R. H.Lindsay, *Anal. Biochem.*, **25**, 192 (1968).

98. M. Bielavská, J. Kassa, *Collect. Czech. Chem. Commun.*, **65**, 1677 (2000).

99. R.W. Bonsnes, H.H. Taussky, *J. Biol. Chem.*, **158,** 581 (1945).

100. A. Mishra, A. Upadhyay, A. Patra, S. Chaudhury, P. Chattopadhyay, *Sci. Pharm.*, **77**, 367 (2009).

101. M. J. Levine, A. Aguirre, M. N. Hatton, L. A. Tabak, *J. Dent. Res*., **66,** 693 (1987**)**.

102. R. M. Kark, J. R. Lawrence, V. E. Pollack, C. L. Pirani, R. C. Muehrcke, H. Silva, *A primer of urinalysis*, 2nd ed., Hoeber Medical Division, Harper & Row, New York (1964).

103. Ringer's solution (pH 7.3 - 7.4), *Cold Spring Harb. Protoc.* (2008).

104. B. Saad, Y. Y. Sing, M. A. Nawi, N. H. Hashim, S. M. Ali, M. I. Saleh, *Food Chem.*, **105**, 389 (2007).

105. G. M. Williams, *Toxicol. Ind. Health*, **9**, 303 (1993).

106. M. Pemberton, C. M. Yeoman, A. Clark, G. T. Craig, C. D. Franklin, D. J. Gawkrodger, *Br. Dent. J.*, **175**, 106 (1993).

107. M. Inoue, R. Susuki, T. Koide, N. Sakaguchi, Y. Ogihara, Y. Yabu, *Biochem. Biophys. Res. Commun.*, **204**, 898 (1994).

108. L. S. Campos, M. A. Valdez- Solana, D. Mahz- Mares, I. Velazquez, J. P. Pardo. *Microbiology*, **155**, 604 (2009).

109. R. K. Shervendani, M. Bagherzadeh, S. A. Mozaffari, *Sens. Actuators, B*, **115**, 614 (2006).

110. T. Luczak, *Electrochim. Acta*, **54**, 5863 (2009).

111. X. Dai, R. G. Compton, *Anal. Sci.*, **22**, 567 (2006).

112. EFSA Panel on food additive and nutrient sources added to food, *EFSA Journal*, **12**, 3642 (2014).

113. J. H. Mahon, *The determination of certain antioxidants in Fats and their behavior in food products*, Dissertation, Mc Gill University (1953).

114. D. L. Madhavi, S. S. Deshpande, D. K. Salunkhe, *Food antioxidants: Technological, Toxicological and Health perspectives*, Marcel Dekker, New York, 160 (1996).

115. H. Chen, C. K. Heng, P. D. Puiu, X. D. Zhou, A. C. Lee, T. M. Lim, S. N. Tan, *Anal. Chim. Acta*, **554**, 52 (2005).

116. S. Campuzano, M. Pedrero, C. Montemayor, E. Fatas, J. M. Pingarron, *J. Electroanal. Chem.*, **586**, 112 (2006).

117. Z. Rasheed, A. E. Vikraman, D. Thomas, J. S. Jagan, K. Girish Kumar, *Food Anal. Methods*, **8**, 213 (2015).

118. A. E. Vikraman, D. Thomas, S. T. Cyriac, K. Girish Kumar, *J. Electrochem. Soc.*, **161**, B305 (2014).

119. R. Gupta, S. K. Guin, S. K. Aggarwal, *RSC Adv.*, **2**, 1810 (2012).

120. J. E. B. Randles, *Trans. Faraday Soc.*, **44**, 322 (1948).

121. M. Luque, A. RõÂos, M. V. Ârcel, *Anal. Chim. Acta*, **395**, 217 (1999).

122. Y. Ding, M. F. Mora, C. D. Garcia, *Anal. Chim. Acta*, **561**,126 (2006).

123. A. Andreu-Navarro, J. M. Fernández-Romero, A. Gómez-Hens. *Anal. Chim. Acta*, **695**, 11 (2011).

124. M. M. Delgado-Zamarren˜o, A. Sa´nchez-Pe´rez, I. Gonza´lezMaza, J. Herna´ndez-Me´ndez, *J. Chromatogr. A*, **871**, 403 (2000).

125. E. Laviron, *J. Electroanal. Chem. Interfacial Electrochem.*, **52**, 355 (1974).

126. T. Gan, J. Sun, S. Cao, F. Gao, Y. Zhang, Y. Yang, *Electrochim. Acta*, **74**,151 (2012).

127. T. Yoshida, K. Mori, T. Hatano, T. Okumura, I. Uehara, K. Komage, Y. Fugita, T. Okuda, *Chem. Pharm. Bull.*, **37**, 1919 (1989).

128. 3B Scientific Therapy and wellness insight, Why Is Gout On The Increase?, http://blog.3bscientific.com/therapy_wellness/2015/05/why-is-gout-on-the-increase.html (Accessed 28 October 2016).

129. E. P. de Oliveira, R. C. Burini, *Diabetol. Metab. Syndr.*, **4**, 12 (2012).

130. Wikipedia, Hyperuricemia, https://en.wikipedia.org/wiki/Hyperuricemia (Accessed 28 October 2016).

131. J. Maiuolo, F. Oppedisano, S. Gratteri, C. Muscoli, V. Mollace, *Int. J. Cardiol. Heart Vessels*, **213,** 8 (2016).

132. Wikipedia, Uric acid, https://en.wikipedia.org/wiki/Uric_acid#Biology (Accessed 28 October 2016).

133. L. Liddle, J. E. Seegmiller, L. Laster, *J. Lab. Clin. Med.*, **54**, 903 (1959).

134. P. Yang, W. Wei, C. Tao, J. Zeng, *Bull. Environ. Contam. Toxicol.*, **79**, 5 (2007).

135. A. Thomas, A. E. Vikraman, D. Thomas, K. Girish Kumar, *Food Anal. Methods*, **8**, 2028 (2015).

136. J. Q. Chambers, *J. Electroanal. Chem.*, **130**, 381(1981).

137. E. Colín-Orozco1, S. Corona-Avendaño1, M. T. Ramírez-Silva, M. Romero-Romo1, M. Palomar-Pardavé, *Int. J. Electrochem. Sci.*, **7,** 6097 (2012).

138. M. A. Kamyabi, M. A. Shafiee, *J. Braz. Chem. Soc.*, **23**, 593 (2012).

139. H. L. Zou, B. L. Li, H. Q. Luo, N. B. Li, *Sens. Actuators, B,* **207**, 535 (2015).

140. X. Zheng, Y. Guo, J. Zheng, X. Zhou, Q. Li, R. Lin, *Sens. Actuators, B,* **213,** 188 (2015).

141. P. F. Bolado, D. H. Santos, V. M. Montoya, A. C. Garc, *Electroanalysis*, **27**, 1276 (2015).

142. F. Wu, T. Huang, Y. Hu, X. Yang, Y. Ouyang, Q. Xie, *Microchim. Acta*, **183**, 2539 (2016).

143. R. Guidelli, R. G. Compton, J. M. Feliu, E. Gileadi, J. Lipkowski, W. Schmickler, S. Trasatti, *Pure Appl. Chem.*, **86**, 245 (2014).

144. S. Michalkiewicz, M. Mechanik, J. Malyszko, *Electroanal*., **16**, 588 (2004).

145. L. Guo, M. Y. Xie, A. P. Yan, Y. Q. Wan, Y. M. Wu, *Anal. Bioanal. Chem.*, **386**, 1881 (2006).

146. J. L. Zurita, A. Jos, A. Peso, M. Salquero, M. López-Artíguez, G. Repetto, *Water Res.*, **41**, 2599 (2007).

147. G. J. A. Speijers, M. E. Apeldoorn, JECFA, Joint FAO/WHO Expert Committee on Food Additives from: http://www.inchem.org/documents/jecfa/jecmono/v32je02.htm (Accessed 10 January 2017).

148. Liumeimei, https://hong24608.wordpress.com/2013/08/16/is-propyl-gallate-bad-or-not/ (Accessed 10 January 2017).

149. Wageningen University, http://www.food-info.net/uk/e/e310.htm (Accessed 10 January 2017).

150. Fooducate, http://www.fooducate.com/app#!page=postandid=57A32809-8AFF-6E5E-44B8-A98F8ED0D3BC (Accessed 10 January 2017).

151. Y. Ni, L. Wang, S. Kokot, *Anal. Chim. Acta*, **412**, 185 (2000).

152. C. De la Fuenta, J. A. Acuña, M. D. Vázquez, M. L. Tascón, M. I. Gómez, P. S. Batanero, *Talanta*, **44**, 685 (1997).

153. L. Agui, M. A. Lopez-Huertas, P. Yanez-Sedeno, J. M. Pingarron, *J. Elecroanal. Chem.*, **414**, 14 (1996).

154. R. A. Mederos, C. Romeu, R. Filho, O. F. Filho, *Food Chem.*, **123**, 886 (2010).

155. S. P. Alves, D. M. Brum, E. C. Branco de Andrade, A. D. P. Netto, *Food Chem.*, **107**, 489 (2008).

156. A. G. Newsome, C. A. Culver, R. B. van Breemen, *J. Agric. Food Chem.*, **62**, 6498, (2014).

157. P. Amchova, H. Kotolova, J. Ruda-Kucerova, *Regul. Toxicol. Pharmacol.* **73**, 914 (2015).

158. D. Narayan, Issues related to artificial food colours. http://www.biotecharticles.com/Issues-Article/Issues-related-to-Usage-of-Artificial-Food-Colours-3125.html. (Accessed 15 July 2016).

159. EFSA Panel on Food Additives and Nutrient Sources added to Food (ANS), *EFSA Journal*, **8**, 1853 (2010).

160. J. Chen, A. Zheng, Y. Gao, C. He, G. Wu, Y. Chen, X. Kai, C. Zhu, *Spec. Chim. Acta, Part A*, **69**, 1044 (2008).

161. Manual of methods of analysis, Food safety and standards authority of India, http://www.fssai.gov.in/Portals/0/Pdf/15Manuals/BEVERAGES,%20SUGARS%20&%20CONFECTINERY.pdf (Accessed 15 July 2016).

162. I.C.M.R, *Manual methods of analysis for adulterants and contaminants in food*, Page 56. (1990).

163. A. E. Vikraman, A. R. Jose, M. Jacob, K. Girish Kumar, *Anal. Methods*, **7**, 6791 (2015).

164. M. Koneswaran, R. Narayanaswamy, *Sens. Actuators B*, **139**, 91 (2009).

165. C. Yu, J. Yan, Y. Tu, *Microchim. Acta*, **175**, 347 (2011).

166. M. Florian, H. Yamanaka, P. A. Carneiro, M. V. Zanoni, *Food Addit. Contam.*, **19**, 803 (2002).

167. K. Sugaya, *BNSKAK*, **61**, 127 (2012).

168. X. Chen, J. Yin, C. Zhang, N. Lu, Z. Chen, *Anal. Sci.*, **33**, 1123 (2017).

169. J. Guo, H. Wu, L. Du, Y. Fu, *Anal. Methods*, **5**, 4021 (2013).

170. M. Zhang, X. Cao, H. Li, F. Guan, J. Guo, F. Shen, Y. Luo, C. Sun, L. Zhang, *Food Chem.*, **135**, 1894 (2012).

171. A. Fang, Q. Long, Q. Wu, H. Li, Y. Zhang, S. Yao, *Talanta*, **148**, 129 (2016).

172. M. Elangovan, R. N. Day, A. Periasamy, *J. Microsc.*, **205**, 3 (2002).

173. M. Maity, S. Dolui, N. C. Maiti, *Phys. Chem. Chem. Phys.*, **17**, 31216 (2015).

174. S. T. Handy, *Applications of Ionic Liquids in Science and Technology*, InTech, Croatia (2011).

175. Quinoline yellow WS, https://en.wikipedia.org/wiki/Quinoline Yellow (Accessed 16 May 2017).

176. A. Williams, Quinoline Yellow WS (E104), http://juicingtherainbow.com/702/supermarket-juices/quinoline-yellow-ws-e104/ (Accessed 16 May 2017).

177. EFSA Panel on Food Additives and Nutrient Sources added to Food (ANS), *EFSA Journal*, **7,** 1329 (2009).

178. X. Yang, Y. Feng, S. Zhu, Y. Luo, Y. Zhuo, Y. Dou, *Anal. Chim. Acta*, **847**, 49 (2014).

179. R. J. Hunter, *Zeta Potential In Colloid Science: Principles And Applications*, Academic Press, UK (1988).

180. G. Rajkumar, M. G. Sethuraman, *Self Assembled Monolayer of 3-Amino-5-Mercapto-1, 2, 4-Triazole on Copper and its Corrosion Protection in 1% NaCl Solution, Recent Advances in Surface Science*, ISBN 978-93-82338-36-9, 246-247 (2013).

181. A. Shrivastava, V. B. Gupta, *Chron. Young Sci.*, **2,** 21 (2011).

182. M. H. Sorouraddin, M. Saadati, F. Mirabi, *J. Food Drug Anal.*, **23**, 447 (2015).

183. F. Martin, J. M. Oberson, M. Meschiari, C. Munari, *Food Chem.*, **197**, 1249 (2016).

184. S. Zhang, Z. Shi, J. Wang, *Food Chem.*, **173**, 449 (2015).

185. Ş. D. Zor, B. Aşçı, Ö. A. Dönmez, D. Y. Küçükkaraca, *J. Chromatogr. Sci.*, **54**, 952 (2016).

186. K. A. Zeynali, S. M. Khoshmanesh, *J. Chin. Chem. Soc.*, **62,** 772 (2015).

187. U. Sivasankaran, S. T. Cyriac, S. Menon, K. Girish Kumar, *J. Fluoresc.*, **27**, 69 (2017).

188. G. X. Song, Q. Tang, Y. Huang, R. Wang, Y. Y. Xi, X. L. Ni, Z. Tao, S. F. Xue , J. X. Zhang, *RSC Adv.*, **5**, 100316 (2015).

189. B. Halliwell, J. M. C. Gutteridge, *Free radicals in Biology and Medicine*, 2nd ed., Oxford, Clarendon, UK, 1989.

190. W. Droge, *Physiol. Rev.,* **82**, 47 (2002).

191. C. Arana, A.Cutando, M. J. Ferrera, G.. Go´mez-Moreno, C. V. Worf, M. J. Bolanos, G. Escames, D. A. Castroviejo, *J. Oral Pathol., Med.,* **35**, 554 (2006).

192. B. Halliwell, *Am. J. Med.,* **91**, 14S (1991).

193. A. Pastore, G. Federici, E. Bertini, F. Piemonte, *Clin. Chim. Acta*, **333**, 19 (2003).

194. S. C. Lu, *Mol. Asp. Med.,* **30**, 42 (2009).

195. D. M. Townsend, K. D. Tew, H. Tapiero, *Biomed. Pharmacother.,* **57**,145 (2003).

196. N. Zang, F. Qu, H. Q. Luo, N. B. Li, *Biosens. Bioelectron.,* **42**, 214 (2013).

197. Y. Shi, Y. Pan, H. Zhang, Z. Zhang, M. Li, C. Yi, M. Yang, *Biosens. Bioelectron.,* **56**, 39 (2014).

198. X. Tan, J. Yang, Q. Lid, Q. Yang, *Analyst,* **140**, 6748 (2015).

199. D. Thomas, L. Lonappan, L. Rajith, S. T. Cyriac, Kumar K. G., *J. Fluoresc.,* **23**, 473 (2013).

200. S. C. Ray, A. Saha, N. R. Jana, R. Sarkar, *J. Phys. Chem. C,* **113**, 18546 (2009).

201. J. Zhou, C. Booker, R. Li, X. Zhou, T. K. Sham, X. Sun, Z. Ding, *J. Am. Chem. Soc.,* **129**, 744 (2007).

202. S. L. Hu, K. Y. Niu, J. Sun, J. Yang, N. Q. Zhao, X. W. Du, *J. Mater. Chem.,* **19**, 484 (2009).

203. H. Zhu, X. Wang, Y. Li, Z. Wang, F. Yang, X. Yang, *Chem. Commun.,* **34**, 5118 (2009).

204. H. Peng, J. T. Sejdic, *Chemistry of Materials,* **21**, 5563 (2009).

205. Microwave-assisted synthesis in the pharmaceutical industry a current perspective and future prospects. http://www.ddw-online.com/chemistry/p97060-microwave-assisted-synthesis-in-the-pharmaceutical-industry-a-current-perspective-and-future-prospectssummer-06.html (Accessed 28 May 2016).

206. S. Menon, A. E. Vikraman, S. Jesny, K. G. Kumar, *J. Fluoresc.,* **26**,129 (2016).

207. S. N. Baker, G. A.Baker, *Angew. Chem. Int. Ed.,* **49**, 6726 (2010).

208. S. Banerjee, S. Kar, J. M. Perez, S. Santra, *J. Phys. Chem. C,* **113**, 9659 (2009).

209. R. Deng, X. Xie, M. Vendrell, Y. T. Chang, Liu X, *J. Am. Chem. Soc.*, **133**, 20168 (2011).

210. R. Gui, X. An, H. Su, W. Shen, L. Zhu, X. Ma, Z. Chen, X. Wang, *Talanta,* **94**, 295 (2012).

211. K. S. Park, M. I. Kim, M. A. Woo, H. G. Park, *Biosens. Bioelectron.,* **45**, 65 (2013).

212. S. L. Hu, K. Y. Niu, J. Sun, J. Yang, N. Q. Zhao, X. W. Du, *J. Mater. Chem.,* **19**, 484 (2009).

213. Y. Fang, S. Guo, D. Li, C. Zhu, W. Ren, S. Dong, E. Wang, *ACS Nano,* **6**, 400 (2012).

214. R. J. Brainard, A. B. Ellis, *J. Phys. Chem. B,* **101**, 2533 (1997).

215. K. D. Kepler, G. C. Lisensky, M. Patel, L. A. Sigworth, A. B. Ellis, *J. Phys. Chem.,* **99**, 16011 (1995).

216. A. Y. Nazzal, X. Wang, L. Qu, W. Yu, Y. Wang, X. Peng, M. Xiao, *J. Phys. Chem. B,* **108**, 5507 (2004).

217. J. J. Li, Y. A. Wang, W. Guo, J. C. Keay, T. D. Mishima, M. B. Johnson, X. Peng, *J. Am. Chem. Soc*., **125**, 12567 (2003).

218. J. Liang, S. Huang, D. Zeng, Z. He, X. Ji, X. Ai, H. Yang, *Talanta*, **69**, 126 (2006).

219. P. Teengam, W. Siangproh, A. Tuantranont, T. Vilaivan, O. Chailapakul, C. S. Henry, *Anal. Chem.*, **89,** 5428 (2017).

220. P. Mulvaney, *Langmuir*, **12**, 788 (1996**).**

221. S. Niu, Z. Lv, J. Liu, W. Bai, S. Yang, A. Chen, *PLoS ONE*, **9**, 1 (2014).

222. H. Li, L. Rothberg, *J. Am. Chem. Soc*., **126**, 10958 (2004).

223. X. J. Xue, F. Wang, X. G. Liu, *J. Am. Chem. Soc*., **130**, 3244 (2008).

224. L. Li, B. Li, Y. Qi, Y. Jin, *Anal. Bioanal. Chem*., **393**, 2051 (2009).

225. L. Lua, J. Zhanga, X. Yang, *Sens. Actuators, B*, **184,** 189 (2013).

226. G. Cao, F. Xu, S. Wang, K. Xu, X. Hou, P. Wu, *Anal. Chem.*, **89**, 4695 (2017).

227. A. Safavi, R. Ahmadi, Z. Mohammadpour, *Sens. Actuators, B*, **242**, 609 (2017).

228. N. Ding, H. Zhao, W. Peng, Y. He, Y. Zhou, L. Yuan, Y. Zhang, *Colloids Surf., A*, **395,** 161 (2012).

229. Y. Li, P. Wu, H. Xu, H. Zhang, X. Zhong, *Analyst*, **136**, 196 (2011).

230. M. Jalili, *OJCHEG*, **32**, 1589 (2016).

231. S. Cho, S. H. Kim, *J. Colloid Interface Sci.,* **458**, 87 (2015).

232. D. R. Dreyer, D. J. Miller, B. D. Freeman, D. R. Paul, C. W. Bielawski, *Langmuir*, **28**, 6428 (2012).

233. C. Li, D. Li, G. Wan, J. Xu, W. Hou, *Nanoscale Res. Lett.*, **6**, 440 (2011).

234. X. Liu, J. Cao, H. Li, J. Li, Q. Jin, K. Ren, J. Ji, *ACS Nano*, **7**, 9384 (2013).

235. P. M. Arnal, M. Comotti, F. Schiith, *Angew. Chem. Int. Ed.*, **45**, 8224 (2006).

236. J. W. Park, J. S. S. Parry, *J. Am. Chem. Soc.*, **136**, 1907 (2014).

237. J. G. Mehtala, D. Y. Zemlyanov, J. P. Max, N. Kadasala, S. Zhao, A. Wei, *Langmuir*, **30**, 13727 (2014).

238. A. Jakhmola, M. Celentano, R. Vecchione, A. Manikas, E. Battista, V. Calcagno, P. A. Netti, *Inorg. Chem. Front.*, **4,** 1033 (2017).

239. K. Juodkazis, J. Juodkazyte, V. Jasulaitiene, A. Lukinskas, B. Sebeka, *Electrochem. Commun.*, **2,** 503 (2000).

240. R. A. Zangmeister, T. A. Morris, M. J. Tarlov, *Langmuir*, **29**, 8619 (2013).

241. N. Wei, Y. Jiang, Y. Ying, X. Guo, Y. Wu, Y. Wen, H. Yang, *RSC Adv.*, **7**, 11528 (2017).

242. J. Park, T. F. Brust, H. J. Lee, S. C. Lee, V. J. Watts, Y. Yeo, *ACS Nano.*, **8**, 3347 (2014).

243. S. Govindaraju, S. R. Ankireddy, B. Viswanath, J. Kim, K. Yun, *Sci. Rep.*, **7**, 40298 (2017).

244. A.M. Ektessabi, S. Hakamata, *Thin Solid Films*, **377**, 621 (2000).

245. U. Sivasankaran, S. Jesny, A. R. Jose, K. Girish Kumar, *Anal. Sci.*, **33**, 281 (2017).

246. Y. Leng, K. Xie, L. Ye, G. Li, Z. Lu, J. He, *Talanta*, **139**, 89 (2015).

247. B. Kong, A. Zhu, Y. Luo, Y. Tian, Y. Yu, G. Shi, *Angew. Chem. Int. Ed.*, **50**, 1837 (2011).

248. J. Feng, H. Guo, Y. Li, Y. Wang, W. Chen, A. Wang, *ACS Appl. Mater. Interfaces*, **5,** 1226 (2013).

249. Z. Chen, C. Zhang, T. Zhou, H. Ma, *Microchim. Acta*, **182**, 5 (2015).

250. Y. Zheng, Y. Wang, X. R. Yang, *Sens. Actuators, B*, **156**, 95 (2011).

251. J. M. Liu, X. X. Wang, M. L. Cui, L. P. Lin, S. L. Jiang, L. Jiao, L. H. Zhang, *Sens. Actuators, B,* **176**, 97 (2013).

252. https://en.wikibooks.org/wiki/Human_Physiology/The_Urinary_System (Accessed 15 April 2017).

253. N. N. Turner, N. Lameire, D. J. Goldsmith, C. G. Winearls, J. Himmelfarb, G. Remuzzi, W. G. Bennet, M. E. de Broe, J. R. Chapman, A. Covic, V. Jha, N. Sheerin, R. Unwin, A. Woolf, *Oxford Textbook of Clinical Nephrology,* 4th ed., Oxford: Oxford University Press (2015).

254. S. Gowda, P. B. Desai, S. S. Kulkarni, V. V. Hull, A. A. K. Math, S. N. Vernekar, *N. Am. J. Med. Sci.,* **2**, 170 (2010).

255. A. K. Parmar, N. N. Valand, K. B. Solankia, S. K. Menon, *Analyst*, **141**, 1488 (2016).

256. Creatinine, Health Encyclopedia, https://www.urmc.rochester.edu/encyclopedia/content.aspx?ContentTypeID=167&ContentID=creatinine_serum (Accessed 15.04.2017).

257. C. S. Pundir, S. Yadav, A. Kumar, *Trends Analyt. Chem.,* **50,** 42 (2013).

258. M. Peake, M. Whiting, *Clin. Biochem. Rev.,* **27,** 173 (2006).

259. W. Marshall, *ACB*, 1, http://www.acb.org.uk/Nat%20Lab%20Med%20Hbk/Creatinine.pdf (2012).

260. J. Siedel, R. Deeg, H. Seidel, H. Möllering, J. Staepels, H. Gauhl, J. Ziegenhorn, *J. Anal. Lett.,* **21**, 1009 (1988).

261. Copper nanoparticle, https://en.wikipedia.org/wiki/Copper_nanoparticles (Accessed 15.04.2017).

262. A. Krishnegowda, N. Padmarajaiah, S. Anantharaman, K. Honnur, *Arab. J. Chem.,* **10,** S2018 (2017).

263. G. Campo, A. Irastorza, J. A. Casado, *Fresenius J. Anal. Chem.,* **352**, 557(1995).

264. M. J. Pugia, J. A. Lott, J. F. Wallace, T. K. Cast, L. D. Bierbaum, *Clin. Biochem.*, **33**, 63 (2000).

265. H. Du, R. Chen, J. Du, J. Fan, X. Peng, *Ind. Eng. Chem. Res.*, **55**, 12334 (2016).

266. S. Mohammadi, G. Khayatian, *Microchim. Acta*, **182**, 1379 (2015).

267. P. K. Jain, K. S. Lee, I. H. El-Sayed, M. A. El-Sayed, *J. Phys. Chem. B*, **110**, 7238 (2006).

268. A. Barth, *Biochimica et. Biophysica Acta*, **1767**, 1073 (2007).

269. S. Masoomeh, J. L. Manzoori, J. Abolghasem, *IJPR*, **3**, 111 (2007).

270. D. Molinnus, A. Bartz, M. Bäcker, P. Siegert, H. Willenberg, A. Poghossian, M. Keusgen, M. J. Schöning, *Procedia Eng.*, **120**, 540 (2015).

271. Adrenalin, https://www.rxlist.com/adrenalin-drug.htm (Accessed 08 February 2018).

272. D. Brondani, C. W. Scheeren, J. Dupont, I. C. Vieira, *Sens. Actuators, B*, **140**, 252 (2009).

273. H. P. Wu, T. L. Cheng, W. L. Tseng, *Langmuir*, **23**, 7880 (2007).

274. Y. Xie, H. Huang, Q. Zhang, S. Jin, *Chem. Res. Chin. Univ.*, **25**, 433 (2009).

275. S. Menon, S. Jesny, U. Sivasankaran, K. Girish Kumar, *Anal. Sci.*, **32**, 999 (2016).

276. Z. Chen, Y. Hu, Q. Yang, C. Wan, Y. Tan, H. Ma, *Sens. Actuators, B,* **207,** 277 (2015).

277. I. N. Pulidindi, A. Gedanken, *Int. J. Environ. Anal. Chem.*, **94**, 28 (2014).

278. J. Li, W. Tu, H. Li, M. Han, Y. Lan, Z. Dai, J. Bao, *Anal. Chem.*, **86**, 130 (2014).

279. M. Wang, Y. Li, L. Wang, X. Su, *Anal. Methods*, **9**, 4434 (2017).

280. D. Molinnus, A. Bartz, M. Bäcker, P. Siegert, H. Willenberg, A. Poghossian, M. Keusgen, M. J. Schöning, *Procedia Eng.*, **120**, 540 (2015).

281. N. Nasirizadeh, Z. Shekari, M. Dehghani, S. Makarem, *J. Food Drug Anal.*, **24**, 406 (2016).

282. M. R. Siddiqui, M. Z. A. Rafiquee, S. M. Wabaidur, Z. A. Alothman, M. S. Ali, H. A. Allohedan, *Anal. Sci.*, **31**, 437 (2015).

283. W. F. El-Hawary, R. G. Orabi, S. A. Al-Yami, *Int. J. Chem. Sci.*, **13**, 563 (2015).

284. P. Böck, *Morphological and Histochemical Methods for the Study of Paraganglionic Cells, The Paraganglia*, Vol. 6, Springer, Berlin, Heidelberg (1982).

285. W. H. Harrison, *Arch. Biochem. Biophys.*, **161**, 116 (1963).

286. U. Sivasankaran, T. C. Jos, K. Girish Kumar, *Anal. Biochem.*, **544,** 1 (2018).

287. L. Y. Zhong, W. W. Tao, C. Wei, *Chin. Sci. Bull.*, **57**, 41 (2012).

288. C. Chen, Z. Hu, Y. Li, L. Liu, H. Mori, Z. Wang, *Sci. Rep.*, **6**, 19545 (2016).

289. R. Sierra-Á vila, M. Perez-Alvarez, G. Cadenas-Pliego, V. C. Padilla, C. Á vila-Orta, O. P. Camacho, E. Jimenez-Regalado, E. Hernandez-Herna´ ndez, R. M. Jime´ nez-Barrera, *J. Nanomater.*, **2015**, 1 (2015).

.....ꕥ.....

List of Publications and Presentations

Publications

1. **U. Sivasankaran**, T. C. Jos, K. Girish Kumar, Selective recognition of creatinine – Development of a colorimetric sensor, *Analytical Biochemistry*, **544**, 1 - 6 (2018).
2. **U. Sivasankaran,** A. Thomas, A. R. Jose, K. Girish Kumar, Poly (Bromophenol Blue) - Gold Nanoparticle Composite: An Efficient Electrochemical Sensing Platform for Uric Acid, *Journal of the Electrochemical Society*, **164**, B292 - B297 (2017).
3. **U. Sivasankaran,** S. Jesny, A. R. Jose, K. Girish Kumar, Fluorescence Determination of Glutathione using tissue paper – derived carbon dots as fluorophores, *Analytical Sciences*, **33**, 281-285 (2017). ***(Selected as Hot Article)***
4. **U. Sivasankaran,** S. T. Cyriac, S. Menon, K. Girish Kumar, Fluorescence Turn off Sensor for Brilliant Blue FCF- an Approach Based on Inner Filter Effect, *Journal of Fluorescence*, **27**, 69-77 (2017).
5. **U. Sivasankaran,** A. E. Vikraman, D. Thomas, K. Girish Kumar, Nanomolar level determination of octyl gallate in fats and oils, *Food Analytical Methods*, **9**, 2115-2123 (2016).
6. A. Thomas, **U. Sivasankaran,** K. Girish Kumar, Biothiols induced colour change of silver nanoparticles: A colorimetric sensing strategy, *Spectrochimica Acta Part A: Molecular and Biomolecular Spectroscopy*, **188**, 113-119 (2018).

7. A. R. Jose, **U. Sivasankaran,** S. Menon, K. Girish Kumar, A silicon nanoparticle based turn off fluorescent sensor for sudan I, *Analytical Methods*, **8**, 5701-5706 (2016).
8. S. Menon, S. Jesny, **U. Sivasankaran,** K. Girish Kumar, Fluorometric determination of Epinephrine: A green approach, *Analytical Sciences*, **32**, 999-1001 (2016).
9. T. C. Jos, A. R. Jose, **U. Sivasankaran,** K. Girish Kumar, Electrochemical sensing of Tinidazole on modified glassy carbon electrodes, *Journal of the Electrochemical Society*, **162**, B94-B100 (2015).

Presentations

1. Determination of Quinoline yellow via fluorescence quenching of copper nanoclusters (Current trends in Chemistry, CUSAT, February 2018).
2. Voltammetric determination of Propyl gallate using nickel nanoparticles modified glassy carbon electrode, (International Symposium on New Trends in Applied Chemistry, Sacred Heart College, Thevara, February 2017).
3. Quantification of Propyl Gallate in Food samples using Differential Pulse Voltammetry (Current trends in Chemistry, CUSAT, February 2017).
4. Square wave voltammetric determination of Uric acid using poly (Bromophenol blue) film and Gold nanoparticles modified glassy carbon

electrode (26th Swadeshi Science Congress, CMFRI, Kochi, November 2016).

5. Sensing of Brilliant Blue FCF by using cadmium sulphide quantum dots, (International Conference on Material for the Millennium, CUSAT, January 2016).

6. Fluorescence determination of blue colorant in soft drinks (25th Swadeshi Science Congress, Sree Sankara Sanskrit University, Kalady, November 2015).

7. Voltammetric determination of octyl gallate using SAM modified glassy carbon electrode, (New Frontiers in Chemical Research, Sacred Heart College, Thevara, December 2014).

.....ൟ.....